

**Determination of regional surface heat fluxes over
heterogeneous landscapes by
integrating satellite remote sensing with
boundary layer observations**

Yaoming Ma

Promotoren: Prof. Dr. R. A. Feddes

Hoogleraar in de bodemnatuurkunde, agrohydrologie en het grondwaterbeheer,
Wageningen Universiteit, Nederland

Prof. Dr. M. Menenti

Istituto per i Sistemi Agricoli e Forestali del Mediterraneo (ISAFoM),
Consiglio Nazionale delle Ricerche (CNR), Italy

Co-promotor: Prof. J. M. Wang

Cold and Arid Regions Environmental and Engineering Research Institute
(CAREERI), Chinese Academy of Sciences (CAS), China

Samenstelling Promotiecommissie:

Prof. Dr. A. A. M. Holtslag, Wageningen Universiteit

Prof. Dr. B. J. J. M. van den Hurk, Universiteit Utrecht

Prof. Dr. W. G. M. Bastiaanssen, Waterwatch, Wageningen

Prof. Dr. Z. (Bob) Su, International Institute for Geo-Information Science and Earth
Observation (ITC), Enschede

**Determination of regional surface heat fluxes over
heterogeneous landscapes by
integrating satellite remote sensing with
boundary layer observations**

Yaoming Ma

Proefschrift
ter verkrijging van de graad van doctor
op gezag van de rector magnificus
van Wageningen Universiteit
Prof. Dr. M. J. Kropff
in het openbaar te verdedigen
op woensdag 4 oktober 2006
des namiddags te 16.00 uur in de Aula

Yaoming Ma, 2006

Determination of regional surface heat fluxes over heterogeneous landscapes by integrating satellite remote sensing with boundary layer observations

PhD dissertation, Wageningen, The Netherlands - with references - with summaries in English and Dutch

ISBN 90-8504-483-9

Abstract

Yaoming Ma, 2006, *Determination of regional surface heat fluxes over heterogeneous landscapes by integrating satellite remote sensing with boundary layer observations*, PhD thesis, Wageningen University, Wageningen, The Netherlands.

Arid areas such as the Heihe River Basin and high elevation areas as the Tibetan Plateau with a heterogeneous landscape are characterized by extreme gradients in land surface properties such as wetness and roughness which have a significant but local impact on the Atmospheric Boundary Layer (ABL). Observation of the actual extent of these areas and their properties is essential to understand the mechanisms through which heterogeneous land surfaces may have a significant impact on the structure and dynamics of the overlying ABL. The latter applies specifically to energy and water fluxes. Progress in this research area requires spatial measurements of variables such as surface hemispherical reflectance, radiometric surface temperature, vegetation fractional cover, Leaf Area Index (*LAI*) and local aerodynamic and thermodynamic roughness lengths. It also requires the measurements of Normalized Difference Vegetation Index (*NDVI*), Modified Soil Adjusted Vegetation Index (*MSAVI*). Imaging radiometers on-board satellites can provide useful estimates of most of these variables. Using these variables in combination with the Surface Layer (SL) and ABL observations we are able to derive the distribution of land surface heat fluxes over heterogeneous landscapes.

Based on the analysis of the land surface heterogeneity and its effects on the overlying air flow, SL observations, ABL observations and satellite Remote Sensing (RS) measurements [Landsat-5(7) TM (ETM) and NOAA/AVHRR measurements], *three parameterization methodologies, which are called RS approach (RS + SL-assumptions), Tile approach (RS + SL-observations) and Blending height approach (RS + SL-observations + ABL-observations) are developed and demonstrated to estimate the surface heat flux densities over heterogeneous landscapes*. The RS approach (see Figures 3.4 and 5.1) uses satellite measurements in combination with assumptions on the SL at and below a reference height of about 2m. The Tile approach (see Figures 3.4, 3.5 and 7.1) uses satellite measurements in combination with SL observations at and below a reference height of about 20 m. The Blending height approach (see Figures 3.4, 3.6 and 7.2) uses satellite measurements in combination with SL and ABL observations at and below the blending height of about 200 m.

The approaches were applied to heterogeneous areas: the Heihe basin Field Experiment (HEIFE), the Arid Environment Comprehensive Monitoring Plan, 95

(AECMP'95), the Global Energy and Water cycle EXperiment Asian Monsoon Experiment on the Tibetan Plateau (GAME/Tibet), the Coordinated Enhanced Observing Period Asia-Australia Monsoon Project on the Tibetan Plateau (CAMP/Tibet) and the DunHuang EXperiment (DHEX). The distributions of *NDVI*, *MSAVI*, vegetation fractional cover, *LAI*, surface reflectance, surface temperature, net radiation flux, soil heat flux, sensible heat flux and latent heat flux have been determined over five different heterogeneous areas. These estimates have been compared with independent ground measurements of flux densities. At the validation sites relative deviations ($\delta V / V$) were less than 10 %. The results derived from the Blending height approach were also compared over the HEIFE area with that derived from the RS approach.

The results clearly show that *the Tile approach and the Blending height approach using satellite measurements in combination with SL observations and ABL observations provided much better estimates of heat flux densities than the RS approach.*

Key words: satellite remote sensing, surface layer observations, atmospheric boundary layer observations, land surface variables, vegetation variables, land surface heat fluxes, validation, heterogeneous landscape, GAME/Tibet, CAMP/Tibet, HEIFE, AECMP'95, DHEX, NOAA/AVHRR, Landsat-5(7) TM(ETM)

Preface

The idea for this research was formed after the HEIhe basin Field Experiment (HEIFE) project in the summer of 1995 when I met my promotor Prof. Dr. Massimo Menenti during the field experiment of the Arid Environment Comprehensive Monitoring Plan, 95 (AECMP'95), and it was strengthened during my first visit at SC-DLO undertaking a cooperative project between the Chinese Academy of Sciences (CAS) and the Netherlands Royal Academy of Sciences (KNAW) and the Intensive Observational Period (IOP) of the Global Energy and Water cycle EXperiment (GEWEX) Asian Monsoon Experiment on the Tibetan Plateau (GAME/Tibet), the Coordinated Enhanced Observing Period (CEOP) Asia-Australia Monsoon Project on the Tibetan Plateau (CAMP/Tibet) and the DunHuang EXperiment (DHEX).

My special appreciation goes to my promotor Prof. Dr. Massimo Menenti. I have been impressed by his tremendous ideas over a wide range of research projects and by his solid physics back ground. And he let me know what is remote sensing and how to do the research on satellite remote sensing. I thank him for spending time and patience in explaining theories, discussing the meeting problems and suggesting on the contracture of thesis. I am grateful to my promotor Prof. Dr. Reinder Feddes of Wageningen University for constructive criticism and encouragement in this thesis. His scientific and moral support was indispensable for the successful completion of this thesis. His interest in my research has been a constant source of inspiration. Without his critical comments and detailed discussions, there could have been no guarantee of the academic quality of this dissertation.

My deep thanks go to my Co-promotor Prof. Jiemin Wang of Cold and Arid Regions Environmental and Engineering Research Institute (CAREERI), the Chinese Academy of Sciences (CAS). My research career started working with him in 1987 and he convinced me to take scientific research as my profession. His scientific and moral support was indispensable for the successful completion of this thesis. His critical comments and suggestions on the manuscripts of all the chapters of this thesis have been extremely valuable to me.

My special thanks to Prof. Dr. Zhongbo Su (International Institute for Geo-Information Science and Earth Observation-ITC). Discussions with him have greatly contributed to this study. His wide interest in various scientific issues impressed me. I also thank him for the

offer of facilities when I was visit Alterra Green World Research, WUR and ITC.

I wish to express my sincere thanks to Profs. Tandong Yao (Institute of Tibetan Plateau Research, CAS), Shihua Lu (CAREERI, CAS), W. G. M. Bastiaanssen (Water Watch), Hirohiko Ishikawa (Kyoto University), Toshio Koike (University of Tokyo), Ronghui Huang (Institute of Atmospheric Physics, CAS), Zhaoliang Li (Universite Louis Pasteur – Strasbourg), Tetsuzo Yasunari (Nagoya University), Toshihiko Maitani (Okayama University), Eiji Ohtaki (Okayama University), Osamo Tsukamoto (Okayama University), Ichiro Tamagawa (Gifu University) and Kenji Nakamura (Nagoya University) for many very useful discussions, good suggestions and supports during the field experiments of the HEIFE, the GAME/Tibet, the CAMP/Tibet, the AECMP'95, the DHEX and the data analysis. I can finish this thesis due to their very kindly help and encouragement.

I am indebted to Dr. Li Jia (Alterra Green World Research, Wageningen UR). When I come to Wageningen again, she gives me many helps in the thesis, even living help. And we have also depth discussion on the structure and the contents of this thesis.

Many thanks to Ir. Gerbert Roerink (Alterra Green World Research, Wageningen UR), Dr. Henk Pelgrum(Water Watch), Prof. Jun Wen, Prof. Zeyong Hu, Prof. Feng Gao (CAREERI,CAS), Prof. Zhiqiu Gao, Dr. Yuping Yan (Chinese Meteorological Administration Bureau) and my students (Mr. Weiqiang Ma, Mr. Maoshan Li, Mr Lei Zhong, Mr. Hui Tian, Mr. Fanglin Sun, Mr. Yongjie Wang, Miss Xiao Hu, Ms. Minhong Song, Mr. Yizhou Zhao, Miss Yaqiong Lu, and Mr. Zhikun Zhu) for their deeply discussion and very kindly help in the field experiments, the field data analysis and satellite data processing.

I am also express my very deeply thanks to all the participants, who came from China, Japan and Korea, in the field experiments of the HEIFE, the GAME/Tibet, the CAMP/Tibet, the AECMP'95 and the DHEX for their very hard work in the field.

I acknowledge all the peoples in the Satellite Earth Observation Group of Alterra Green World Research, Wageningen UR, the peoples in the Disaster Prevention Research Institute, Kyoto University and the peoples in the International Institute for Geo-Information Science and Earth Observation. During my staying in these universities and institutes I had plenty of time to lay down the structure of the thesis.

Finally, special thanks to my wife Rong Han for her fully understandings and supports on my field work and research work for more than fifteen years. Her hard work in my family led to this thesis finishing smoothly. Deep thanks to my mother Huizhen Cao, who is the most patient mother in the world. She asked me do my best for my research and this thesis even she cannot see this thesis now. Thanks also to my father Jucai Ma, my mother in law Yuzhen Liu, my father in law Demeng Han, my elder brother Wei Han for their

understanding and moral support. Surely, many thanks give my daughter Yuan Ma for her understanding in my work. And I have to say that “sorry, YuanYuan and Rong, I have too many works to do in the field and my office and I miss you too long time!”

Yaoming Ma (马耀明)

September 2006

Wageningen, The Netherlands

Content

Abstract	i
Preface	iii
Abbreviations and acronyms	xi
List of frequently used symbols	xiii
1 Introduction	1
1.1 Background	1
1.2 Objectives	4
1.3 Outline of the thesis	5
2 Theoretical framework of parameterization of heat exchanges at the land surface	7
2.1 Net radiation flux $R_n(x,y)$	8
2.2 Soil heat flux $G_0(x,y)$	14
2.3 Sensible heat flux $H(x,y)$	16
2.4 Latent heat flux $\lambda E(x,y)$	24
2.5 Summary and conclusions	24
3 Parameterizations of heat fluxes at heterogeneous surfaces using surface and atmospheric boundary layer observations	27
3.1 Introduction	27
3.2 Heterogeneous land surface and the length scales of heterogeneity	28
3.3 Characteristics of the atmospheric boundary layer over a heterogeneous landscape	30
3.3.1 General characteristics of the atmospheric boundary layer	31
3.3.2 A slab model for the diurnal behaviour of the atmospheric boundary layer	32
3.3.3 Time scales of the atmospheric boundary layer	33
3.3.4 Air flow over a heterogeneous land surface	35
3.4 Blending height assumption	37
3.5 Generic constraints over heterogeneous land surfaces	40
3.6 Parameterization of land-atmospheric interactions using satellite measurements in combination with surface layer and atmospheric boundary layer observations	42

3.7	Summary and conclusions	48
4	Descriptions of land surface processes experiments and satellite data	51
4.1	Global Energy and Water cycle EXperiment Asian Monsoon Experiment on the Tibetan Plateau (GAME/Tibet) and Coordinated Enhanced Observing Period Asia-Australia Monsoon Project on the Tibetan Plateau (CAMP/Tibet)	51
4.1.1	The GAME/Tibet experiment	52
4.1.2	The CAMP/Tibet experiment	52
4.2	HEIhe basin Field Experiment (HEIFE)	60
4.3	Arid Experiment Comprehensive Monitor Plan, 95 (AECMP'95)	64
4.4	DunHuang Experiment (DHEX)	66
4.5	Landsat-5(7) TM(ETM) data and NOAA/AVHRR data	68
4.6	Summary and conclusions	69
5	Application of the parameterization scheme using satellite measurements and surface layer assumptions: the HEIFE case	71
5.1	Introduction	71
5.2	Methodology	72
5.2.1	Land surface variables	72
5.2.2	Net radiation flux R_n and soil heat flux G_0	78
5.2.3	Sensible heat flux H	79
5.2.4	Latent heat flux λE	80
5.3	Analysis of the results	80
5.4	Summary and conclusions	87
6	Analysis of momentum and heat fluxes at the surface using local surface layer and atmospheric boundary layer observations	89
6.1	Introduction	89
6.2	Land surface heterogeneity and its influences on the overlying surface layer and atmospheric boundary layer	90
6.2.1	Diurnal variations of surface reflectance, surface temperature and surface heat fluxes over heterogeneous land surfaces	90
6.2.2	Influences of surface heterogeneity on the overlying convective atmospheric boundary layer	93
6.2.3	Vertical variation of surface heat fluxes	98

6.3	Aerodynamic and thermodynamic parameters over the different land surfaces	99
6.3.1	Aerodynamic roughness length z_{0m}	99
6.3.2	Thermodynamic roughness length z_{0h}	103
6.3.3	Excess resistance to heat transfer kB^{-1}	105
6.4	Summary and conclusions	111
7	Estimation of regional surface heat fluxes using satellite measurements in combination with surface layer and atmospheric boundary layer observations	113
7.1	Introduction	113
7.2	Implementation of the Tile approach and the Blending height approach	114
7.2.1	Tile approach	114
7.2.2	Blending height approach	117
7.2.3	Comparison between the RS approach, the Tile approach and the Blending height approach	122
7.3	Experimental case studies	123
7.3.1	HEIFE	125
7.3.2	AECMP'95	129
7.3.3	DHEX	131
7.3.4	CAMP/Tibet	133
7.3.5	GAME/Tibet	136
7.4	Summary and conclusions	141
	Summary and conclusions	145
	Samenvatting en conclusies	151
	References	157
	List of peer-reviewed publications by the candidate during the PhD study period	177
	First-author publications	
	Co-author publications	
	Curriculum vitae	181

Abbreviations and acronyms

ABL	Atmospheric Boundary Layer
AECMP'95	Arid Experiment Comprehensive Monitor Plan, 95
AVHRR	Advanced Very High Resolution Radiometer
AWS	Automatic Weather Station
BJ	BuJiao
BL	Balance Layer
BST	Beijing Standard Time
CABL	Convective Atmospheric Boundary Layer
CAREERI	Cold and Arid Regions Environmental and Engineering Research Institute
CAS	Chinese Academy of Sciences
CAMP	CEOP Asia-Australia Monsoon Project
CAMP/Tibet	CEOP Asia-Australia Monsoon Project on the Tibetan Plateau
CE	Combination Equation
CEOP	Coordinated Enhanced Observing Period
DHEX	DunHuang EXperiment
DN	Digital Number
EFEDA	Echival First field Experiment in Desertification threatened Area
ETM	Enhanced Thematic Mapper
FIFE	First ISLSCP Field Experiment
GAME	GEWEX Asian Monsoon Experiment
GAME/Tibet	GEWEX Asian Monsoon Experiment on the Tibetan Plateau
GEWEX	Global Energy and Water cycle EXperiment
GMT	Greenwich Mean Time
HAPEX	Hydrological and Atmospheric Pilot EXperiments
HEIFE	HEIhe basin Field Experiment
IAHS	International Association of Hydrological Sciences
IBL	Internal Boundary Layer
IOP	Intensive Observational Period
ISLSCP	International Satellite Land Surface Climatologic Project
ITC	International Institute for Geo-Information Science and Earth Observation
ITP	Institute of Tibetan Plateau Research

LIPAP	Lanzhou Institute of Plateau Atmospheric Physics
LOWTRAN	LOW resolution atmospheric TRANsmission model
LSPE	Land Surface Processes Experiment
LST	Land Surface Temperature
LT	Local Time
MODTRAN	MODerate spectral resolution atmospheric TRANsmittance algorithm
MOS	Monin-Obukhov Similarity theory
NIR	Near-InfraRed
NOAA	National Oceanic and Atmospheric Administration
NPAM	North Portable Automated Meso-net station
NSFC	National Natural Science Foundation of China
PAM	Portable Automated Meso-net
PBL	Planetary Boundary Layer
RASS	Radio Acoustic Sounding System
SEB	Surface Energy Balance
SEBAL	Surface Energy Balance Algorithm for Land
SEBI	Surface Energy Balance Index
SEBS	Surface Energy Balance System
SL	Surface Layer
SPAM	South Portable Automated Meso-net station
SWT	Split-Window Technique
SVAT	Soil Vegetation Atmosphere Transfer
TIR	Thermal-InfraRed
TM	Thematic Mapper
TOA	TOp of Atmosphere
VIS	VISible
UTM	Universal Transfer Mercator
WCRP	World Climate Research Progrmme

List of frequently used symbols

Symbol	Interpretation	Unit
B_λ	Black emitted radiance	W m^{-2}
C_D	Drag coefficient	-
C_{DN}	Drag coefficient in the neutral state	-
C_H	Bulk transfer coefficient of sensible heat	-
C_{HN}	Bulk transfer coefficient of sensible heat in neutral state	-
C_E	Bulk transfer coefficient of latent heat	-
C_{EN}	Bulk transfer coefficient of latent heat in the neutral state	-
c_p	Air specific heat at constant pressure	$\text{J kg}^{-1} \text{K}^{-1}$
c_s	Soil specific heat	$\text{J kg}^{-1} \text{K}^{-1}$
d_0	Zero-plane displacement	m
E	Evaporation flux	$\text{kg m}^{-2} \text{s}^{-1}$
e_a	Water vapor pressure	Pa
e_{a-b}	Air vapour pressure at the blending height	Pa
f_A	Air-to-surface flux of available energy	W m^{-2}
F_C	Scalar flux at the surface	W m^{-2}
f_C	Sum of turbulent and molecular flux density vectors	W m^{-2}
f_E	Latent heat flux	W m^{-2}
f_H	Sensible heat flux	W m^{-2}
g	Acceleration due to gravity	m s^{-2}
G_0	Soil heat flux	W m^{-2}
h_v	Vegetation height	m
h_{ABL}	Height of the atmospheric boundary layer	m
h_{CBL}	Height of the convective atmospheric boundary layer	m
H	Sensible heat flux	W m^{-2}
k	Von Karman constant	-
kB^{-1}	Excess resistance to heat transfer	-
K^*	Net short-wave radiation flux	W m^{-2}
K_\downarrow	Incoming short wave radiation flux	W m^{-2}
$K_{\text{exo}}^\downarrow(b)$	Mean in-band solar exo-atmospheric irradiance flux	W m^{-2}
$K_{\text{TOA}}^\downarrow$	Radiation flux perpendicular to the Top Of Atmosphere	W m^{-2}
K_\uparrow	Outgoing short wave radiation flux	W m^{-2}
L_\downarrow	Incoming Long wave radiation flux	W m^{-2}

Symbol	Interpretation	Unit
L_{\uparrow}	Outgoing Long wave radiation flux	W m^{-2}
L_0	Emitted band radiance flux from the land surface	W m^{-2}
LAI	Leaf Area Index	$\text{m}^2 \text{m}^{-2}$
$MSAVI$	Modified Soil Adjusted Vegetation Index	-
$NDVI$	Normalized Difference Vegetation Index	-
$NDVI_{\max}$	Maximum $NDVI$	-
$NDVI_{\min}$	Minimum $NDVI$	-
$NDVI_s$	$NDVI$ values for bare soil	-
$NDVI_v$	$NDVI$ values for full vegetation	-
p	Pressure	Pa
q	Specific humidity	kg kg^{-1}
q^*	Characteristic humidity,	kg kg^{-1}
q_0	Specific humidity at the land surface	kg kg^{-1}
q_z	Specific humidity at reference height z	kg kg^{-1}
q_{z1}	Specific humidity at height z_1	kg kg^{-1}
q_{z2}	Specific humidity at height z_2	kg kg^{-1}
Q_m	Mean specific humidity	kg kg^{-1}
r_0	Surface reflectance (surface albedo)	-
r_a	Aerodynamic resistance	s m^{-1}
r_{a-b}	Aerodynamic resistance at the blending height	s m^{-1}
r_{ac-b}	Aerodynamic resistance for vapor transfer between land surface and the blending height	s m^{-1}
r_{ah-b}	Aerodynamic resistance for heat between land surface and the blending height	s m^{-1}
r_{sh}	Soil heat transportation resistance	s m^{-1}
R_n	Net radiation flux	W m^{-2}
t	Time	s
t_d	Dynamical time scale	s
t^*	Mixing time-scale	s
t_e	Entrainment time scale	s
T	Temperature	K
T_0	Surface temperature	K
T_a	Air temperature	K
T_{air-b}	Air temperature at the blending height	K

Symbol	Interpretation	Unit
T^B	Brightness temperature	K
T^*	Characteristic temperature	K
T_r	Reference absolute temperature	K
T_{rad}	Radiation surface temperature	K
T_z	Air temperature at the reference height z	K
T_{z1}	Air temperature at the height z_1	K
T_{z2}	Air temperature at the height z_2	K
u	Horizontal component of wind speed	m s^{-1}
$u(x,z)$	Time-mean velocity	m s^{-1}
u_*	Friction velocity	m s^{-1}
u_{*b}	Friction velocity at blending height	m s^{-1}
u_b	Wind speed at blending height	m s^{-1}
u_z	Wind speed at the reference height z	m s^{-1}
U	Averaged wind speed	m s^{-1}
\mathbf{U}	Mean velocity vector	m s^{-1}
U_m	Mean wind speed in the well-mixed bulk of the CABL	m s^{-1}
U_b	Background advection velocity	m s^{-1}
$\overline{U_b}$	Mean velocity scale for the equilibrated layer	m s^{-1}
$\overline{U_*}$	Background friction velocity	m s^{-1}
w	Mean vertical velocity	m s^{-1}
w	Vertical wind velocity	m s^{-1}
w_*	Convective velocity scale	m s^{-1}
W	Water vapor content	g m^{-3}
X	Patch length scale	m
z	Reference height	m
z_{0h}	Thermodynamic roughness length	m
z_{0m}	Aerodynamic roughness length	m
Z_{0m}	Effective aerodynamic roughness length	m
z_b	Blending height	m
z_i	Convective inversion height	m
θ	View angle of satellite	degree
θ	Radiation incident zenith angle	degree
θ_{sun}	Sun zenith angle	degree
Θ	Potential air temperature	K

Symbol	Interpretation	Unit
θ_b	Potential temperature at the blending height	K
Θ_m	Mean potential air temperature	K
θ_v	Vertical potential temperature	K
λ	Wave length	μm
λE	Latent heat flux	W m^{-2}
ρ	Air density	kg m^{-3}
ρ_s	Soil bulk density	kg m^{-3}
$\rho_s c_s$	Volumetric soil heat capacity	$\text{J m}^{-3} \text{K}^{-1}$
ρc_p	Volumetric air heat capacity	$\text{J m}^{-3} \text{K}^{-1}$
σ	Stefan Boltzmann constant	$\text{W m}^{-2} \text{K}^{-4}$
τ	Band average transmittance	-
τ_{sw}	Atmospheric short-wave transmittance	-
τ_λ	Spectral atmospheric transmittance	-
ϕ_m	Monin-Obkuhov function for atmospheric momentum transport	-
ϕ_h	Monin-Obkuhov function for atmospheric heat transport	-
ψ_h	Stability correction for atmospheric heat transport	-
$\psi_{\text{h-b}}$	Stability correction for atmospheric heat transport at the blending height	-
ψ_m	Stability correction for atmospheric heat transport	-
$\psi_{\text{m-b}}$	Stability correction for atmospheric heat transport at the blending height	-
ε_0	Surface emissivity	-
ε_a	Effective atmospheric emissivity	-
ε_v	Surface emissivity for full vegetation	-
ε_g	Surface emissivity for bare soil	-
ζ	Stability parameter	-
$\omega(x)$	Solar angle hour	rad

1. Introduction

1.1 Background

The growing concern about the change of climate and environment has increased the number of land surface processes studies over heterogeneous areas (Table 1.1).

The regional heat flux exchange between the land surface and atmosphere is of paramount importance for the land surface processes. It is also the main objective in a number of the land surface process experiments. *How can one determine the regional distribution of surface heat fluxes on a quantitative level over heterogeneous landscapes?*

One approach is to operate an atmospheric model. Numerical simulation models of regional heat fluxes have been developed for a range of scales and with different levels of physical complexity (e.g. Manabe, 1969; Feddes et al., 1978; Anthes, 1983; Anthes et al., 1987; Dickinson et al., 1986; Sellers et al., 1986; Avissar and Pielke, 1989; Entekhabi and Eagleson, 1989; Avissar, 1991; Famiglietti and Wood, 1991; Koster and Suarez, 1992; Sellers and Pitman, 1992; Xue and Shukla, 1993; Kroon and De Bruin, 1993; Walko et al., 1995; Pielke et al., 1995; Sellers et al., 1995; Holtslag and EK, 1996; Van den Hurk et al., 1997; Yan, 1999; Xue et al., 2001; Strack et al., 2003; Hu, 2004).

Because the interactions between soil, vegetation and atmosphere vary both spatially and temporally, regional heat fluxes in heterogeneous natural landscapes are difficult to predict accurately by means of atmospheric models only. Most atmospheric models deal with terrestrial landscapes by assuming homogeneity of system variables and processes within each model grid. The so-called tile approach (Avissar and Pielke, 1989) has been proposed to build a more realistic description of heterogeneous land surfaces. Recently, sparse but growing evidence has been put forward on the relation between nature and spatial organization of the processes in the Surface Layer (SL) and Atmospheric Boundary Layer (ABL) and spatial heterogeneity of land surfaces (Avissar, personal communication). This trend will lead eventually to a more accurate prediction of heat fluxes at the land – atmosphere interface. *Ground and satellite measurements that characterize the actual spatial variability of terrestrial landscapes will be needed to achieve this objective.*

Remote sensing from satellites offers the possibility to derive regional distribution of land surface heat fluxes over heterogeneous land surfaces in combination with sparse

Table 1.1 Major Land Surface Processes Experiments (LSPE) in the world (1986-2005)

Experiments	Experimental period	Scale (km × km)	Major objectives	References
HAPEX-MOBILHY	1986	100 × 100	Water and energy exchange, regional hydrology	Schmugge and Andre (1991)
FIFE	1988,1990	10 × 10	Water and energy exchange, biometeorology, remote sensing	Sellers and Hall (1992)
HEIFE AECMP'95	1988, 1990-1992, 1994, 1995	70 × 90	Water and energy exchange in arid regions, regional hydrology, biometeorology, remote sensing	Wang et al. (1993), Hu et al. (1994)
EFEDA	1991, 1995	85 × 130	Desertification, biometeorology, remote sensing	Bolle et al. (1993)
HAPEX-Sahel	1992	100 × 100	Biometeorology, remote sensing	Goutorbe et al. (1994)
BOREAS	1993-1994	1000 × 1000	Biometeorology, remote sensing	Hall and Sellers (1993)
GCIIP	1995-2000	2000 × 200	Meteorology and remote sensing	IGBP (1992)
GAME/Tibet and TIPEX, GAME-Siberia, GAME-HUBEX GAME-Tropic	1996-2000	200 × 100 (meso-scale) 2000 × 1300 (plateau area), 100 × 100 for the other three area	Water and energy exchange over the experimental areas, regional hydrology, snow cover, precipitation, biometeorology, remote sensing	GAME ISP (1998)
CEOP (CAMP/Tibet)	2001-2005	36 reference areas (250 × 150)	Water and energy exchange over the experimental areas, regional hydrology, snow cover, precipitation, biometeorology, remote sensing	Koike (2002)
IMGRASS	1997, 1998	100 × 150	Water and energy exchange over the grass land, regional hydrology, precipitation, remote sensing, biometeorology	Lu (1997)
MAGS	1998, 1999	1000 × 1000	Hydrological process, climatic effect	JSC (1994)
AMAZON	1998-2000	3000 × 2000	biometeorology, remote sensing	Sellers et al. (1993)

ground experimental stations. Remote sensing data provided by satellites are a means of obtaining consistent and frequent observations of spectral reflectance and emittance at elements in a patch landscape and on a global scale (Sellers et al., 1990). The land surface variables and vegetation variables, such as surface temperature T_0 , surface hemispherical reflectance r_0 , Normalized Difference Vegetation Index (*NDVI*), Modified Soil Adjusted Vegetation Index (*MSAVI*), vegetation fractional cover P_v , Leaf Area Index (*LAI*) and surface thermal emissivity ε_0 can be derived directly from satellite measurements (e.g. Susskind et al., 1984; Perry and Lautenschlager, 1984; Justice et al., 1985; Tucker, 1987; Pinty and Ramond, 1987; Clevers, 1988; Menenti et al., 1989; Wan and Dozier, 1989; Becker and Li, 1990; Watson et al., 1990; Baret and Gauyot, 1991; Price, 1992; Kahle and Ally, 1992; Li and Becker, 1993; Qi et al., 1994; Norman et al., 1995; Schmugge et al., 1995; Becker and Li, 1995; Kustas and Norman, 1997; Ma et al., 1997; Wen, 1999; Ma et al., 1999; Ma et al., 2002a; Ma et al., 2003a; Liang, 2004; Jia, 2004; Oku and Ishikawa, 2004).

Regional heat fluxes can be determined indirectly with the aid of these land surface variables (Pinker, 1990).

Recent studies have explored several approaches to estimate the regional distribution of surface heat fluxes. These methods bridge the gap between the point/local measurements and the regional scale, and they required specification of the vertical temperature difference between T_0 and the air temperature T_a and an exchange resistance (e.g. Kustas et al., 1989; Kustas, 1990; Menenti et al., 1991; Menenti and Choudhury, 1993; Wang et al., 1995; Bastiaanssen, 1995; Menenti and Bastiaanssen, 1997; Roerink and Menenti 1997; Ma et al., 1997; Su et al., 1998; Su et al., 1999; Ma et al., 1999; Van den Hurk, 2001; Su, 2002; Jia 2004).

Remote sensing methods to estimate heat fluxes at the surface are still in a developing stage, and some shortcomings exist, such as:

- Remote sensing retrieval algorithms did not pay sufficient attention to ABL aspects, in other words, the analysis of the characteristics of structure and transfer of the ABL was not robust, i.e. in the existing methods too many semi-empirical relationships and assumptions on the ABL were embedded, particularly in the procedures to calculate the surface roughness length (aerodynamic roughness length z_{0m} and thermodynamic roughness length z_{0h}), momentum flux (τ) and sensible heat flux (H).
- T_0 , which is usually replaced by the surface radiative temperatures T_{rad} and the near surface T_a is not determined by a robust approach.

- Most studies of the regional distribution of land surface heat fluxes have been performed in homogeneous moist or semi-arid regions. Investigations in heterogeneous landscapes of arid areas and high altitudes were rare.

1.2 Objectives

In this thesis a general conceptual framework is described to achieve the following ultimate objective: *Providing a better satellite remote sensing parameterization methodology of regional land surface heat fluxes over heterogeneous landscapes by including SL and ABL observations.*

This study will pay more attention to the following.

- Deriving a more accurate regional distribution of the land surface variables and vegetation variables over heterogeneous landscapes.
- Deriving a more accurate regional distribution of the net radiation flux R_n and the soil heat flux G_0 over heterogeneous landscapes.
- Limiting assumptions in the existing remote sensing retrieval methodology to estimate H :
 - To derive the structure characteristics of the Surface Layer (SL) and ABL with the available SL and ABL observational data (tethered balloon, radio-sonde, the PBL tower etc.).
 - To determine aerodynamic and thermodynamic variables (aerodynamic roughness z_{0m} , thermodynamic roughness z_{0h} and excess resistance to heat transfer kB^{-1}) by means of SL observations and remote sensing measurements at high spatial resolution over heterogeneous land surfaces.
 - To derive the regional distribution of T_0 at a high spatial resolution from the remote sensing surface brightness temperature T^B .
 - To derive the regional distribution of T_a at high spatial resolution from the distribution of T_0 and ground observations using a simple numerical interpolation model.
- Assimilating the previous improvements into the remote sensing parameterization methodology to estimate the regional distribution of H and its temporal variation over heterogeneous landscapes.
- Validating the improvement remote sensing parameterization methodology by using the surface, SL and ABL observations.

1.3 Outline of the thesis

The theoretical framework of parameterization of heat exchanges at the land surface will be described in Chapter 2. The procedure to determine the four components of the surface energy budget will be given in detail in this chapter.

In Chapter 3, three parameterization schemes will be proposed to determine the heat fluxes over heterogeneous surfaces. *The first* is to use satellite measurements and assumptions on the surface layer to estimate the regional land surface heat fluxes, which is called *RS approach* (RS+SL-assumptions). *The second* is to use satellite measurements and surface layer observations, which called *Tile approach* (RS+SL-observations). *The third* is to use satellite measurements and ABL observations, which named *Blending height approach* (RS+SL-observations+ABL-observations). Because both the surface heterogeneity and the SL and ABL characteristics are very important in the parameterization procedures, they will also be analyzed in detail in this chapter.

In Chapter 4, land surface processes experiments of the Global Energy and Water cycle EXperiment (GEWEX) Asian Monsoon Experiment on the Tibetan Plateau (GAME/Tibet, 1996-2000), the Coordinated Enhanced Observing Period (CEOP) Asia-Australia Monsoon Project on the Tibetan Plateau (CAMP/Tibet, 2001-2005), the HEIhe basin Field Experiment (HEIFE, 1988-1993), the Arid Environment Comprehensive Monitoring Plan, 95 (AECMP'95, 1 August–21 August 1995) and the DunHuang EXperiment (DHEX, 1 May 2000–31 August 2002), with ground observational data, will be described.

In Chapter 5, regional land surface heat fluxes over heterogeneous landscapes will be determined using the *RS approach*. It will be shown that the derived land surface heat fluxes over some areas determined in this way may not be accurate. In other words, the parameterization method has to be improved. Also the input land surface and atmospheric variables have to be determined over heterogeneous landscapes by using the SL and ABL observations and not from assumptions.

Therefore, in Chapter 6, the SL and ABL processes will be analyzed in detail. Surface heterogeneity, the influences of the surface heterogeneity on the variables of the SL and ABL (wind speed u , T_a and specific humidity q) and land surface heat fluxes (the different

heat fluxes over the different land surface and in the different month) and some of the atmospheric variables (z_{0m} , z_{0h} and kB^{-1}) will be analyzed and determined.

In Chapter 7, the *Tile approach* (RS + SL-observations) and the *Blending height approach* (RS + SL-observations + ABL-observations) will be used to derive land surface heat fluxes over heterogeneous landscapes. They will be applied to the areas of the GAME/Tibet, the CAMP/Tibet, the HEIFE, the AECMP'95 and the DHEX. The distributions of *NDVI*, *MSAVI*, vegetation fractional cover P_v , LAI , r_0 , T_0 , R_n , G_0 , H and the latent heat flux λE will be determined over these areas. "Ground truth" will be used to validate the derived results. A comparison between the results derived from the *Blending height approach* and the results derived from the *RS approach* over the HEIFE area will also be given in this chapter.

Finally, a summary and conclusions will be given.

2. Theoretical framework of parameterization of heat exchanges at the land surface

The exchange processes occurring at the land surface are of paramount importance for the re-distribution of moisture and heat in soil and atmosphere. In any given system at the earth's surface, evapotranspiration is the connecting link between the water budget and the energy budget. For a simple lumped system, when effects of unsteadiness, ice melt, photosynthesis and lateral advection can be neglected, the energy budget is (Brutsaert, 1984):

$$R_n = H + \lambda E + G_0 \quad (\text{W m}^{-2}) \quad (2.1)$$

where R_n is the net radiation flux at the land surface, H and λE are the sensible and latent land surface heat fluxes respectively, and G_0 is the soil heat flux (Figure 2.1). The sign convention of Eq.2.1 is that R_n is considered positive when radiation is directed towards the land surface, while G_0 , H and λE are considered positive when directed away from the land surface (Bastiaanssen, 1995).

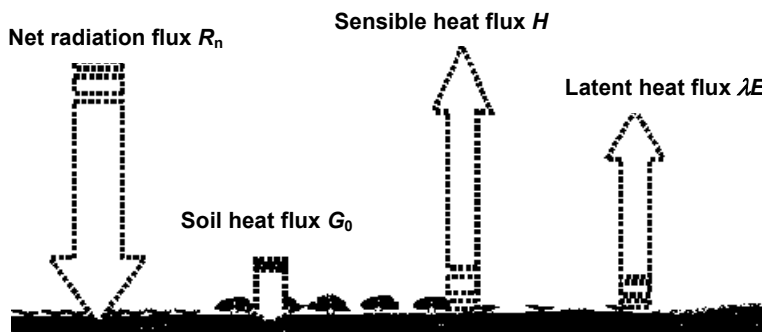


Figure 2.1 Schematic illustration of the energy balance at the land surface.

For the regional land surface heat fluxes, the energy balance equation can be rewritten as (e.g. Bastiaanssen, 1995; Wang et al., 1995; Ma et al., 2002a; Ma et al., 2003a; Ma et al., 2003b; Ma et al., 2004a; Ma et al., 2006):

$$R_n(x, y) = H(x, y) + \lambda E(x, y) + G_0(x, y) \quad (\text{W m}^{-2}) \quad (2.2)$$

The (x,y) notation indicates that a certain parameter is variable in the horizontal space domain with a resolution equal to the size of a pixel of a satellite image.

2.1 Net radiation flux $R_n(x, y)$

The regional net radiation flux $R_n(x, y)$ can be derived from

$$\begin{aligned} R_n(x, y) &= K_{\downarrow}(x, y) - K_{\uparrow}(x, y) + L_{\downarrow}(x, y) - L_{\uparrow}(x, y) & (\text{Wm}^{-2}) & (2.3) \\ &= (1 - r_0(x, y)) \bullet K_{\downarrow}(x, y) + L_{\downarrow}(x, y) - \varepsilon_0(x, y) \sigma T_0^4(x, y) \end{aligned}$$

where $K_{\downarrow}(x,y)$ and $K_{\uparrow}(x,y)$ are the incoming and outgoing solar radiation flux respectively, $L_{\downarrow}(x,y)$ and $L_{\uparrow}(x,y)$ are the incoming and outgoing long wave radiation flux respectively. $r_0(x,y)$ is the surface reflectance, $T_0(x,y)$ is the surface temperature and σ ($=5.678 \times 10^{-8} \text{ W m}^{-2} \text{ K}^{-4}$) is the Stefan-Boltzman's constant.

In Eq.2.3, $r_0(x,y)$ can be derived from a linear relationship between the surface reflectance r_0 and the spectrally integrated planetary reflectance r_p (e.g. Menenti, 1984; Wang et al., 1995; Bastiaanssen, 1995; Ma et al., 1997; Ma et al., 1999) as

$$r_0(x, y) = a r_p(x, y) + b \quad (-) \quad (2.4)$$

where parameters a and b can be determined from the ground observations.

To avoid the shortcoming of using the linear relationships to estimate r_0 from r_p (e.g. Wen, 1999), a four-stream radiative transfer assumption (e.g. Verhoef, 1997; Wen, 1999; Ma et al., 2002c; Ma, 2003c) is used to determine $r_0(x,y)$. The assumption is based on the radiative transfer among the satellite sensor, atmosphere layer and the land surface. By using the MODerate spectral resolution atmospheric TRANsmittance algorithm (MODTRAN) model, the surface narrow band reflectance can be derived, and the broadband reflectance of the land surface can be calculated as a weighted sum formula from the different band reflectance.

The determination of r_0 from satellite remote sensing data is affected by the atmospheric effects in the radiative transfer path (Verhoef, 1997). A schematic diagram (Figure 2.2) provides an illustration of radiative transfer process (Wen, 1999). The radiance which reaches the satellite remote sensor consists of four contributions:

- 1) Direct sunlight reflected by the target.

- 2) Target reflected diffuse radiance.
- 3) Molecular and aerosol particles back-scattered sunlight.
- 4) A contribution from “background” outside the target.

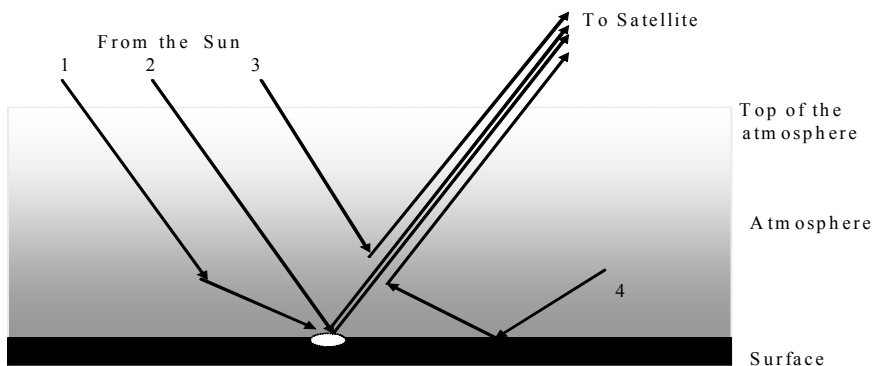


Figure 2.2 The diagram of the radiative transfer process between the sun, atmosphere, land surface and satellite sensor in solar spectra.

Based on Figure 2.2, the broadband surface reflectance has been calculated from a weighted sum of the band reflectance as (Wen, 1999):

$$r_s^b = \sum_{i=1}^{7(i \neq 6)} a(i) r_s^i \quad (-) \quad (2.5)$$

where i is band number of the sensor, $a(i)$ is the weight of each band at surface, r_s^b is the broadband surface reflectance, r_s^i is the band reflectance. Hence, the distribution of land surface reflectance can be derived as

$$r_s^b(x, y) = \sum_{i=1}^{7(i \neq 6)} a(i) r_s^i(x, y) \quad (-) \quad (2.6)$$

Using the NOAA/AVHRR data, surface reflectance can be determined from linear relationships (Valiente et al., 1995) as:

$$r_{\text{broadband}}(x, y) = ar_{\text{AVHRR-1}}(x, y) + br_{\text{AVHRR-2}}(x, y) + c \quad (-) \quad (2.7)$$

where a , b and c are constant depending on different experimental areas, $r_{\text{broadband}}$ is the surface reflectance, $r_{\text{AVHRR-1}}$ and $r_{\text{AVHRR-2}}$ are the band reflectance of AVHRR channel-1 and channel-2, respectively

In Eq. 2.3, regional distribution of surface temperature $T_0(x, y)$ can be derived in different ways depending on the different satellite data. Using the NOAA/AVHRR data, $T_0(x, y)$ can be derived from Split Window Technique (SWT) (e.g. Becker and Li, 1990; Becker and Li, 1995; Sobrino et al., 1994; Sobrino and Raissouni, 2000). It means that T_0 can be thought as a simple linear combination of the brightness temperatures T_i and T_j measured at two adjacent thermal infrared channels i and j , i.e.

$$T_0 = A_0 + A_1T_i + A_2T_j \quad (\text{K}) \quad (2.8)$$

where A_0 , A_1 and A_2 are local coefficients which depend on spectral emissivities of surface and on the spectral transmittance of the atmosphere. The accuracy of T_0 retrieval is dependent on the correct choice of the coefficients A_0 , A_1 and A_2 (Becker and Li, 1995). The derived from NOAA AVHRR can be expressed as

$$T_0 = F(T_4, T_5, \varepsilon_4, \varepsilon_5, W, \theta) \quad (\text{K}) \quad (2.9)$$

where T_4 and T_5 are the brightness temperatures of channel 4 and 5 of AVHRR; ε_4 and ε_5 are the spectral emissivities of channel 4 and 5 respectively; W is water vapor content, and θ represents the view angle of satellite.

$T_0(x, y)$ in Eq.2.3 can also be derived from Landsat TM thermal infrared band-6 (10.2-12.5 μm) spectral radiance. Because the 10.2-12.5 μm TM band is relatively transparent to radiation transfer in the atmospheric layer under the cloud-free sky, the absorption in this band is relatively small except under the turbid weather condition, the main substance of continuous absorption are water vapor and aerosol. The upward thermal

radiance at wavelength λ passing through the local atmosphere layer L_λ is described by (Ma et al., 2002a)

$$\chi \frac{dL_\lambda}{d\delta} = L_\lambda - B_\lambda \quad (\text{Wm}^{-2}) \quad (2.10)$$

where δ is atmospheric optical thickness, $\chi = \cos\theta$, θ is the zenith angle between normal of the horizon and radiative stream, and B_λ is black body radiance as given by Planck function

$$B_\lambda(T_0) = \frac{c_1}{\pi\lambda^5 \left[\exp\left(\frac{c_2}{\lambda T_0}\right) - 1 \right]} \quad (\text{Wm}^{-2}) \quad (2.11)$$

where c_1 and c_2 are constants. Boundary conditions for radiative transfer are:

$$\begin{cases} L_\lambda(\delta_0, \chi) = B_\lambda(T_0) & \delta = \delta_0 \\ L_\lambda(0, \chi) = 0 & \delta = 0 \end{cases} \quad (\text{Wm}^{-2}) \quad (2.12)$$

Then the upward radiance can be derived after integrating Eq.2.17as

$$L_\lambda(\delta, \chi) = L_\lambda(T_0) e^{-\frac{\delta - \delta_0}{\chi}} + \int_{\delta_0}^{\delta} B_\lambda[T(\delta')] e^{-\frac{\delta' - \delta}{\chi}} d\delta' \quad (\text{Wm}^{-2}) \quad (2.13)$$

where $L_\lambda(T_0)$ is upward radiance emitted from land surface, δ' is atmospheric optical thickness at an arbitrary altitude. The satellite sensor detected radiance $L_S(x, y)$ for each pixel is composed of two parts: contributions from land surface and the atmosphere

$$L_S(x, y) = \tau L_0(x, y) + S(x, y) \quad (\text{Wm}^{-2}) \quad (2.14)$$

where $L_0(x, y)$ is emitted band radiance from the land surface, $S(x, y)$ is band upward radiance at the top of atmosphere emitted from the atmosphere, and τ is band average transmittance. $S(x, y)$ and τ can be derived from the MODTRAN model. Eq.2.14 can be rewritten as

$$L_0(x, y) = [L_S(x, y) - S(x, y)] / \tau \quad (\text{Wm}^{-2}) \quad (2.15)$$

Hence, the brightness temperature for each pixel at the land surface $T^B(x, y)$ can be expressed from Eq.2.15 for a given wavelength or remote sensor band as (e.g. Wang et al., 1995; Ma, et al., 1997; Ma et al., 1999)

$$T^B(x, y) = \frac{c_2}{\ln\left(\frac{c_1}{L_0(x, y)} - 1\right)} \quad (\text{K}) \quad (2.16)$$

where c_1 and c_2 are constants. Therefore, the distribution of T_0 can be obtained as:

$$T_0(x, y) = \varepsilon_0(x, y)^{\frac{1}{4}} T^B(x, y) \quad (\text{K}) \quad (2.17)$$

where surface emissivity $\varepsilon_0(x, y)$ can be determined from *NDVI* (e.g. Van de Griend and Owe, 1993; Bastiaanssen, 1995) and vegetation fractional cover (e.g. Sobrino et al., 1990; Valor and Caselles, 1996). i.e.

$$\varepsilon_0(x, y) = 1.009 + 0.047 \ln \text{NDVI}(x, y) \quad (-) \quad (2.18)$$

or

$$\varepsilon_0(x, y) = \varepsilon_v(x, y)P_v(x, y) + \varepsilon_g(x, y)(1 - P_v(x, y)) + 4 < d\varepsilon > (1 - P_v(x, y))P_v(x, y) \quad (-) \quad (2.19)$$

where $\varepsilon_v(x, y) = 0.985(\pm 0.007)$ and $\varepsilon_g(x, y) = 0.960(\pm 0.010)$ are surface emissivity for full vegetation and bare soil respectively, $< d\varepsilon > = 0.015(\pm 0.008)$ is the error, and vegetation fractional cover (Carlson and Ripley, 1997)

$$P_v(x, y) = \left[\frac{\text{NDVI}(x, y) - \text{NDVI}_{\min}}{\text{NDVI}_{\max} - \text{NDVI}_{\min}} \right]^2 \quad (-) \quad (2.20)$$

where NDVI_{\min} and NDVI_{\max} are the *NDVI* values for bare soil and full vegetation respectively. Normalized Difference Vegetation Index (*NDVI*) is:

$$NDVI(x, y) = \frac{r_{NIR}(x, y) - r_{VIS}(x, y)}{r_{NIR}(x, y) + r_{VIS}(x, y)} \quad (-) \quad (2.21)$$

where r_{VIS} and r_{NIR} present surface reflectance averaged over ranges of wavelengths in the visible and near infrared regions of the spectrum, respectively

In Eq.2.3, the regional downward short wave radiation flux $K_{\downarrow}(x, y)$ can be obtained as

$$K_{\downarrow}(x, y) = \tau_{sw} K^{\downarrow}_{TOA}(x, y) \quad (\text{W m}^{-2}) \quad (2.22)$$

where the atmospheric short wave transmittance τ_{sw} can be derived directly from MODTRAN, and the regional variation of the radiation flux perpendicular to the top of atmosphere $K^{\downarrow}_{TOA}(x, y)$ is a spectrally integrated form of in-band radiation flux perpendicular to the top of atmosphere, which can be derived from

$$K^{\downarrow}_{TOA}(x, y) = \frac{K^{\downarrow}_{exo}(b) \cos \theta_{sun}(x, y)}{d_s^2} \quad (\text{W m}^{-2}) \quad (2.23)$$

where $K^{\downarrow}_{exo}(b)$ is the mean in-band solar exo-atmospheric irradiance undisturbed by the atmosphere $\theta_{sun} = 0^0$, d_s is the relative earth-sun distance, and θ_{sun} represents the sun zenith angle.

$L_{\downarrow}(x, y)$ in Eq.2.3 can be calculated from MODTRAN directly (e.g. Ma et al., 2002c; Ma, 2003c), and it can also be estimated as a function of mean air temperature T_a in the atmospheric boundary layer (Jia, 2004)

$$L_{\downarrow}(x, y) = \varepsilon_a \sigma T_a^4 \quad (\text{W m}^{-2}) \quad (2.24)$$

According to Brutsaert (1984), the effective atmospheric emissivity ε_a is a function of water vapor pressure e_a and air temperature T_a

$$\varepsilon_a = 1.72 \left(\frac{e_a}{T_a} \right)^{\frac{1}{7}} \quad (-) \quad (2.25)$$

2.2 Soil heat flux $G_0(x,y)$

The regional soil heat flux $G_0(x,y)$ can be determined by (Choudhury and Monteith, 1988)

$$G_0(x, y) = \rho_s c_s [(T_0(x, y) - T_s(x, y))] / r_{sh}(x, y) \quad (\text{W m}^{-2}) \quad (2.26)$$

where ρ_s is soil dry bulk density, c_s is soil specific heat, $T_s(x,y)$ stands for soil temperature at a determined depth, $r_{sh}(x,y)$ represents soil heat transfer resistance.

$G_0(x, y)$ cannot directly be mapped from satellite measurements through Eq.2.26. The difficulty is to derive $r_{sh}(x,y)$ and $T_s(x,y)$ (e.g. Bastiaanssen, 1995; Wang et al., 1995; Ma et al., 1999; Ma et al., 2002a; Ma et al., 2003a; Ma et al., 2004a; Ma et al., 2006).

To calculate the values of $G_0(x, y)$ solely from remote sensed data requires that it is to be made proportional to another term in the energy balance equation. A good candidate is $R_n(x, y)$, which can be calculated with a minimal amount of meteorological information (Jackson et al., 1985). Indeed, early studies over bare soil (Fuchs and Hadas, 1972; Perrier, 1975; Idso et al., 1975) suggested that for practical applications $G_0(x, y)/R_n(x, y)$ is about 0.3. However, Idso et al. (1975) found the ratio to vary with moisture being about 0.5 for dry soil and 0.3 for wet conditions. Brutsaert (1984) argued that combining all of Idso's data together produced a coefficient 0.4. For vegetation surfaces under full cover, Monteith (1973) suggested values for the ratio would most likely vary between 0.05 and 0.1. Monteith's conclusion was supported by a large quantity of hourly data for a short grass pasture where the daytime average was about 0.1 (De Bruin and Holtslag, 1982).

For application to agriculture, the ratio must be made a function of some easily measured quantity that will allow the value of $G_0(x, y)/R_n(x, y)$ to take intermediate values between around 0.3 at planting and around 0.1 when full cover is reached. Reginato et al. (1985) obtained an empirical equation for wheat where the coefficient was calculated from the height of crop. Choudhury et al. (1987) expressed the ratio as an exponential function of leaf area index yielding a correlation of 0.90.

For regional energy studies, typically very little information on crop height and phytomass is available. However, there are indications that remotely sensed vegetation indices may be a surrogate for plant phytomass, Leaf Area Index (*LAI*) and vegetation fractional cover (Hinzman et al., 1986; Kollenkark et al., 1982a). As a result, G_0/R_n has been related to some vegetation index. For example, Jackson et al. (1987) employed an

equation give by K.L.Clawson (personal communication) that calculates G_0/R_n using an exponential function of $NDVI$. Clothier et al. (1986) show that for alfalfa under full and sparse cover situations the Simple Ratio vegetation index (SR) was linearly related to midday G_0/R_n with a linear regression coefficient $r^2= 0.76$. Kustas and Daughtry (1990) showed that the midday values of G_0/R_n were linearly related to SR and $NDVI$.

Nevertheless, vegetation indices like $NDVI$ and SR are sensitive to solar position (i.e. to the zenith and azimuth view angles) and to the variability in soil reflectance factors. The effects of sun and view angle on the spectral response of vegetation canopies are dependent on the physiological properties of the vegetation such as canopy architecture and leaf angle distribution (Cowan, 1968; Kirchner et al., 1982; Kimes et al., 1985; Sellers, 1985). If it is an arable crop, row spacing, orientation and stage of growth will also affect the spectral behavior of the surface (Jackson et al., 1979; Kollenkark et al., 1982b; Kimes, 1983; Ranson et al., 1985). The view angle of the sensor has as well a significant effect (Ranson et al., 1986; Gutman, 1987; Pinter et al., 1987). The variability in soil reflectance can have a major impact on vegetation indices (Huete et al., 1985; Huete, 1987) which are normally used for the modeling radiation absorption, vegetation fractional cover, biomass, and net photosynthesis of plant communities (Choudhury, 1987).

An improved relationship of $G_0/R_n = \Gamma(r_0, T_0, NDVI)$ was given by Menenti et al. (1991) and Bastiaanssen (1995) as

$$G_0(x, y) = R_n(x, y) \cdot \frac{T_0(x, y)}{r_0(x, y)} \cdot (0.0032\bar{r}_0 + 0.0062\bar{r}_0^2) \cdot [1 - 0.978NDVI(x, y)^4] \quad (\text{W m}^{-2}) \quad (2.27)$$

where \bar{r}_0 is a daily mean reflectance value.

Soil effects are not accounted for the definition of $NDVI$ (Huete et al., 1985; Huete, 1989), parameterization based on Modified Soil Adjusted Vegetation Index ($MSAVI$, Qi et al., 1994) has been proposed over the arid area and high altitude area by Ma et al. (2002a), Ma et al. (2003a), and Ma et al. (2003b) as

$$G_0(x, y) = R_n(x, y) \cdot (T_0(x, y)/r_0(x, y)) \cdot (a + b\bar{r}_0 + c\bar{r}_0^2) \cdot [1 + dMSAVI(x, y)^e] \quad (\text{W m}^{-2}) \quad (2.28)$$

where the parameters a , b , c , d and e were determined by using the field data observed at six observation stations, and $MSAVI$ is:

$$MSAVI = \frac{2r_{NIR} + 1 - \sqrt{[2r_{NIR} + 1]^2 - 8[r_{NIR} - r_{VIS}]}}{2} \quad (-) \quad (2.29)$$

2.3 Sensible heat flux $H(x,y)$

The sensible heat flux H can be estimated with a bulk transfer equation written in the form (Monteith, 1973):

$$H = \rho c_p \frac{T_0 - T_a}{r_a} \quad (\text{W m}^{-2}) \quad (2.30)$$

where r_a is the resistance to heat flow in the boundary above the land surface, T_a is the air temperature at the reference height, ρ is the air density, and c_p is the air specific heat at constant pressure.

Figure 2.3 is a schematic description of the model for sensible heat transfer nearby the land surface. It implies that the regional distribution of H can be rewritten as (e.g. Menenti et al., 1991; Menenti and Choudhury, 1993; Bastiaanssen, 1995; Wang et al., 1995; Ma et al., 1999; Ma et al., 2002a; Ma et al., 2003a; Ma et al., 2004a; Ma et al., 2006)

$$H(x,y) = \rho c_p \frac{T_0(x,y) - T_a(x,y)}{r_a(x,y)} \quad (\text{W m}^{-2}) \quad (2.31)$$

The aerodynamic resistance in Eq.2.31 is

$$r_a(x,y) = \frac{1}{ku_s(x,y)} \left[\ln\left(\frac{z - d_0(x,y)}{z_{0m}(x,y)}\right) + kB^{-1}(x,y) - \psi_h(x,y) \right] \quad (\text{s m}^{-1}) \quad (2.32)$$

and

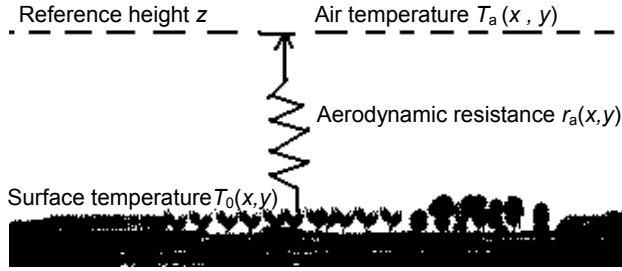


Figure 2.3 Schematic description of the model for sensible heat flux H transfer over a heterogeneous landscape.

$$u_* (x, y) = ku(x, y) \left[\ln \left(\frac{z - d_0(x, y)}{z_{0m}(x, y)} \right) - \psi_m(x, y) \right]^{-1} \quad (\text{m s}^{-1}) \quad (2.33)$$

where k is the Von-Karman constant, u_* is the friction velocity, z is reference height, d_0 is zero-plane displacement height, u is wind speed at the reference height, z_{0m} is the aerodynamic roughness, $kB^{-1} = \ln(z_{0m}/z_{0h})$ (Owen and Thomson, 1963; Chamberlain, 1968) is excess resistance to heat transfer, and ψ_m and ψ_h is the stability correction function.

Combining Eqs.2.31, 2.32 and 2.33 yields:

$$H(x, y) = \rho c_p k^2 u(x, y) \frac{T_0(x, y) - T_a(x, y)}{\left[\ln \frac{z - d_0(x, y)}{z_{0m}(x, y)} + kB^{-1}(x, y) - \psi_h(x, y) \right] \bullet \left[\ln \frac{z - d_0(x, y)}{z_{0m}(x, y)} - \psi_m(x, y) \right]} \quad (\text{W m}^{-2}) \quad (2.34)$$

Therefore, $H(x, y)$ can be determined by Eq.2.34.

Air temperature $T_a(x, y)$

$T_a(x, y)$ in Eq.2.34 is the air temperature at each pixel, which can be derived from the distribution of $T_0(x, y)$ and ground observations by using the linear relationship between $T_a(x, y)$ and $T_0(x, y)$ (e.g. Davies and Tarpley, 1983; Wang et al., 1995; Bastiaanssen, 1995; Ma et al., 1999) In other words, the regional distribution of air temperature can be estimated as:

$$T_a(x, y) = aT_0(x, y) + b \quad (\text{K}) \quad (2.35)$$

where the parameters a and b can be determined using ground observations.

A numerical interpolation method (Ding et al., 1989) to derive the distribution of air temperature from remote sensing surface temperature was used to analyze the “urban heat island effect” (Wu et al., 1993). It is used here to derive $T_a(x,y)$ over heterogeneous landscape when there are observations of T_a and T_0 at the stations (Ma et al., 2002a). T_0 is taken as initial temperature field and it is smoothed using nine points filter (Figure 2.4).

$$T_{0(i,j)}^* = [4T_{0(i,j)} + 2(T_{0(i+1,j)} + T_{0(i-1,j)} + T_{0(i,j+1)} + T_{0(i,j-1)}) + T_{0(i+1,j+1)} + T_{0(i-1,j+1)} + T_{0(i+1,j-1)} + T_{0(i-1,j-1)}] / 16 \quad (\text{K}) \quad (2.36)$$

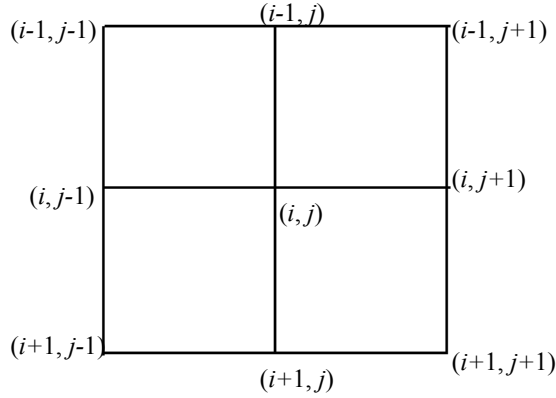


Figure 2.4 The scheme of the interpolation method of nine points.

This gives that the smoothed value of surface temperature $T_{0(i,j)}^*$ at the point (i,j) . If there are a number of observation sites, the difference between the smoothed surface temperature $T_{0(k)}^*$ and the observed air temperature $T_{a(k)}$ can be derived from

$$dT_{a(k)} = T_{0(k)}^* - T_{a(k)} dT_{a(k)} \quad (\text{K}) \quad (2.37)$$

If the difference between the smoothed surface temperature and the air temperature at grid point (i,j) is $DT_a(i,j)$ and dT_1, dT_2, \dots, dT_m are the differences between the smoothing surface temperature and the observed air temperature at the No.1, No.2, ..., No.m observation sites, $DT_a(i,j)$ can be written as

$$DT_a(i, j) = \frac{\sum_{k=1}^m \frac{dT_a(k)}{r_k^2}}{\sum_{k=1}^m r_k^{-2}} \quad (\text{K}) \quad (2.38)$$

where r_k is the distance between the observation point k and the grid point (i, j) . The difference $dT_a(k)$ at an observation point can be interpolated to all the grid point (i, j) from Eq.2.37. Therefore, T_a value estimated by Eq.2.35 can here be corrected using DT_a from Eq.2.38:

$$T_a(i, j) = T_0(i, j) - DT_a(i, j) \quad (\text{K}) \quad (2.39)$$

In other words, $T_a(x, y)$ can be derived by using this improved numerical interpolation method based on a number of ground observations of air temperature and regional surface temperature as

$$T_a(x, y) = T_0(x, y) - DT_a(x, y) \quad (\text{K}) \quad (2.40)$$

Aerodynamic roughness length $z_{0m}(x, y)$

In Eq.2.34, $z_{0m}(x, y)$ can be roughly determined by using the Surface Layer (SL) and Atmospheric Boundary Layer (ABL) observations. Wieringa (1992) proposed typical values of $z_{0m}(x, y)$ for homogeneous surfaces and heterogeneous landscapes (Table 2.1). In this case, to be representative either a number of point measurements at moderate heights or one point measurement at a height above the reference height is required. As these measurements require a high tower, aircraft or tethered balloons, the ABL observations are generally very expensive and cumbersome. Bastiaanssen (1995) and Jia et al. (1999a) pointed out there were relationships between z_{0m} and $NDVI$. The relationships can be used to estimated $z_{0m}(x, y)$.

Zero-plane displacement $d_0(x, y)$

$d_0(x, y)$ in Eq.2.34 can be roughly determined in two ways:

- 1) As regards a complete canopy surface, there is a commonly accepted equation between d_0 and vegetation height h_v (Stanhill, 1969; Brutsaert, 1984)

Table 2.1 Typical values for aerodynamic roughness length z_{0m} over homogeneous surfaces and heterogeneous landscapes (after Wieringa, 1992)

Surface	z_{0m} (m)
Homogeneous surface	
Sea loose sand and snow	0.0002
Concrete, flat desert, tidal flat	0.0002-0.0005
Flat snow field	0.0001-0.0007
Rough ice field	0.001-0.004
Fallow ground	0.008-0.03
Short grass and moss	0.02-0.06
Long grass and heather	0.04-0.09
Low mature agricultural crops	0.12-0.18
High mature crops	0.35-0.45
Continuous bush land	0.8-1.6
Mature pine forest	0.4-0.7
Dense low buildings	0.7-1.5
Regularly-built large town	1.7-2.3
Tropical forest	≥ 2.0
Heterogeneous landscape	
Sea: tidal sea lake, tidal flat, snow-covered flat plain, featureless desert, tarmac and concrete, with a free fetch of several kilometers	0.0002
Smooth: featureless land surfaces without any noticeable obstacles and with negligible vegetation	0.005
Open: level country with low vegetation and isolated obstacles with separations of at least 50 obstacle heights	0.03
Roughly open: cultivated area with regular cover of low crops, or moderately open country with occasional obstacles at relatively horizontal distance of at least 20 obstacle heights	0.1
Rough: recently developed 'young' landscape with high crops or crops of varying height, and scattered obstacles at relative distances of about 15 obstacle heights	0.25
Very rough: 'old' cultivated landscape with many rather large obstacle groups separated by open spaces of about 10 obstacle heights and low large vegetation with small interspaces	0.5
Closed: landscape totally and quite regularly covered with similar size large obstacles with open spaces comparable to obstacle heights	1.0
Chaotic: centers of large towns with mixture of low-rise and height-rise buildings and irregular large forests with many clearings	≥ 2.0

$$\frac{d_0(x, y)}{h_v(x, y)} = c \quad (-) \quad (2.41)$$

where c is constant, $c_{\text{Brutsaert}}=2/3$ and $c_{\text{Stanhill}}=0.64$. Seginer (1974) pointed out

$$\frac{d_0(x, y)}{h_v(x, y)} = 1 - \frac{l_h}{kh_v(x, y)} \quad (-) \quad (2.42)$$

where l_h is the mixing length at the top of the canopy.

- 2) As regards a partial canopy, a simple description d_0/h_v given by Raupach (1994) can be used.

$$1 - \frac{d_0(x, y)}{h_v(x, y)} = \frac{1 - \exp(-\sqrt{c_{d1}LAI(x, y)})}{\sqrt{c_{d1}LAI(x, y)}} \quad (-) \quad (2.43)$$

where c_{d1} is a free parameter (Raupach, 1994). For a range of partial vegetation canopies, Raupach (1994) proposed to use $c_{d1}=7.5$. Leaf Area Index (LAI) in Eq.2.43 can be derived using spectral vegetation indices. For normal sparse canopy, Kustas and Norman (1997) proposed:

$$LAI = -2\ln(1 - P_v) \quad (\text{m}^2 \text{ m}^{-2}) \quad (2.44)$$

and Li et al. (1997) proposed:

$$LAI = -\frac{1}{2k} \ln\left[\frac{r - r_v}{r_s - r_v}\right] \quad (\text{m}^2 \text{ m}^{-2}) \quad (2.45)$$

where r is the surface reflectance of a soil-vegetation mixture, r_s and r_v is the surface reflectance values for bare soil and full vegetation respectively.

Excess resistance to heat transfer $kB^{-1}(x, y)$

Since the 1930s scientists have been studying kB^{-1} in Eq.2.34 for all kinds of natural and artificial surface ranging from aerodynamically smooth to rough. These studies led to a number of formulations for kB^{-1} (e.g. Sverdrup, 1937; Sheppard, 1958; Owen and Thomson,

Table 2.2 Some practical equations on the excess resistance to heat transfer kB^{-1}

Landscape	Equation	Reference
Sparse vegetation	$kB^{-1} = \text{Re}^* \text{Pr} = \ln(k u_* z_{0m} / k_\theta)$ <ul style="list-style-type: none"> • Reynolds number: $\text{Re}^* = u_* z_{0m} / \nu$ • Prandtl number: $\text{Pr} = \nu / k_\theta$ <p>ν: kinematic molecular viscosity k_θ: molecular thermal diffusivity</p>	Sheppard (1958)
Rough surfaces and based on wind tunnel experiments	$kB^{-1} = k\alpha(8\text{Re}^*)^m \text{Pr}^n$ <ul style="list-style-type: none"> • $\alpha(\sim 0.52)$ depending to some extent on the shape of the roughness elements; • $m(\sim 0.45)$ and $n(\sim 0.8)$ depend on the diffusivities in the sub-layer 	Owen and Thomson (1963)
Bean crop	$kB^{-1} = 1.35k(100u_*)^{1/3}$	Thom (1972)
Uniform vegetative surface	2.0	Garratt and Hicks (1973)
Smooth surface	$kB^{-1} = k\lambda \text{Pr}^{2/3} + \ln\left(\frac{R^* \text{Pr}^{1/3}}{\lambda}\right)$	Kondo (1975)
Heterogeneous surface :25% 8m high trees, 65% 1 m high dry grass and 10% bare soil	2.5±0.5	Garratt (1978)
Sparse vegetation	$kB^{-1} = 2.46(\text{Re}^*)^{0.25} - 2.0$	Brutsaert (1984)
Bushes (~30%) and bare soil (70%)	$kB^{-1} = 0.17u(T_s - T_a)$	Kustas et al.(1989)
Sparse vegetation	$kB^{-1} = k\left(\frac{120}{LAI} \sqrt{wu_*} - 2.5\right),$ <p>w is leaf width</p>	Jensen and Hummelshøj (1995), McNaughton and Van den Hurk (1995) and Qualls and Brutsaert (1995)

1963; Chamberlain, 1968; Thom, 1972; Garratt and Hicks, 1973; Kond, 1975; Garratt, 1978; Brusaert, 1984; Kustas et al., 1989; Kohsiek et al., 1993; Verhoef et al., 1997; Jia, 1999a; Ma et al., 2002d; Jia, 2004).

Some practical equations proposed by some scientists are shown in Table 2.2. During the last two decades, the interest in the topic of kB^{-1} has been revived by the remote sensing community (e.g. Kustas et al., 1989; Sugita and Brutsaert, 1990; Stewart, 1995; Stewart et al., 1998; Jia, 2004) by using the bulk transfer equation to calculate H from the remotely sensed surface radiative temperature obtained from a satellite or aircraft, and the relationships between kB^{-1} and T_0 , kB^{-1} and T_0-T_a , and kB^{-1} and u (T_0-T_a) were found by Kustas et al. (1989), Guo and Wang (1993) and Ma et al.(2002d). The concept of kB^{-1} is being applied in many meteorological models, used for weather forecasting in recent years.

Integrated stability functions $\psi_h(x,y)$ and $\psi_m(x,y)$

For unstable conditions, the integrated stability functions $\psi_h(x,y)$ and $\psi_m(x,y)$ in Eq.2.34 can be written as (Paulson, 1970):

$$\begin{cases} \psi_m(x, y) = 2 \ln\left(\frac{1+X}{2}\right) + \ln\left(\frac{1+X^2}{2}\right) + 2 \arctan(X) + 0.5\pi \\ \psi_h(x, y) = 2 \ln\left(\frac{1+X^2}{2}\right) \end{cases} \quad (-) \quad (2.46)$$

where $X = \{1 - 16 * [z - d_0(x, y)] / L(x, y)\}^{0.25}$.

For stable conditions, $\psi_h(x,y)$ and $\psi_m(x,y)$ in Eq.2.34 become (Webb, 1970):

$$\psi_m(x, y) = \psi_h(x, y) = 5 \frac{z - d_0(x, y)}{L(x, y)} \quad (-) \quad (2.47)$$

The stability function $[z - d_0(x, y)] / L(x, y)$ will be solved by using the Businger scheme (Businger, 1988):

$$\begin{cases} \frac{z - d_0(x, y)}{L(x, y)} = R_i(x, y) & \text{(unstable)} \\ \frac{z - d_0(x, y)}{L(x, y)} = R_i(x, y) / [1 - 5.2R_i(x, y)] & \text{(stable)} \end{cases} \quad (-) \quad (2.48)$$

where L is Monin Obukhov stability length, $R_i(x,y)$ is the Richardson number, and according to the definition of Richardson number, it can be approximately written as

$$R_i(x,y) = \frac{g[z - d_0(x,y)]}{T_a(x,y) \cdot u^2} \cdot [T_0(x,y) - T_a(x,y)] \quad (-) \quad (2.49)$$

where g is acceleration due to gravity, u is the wind speed at the reference height z .

2.4 Latent heat flux $\lambda E(x,y)$

The latent heat flux can be determined as (e.g. Brutsaert, 1984; Rowntree, 1991)

$$\lambda E = \frac{\rho c_p}{\gamma} \left[\frac{e^*(T_0) - e_a}{r_a + r_s} \right] \quad (\text{W m}^{-2}) \quad (2.50)$$

where γ is the psychrometric constant, e_a is vapor pressure of the air at the reference height z above the land surface, r_a is the atmospheric resistance to transfer from the surface to the atmosphere, r_s is the surface resistance to transfer from the soil (or the stomatal resistance in the case of vegetation), $e^*(T_0)$ is the saturated vapor pressure at the surface temperature T_0 .

The difficulty of using Eq.2.50, especially at the regional scale, is the estimation of r_a and r_s (e.g. Menenti and Choudhury, 1993; Bastiaanssen, 1995; Su, 2002; Jia, 2004). To avoid the difficulty, $\lambda E(x,y)$ can be derived as a residual in the surface energy balance equation of the land surface based on the condition of zero horizontal advection at $z < z_{\text{sur}}$ (e.g. Bastiaanssen, 1995; Wang et al., 1995; Ma et al., 1999; Su, 2002; Ma et al., 2002a; Ma et al., 2003a; Ma et al., 2004a; Ma et al., 2005; Ma et al., 2006), i.e.

$$\lambda E(x,y) = R_n(x,y) - H(x,y) - G_0(x,y) \quad (\text{W m}^{-2}) \quad (2.51)$$

2.5 Summary and Conclusions

Based on satellite remote sensing and observations of the Surface Layer (SL) and Atmospheric Boundary Layer (ABL), the methodologies to determine the regional distribution of net radiation heat flux $R_n(x,y)$, soil heat flux $G_0(x,y)$, sensible heat flux $H(x,y)$ and latent heat flux $\lambda E(x,y)$ at the land surface were established. The procedure given in the previous sections can be summarized as:

- The distribution of $R_n(x,y)$ at the land surface can be determined from Eq. 2.3. Where incoming solar radiation flux $K_{\downarrow}(x,y)$ and incoming long-wave radiation flux $L_{\downarrow}(x,y)$ can be calculated from the MODerate spectral resolution atmospheric TRANsmittance model (MODTRAN) directly, surface reflectance $r_0(x,y)$ can be derived from a linear relationship between it and the spectrally integrated planetary reflectance r_p or from four-stream radiative transfer assumption, surface temperature $T_0(x,y)$ can be derived from a Split Window Techniques (SWT) or from a radiative transfer model, and surface emissivity $\varepsilon_0(x,y)$ can be estimated from Normalized Difference Vegetation Index (NDVI) or from vegetation fractional cover P_v .
- The distribution of $G_0(x, y)$ at the land surface cannot be calculated from the definition equation directly, but from Eqs.2.27 and 2.28, if the parameters a, b, c, d, e and the Modified Soil Adjusted Vegetation Index (MSAVI) can be derived from ground observational data and satellite data respectively.
- The distribution of $H(x,y)$ at the land surface can be derived from Eq.2.34 once the pixel values of surface temperature T_0 , the wind speed at the reference height u , air temperature T_a , zero-plane displacement height d_0 , excess resistance to heat transfer kB^{-1} and the stability correction function ψ_m and ψ_h have been determined.
- Because of the difficulties to estimate the heat transfer resistances between the atmosphere, land surface and soil, the distribution of $\lambda E(x, y)$ at the land surface is difficult to solve directly from Eq.2.50. Therefore, it is preferred to consider $\lambda E(x, y)$ as a residual of the surface energy balance equation at the land surface (Eq. 2.51).

Due to insufficient knowledge some assumptions and approximations have been involved in the methodology, especially in the procedure of determining $H(x,y)$. But the assumptions and approximations in the procedure can be reduced to a minimum level when the micrometeorological parameters have been determined by using the SL and ABL observations. In other words, the land surface heat fluxes can be determined more accurately when the input variables in the methodology have been improved.

As a conclusion, *the heat fluxes at the land surface can be determined accurately by integrating satellite remote sensing with the SL and ABL observations.* The ABL observations give the ground truth of each parameter and satellite remote sensing can directly measure land surface properties over large areas. Therefore, combining satellite remote sensing with the SL and ABL observations can yield better results for land surface

heat fluxes over heterogeneous landscapes.

3. Parameterization of heat fluxes at heterogeneous surfaces using surface and atmospheric boundary layer observations

3.1 Introduction

Land-atmosphere interactions are strongly heterogeneous spatial processes at the interface between the land surface and the Atmospheric Boundary Layer (ABL). This is true for practically every spatial scale varying from individual stomata to the whole earth. Heat fluxes are the key topic in the study of land-atmosphere interactions.

Theories and models for energy exchange between heterogeneous land surface and the overlying atmosphere always involve some kind of implicit or explicit spatial averaging till now. These models usually express fluxes in terms of transfer coefficients over various exchange pathways, such as aerodynamic or surface resistances. Models are also usually nonlinear in the spatially changing independent variables. Because of the nonlinearities, it is not always easy to use transfer coefficients across spatial scales (Stewart et al., 1998), such as using empirical knowledge of conductance at a small scale to infer an averaged conductance for use in a bulk model at a large scale. Therefore, the ‘scaling problem’ in land-atmosphere interactions is essentially the problem of using information about exchange processes at one small scale, such as transfer coefficients, to characterize the same processes at the larger scale.

Three spatial scales of great practical importance are the single energy-exchanging element, the homogenous land surface patch, and the heterogeneous landscape of linear scale up to a few hundred kilometers. For brevity, these will be called the leaf, canopy and regional scales, respectively (Raupach, 1995). The two primary scale transitions in practice are therefore leaf to canopy and canopy to region. Leaf-canopy scaling has been an issue for several decades, following the postulate by Monteith (1965) that a canopy acts as ‘big leaf’ with a canopy conductance equal to the parallel sum of the leaf stomata conductances. Canopy-regional scaling has advanced in part through the need for spatially averaged lower boundary conditions in large scale atmospheric models (Raupach, 1995), which is based on the scaling principle of conservation of mass and energy, and it is also the main focus of this chapter and this thesis. Using the idea of a ‘blending height’ above which the air flow is approximately spatially uniform, several researchers have proposed canopy-region scaling rules for momentum transfer, by quantifying the regionally momentum roughness length (e.g. Wieringa, 1986; Mason, 1988; Claussen, 1991; Menenti et al., 1991; Menenti and

Choudhury 1993; Menenti and Ritchie, 1994; Bastiaanssen, 1995; Wang et al., 1995; Ma et al., 1999; Ma et al., 2002a; Ma et al., 2003a; Ma et al., 2006). A similar treatment of heat exchange was given by Wood and Mason (1991), whereas Blyth et al. (1993) considered coupled sensible heat and latent heat exchange on the basis of heuristic scaling argument for transfer resistances.

This chapter will consider the features of scaling problems for energy exchange over heterogeneous land surfaces, which are including the effects of the ABL, i.e. canopy-region scale translations. Because both surface heterogeneity and ABL are very important in the parameterization procedure of heat fluxes in the ABL overlying a heterogeneous surface, the plan of this chapter is as follows.

- The characteristics of a heterogeneous land surfaces and its length scale of heterogeneity will be described in Section 3.2.
- Section 3.3 will analyze the response of the ABL to the surface energy balance and large scale heterogeneity.
- Blending height assumptions will be introduced and its height and relative length scale will be determined in Section 3.4.
- In Section 3.5, constraints will be established to define larger-scale surface properties from their smaller-scale counterparts.
- Three parameterization methodologies to determine land surface heat fluxes (i.e. the *RS approach*, the *Tile approach* and the *Blending height approach*) will be presented in Section 3.6.
- Summary and conclusions are given in Section 3.7.

3.2 Heterogeneous land surface and the length scales of heterogeneity

The global land surface consists of landscape mosaics that are mixtures of natural and human managed patches that vary in size, shape and arrangement. This *horizontal variability*, i.e. *heterogeneity*, affects the processes taking place at the surface of the earth. Understanding how to account for and how to include heterogeneity in the climate models is essential for understanding the regional and global hydro-meteorological processes. *Heterogeneity is defined in terms of contrast and scale. Contrast is the difference between patches and scale. Scale is the horizontal dimension of patches in the direction of the prevailing wind. Each patch represents a surface area differing from its surrounding, thus defining a discrete and internally homogeneous entity.*

Land surface heterogeneity influences the atmospheric flow and the energy and mass exchange with the surface. The influence depends on the scale of heterogeneity. As the surface conditions vary horizontally, only the lower layer of the ABL is in equilibrium with the underlying surface. In case of large scales, the entire ABL will adapt to heterogeneities, while for smaller scales only the lower part of the ABL responds to the heterogeneity before an air mass moves forward and over a different patch.

Length scales of heterogeneity have been classified in several ways in the past (e.g. Avissar, 1995; Raupach and Finnigan, 1995). Here we use two dynamic time-scales for the ABL processes:

- 1) The *mixing time-scale* $t_* = z_i / w_*$ (the time-scale for a scalar to mix fully through the ABL, where w_* is the convective velocity scale, and z_i is the convective inversion height).
- 2) The *entrainment time scale* $t_e = z_i / (dz_i / dt - w_+)$. It is the time scale for renewal of the air in the ABL by entrainment from above, where w is the mean vertical velocity, and the ‘+’ subscript denotes conditions in the troposphere just above $z = z_i$.

Typically, t_* is of the order of 10^2 s in the early morning, quickly rising to around 10^3 s later in the day as z_i increases, and t_e is of the order of the time since dawn (Raupach and Finnigan, 1995).

The corresponding *length scales* are $U_m t_*$ (typically 1-5 km) and $U_m t_e$ (typically 100 km or more) for the typical values of t_* and t_e , where U_m is the mean wind speed in the well-mixed bulk of the ABL (Raupach and Finnigan, 1995). For different length scales, their characteristics can be defined as follows.

- Over *micro-scale heterogeneity* with patch length scale $X \leq U_m t_*$, air temperature and humidity respond to surface conditions only in a thin surface layer of depth $\ll z_i$, above which they take the uniform, average values Θ_m and Q_m . Micro scale advection (the interaction between vertical and horizontal gradients) in the surface layer is significant in these conditions. At this scale, methods have been developed that take into account the effect of small scale heterogeneities on surface-atmosphere fluxes (Raupach and Finnigan, 1995).
- For *macro-scale heterogeneity* with patch length scale $X \geq U_m t_e$, the ABLs over adjacent patches are energetically independent, because air cannot flow from patch to patch during the time it takes for the daytime ABL to evolve. The ABL evolution is controlled by the surface fluxes and tropospheric conditions above the ABL. This is the scale at which the ABL can be regarded as self-organizing, subject to these external

conditions.

- Between micro-scale heterogeneity and macro-scale heterogeneity, *meso-scale heterogeneity* occurs when $U_m t_* \leq X \leq U_m t_c$. Patches of this scale are not necessarily energetically independent, because the potential air temperature Θ and humidity Q (although well-mixed vertically through the bulk of the ABL) continue to adjust to changes in the surface state over distances much larger than $U_m t_*$. This is advection at the ABL scale, rather than at the surface layer scale as for micro-scale heterogeneity. Aggregation of heterogeneity at the meso-scale is often parameterized in climate modelling. In the first generation models, the average grid fluxes were computed from the dominant surface type. Avissar and Pielke (1989) and Koster and Suarez (1992) improved this approach by calculating the flux for each surface type and deriving the average flux. Their approach assumes that each surface type is independently coupled to the ABL. It should be noted that the lower part of the ABL is adjusted to surface conditions, while the upper part conditions to evolve. Under these conditions observations of Θ and Q in the lower ABL allow us to treat meso-heterogeneous patches as independent.

3.3 Characteristics of the atmospheric boundary layer over a heterogeneous landscape

The controlling role of the ABL on the regional surface energy balance has been recognized by many researchers (e.g. Deardorff, 1978; Menenti, 1984; Troen and Mahrt, 1986; McNaughton and Spriggs, 1986; Avissar and Pielke, 1989; Menenti et al., 1989; Menenti et al., 1991; Menenti and Choudhury, 1993; Xue and Shukla, 1993; Pielke et al., 1995; Bastiaanssen, 1995; Wang et al., 1995; McNaughton and Raupach, 1996; Kustas and Norman, 1997; Ma et al., 2002a; Ma et al., 2003a; Jia, 2004; Ma et al., 2005; Ma et al., 2006). In the context of land-atmosphere interactions, the ABL has two key general properties. *First*, it acts as a natural integrator by accumulating entities exchanged at the surface, such as heat, water vapor, and CO_2 . This means that the spatial variability of concentrations of these entities in the ABL is limited even when their fluxes at the surface change rapidly, so that the ABL concentrations are relatively insensitive to short-term small scale details of the surface fluxes, and are mainly determined by the long history of the surface fluxes over the lifetime of the ABL (the time since dawn). *Second*, for the key ABL state variables such as air temperature, wind speed and humidity involved in the Surface Energy Balance (SEB)-heat and water vapor-the ABL concentrations influence fluxes,

forming a negative-feedback loop. The coupled concentrations and fluxes therefore tend to evolve toward equilibrium values, at rates determined by characteristic time scales. The nature of SEB-ABL feedback also depends fundamentally on the entrainment processes at the top of the ABL, because these are largely driven by the surface heat fluxes (e.g. McNaughton and Spriggs, 1986; McNaughton and Jarvis, 1991; Raupach, 1991; Raupach and Finigan, 1995; McNaughton and Raupach, 1996).

In order to describe the response of the ABL to the SEB at large scale heterogeneities, a slab ABL model (McNaughton and Raupach, 1996) will be discussed, to explain the ABL behaviour, two important ABL time scales, and changes in air flow over heterogeneous land surface will be discussed in this section.

3.3.1 General characteristics of the atmospheric boundary layer

The interaction of air flow with the land surface results in boundary-layer flow. The ABL or the Convective Atmospheric Boundary Layer (CABL) is caused by the frictional drag of the land surface and heating from the surface. The height of this layer depends on the strength of the surface-atmosphere interaction. In the absence of strong meso-scale circulation and in cloud-free conditions, the height is controlled by the surface sensible heat and momentum flux at the atmosphere-land interface. During daytime there is an upward transfer of heat caused by warming of the surface of the earth resulting in a ABL thickness of 1 to 2 km. At night the height shrinks to less than 100 m due to a downward transfer of heat. During daytime the momentum exchange is a negligible factor controlling the thickness of the ABL, while at night it is dominant. The magnitude of this influence strongly depends on the wind speed and surface roughness. The greater the roughness, the more effective the exchange of momentum will be, causing a stronger development of ABL. The vertical fluxes in the ABL tend to decrease with height. Above the ABL, turbulence weakens through the diminishing shear while large-scale eddies (e.g. depressions and fronts) become more important. The lowest level where shear becomes insignificant is known as the gradient level or the upper limit of the ABL.

Usually the *ABL* is divided into different layers, including a *Surface Layer (SL)* and *Outer layer* (see Figure 3.1). In the outer layer the flow depends on the Coriolis force in near-geostrophic balance and is hardly sensitive to surface friction. In unstable conditions strong convective forces mainly drive the motions in this layer and it is therefore called

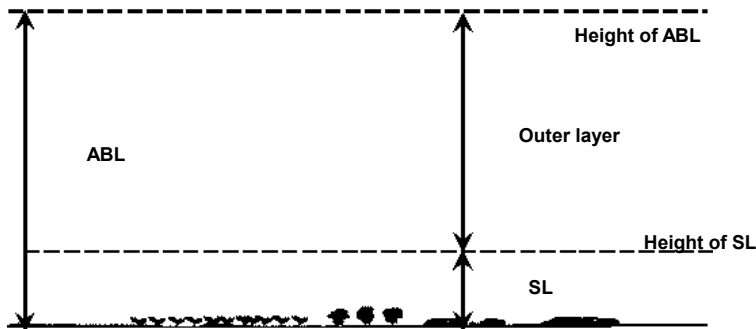


Figure 3.1 Schematic diagram of the layers of the Atmospheric Boundary Layer (ABL). The ABL is divided into different layers, including a Surface Layer (SL) and outer layer.

mixed layer.

The SL develops within the lower 10 % of the ABL (e.g. Garratt, 1992). In the SL the change in fluxes with height is negligibly small, as compared to the outer layer, where the fluxes change significantly with the height. The SL is therefore also known as the constant flux layer in dynamic equilibrium with the underlying land surface. The SL is only quasi steady-state, since the height of the layer may vary with time, even if the surface conditions stay constant. The SL may extend to 200 m in daytime, while at night it shrinks and may only be a few meters thick. The thickness is hardly affected by the Coriolis force but strongly affected by the heat fluxes from the surface to the atmosphere.

3. 3. 2 A slab model for the diurnal behaviour of the atmospheric boundary layer

An analytical approach is to use a simple ‘slab’ or ‘mixed-layer’ model for the development of the day time ABL. McNaughton and Spriggs (1986), McNaughton (1989), and Cleugh and Grimmond (1993) argued that a slab ABL model provides a rational link between the surface energy balance and large scale atmosphere motions. The dynamic simplifications of the slab ABL model are appropriate for studies of land-atmosphere energy exchanges because the key property of the ABL which influences the surface energy balance is the rate of entrainment of overlying air into the ABL. With an appropriate entrainment parameterization to describe the ABL growth rate, this property can be described fairly

realistically in a slab model.

The slab model assumes that the ABL is well mixed by convective turbulence and is bounded above by a capping inversion at height $z_i(t)$. The scalar conservation equation, height-integrated from $z=0$ to $z=z_i$ in an air column moving with the mean wind field, is then:

$$\frac{dC_m}{dt} = \frac{F_C}{Z_i} + \left(\frac{C_+(Z_i) - C_m}{Z_i} \right) \left(\frac{dZ_i}{dt} - w_+ \right) \quad (\text{W m}^{-3}) \quad (3.1)$$

where $C_m(t)$ is the mixed-layer scalar concentration (uniform in the ABL), w is the mean vertical velocity, the + subscript denotes conditions in the troposphere just above $z=z_i$, and F_C is the scalar flux at the surface and t is time. This equation prescribes that C_m should change when F_C changes because of heterogeneity under the condition of dynamic equilibrium.

The slab model can be solved for the daytime evolution with time t of five variables, all of which are averaged over small-scale heterogeneities (therefore capitalized here): the mixed layer potential temperature $\Theta_m(t)$ and specific humidity $Q_m(t)$, the land-atmosphere fluxes of sensible heat flux $F_H(t)$ and latent heat flux $F_E(t)$ and the convective inversion height $z_i(t)$. However, there are clear restrictions to the applicability of the ABL slab models: they are inappropriate over terrain with large topographic variations, or in disturbed meteorological conditions such as fronts.

3.3.3 Time scales of the atmospheric boundary layer

The ABL has two significant time (and therefore length) scales. One is the dynamical time scale t_d , and another is the time t_q for thermodynamic adjustment of the ABL to changes in the surface energy balance.

The dynamical time scale t_d is a scale for the overturning time of convective motions in the ABL, and also for the time needed for these motions to adjust dynamically after a sudden change in surface flux (e.g. Briggs, 1988; Raupach, 1991; Garratt, 1992; Raupach and Finnigan, 1995) or in the surface characteristics. This time scale is defined as

$$t_d = h_{\text{ABL}} / w_* \quad (\text{s}) \quad (3.2)$$

where h_{ABL} is the height of the ABL and w_* is the convective velocity scale in the ABL:

$$w_* = \left(\frac{h_{\text{ABL}} w \theta_v g}{T_r} \right)^{\frac{1}{3}} \quad (\text{ m s}^{-1}) \quad (3.3)$$

where g is acceleration due to gravity, T_r is a reference absolute temperature, w is the vertical velocity and $w\theta_v$ is the surface layer virtual flux of vertical potential temperature θ_v . Full adjustment occurs in a time around $4h_{\text{ABL}}/w_*$ which is also the time required for complete vertical mixing of scalars through the depth of the ABL (McNaughton and Raupach, 1996). At midday, taking the ABL height $h_{\text{ABL}} = 1000$ m and $w_* = 2$ m s⁻¹ as typical values, full adjustment takes about half an hour, though it is quicker in the early morning when h_{ABL} is lower. During this time the ABL air mass moves with the averaged wind speed in the ABL, U , through a distance $4Uh_{\text{ABL}}/w_*$. If $U = 5$ m s⁻¹, then the adjustment distance is about 10 km at the midday. To resolve processes at scales less than these, we have to use a model which describes the mixing in detail. If our scale of interest is larger, then the assumption of well-mixed ABL is satisfactory.

We define t_q as the time scale for the saturation deficit $D(t)$ to become independent of the initial saturation deficit D_0 , following a transition in surface properties time for thermodynamic adjustment of the ABL to changes in the SEB. The saturation deficit is a significant quantity because of its link with evaporation. If t_q is short, then the local ABL state is controlled by local conditions only and is influenced little by upwind surface. If however t_q is long, then the state of the upwind surface is significant and past history of the ABL air mass has a significant influence on the local ABL state, and hence, via $D(t)$ on the local surface energy balance.

Air flow and mixing impose an influence from distant events on local energy balance, and therefore naturally integrate events at one scale into a larger scale. As the length scale increases, the range and extent of air mixing also increases through a hierarchy of physical processes encompassing many orders of magnitude in both space and time-scales. This hierarchy of processes for the atmosphere is shown in Table 3.1 (Raupach and Finnigan, 1995). At the largest scale, the time scale for mixing is significantly longer than that of the energy source that drives the hydrological and climate systems (diurnal radiative forcing), so that on a diurnal time scale, little mixing occurs. It is this property that defines from the atmospheric viewpoint the regional scale as the area over which the ABL is self-organizing on diurnal time-scales, and largely not affected by events in neighbouring regions.

Table 3.1 Atmospheric mixing processes (after Raupach and Finnigan, 1995)

Length scale (m)	Time scale (s)	Process	Typical situation
10^{-5}	10^{-5}	Molecular diffusion in static fluid	Substomatal cavity
10^{-3}	10^{-1}	Advection diffusion in laminar flow	Leaf boundary layer
10^{-1} - 10^2	10^{-1} - 10^2	Shear-driven turbulence	Canopy layer and surface layer
10^2 - 10^3	10^2 - 10^3	Buoyancy-driven turbulence	Convective mixed layer
10^3 - 10^5	10^3 - 10^5	Buoyancy-driven mean flow	Meso-scale circulations; thermally driven hill and valley flows; mountain waves, bores, hydraulic jumps (flow systems locked into topography) frontal systems; convective storms
10^5 - 10^7	10^5 - 10^6	Two dimensional turbulence, gyres	Weather systems on continent scale

The above approach uses a slab or mixed-layer model of the ABL, according to the semi-Lagrangian view in which we track the properties of columns of air as they move across the landscape. ‘Semi-Lagrangian column view’ means that the ABL is envisaged as a well-mixed column of air moving across the landscape, accumulating and integrating scalar entities along its path as it passes over a succession of different surface types. Two constraints upon this approach must be noted. *Firstly*, a mixed-layer model is only meaningful when applied over time t_d (and therefore length) scales large enough for the ABL to be treated as fully mixed, that is, over times larger than about $4h_{ABL}/w_*$ and lengths larger than $4Uh_{ABL}/w_*$ (Mcnaughton and Raupach, 1996). Mixed layer models cannot describe ABL evolution on shorter space and time scales. Therefore, in considering the evolution of a moving column of air with a mixed layer model, we are implicitly speaking of a column at least $4Uh_{ABL}/w_*$ in linear extent. *Secondly*, we must ask to what extent a column of air remains unchanged during its motion, given that the column is continuously smeared or mixed with neighboring columns by the horizontal dispersion induced mainly by wind shear in combination with vigorous vertical mixing. This smearing is the reason for calling the approach ‘semi-Lagrangian’.

3.3.4 Air flow over a heterogeneous land surface

In case of heterogeneous surfaces an important effect of changes in the surface characteristics on wind speed is the change in surface roughness from one patch to another (see Figure 3.2). Flow over a change in surface roughness will result in an Internal Boundary

Layer (IBL) developing over the new surface. The IBL is usually much shallower than the ABL, since the horizontal extent of the surface patches is usually small. The height of the IBL depends on the scale of heterogeneity and on the height of the surface layer. At the same time, the height of the IBL depends on the fetch or distance from the leading edge (the edge between two surfaces or patches, see Figure 3.2) as well as on the roughness of the surface. Only in the lower 1-10 % of the IBL, the air is fully adjusted to the surface, and this layer is called fully adjusted layer (Figure 3.2). The remainder of the layer is a transition zone where air is modified but not fully adjusted. The air above the IBL is only affected by the surface upwind direction. Any difference in roughness between the adjacent patches will result in a change of momentum exchange downwind of the discontinuity, influencing the wind speed in the fully adjusted layer. For example, a change from a smooth to a rough surface would result in a greater drag, increasing the stress and decreasing the wind speed.

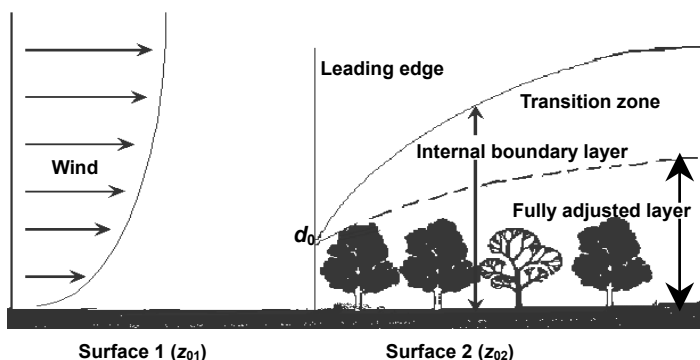


Figure 3.2 The development of an internal boundary layer as air flows from a smooth dry surface (e.g. Gobi desert) to a rough vegetated wet surface. The quantities z_{01} and z_{02} represents aerodynamic roughness length on the land surface No.1 and No.2 respectively, and d_0 is zero-plane displacement.

Thus types of landscape roughness elements at different scales are important as they have a major impact on the local state of ABL. The obstacles may vary from tree lines to hills. Every hill, dune, valley or tree line creates a perturbation in the flow pattern. Topography or obstacles create an area of high pressure on the upstream slowing the wind and resulting in absorption of momentum. Separation may take place behind a sudden drop in topography or behind an obstacle. Obstacles like tree lines are usually sufficiently porous to prevent separation of air flow. The effect on roughness depends on the shape, size, and spatial distribution of these obstacles. For air flow over an area with a low density of obstacles,

aerodynamic roughness increases with obstacle density. For dense arrays of obstacles, the roughness of the surface will decrease again, as the flow raises above the obstacles.

Many researchers have stated clearly that air flow has an auto-conservative property in the IBL (e.g. Zhou et al., 1988; Hu et al., 1990). Theoretical research and observational results (e.g. Brandley, 1968; Zhou et al., 1988, Hu et al., 1990) stated that there is a “4/5 power law” between the depth of IBL i.e. z_{IBL} and the fetch x past the change in the IBL, i.e. $z_{IBL} \sim x^{4/5}$ or $(1/10)x$. z_{IBL} does not have any obvious relationship with stratification. The depth of the fully adjusted layer or Balance Layer (BL) is about $z_{BL} \sim (1/200)x$ or $(1/10)z_{IBL}$. In order to carry out flux observations it is estimated that the BL depth should be about $z_{BL} \approx (1/50)x \sim (1/300)x$ (Hu, et al., 1990). It means that if an observation is done at the height Z_{BL} , the footprint on the underlying surface is $x=50 z_{IBL} \sim 300 z_{IBL}$. For example, if the footprint x is 1000 m, the observation height (or the reference height) should be 3 m~20 m.

3.4 Blending height assumption

One of the key ABL properties related to the scale of heterogeneity is the *blending height* z_b above the surface, at which atmospheric properties such as wind, and scalars such as air temperature and humidity become horizontally well mixed (i.e. uniform) (Wieringa, 1986; Mason, 1988; Claussen, 1990; Claussen, 1991).

In micro-scale heterogeneity, z_b has been studied both for wind speed (e.g. Wieringa, 1986; Mason, 1988) and scalars (e.g. Claussen, 1990; Claussen, 1991; Wood and Mason 1991; Blyth et al., 1993). For steady flow over a flat but heterogeneous surface in thermal neutral conditions, the perturbation part of the linearized equation of motion is

$$U(z) \frac{\partial u'}{\partial x} = \frac{\partial \tau'}{\partial z} \quad (\text{m s}^{-2}) \quad (3.4)$$

where $u(x,z) = U(z) + u'(x,z)$ is the time-mean velocity and $\tau(x,z) = \Gamma + \tau'(x,z)$ is the time-mean stress, and the capitals denote horizontal averages. The pressure term is ignored (Kaimal and Finigan, 1994). Using a mixing-length model to estimate τ for neutral conditions, we can write

$$\tau = k^2 z^2 \left(\frac{\partial u}{\partial z} \right)^2; \quad \tau' = 2kU_* z \frac{\partial u'}{\partial z} \quad (\text{N m}^{-2}) \quad (3.5)$$

where $U_* = \Gamma^{0.5} = kz(\partial u / \partial z)$ is the background friction velocity, and the second equation is linearized by neglecting products of perturbation terms. We now equate order of magnitude estimates for the left-and-right-hand sides of Eq.3.4. The term on the left is of order $U_b u' / X$, where X is a length scale for stream-wise heterogeneity and U_b a background advection velocity. The term on the right is estimated in different ways by different researchers.

- Mason (1988) assumed that u' 'adjusts to the new surface in the usual logarithmic way', implying

$$\frac{\partial u'}{\partial z} \sim \frac{u'}{U(z)} \frac{U_*}{kz} \quad (\text{s}^{-1}) \quad (3.6)$$

and

$$\tau' = 2U_*^2 \frac{u'}{U(z)} \quad (\text{N m}^{-2}) \quad (3.7)$$

The height z_b is defined by assuming Eq.3.4 being in balance. Mason assumed $\partial \tau' / \partial z \sim \tau' / z_b$, Eq.3.7 can be rewritten to

$$\frac{z_b}{X} = 2 \left[\frac{U_*}{U(z_b)} \right]^2 \quad (-) \quad (3.8)$$

and

$$z_b \left[\ln \left(\frac{z_b}{Z_{0m}} \right) \right]^2 = 2k^2 X \quad (\text{m}) \quad (3.9)$$

where $k=0.4$ is the von Karman constant, and X is a length scale of heterogeneity in the stream-wise direction (e.g. $X=A/2\pi$ for sinusoidal heterogeneity with wavelength A). The resulting z_b is here an estimate of the height up to which equilibrium conditions prevail over the new surface. Z_{0m} in Eq.3.9 is the effective (or averaged) roughness length. If one area is including the effect of topography, low vegetation (e.g. grass), taller plants (e.g. wheat canopy, trees and shrubs), Z_{0m} can be determined by the Arya's model (Arya et al., 1975). It means that the local roughness length z_{0m} can be determined by using the turbulent measurements of anemometer-thermometer, radio sonde and the

PBL tower firstly (see Chapter 6). Then Z_{0m} , can be derived from

$$\ln \frac{Z_{0m}}{z_{0m}} = \frac{4}{5} \left[\ln \frac{h_{\text{obstacle}}}{z_{0m}} + \ln \left(\frac{1}{\lambda} - \frac{b}{h_{\text{obstacle}}} - \frac{X_b}{h_{\text{obstacle}}} \right) \right] \bullet \left[1 - \left\{ 1 - m\lambda + \frac{C_D \lambda}{2k^2} \left(\ln \frac{h_{\text{obstacle}}}{z_{0m}} \right)^2 \right\}^{\frac{1}{2}} \right] \quad (-) \quad (3.10)$$

where $o_{\text{obstacles}}$ is effective (average) obstacle height, C_D is drag coefficient, which is given by Wooding et al. (1973), k is Von Karman's constant, $m = b/h_{\text{obstacle}} + B/h_{\text{obstacle}} + X_b/2h_{\text{obstacle}}$, b the base width of obstacles, B is the base width of the region with separated air flow behind obstacles, X_b is the wind profile recovering distance behind the obstacle, $\lambda = h_{\text{obstacle}}/s_1$, and s_1 is the spacing of obstacles.

If one area is including the effect of topography (mountain) and low vegetation (grass land), effective aerodynamic roughness length Z_{0m} can be determined by the Taylor's model (Taylor et al., 1989), i.e.

$$\ln \left(\frac{Z_{0m}}{z_{0m}} \right) = 3.5 \left(a \frac{2\pi}{\lambda_1} \right)^2 \ln \left(\frac{\lambda_1}{z_{0m}} \right) \quad (-) \quad (3.11)$$

where a is the amplitude of relief and λ_1 is the wavelength of periodic relief. In other words, the local roughness length z_{0m} can be determined by using the turbulent measurements of anemometer-thermometer or the PBL tower (see Chapter 6). Then Z_{0m} can be determined from Eq. 3.11 (see Menenti and Ritchie, 1994).

- Jackson and Hunt (1975) introduced an order of magnitude analysis for inner layer depth in the linear theory of flow over low hills, which has since become standard (see Kaimal and Finigan, 1994 for a review) and has been adapted to roughness changes by Belcher et al. (1990). If z_b is a height scale for the inner layer, then Eq.3.5 gives

$$\frac{\partial \tau'}{\partial z} = 2kU_* \frac{\partial}{\partial z} \left(z \frac{\partial u'}{\partial z} \right) \sim 2kU_* \frac{u'}{z_b} \quad (\text{N m}^{-3}) \quad (3.12)$$

where u' and z_b are here to be understood as velocity and height scales and the second

relationship includes a dimensionless $O(1)$ function of position. Equating this with $U_b u' / X$, we obtain

$$\frac{z_b}{X} = 2k \frac{U_*}{U(z_b)} \quad (-) \quad (3.13)$$

and

$$z_b \ln \left(\frac{z_b}{Z_{0m}} \right) = 2k^2 X \quad (m) \quad (3.14)$$

Eq.3.8 and Eq.3.9 estimate the depth of the equilibrated layer over the downwind surface following a transition in surface properties. This is the layer within which the velocity and scalar concentration profiles have approximately readjusted to logarithmic forms (in neutral conditions) appropriate to downward surface. Its depth is $O[X(U_* / \overline{U_b})^2]$, where $\overline{U_b}$ is a mean velocity scale for the layer.

In contrast, Eq.3.13 and Eq.3.14 estimate the depth of the ‘influenced layer’, or the height to which perturbations can diffuse by turbulent transport. Within a neutral surface layer, its depth is $O[X(U_* / \overline{U_b})]$. Finigan et al. (1990) showed experimentally that this is a good estimate for the height to which mean vorticity perturbations diffuse in the flow over low hills. Many researchers have used similar advection-diffusion principles to suggest equations for the depth of the developing internal boundary layer be in consistent with a depth of $O[X(U_* / \overline{U_b})]$ (see Kaimal and Finigan, 1994 for a comprehensive review).

3.5 Generic constraints over heterogeneous land surfaces

Constraints must be established to define larger-scale surface properties from their smaller-scale counterparts. One generic tool for imposing consistent constraints will be discussed here as i.e. the primary physical constraint, that net fluxes of conserved scalars must average linearly over the land surface.

The scalar conservation equation can be written as

$$\frac{\partial C}{\partial t} + \mathbf{U} \nabla C = -\nabla f_C \quad (\text{W m}^{-2}) \quad (3.15)$$

where C is the concentration of the conserved scalar, f_C is the sum of turbulent and molecular flux density vectors, and U is the mean velocity vector. Eq.3.15 provides a primary physical constraint on areal up scaling. For modeling purposes, this equation is always integrated spatially over air volumes R such as the air space in a canopy layer, a general circulation model grid cell or the entire ABL. Let R be bounded partly by the land-atmosphere interface, so that its closed bounding surface $S = S_L + S_A$ consists of a part S_L coincident with the land-atmosphere interface (vegetation, soil, lake and hill etc.) and a part S_A in the air. Using the divergence theorem, the conservation equation can be integrated over R

$$\frac{\partial}{\partial t} \iiint_R C dx = \iint_S U_n C dS + \iint_{S_A} f_C dS + \iint_{S_L} f_C dS \quad (\text{W m}^{-2}) \quad (3.16)$$

where U_n and f_C are the inward-normal components of U and f_C on S , and x is a position coordinate. The three terms on the right-hand side correspond respectively to advection, atmospheric divergence and the scalar input into R by surface fluxes. If the last term is written as $S_L F_C$, with $F_C = \langle f_C \rangle$ an averaged flux over the surface S_L , then Eq.3.16 requires that

$$F_C = \frac{1}{S_L} \iint_{S_L} f_C dS = \sum_{i=1}^n a_i f_{C_i} \quad (\text{W m}^{-2}) \quad (3.17)$$

where S_L consists of several patches i ($i=1$ to n) with area S_i , normalized areas $a_i = S_i / S_L$ and flux densities f_{C_i} . Eq.3.17 means that scalar mass conservation requires elemental surface fluxes to average linearly, with area weighting, across the land surface. To satisfy mass conservation area averages of other land-atmosphere interaction parameters (surface temperature, conductance and so on) need to be consistent with this constraint. Eq.3.17 applies to net fluxes of conserved scalars, in particular, sensible heat flux f_H , latent heat flux f_E and their sum $f_A = f_H + f_E$, i.e. the available energy flux. Eq.3.17 also applies to net irradiances (quantum fluxes) in any spectral waveband, as these are also net scalar fluxes.

3.6 Parameterization of land-atmospheric interactions using satellite measurements in combination with surface layer and atmospheric boundary layer observations

Satellite Remote Sensing (RS) data provide consistent and frequent observations of spectral reflectance and emittance of radiation at patches landscape. Therefore, combining them with ABL observations we can analyze the interaction between the land surface and atmosphere. Based on the theory presented in the previous sections and in combination with satellite measurements, three methodologies can be identified to estimate the heat fluxes over heterogeneous landscapes if the land surface can be classified into n categories according to the surface characteristics (Figure 3.3).

- *The first* is to use satellite measurements and *assumptions* on the Surface Layer (SL) nearby the surface (e.g. 2 m), which is called **RS approach** (RS+SL-assumptions)
- *The second* is to use satellite measurements and SL observations, which called **Tile approach** (RS+SL-observations).
- *The third* is to use satellite measurements in combination with SL and ABL observations, which called **Blending height approach** (RS+SL-observations+ABL-observations).

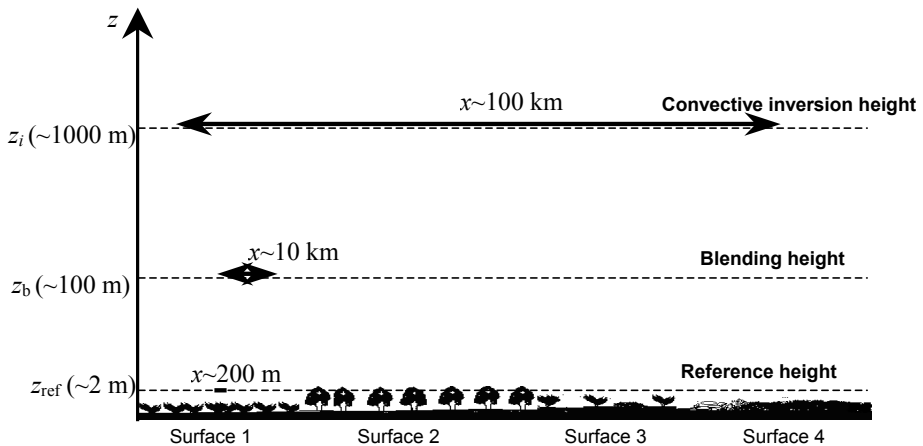


Figure 3.3 Different approaches at three different scales. z_i is the convective inversion height, z_b is the blending height, z is the reference height nearby the surface and x is the footprint .

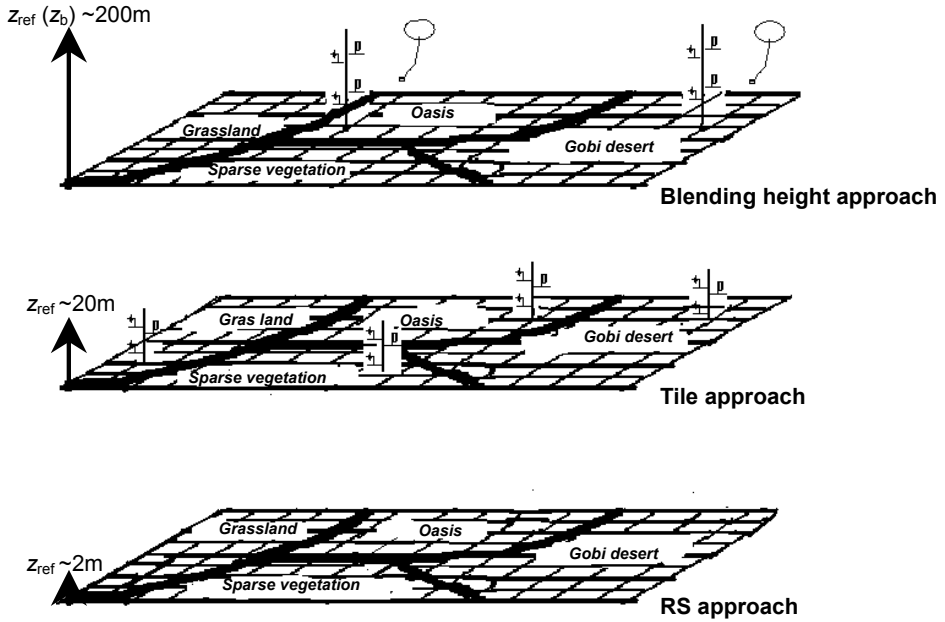


Figure 3.4 Conceptual scheme of the *RS approach*, the *Tile approach* and the *Blending height approach*. The variable z_{ref} denotes reference height.

In the *RS approach*, surface albedo-surface reflectance r_0 , surface temperature T_0 , surface emissivity ϵ_0 and Normalized Difference Vegetation Index (*NDVI*) at the surface can be derived from satellite measurements (Figure 3.4). It also takes the reference height nearby the surface (e.g. 2m), full adjustment occurs above the overlying new land surface in a time around $4z_{\text{ref}}/w_*$. It means that the air flow adjusts to the new surface properties very quickly, i.e. during the time the air mass nearby the surface moves with the averaged wind speed, U , through a distance $4Uz_{\text{ref}}/w_*$. For example, $U=3\text{ m s}^{-1}$ and the convective velocity scale, $w_*=1\text{ m s}^{-1}$ as a typical value at 10 o'clock of the local time, therefore, the full adjustment time is about 8 s and the full adjustment distance is about 24 m. This distance is equal and like the satellite pixel size.

Hence, the values of atmospheric variables (air temperature T_a and specific humidity q at the reference height, zero-plane displacement d_0 , aerodynamic roughness length z_{0m} , thermodynamic roughness length z_{0h} and the excess resistance to heat transfer kB^{-1}) above each satellite pixel should be used when surface heat fluxes are estimated. It means that the *RS approach* needs many measurements at each satellite pixel. But it is difficult to determine these values at each satellite pixel. Therefore, assumptions and approximations

were involved in the approach.

In the *Tile approach* (Figures 3.4 and 3.5), taking the reference height z_{ref} on SL (e.g. 20 m), full adjustment occurs above the overlying new land surface in a time around $4z_{\text{ref}}/w_*$. It means that during the time the air mass in the surface layer moves with the averaged wind speed, U , through a distance $4Uz_{\text{ref}}/w_*$. For example, $U=4\text{ m s}^{-1}$ and the convective velocity scale, $w_* = 1\text{ m s}^{-1}$ as a typical value at 10 o'clock of the local time, therefore, the full adjustment time is about 80 s and the *full adjustment distance* on the new surface is about 320 m. The new surface can be considered as a *tile* if it is homogeneous, and only one resistance can be used above it. In other words, the *tile* is a linear combination of the *full adjusted distance*.

Then, using the satellite measurements at the surface and the Surface Layer (SL) observations on a *tile* at and below the reference height, the heat fluxes over a heterogeneous landscape can be estimated.

- *Firstly*, surface reflectance r_0 , surface temperature T_0 , surface emissivity ϵ_0 , Normalized Difference Vegetation Index (*NDVI*), Modified Soil Adjusted Vegetation (*MSAVI*), vegetation fractional cover P_v , Leaf Area Index (*LAI*) at the surface are derived from satellite measurements.
- *Secondly*, SL observations on a *tile*: wind speed u , air temperature T_a and specific humidity q at the reference height. Zero-plane displacement d_0 , aerodynamic roughness length z_{0m} , thermodynamic roughness length z_{0h} and the excess resistance to heat transfer kB^{-1} and the like in SL below the reference height over the *i-tile* are used to estimate the sensible heat flux H and the latent heat flux λE .

Hence, in mathematical terms:

$$\begin{aligned}
 H_1(x, y) &= \rho c_p k^2 u_1 \frac{[T_0(x, y) - T_{a1}]}{r_{ah1}}, & \lambda E_1(x, y) &= \frac{\rho c_p}{\gamma} \frac{[e_0(x, y) - e_{a1}]}{r_{ae1}} \\
 H_2(x, y) &= \rho c_p k^2 u_2 \frac{[T_0(x, y) - T_{a1}]}{r_{ah2}}, & \lambda E_2(x, y) &= \frac{\rho c_p}{\gamma} \frac{[e_0(x, y) - e_{a2}]}{r_{ae2}} \quad (\text{Wm}^{-2}) \quad (3.18) \\
 & \dots & \dots & \\
 H_n(x, y) &= \rho c_p k^2 u_n \frac{[T_0(x, y) - T_{an}]}{r_{ahn}}, & \lambda E_n(x, y) &= \frac{\rho c_p}{\gamma} \frac{[e_0(x, y) - e_{an}]}{r_{aen}}
 \end{aligned}$$

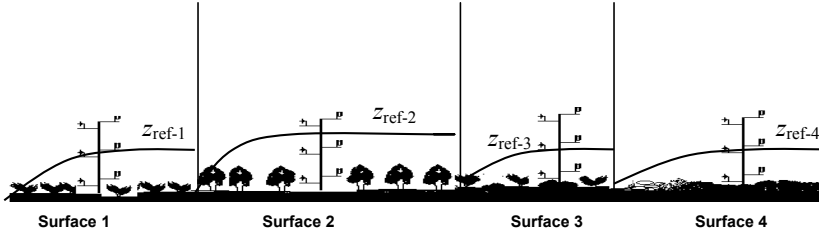


Figure 3.5 The diagrammatic sketch of the *Tile approach* using the observed data and the derived parameters from the ABL measurements at (and below) the reference height nearby the surface and satellite measurements at the surface to estimate the surface heat fluxes. $z_{\text{ref-1}}$, $z_{\text{ref-2}}$, $z_{\text{ref-3}}$ and $z_{\text{ref-4}}$ are the reference height nearby the surface.

where γ is the psychrometric constant, e_0 is the vapor pressure at the surface, e_a is air vapor pressure at the reference height, r_{ah} is aerodynamic resistance for heat between land surface and reference height, and r_{ae} is aerodynamic resistance for vapor transfer between land surface and reference height. Therefore, H and λE over whole area can be derived from Eq.3.17 as

$$H(x, y) = \sum_{i=1}^n a(i)H_i(x, y), \quad \lambda E(x, y) = \sum_{i=1}^n a(i)\lambda E_i(x, y) \quad (\text{Wm}^{-2}) \quad (3.19)$$

where $a(i)$ is the fractional ratio of each *tile*.

In the *Blending height approach* (Figures 3.4 and 3.6), taking the blending height z_b as the reference height, full adjustment occurs above the overlying new land surface in a time around $4z_b/w_*$. During the time the air mass below z_b moves with the averaged wind speed, U , through a full adjustment distance $4Uz_b/w_*$. It means that after a time $t = 4z_b/w_*$, the atmospheric characteristics variables (u , T_a and q) at and above z_b will become well mixed (uniform) horizontally around the distance scale $4Uz_b/w_*$. For example, the blending height z_b is about 300 m, $U = 5 \text{ m s}^{-1}$ and the convective velocity scale $w_* = 1 \text{ m s}^{-1}$ as a typical value at 10 o'clock of the local time, therefore, the full adjustment time is about 20 minutes and the *full adjusted distance* on the new surface is about 6.0 km. If the new surface is homogeneous and its length scale being larger than the *full adjusted distance* (e.g. 6.0km), it can be considered as a linear combination of the *full adjusted distance*. One resistance can

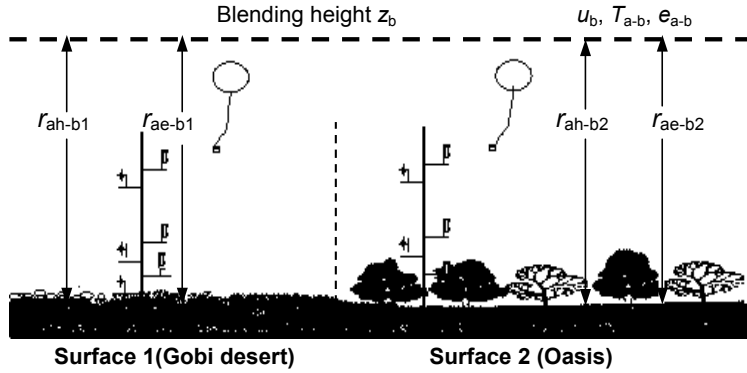


Figure 3.6 Diagrammatic sketch of the *Blending height approach* using satellite measurements at the surface in combination with SL and ABL observations to estimate the heat fluxes. The physical variables r_{ah-b1} and r_{ah-b2} denote the aerodynamic resistances for *heat* between land surface and the blending height; r_{ae-b1} and r_{ae-b2} denote the aerodynamic resistances for *vapour* transfer between land surface and the blending height.

be used above the new land surface (Figure 3.6).

Then, using the satellite measurements at the surface and the ABL observations at the blending height, the heat fluxes over a heterogeneous landscape can be estimated. In other words, using data observed from radio sounding system (or Wind Profiler and RASS, or tethered sonde system), the profiles of u , T_a and q over the different land surface (e.g. over the very different surface, oasis and Gobi desert in Figures 3.4 and 3.6) can be analyzed, and z_b can be determined when the effects of individual different surface on vertical profiles become horizontally blended, and at the same time, the atmospheric characteristics variables (u , T_a and q) at z_b can be obtained. If r_0 , T_0 , ϵ_0 , $NDVI$, LAI , P_v and $MSAVI$ at the surface can also be derived from the satellite measurement on each pixel, and effective atmospheric variables (e.g. effective aerodynamic roughness length, effective thermodynamic roughness length, effective zero-plane displacement and effective excess resistance to heat transfer) in the atmospheric layer below z_b have already been determined by using SL and ABL observations, then, the regional H and λE over heterogeneous landscape can be determined as:

$$H_1(x, y) = \rho c_p k^2 u_b \frac{[T_0(x, y) - T_{a-b}]}{r_{ah-b1}}, \quad \lambda E_1(x, y) = \frac{\rho c_p [e_0(x, y) - e_{a-b}]}{\gamma r_{ae-b1}}$$

$$H_2(x, y) = \rho c_p k^2 u_b \frac{[T_0(x, y) - T_{a-b}]}{r_{ah-b2}}, \quad \lambda E_2(x, y) = \frac{\rho c_p [e_0(x, y) - e_{a-b}]}{\gamma r_{ae-b2}} \quad (\text{Wm}^{-2}) \quad (3.20)$$

... ..

$$H_n(x, y) = \rho c_p k^2 u_b \frac{[T_0(x, y) - T_{a-b}]}{r_{ah-bn}}, \quad \lambda E_n(x, y) = \frac{\rho c_p [e_0(x, y) - e_{a-b}]}{\gamma r_{ae-bn}}$$

where u_b , T_{a-b} and e_{a-b} are wind speed, air temperature and air vapor pressure at z_b respectively, r_{ah-b1} , r_{ah-b2} , ..., r_{ah-bn} are the aerodynamic resistances for heat between land surfaces and z_b , and r_{ae-b1} , r_{ae-b2} , ..., r_{ae-bn} are the aerodynamic resistances for vapor transfer between land surfaces and z_b . The resistances r_{ah-b1} , r_{ah-b2} , ..., r_{ah-bn} and r_{ae-b1} , r_{ae-b2} , ..., r_{ae-bn} can be defined as:

$$r_{ah-b1} = \int_0^{z_b} \frac{1}{K_{h1}(z)} dz, \quad r_{ah-b2} = \int_0^{z_b} \frac{1}{K_{h2}(z)} dz, \quad \dots, \quad r_{ah-bn} = \int_0^{z_b} \frac{1}{K_{hn}(z)} dz \quad (\text{s m}^{-1}) \quad (3.21)$$

$$r_{ae-b1} = \int_0^{z_b} \frac{1}{K_{e1}(z)} dz, \quad r_{ae-b2} = \int_0^{z_b} \frac{1}{K_{e2}(z)} dz, \quad \dots, \quad r_{ae-bn} = \int_0^{z_b} \frac{1}{K_{en}(z)} dz, \quad (\text{s m}^{-1}) \quad (3.22)$$

where K_{h1} , K_{h2} , ..., K_{hn} are the eddy diffusion coefficients for heat transport, K_{e1} , K_{e2} , ..., K_{en} are the eddy diffusion coefficients for vapour transport. Hence, H and λE over whole area can be derived from Eq.3.17 as

$$H(x, y) = \sum_{i=1}^n a(i) H_i(x, y) = \rho c_p k^2 u_b [T_0(x, y) - T_{a-b}] \sum_{i=1}^n a(i) \frac{1}{r_{ah-bi}} \quad (\text{Wm}^{-2}) \quad (3.23)$$

$$\lambda E(x, y) = \sum_{i=1}^n a(i) \lambda E_i(x, y) = \frac{\rho c_p}{\gamma} [e_0(x, y) - e_{a-b}] \sum_{i=1}^n a(i) \frac{1}{r_{ae-bi}} \quad (\text{Wm}^{-2}) \quad (3.24)$$

where $a(i)$ is the fractional ratio of each land cover type. r_{ah-bi} is the aerodynamic resistance

for heat between land surfaces and z_b over land cover type i , and r_{ae-bi} is the aerodynamic resistances for vapor transfer between land surfaces and z_b over land cover type i .

3.7 Summary and conclusions

Based on the analysis of the land surface heterogeneity and its influences on the overlying air flow and the observations in the Surface Layer (SL) and the Atmospheric Boundary Layer (ABL), the parameterization methodologies of heat fluxes in the layers overlying a heterogeneous surface were established. The procedure and characteristics of the parameterization given in the previous sections can be summarized as follows.

- The length scales of land surface heterogeneity can be classified to micro-scale, meso-scale and macro-scale by using two dynamic time-scales (the mixing time-scale and the entrainment time scale). Each length has different characteristics.
- Characteristics of the ABL over heterogeneous landscape can be described by a slab ABL model, two important ABL time scales (the dynamical time scale $t_d = h_{ABL} / w_*$ and the time for thermodynamic adjustment of the ABL to changes in the surface energy balance t_q) and the air flow change feature.
- Blending height z_b is defined as a scale height for turbulent flow above a heterogeneous surface, at which the influences of individual surface patches on vertical profiles or fluxes become horizontally blended. Not only Eq.3.8 and Eq.3.9 but also Eq.3.13 and Eq.3.14 can be used to estimate z_b .
- Based on the scalar conservation equation, generic constraints over heterogeneous land surface have been established to define larger-scale surface properties from their smaller-scale counterparts. Eq.3.17 can be applied to net fluxes of conserved scalars, in particular, sensible heat flux f_H , latent heat flux f_E and their sum $f_A = f_H + f_E$, the available energy flux. Eq.3.17 can also be applied to net irradiances (quantum fluxes) in any spectral waveband.
- Based on the analysis of the land surface heterogeneity and its influences on the overlying air flow, the blending height assumption, satellite measurements, SL and ABL observations, three parameterization methodologies, which are called *RS approach*, *Tile approach* and *Blending height approach* (Figure 3.4) have been developed to estimate the heat fluxes over heterogeneous landscapes. The *RS approach* uses satellite measurements and assumptions on the Surface Layer (SL) nearby the surface. The *Tile approach* (Figures 3.4 and 3.5) uses satellite measurements and SL observations when

the length scales of land surface heterogeneity are relatively small. In other words, the sensible heat flux and latent heat flux can be calculated from Eq.3.18 and Eq.3.19. *The Blending height approach* uses satellite measurements in combination with SL and ABL observations when the length scales of land surface heterogeneity are relatively larger. In other words, the sensible heat flux and latent heat flux can be calculated from Eqs.3.20, 3.23 and 3.24.

4. Descriptions of land surface processes experiments and satellite data

Five land surface processes experiments were performed in the west part of China in the past years. They were the Global Energy and Water cycle EXperiment (GEWEX) Asian Monsoon Experiment on the Tibetan Plateau (GAME/Tibet), the Coordinated Enhanced Observing Period (CEOP) Asia-Australia Monsoon Project on the Tibetan Plateau (CAMP/Tibet), the HEIhe basin Field Experiment (HEIFE), the Arid Environment Comprehensive Monitoring Plan, 95 (AECMP'95) and the DunHuang EXperiment (DHEX). These experiments can be used to validate the theory and approaches presented in Chapter 2 and Chapter 3 due to the heterogeneity of the land surfaces. The experiments and the data collected during these experimental periods are firstly described.

Landsat-5 Thematic Mapper (TM) data, Landsat-7 Enhanced Thematic Mapper (ETM) data and NOAA-14 Advanced Very High Resolution Radiometer (AVHRR) data will also be described.

4.1 Global Energy and Water cycle EXperiment Asian Monsoon Experiment on the Tibetan Plateau (GAME/Tibet) and Coordinated Enhanced Observing Period Asia-Australia Monsoon Project on the Tibetan Plateau (CAMP/Tibet)

The energy and water cycle over the Tibetan Plateau play an important role in the Asian Monsoon system, which in turn are major components of the energy and water cycles of the global climate system. The Tibetan Plateau contains the world's highest elevation (average elevation about 4000 m) relief features, some reaching into the mid-troposphere. It represents an extensive massif extending from sub-tropical to middle latitudes and spanning over 25 degrees of longitude. Due to its topographic character, the plateau surface absorbs a large amount of solar radiation energy (much of which is redistributed by cryospheric processes), and undergoes dramatic seasonal changes of surface heat and water fluxes (e.g. Ye and Gao, 1979; Yanai, 1992).

The lack of quantitative understanding of the interactions between the land surface and the atmosphere makes it difficult to understand the complete energy and water cycle over the Tibetan Plateau and its effect on the Asian Monsoon system (Webster et al., 1998). Therefore, due to heterogeneous nature of the land surface and the different climate features of the plateau (Shi and Smith, 1992) and the relatively few ground-based observational

stations deployed over the plateau, a meso-scale monitoring system should be developed and validated.

4.1.1 The GAME/Tibet experiment

The overall goal of the GAME/Tibet was to clarify the interaction between the land surface and the atmosphere over the Tibetan Plateau in the context of the Asian monsoon system. To achieve this goal, the scientific objectives of this experiment were to improve the quantitative understanding of land-atmosphere interactions over the Tibetan Plateau, to develop process models and methods for applying them over large spatial scales, and to develop and validate satellite-based retrieval methods. The GAME/Tibet was an inter-disciplinary, coordinated effort by field scientists, modelers and remote sensing scientists in meteorology and hydrology (e.g. Ma et al., 2000; Tanaka et al., 2001; Ma et al., 2002d; Ma et al., 2003a; Ma et al., 2005).

Figure 4.1 and Figure 4.2 show the sites layout during the intensive observation period (May to September, 1998) of the GAME/Tibet. A meso-scale observational network (150 km×250 km, 91°-92.5°E, 30.5°-33°N) was implemented on the central plateau:

- Amdo Atmospheric Boundary Layer (ABL) station (91°37'30"E, 32°14'28"N, elevation: 4700 m). A basic PBL tower (17 m, wind speed, wind direction, air temperature and humidity at three-levels), a radiation observational system, turbulent flux measurements (sonic anemo-thermometer), soil temperature and moisture measurement, radio sonde observation system etc. have been set up in this station.
- Automatic Weather Station (AWS) networks. Five AWSs (D66, TTH, Naqu, D110, MS3608) and two sets of Portable Automated Meso-net (PAM) stations (MS3478-NPAM and MS3637-SPAM) have been deployed along the Tibetan (Qinghai-Xizang) high way.
- A basic ABL observational station (NaquFx). A PBL tower (3.5 m, four-levels), a radiation observational system, turbulent flux measurements (sonic anemo-thermometer), soil temperature, moisture measurement and soil water content have been set up in this station in 1998.
- Barometer network (nine sites: Amdo, AQB, Naqu, Noda, North-mt, South-mt, Sexi, Ziri, Wadd), ground truth observation sites for validation of satellite data and a sampling network for isotope studies on the water cycle.

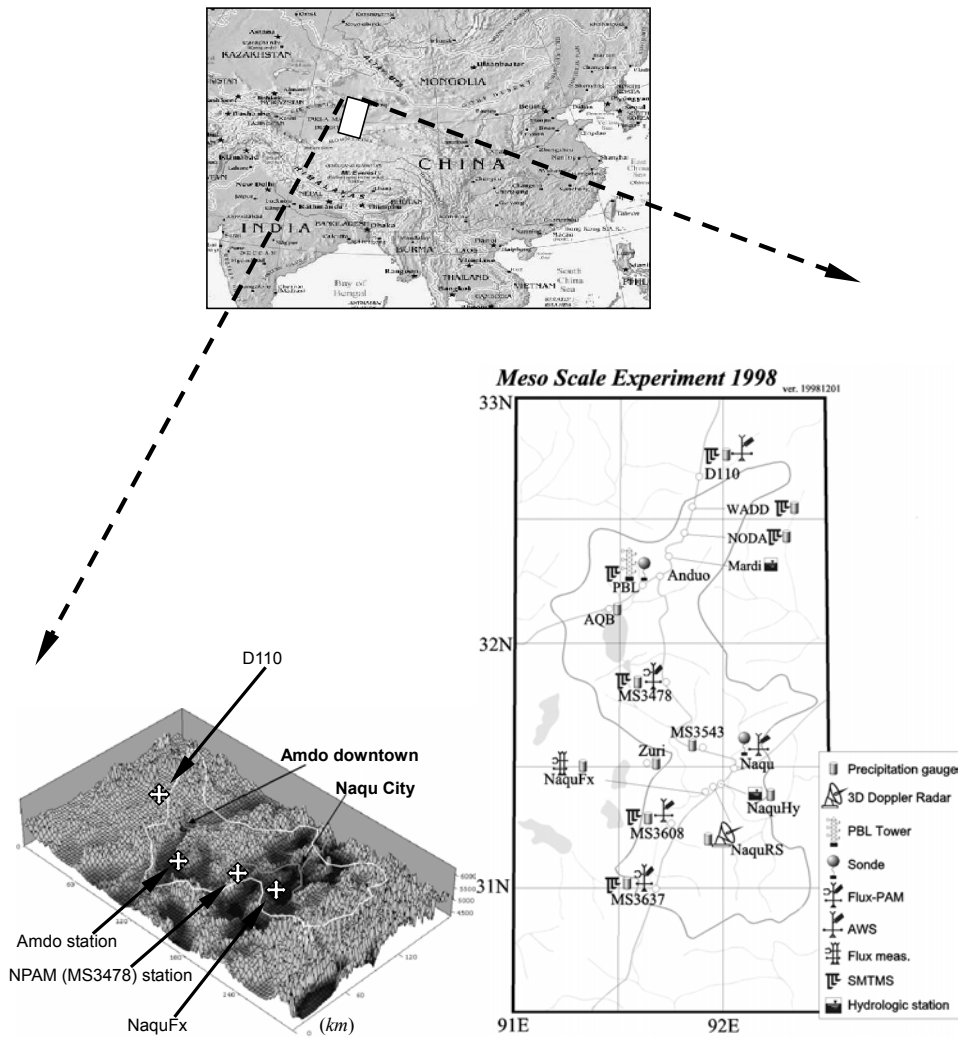


Figure 4.1 The geographic map and the sites layout during the Global Energy and Water cycle EXperiment Asian Monsoon Experiment on the Tibetan Plateau (GAME/Tibet).

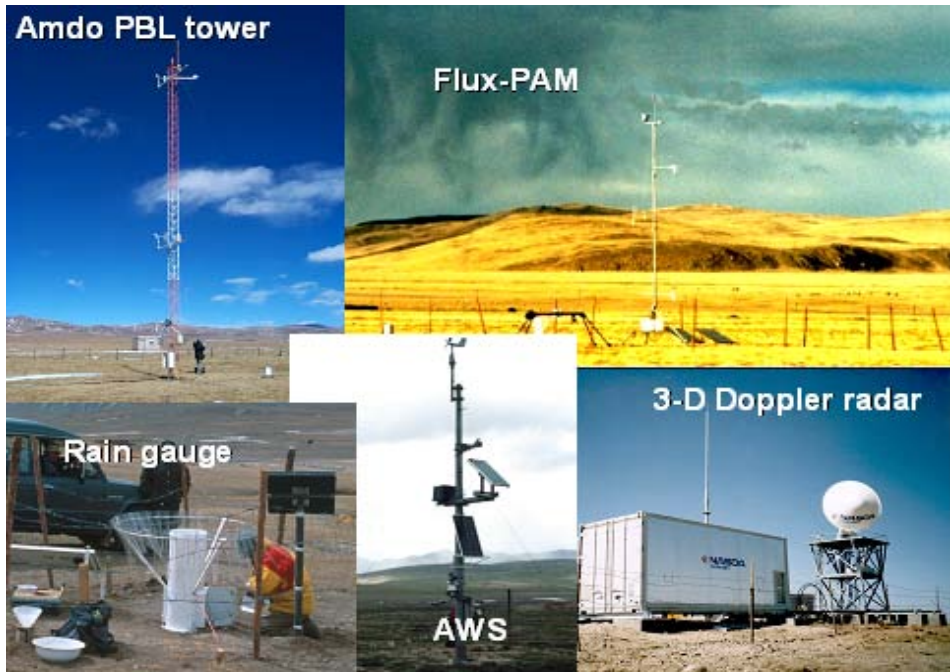


Figure 4.2 Land surface condition and instruments in the stations of the Global Energy and Water cycle EXperiment Asian Monsoon Experiment on the Tibetan Plateau (GAME/Tibet).

- Soil temperature and soil moisture (SMTMS) network. Nine of these sites (D66, TTH, D110, WADD, NODA, Amdo, MS3478, MS3608 and MS3637) have been deployed along the Tibetan highway.
- Three-dimensional Doppler radar and precipitation gauge network. The Doppler radar system has been deployed about 10 km south of Naqu in 1998 ($91^{\circ}56'20''\text{E}$, $31^{\circ}22'59''\text{N}$). Seven rain gauges were set up around the radar station.
- A precipitation gauge net (D110, WADD, NODA, AQB, MS3478, MS3543, Zuri, NaquFx, MS3608, Naquhy, NaquRS and MS3637) has been deployed along the Tibetan highway.
- Two radio-sonde observational systems were set up in the Amdo ABL station and Naqu Meteorological Bureau.

4.1.2 The CAMP/Tibet experiment

The objectives of the CAMP/Tibet were the following:

- Quantitative understanding of an entire seasonal hydro-meteorological cycle including winter processes by solving surface energy "imbalance" problems in the Tibetan Plateau.
- Observation of local circulation and evaluation of its impact on plateau scale water and energy cycle.
- Establishment of quantitative observational methods for entire water and energy cycle between land surface and atmosphere by using satellites.

To achieve the scientific objectives of the CAMP/Tibet, a meso-scale observational network (150×250 km, 91°-92.5°E, 30.7°-33.3°N) has been implemented in the central plateau (see Figure 4.3 and Figure 4.4):

- A basic observational station (BuJiao-BJ). A flux measuring tower (20 m, two levels), a Sky Radiometer, a LIDAR system, a Wind Profiler and Radio Acoustic Sounding System (RASS), a radio sonde system, and 4 Automatic Weather Stations have been set up at this station.
- AWS networks. Six AWSs (D105, D110, MS3478, BJ, MS3608 and ANNI) stations have been deployed in this area; Soil moisture and soil temperature networks.
- Soil moisture and soil temperature networks. Seven of these sites (D105, D110, Amdo, BJ, MS3608, ANNI and MS3637) have been deployed in this area.
- Two deep soil temperature measurements were put in D105 and NaquDS (nearby the BJ basic station).
- Amdo ABL station (91°37'30"E, 32°14'28"N). A basic PBL tower (17 m, wind speed, wind direction, air temperature and humidity at three-levels) and radiation observational system have already been continued for 8 years from 1997 and will be continued till the end of 2010.

The enhanced automated observing period and the intensive observation period of the CAMP/Tibet have been started from October 1, 2002 and ended in September 30, 2004.

A large amount of data has been collected during the GAME/Tibet and the CAMP/Tibet, which was the best data set so far for the study of the Tibetan Plateau hydrometeorology (Ma et al., 2005; Table 4.1, Table 4.2).

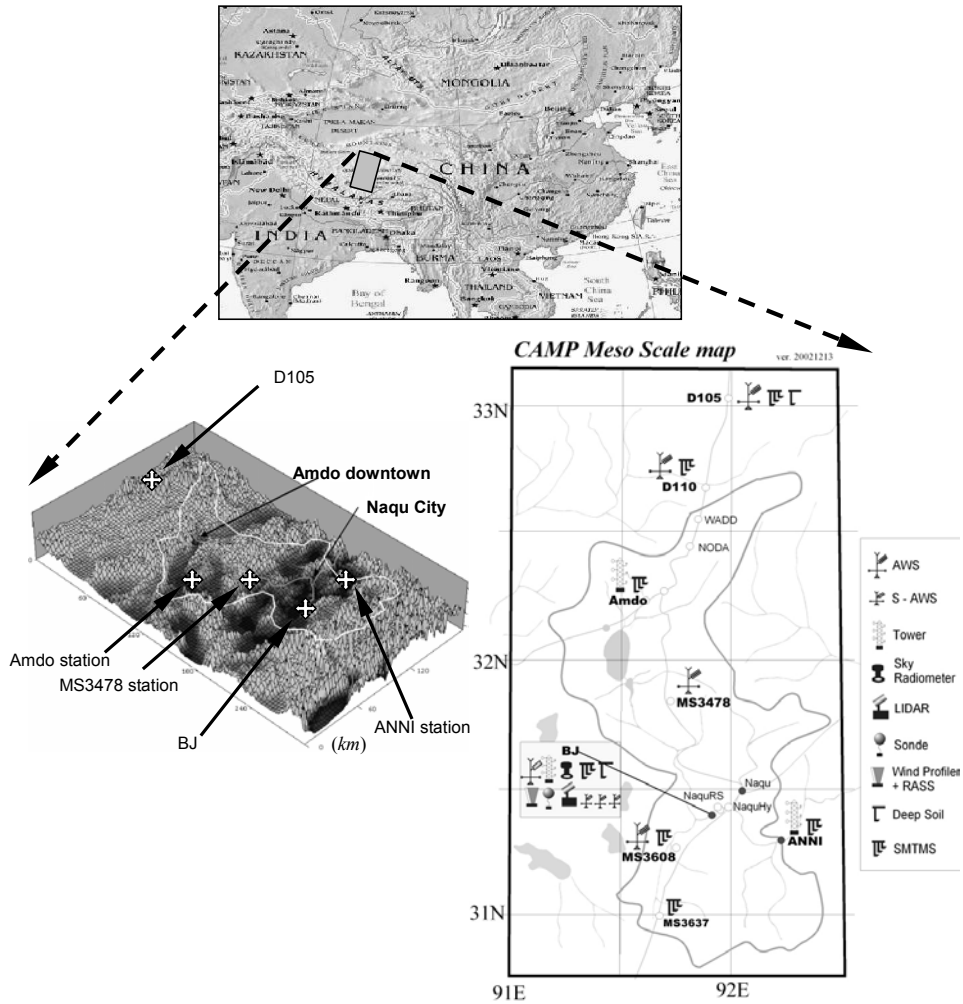


Figure 4.3 The geographic map and the sites layout during the Coordinated Enhanced Observing Period (CEOP) Asia-Australia Monsoon Project on the Tibetan Plateau (CAMP/Tibet).



Figure 4.4 Land surface condition and instruments in the stations of the Coordinated Enhanced Observing Period (CEOP) Asia-Australia Monsoon Project on the Tibetan Plateau (CAMP/Tibet).

Table 4.1 The collected field data of the Global Energy and Water cycle EXperiment Asian Monsoon Experiment on the Tibetan Plateau (GAME/Tibet) over the period 1 May 1998 to 30 August 1998.

Station (site)	Observation item
Amdo	<ul style="list-style-type: none"> ● Tower: wind speed, wind direction, air temperature and humidity (height (m): 1.5, 6.5 and 14.0), surface temperature, soil temperature (depth (cm): -5, -10, and -20), soil heat flux(depth (cm):-10 and -20), solar radiation ,air pressure, rain intensity. ● Radiation: short wave radiation (downward and upward), long wave radiation (downward and upward). ● Turbulence: wind speed, wind direction, air temperature, relative humidity, the characteristic length scales of surface layer (u, T, q), sensible heat flux, latent heat flux, stability parameter.
Automatic Weather Station (D66, Tuotuohe, D110, Naqu, MS3608)	Wind speed, wind direction, air temperature and humidity, surface temperature, soil temperature, soil moisture, solar radiation, air pressure.
Portable Automated Mesonet (MS3437-SPAM, MS3478-NPAM)	Wind speed, wind direction (9.8m), air temperature and humidity (height (m):7.8 and 2.3), short wave radiation(downward and upward, long wave radiation (downward and upward), net radiation, air pressure, turbulent fluxes (5.6m), surface temperature, stability parameter, snow depth, precipitation, soil heat flux (-1cm), soil temperature(depth (cm): -4, -20, -40, -60, -100, -160, -188), soil moisture (depth (cm): -4, -20, -40, -60, -100, -160m, -188).
Soil moisture and soil temperature system (D66, Tuotuohe, D110, MS3608, Amdo, NODA, WADD, MS3478, MS3637)	<ul style="list-style-type: none"> ● Soil temperature (depth (cm)): -4, -20, -60, -100, -160, -258. ● Soil moisture (depth (cm)): -4, -20, -40, -60, -80, -100, -130, -160, -200.
Naqu flux	<ul style="list-style-type: none"> ● Fast response measurement (sonic anemometer): wind velocity, air temperature, absolute humidity fluctuation, frictional velocity, sensible heat flux, latent heat flux ● Short-wave radiation (downward and upward), long wave radiation (downward and upward) ● Soil heat flux(-5cm), soil temperature(depth (m): -1.5 and -4), soil water content(0—15cm layer) ● Tower (3.5 m): wind speed ((height (m): 0.7, 1.3, 2.2, 3.5), wind direction(3.5 m) ,air temperature and humidity((height (m): 1.3 and 3.5)
Radar	Radar reflectivity, Doppler velocity, spectral width, wind speed, wind direction, air temperature
Radio-sonde	Profile of air pressure, air temperature, relative humidity , wind speed and direction
Barometer network (Amdo, AQB, Naqu, Noda, North-mt, South-mt, Sexi, Ziri, Wadd)	Air pressure

Table 4.2 The collected field data of the Coordinated Enhanced Observing Period (CEOP) Asia-Australia Monsoon Project on the Tibetan Plateau (CAMP/Tibet) over the period 1 October 2002 to 30 September 2004.

Station (site)	Observation item
Amdo	<ul style="list-style-type: none"> ● PBL tower: wind speed, wind direction, air temperature and humidity (height (m): 1.5, 6.5 and 14.0), surface temperature, soil temperature(depth (cm): -5, -10 and -20), soil heat flux (depth (cm): -10 and -20), solar radiation ,air pressure, rain intensity ● Radiation: short wave radiation (downward and upward), long wave radiation (downward and upward)
Automatic Weather Station (D66, Tuotuohe, D110, MS3608)	Wind speed, wind direction, air temperature and humidity, surface temperature, soil temperature, soil moisture, solar radiation, air pressure
Automatic Weather Station (D105, MS3478, BJ, ANNI)	Wind speed (height (m): 10, 5, 0.5), wind direction (10m), air temperature and humidity (height (m): 9.5, 2, 0.5), short-wave radiation(downward and upward), long wave radiation (downward and upward), air pressure, surface temperature, snow depth, precipitation, soil heat flux (depth (cm):-10, -20), soil temperature (depth (cm): 0, 0, -4, -10, -20, -40), soil moisture (depth (cm): -4, -20)
Soil moisture and soil temperature system (D66, Tuotuohe, D105, D110, MS3608, Amdo, NODA, WADD, MS3637, ANNI)	<ul style="list-style-type: none"> ● Soil temperature (depth (cm)):-4, -20, -60, -80, -100, -130, -160, -200, -279. ● Soil moisture (depth (cm)): -4, -20, -60, -100, -160, -258.
Turbulent measurement (BJ, ANNI)	Wind speed, wind direction, air temperature, relative humidity, the characteristic length scales of surface layer (u_s, T_s, q_s), sensible heat flux, latent heat flux, stability parameter, CO ₂ flux
Wind Profiler+RASS (BJ, Naqu)	Profile of air temperature, wind speed and direction
Radio-sonde (BJ)	Profile of air pressure, air temperature, relative humidity, wind speed and direction

4.2 HEIhe basin Field Experiment (HEIFE)

HEIFE was an experiment on atmosphere-land surface interactions in the Heihe River Basin in the Hexi Corridor, Gansu Province, northwestern China. It was carried out from 1989 through 1993. It was a Sino-Japanese cooperative investigation program supported by the Chinese Academy of Sciences, the National Natural Science Foundation of China and the Japanese Ministry of Education, Sports and Culture.

The experimental sites of the HEIFE were an area of 70 km × 90 km in the Heihe River Basin with an average elevation of 1500m above sea level. During the experiment period, five basic micrometeorological stations (Linze, Zhangye, Huayin, Pingcuan and Desert), five AWSs and four ground water level stations were operated separately in the oasis and Gobi with distinct underlying surfaces. Each basic micrometeorological station included a PBL tower, which is 20 m high (one was 40 m high with 10 levels in the Linze oasis), with six levels to measure air temperature, humidity, wind velocity and wind direction (only at 10 m level), and also included radiation components of short-wave incoming radiation flux, reflective radiation flux, long-wave incoming radiation flux, outgoing radiation flux and net radiation flux. At the same time, the ground surface temperature and soil temperature at 5 layer depths below the surface and soil heat flux at 2 layer depths were measured at each basic station. Moreover, the meteorological data from three routine weather stations, the surface runoff and the sub-surface hydrological data from three routine hydrological stations in the experimental area were collected for providing the background materials (see Figure 4.5b and Figure 4.6).

The investigations of the HEIFE consisted of six special subjects:

- 1) Observation of the turbulent fluxes in the surface layer and structure of the planetary boundary layer;
- 2) Observation of the surface radiation budget and radiation physical characteristics;
- 3) Observation of the surface evaporation and water budget in the experimental area;
- 4) Bulk data collection, reorganization and analysis;
- 5) Numerical modeling of planetary boundary layer;
- 6) Study of the amount of water required for crops and techniques of economical water irrigation in HEIFE area.

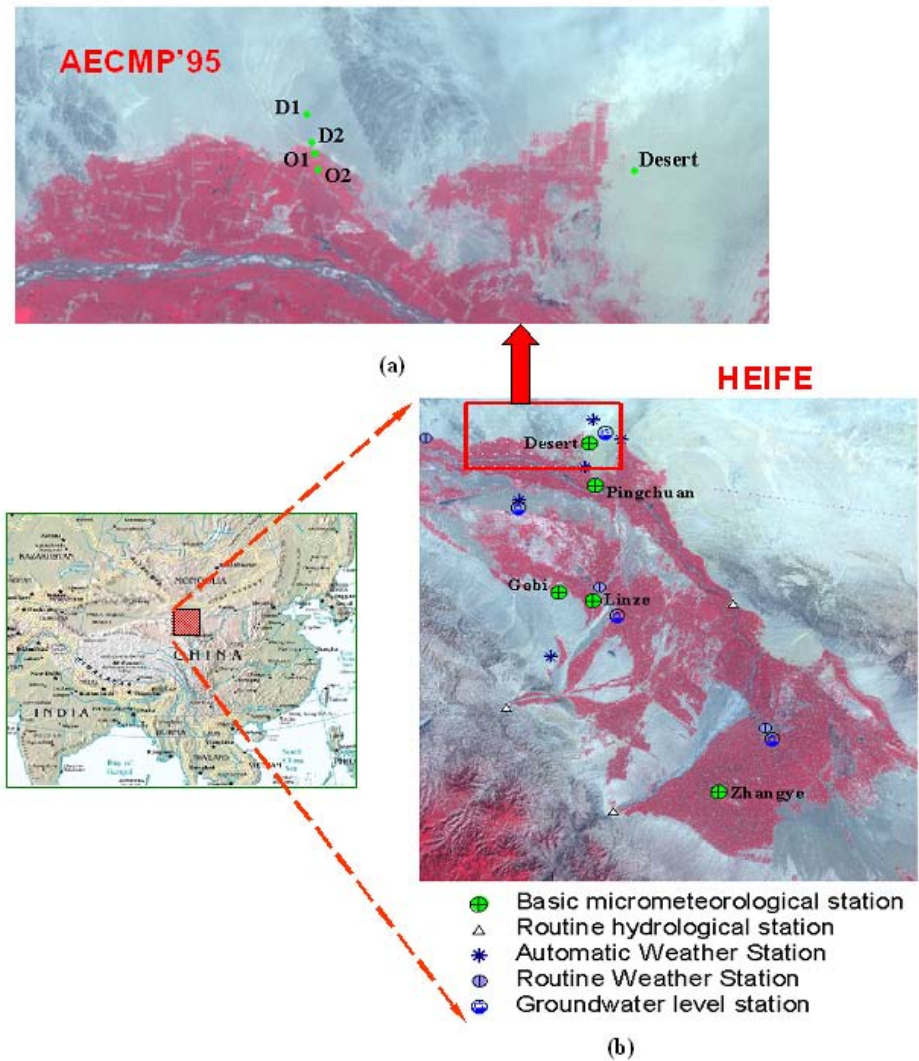


Figure 4.5 The sites layout during intensive observation period of a) Arid Environment Comprehensive Monitoring Plan, 95 (AECMP'95) and b) HEIhe basin Field Experiment (HEIFE), the red part is oasis or irrigated farm and the others are Gobi desert.

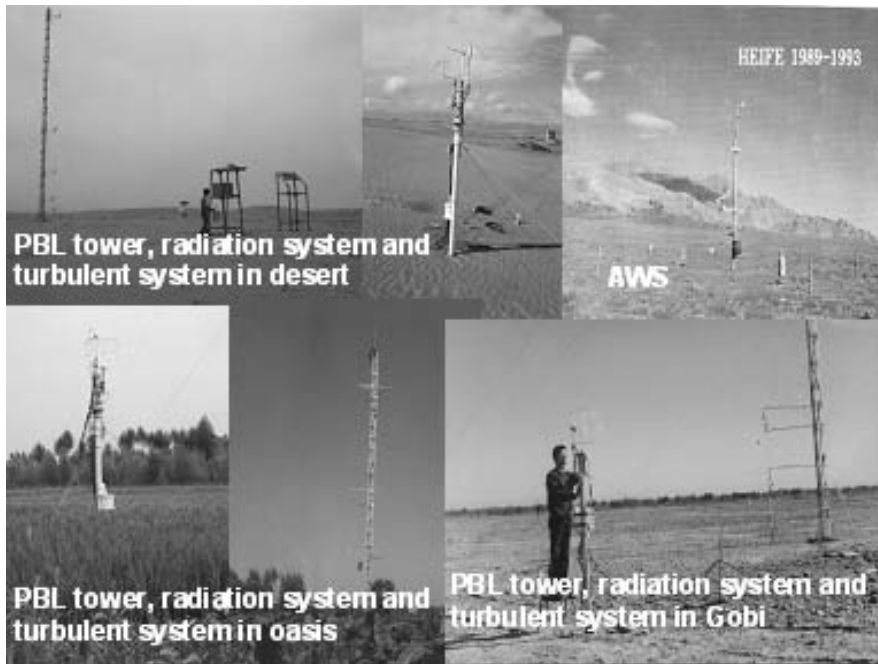


Figure 4.6 Land surface condition and instruments in the stations of the HEIhe basin Field Experiment (HEIFE) and the Arid Environment Comprehensive Monitoring Plan, 95 (AECMP'95).

The schedule of ground observations of the HEIFE was divided in the following types.

- Pilot observing period in September 1988.
- Formal observing period from June 1990 to October 1991 in which the basic stations and the automatic weather stations were operated and some data were collected from the routine weather stations and the routine hydrological stations.
- Four Intensive Observation Periods (IOP), which were separately in 16-30 April (IOP-1), 1-31 August (IOP-2), 1-10 October (IOP-3) and December 1991 (IOP-4). The IOP-1 represents spring in growth stage. The IOP-2 and IOP-3 represent the mature period and the end of the growing season. The IOP-4 represents the winter. The IOP-2 and IOP-3 added the observations about the turbulence with the sonic anemo-thermometers and infrared hygrometers and the planetary boundary layer structure with tethered balloons. Doppler sodars and low-level radiosonde over the distinct underlying surfaces separately in the oasis, desert and Gobi observational sites.

Table 4.3 The collected field data of HEIhe basin Field Experiment (HEIFE).

Content	Station	Observation period	Observation item
PBL tower	Linze (oasis, 40 m)	Jan.1, 1991- Dec.15, 1991	Wind speed, air temperature and humidity (Linze, height (m): 1, 2, 4, 6, 10, 15, 20, 25, 30 and 40; the others, height (m): 0.5, 1, 2, 4, 8 and 16), wind direction (10 m), surface temperature and soil temperature (depth (cm): -5 and -10), soil heat flux (depth (cm):-5 and -10)
	Huayin (Gobi, 20 m)	Jan.1 ,1991- Dec.15, 1991	
	Desert (20 m)	Sep.26, 1990-Jul.17, 1992	
	Zhangye (oasis, 20 m)	Oct.1, 1990-Agu.14, 1992	
	Pingcuan (shrub, 20 m)	oct.1, 1990-Agu.14, 1992	
Radiation	Linze (oasis)	Jan.1, 1991- Dec.15, 1991	Downward (upward) short wave radiation; downward (upward) long wave radiation; soil heat flux; net radiation
	Huayin (Gobi)	Jan.1 ,1991- Dec.15, 1991	
	Desert	Sep.27, 1990-Aug.17,1992	
	Zhangye (oasis)	Oct.1, 1990-Agu.14, 1992	
Automatic Weather Station (AWS)	011 (dsert)	Jun.18, 1991-Jul.1, 1992	Wind speed and wind direction, air temperature and humidity, surface temperature, soil temperature, soil moisture, solar radiation
	012 (Gobi)	Jun.18, 1991-Jul.2, 1992	
	013 (Gobi)	Jun.18, 1991-Jul.1, 1992	
	014 (transitional area)	Jun.18, 1991-Jul.5, 1992	
	015 (transitional area)	Oct.6, 1991-Jul.5, 1992	
Tethered sonde	Huayin (Gobi)	Aug.8-Aug.20, 1991; Oct.6-Oct.13, 1991	Altitude, wind speed and wind direction, air temperature, potential temperature, air pressure, specific humidity, relative humidity
	Xiaotun (oasis)	Aug.6-Aug.20, 1991; Oct.4-Oct.12, 1991	
	Desert	Aug.6,-Aug.20,1991;Oct.8-Oct.12,1991	
Sodar	Huayin (Gobi)	Aug.4-Aug.20, 1991; Oct.3-Oct.13, 1991	Vertical and horizontal wind speed and wind direction, sodar echo intensity, potential temperature
	Xiaotun (oasis)	Aug.5-Aug.20, 1991; Oct.3-Oct.13, 1991	
Turbulent measurement system	Huayin (Gobi)	Aug.5-Aug.20, 1991; Oct.3-Oct.13, 1991; Dec.10-Dec.20, 1991	wind speed and wind direction, air temperature, relative humidity, the characteristic length scales of surface layer (u_* , T_* , q_*), sensible heat flux, latent heat flux, stability parameter
	Linze(oasis)	Jun.25- Jul.13, 1991	
	Desert	Aug.5-Aug.20, 199; Oct.3-Oct.13, 1991; Dec.10-Dec.20, 1991	
	Zhangye (oasis)	Aug.5-Aug.20,1991; Oct.3-Oct.13,1991; Dec.10-Dec.20,1991	

- Bio-meteorological observing period from April to July in 1992 in which at the oasis site the observations about the turbulence and some bio-meteorological parameters in farmland were added.

These stations have been operated successfully for more than two years and a large amount of data of surface observations have been collected (Table 4.3).

4.3 Arid Environment Comprehensive Monitoring Plan, 95 (AECMP'95)

The AECMP'95 has been carried out in a heterogeneous arid area of northwestern China from Aug.1 to Aug.21 1995. The objectives of AECMP'95 were:

- To investigate the interaction between oasis and Gobi desert and to find the advection over the fringe region between oasis and Gobi desert.
- To investigate the development of internal boundary layer over the fringe region between oasis and Gobi desert.
- To investigate the water and energy cycle over the fringe region between oasis and Gobi desert.

The observational sites distributed over an oasis fringe region, where four observational sites, D1, D2, O1 and O2, were set up (Figure 4.5a). A basic PBL tower and radiation system set up in the desert in the HEIFE was working at same time (Figure 4.6). The data collected during AECMP'95 was shown in Table 4.4.

Table 4.4 The collected field data of the Arid Environment Comprehensive Monitoring Plan (AECMP'95, August 1-August 21, 1995)

Sites	Observation item
<p style="text-align: center;">D1 (Gobi)</p>	<ul style="list-style-type: none"> ● Tethered-sonde: altitude, wind speed and wind direction, air temperature, potential temperature, air pressure, specific humidity, relative humidity. ● Turbulent measurement (sonic anemo-thermometer): wind speed, wind direction, air temperature, relative humidity, the characteristic length scales of surface layer (u_*, T_*, q_*), sensible heat flux, latent heat flux, stability parameter. ● Radiation: downward (upward) short wave radiation, downward (upward) long wave radiation. ● Soil heat flux. ● Surface temperature. ● Bowen Ratio.
<p style="text-align: center;">D2 (Gobi)</p>	<p>Turbulent measurement (sonic anemo-thermometer): wind speed, wind direction, air temperature, relative humidity, the characteristic length scales of surface layer (u_*, T_*, q_*), sensible heat flux, latent heat flux, stability parameter.</p>
<p style="text-align: center;">O1 (oasis, crop)</p>	<ul style="list-style-type: none"> ● Tethered-sonde: altitude, wind speed and wind direction, air temperature, potential temperature, air pressure, specific humidity, relative humidity. ● Turbulent measurement (sonic anemo-thermometer): wind speed, wind direction, air temperature, relative humidity, the characteristic length scales of surface layer (u_*, T_*, q_*), sensible heat flux, latent heat flux, stability parameter. ● Radiation: downward (upward) short wave radiation; downward (upward) long wave radiation. ● Soil heat flux. ● Surface temperature.
<p style="text-align: center;">O2 (oasis, crop)</p>	<ul style="list-style-type: none"> ● Tethered-sonde: altitude, wind speed and wind direction, air temperature, potential temperature, air pressure, specific humidity, relative humidity. ● Turbulent measurement (sonic anemo-thermometer): wind speed, wind direction, air temperature, relative humidity, the characteristic length scales of surface layer (u_*, T_*, q_*), sensible heat flux, latent heat flux, stability parameter.
<p style="text-align: center;">Desert (sand desert)</p>	<p>Wind speed (height (m): 0.5, 1, 2, 4, 8 and 20), air temperature and humidity (height (m): 1, 2, 4, 8 and 20), wind direction (height (m): 1, 4 and 20), surface temperature, soil temperature (depth (cm): -5, -10, -20, -40 and -80), soil heat flux (40 cm) and soil moisture (depth (cm): -10, -20, -40 and -80).</p>

4.4 DunHuang EXperiment (DHEX)

The DunHuang EXperiment was selected as a basic experiment for the Chinese National Key Programme for Developing Basic Sciences. It was carried out from 1 May 2000 to 31 August 2002 over a heterogeneous desertification area in Dunhuang, China. A micrometeorological station in Gobi near the Dunhuang oasis, a PAM station at the Dunhuang Meteorological Station located in the Dunhuang oasis, and an automatic weather station in a transition area between the oasis and Gobi, were set up for this experiment (Figure 4.7). The Gobi micrometeorological station is located at $40^{\circ}10'N$ and $94^{\circ}31'E$, with a surface elevation of 1150 m above sea level and an annual mean surface pressure of 873 hPa. The Gobi station is found in the Shuangdunzi Gobi to the west of the Dunhuang oasis. The nearest distance to the edge of the Dunhuang oasis is about 7 km. The Gobi station is located about 20–30 km south of Mountain Mingsha.

There were small buildings for pumping water within several tens of meters to the south of the micrometeorological station. The observational area was flat (upper soil is mainly pebble, the lower is sand). In the Dunhuang Experiment, a series of observations were conducted at the three stations, and large amount of data was collected (Table 4.5).



Figure 4.7 Sites layout, land surface condition and instruments in the DunHuang Experiment (DHEX) stations.

Table 4.5 The field data of the DunHuang EXperiment (DHEX) being collected over the period 1 May 2000 to 31 August 2002.

Station (site)	Observation item
Gobi	<ul style="list-style-type: none"> ● PBL tower: wind speed (height (m): 1, 2, 8 and 18), wind direction (10 m), air temperature and humidity (height (m): 1, 2, 8 and 18), surface temperature, soil temperature (depth (cm): -5, -10, -20, -40, -80 and -180), soil heat flux (depth (cm):-2.5 and -7.5), soil moisture (depth (cm): -5, -10, -20 and -80). ● Radiation: short wave radiation (downward and upward), long wave radiation (downward and upward). ● Turbulence: wind speed, wind direction, air temperature, relative humidity, the characteristic length scales of surface layer (u_*, T_*, q_*), sensible heat flux, latent heat flux, stability parameter. ● Tethered-sonde: profile of air pressure, air temperature, relative humidity, wind speed and direction.
Automatic Weather Station	Wind speed, wind direction, air temperature and humidity, surface temperature, soil temperature, soil moisture, solar radiation, air pressure.
Portable Automated Mesonet (PAM)	Wind speed, wind direction (9.8m), air temperature and humidity (height (m): 7.8and 2.3), short wave radiation (downward and upward), long wave radiation (downward and upward), net radiation, air pressure, turbulent fluxes (5.6 m), surface temperature, stability parameter, snow depth, precipitation, soil heat flux (-1 cm), soil temperature (depth (cm): -4, -20, -40, -60, -100, -160, -188), soil moisture (depth (cm): -4, -20, -40, -60, -100,-160, -188).
Radio-sonde (Dunhuang Meteorological Station)	Profile of air pressure, air temperature, relative humidity, wind speed and direction.

4.5 Landsat-5(7) TM (ETM) data and NOAA/AVHRR data

Landsat-5 Thematic Mapper (TM) and Landsat-7 Enhanced Thematic Mapper (ETM) provide spectral radiance measurements in narrow spectral bands, with a spatial resolution of about $30 \times 30 \text{ m}^2$ for three visible bands (Band 1, 2, 3) and three near infrared bands (Band 4, 5, 7), and $120 \times 120 \text{ m}^2$ for the thermal infrared band 6 of Landsat-5 TM and $60 \times 60 \text{ m}^2$ for the thermal infrared band 6 of Landsat-7 ETM.

The NOAA-14 Advanced Very High Resolution Radiometer (AVHRR) provides spectral information in 5 bands (band-1: $0.58\text{-}0.68\mu\text{m}$, band-2: $0.73\text{-}1.10\mu\text{m}$, band-3:

3.55-3.93 μm , band-4: 10.3-11.3 μm and band-5: 11.5-12.5 μm), with a spatial resolution of about $1 \times 1 \text{ km}^2$.

4.6 Summary and Conclusions

Heterogeneous land surfaces are characterized by extreme gradients in land surface properties such as wetness, roughness and temperature which have a significant but local impact on the Atmospheric Boundary Layer (ABL). Observation of the actual extent over the area is essential to understand the mechanisms through which heterogeneous land surfaces may have a significant impact on the structure and the dynamics of the overlying ABL.

In order to understand heat flux exchange between land surface and atmosphere over heterogeneous landscapes of arid areas and high altitude areas, *five land surface processes ground experiments* were performed in the western part of China.

- The first experiment, the Global Energy and Water cycle EXperiment Asian Monsoon Experiment on the Tibetan Plateau (GAME/Tibet) was performed over the central Tibetan Plateau area, which has the world's highest elevation (average elevation about 4000 m). The intensive observation period was from the middle of May to the middle of September 1998. The experimental area included a variety of land surfaces, such as a large area of grassy marshland, some desertification grass-land areas, many small rivers and several lakes.
- The second experiment, the Coordinated Enhanced Observing Period (CEOP) Asia-Australia Monsoon Project on the Tibetan Plateau (CAMP/Tibet) was carried out over the central Tibetan Plateau from the beginning of 2001 to 30 September 2004. The experimental area of the CAMP/Tibet was the same as that GAME/Tibet.
- The third experiment, the HEIhe Field Experiment (HEIFE) was carried out from 1988 to 1993 over the desertification area in Gansu, China. The HEIFE experimental area consisted of complex land surface conditions with mainly a large area of Gobi and sand desert and various scales of oasis dispersed along the river and irrigation canals.
- The fourth experiment, the Arid Environment Comprehensive Monitoring Plan (AECMP'95) was located in the HEIFE area, which more attention being paid to the interaction between the oasis and the Gobi desert. The intensive observational period

of AECMP'95 was from August 1, 1995 to August 21, 1995.

- The fifth experiment, the DunHuang EXperiment (DHEX) was selected as a basic experiment for the Chinese National Key Programme for Developing Basic Sciences. It was carried out from 1 May 2000 to 31 August 2002 in Dunhuang, China. The experimental area included a variety of land surfaces, such as a large area of Gobi, some sand desert areas and oasis areas.

Many types of instruments (e.g. PBL towers, radiation systems, radio sonde systems, turbulent fluxes measured by eddy-correlation technique, soil moisture and soil temperature measurement systems, PAM, Wind Profiler with RASS, tethered-sonde systems and radar systems and the like) were set up on heterogeneous land surfaces during the experimental periods. A large amount of observational data of soil, surface and atmospheric boundary layer has been collected. It constituted a sound base in deriving the input parameters for determining regional land heat fluxes. The data will be used in the Chapters 5 and 7 to validate the presented theory and approaches in Chapter 2 and Chapter 3.

Satellite remote sensing data can provide consistent and frequent observations of spectral reflectance and emittance of radiation at patches landscape. The data of Landsat-5 Thematic Mapper (TM), Landsat-7 Enhanced Thematic Mapper (ETM) and NOAA-14 Advanced Very High Resolution Radiometer (AVHRR) have been described and they will also be used in the Chapters 5 and 7 to derive the land surface heat fluxes over heterogeneous landscapes.

5. Application of the parameterization scheme using satellite measurements and surface layer assumptions: the HEIFE case

5.1 Introduction

As shown in Chapters 1, 2 and 3, the regional surface heat fluxes over heterogeneous landscapes can be estimated by using satellite measurements. The HEIFE (Chapter 4) provided materials for a case study, which will be dealt with in this chapter to show the advantages as well as the shortcomings of the *RS approach*.

The observational study on the energy and water cycle over the experimental area was an important component in the HEIFE project. Some interesting detail studies concerning the surface water and energy budget in some stations have already been reported. However, the investigation on the areal distribution of water and heat, particularly the evaporation taken as the base of water circulation, was continued towards a better understanding of the landscape of the HEIFE area (Hu, et al., 1994). In order to reach the purpose of a better understanding of the land surface processes to represent in the atmospheric Global Circulation Models (GCM), the aggregation of the individual results to a basin scale is inevitable. An effective approach is to use satellite remote sensing measurements (e.g. Menenti, 1984; Menenti et al., 1989; Menenti et al., 1991; Bastiaanssen, 1995; Wang et al., 1995; Ma et al., 1997; Stewart et al., 1998; Ma et al., 1999). The objectives of this chapter are:

- (1) To estimate the distributions of surface reflectance r_0 , surface temperature T_0 , $NDVI$, net radiation flux R_n and soil heat flux G_0 over the HEIFE area with the aid of satellite remote sensing measurements.

This chapter is based on:

- (1) **Ma, Y.**, J. Wang, M. Menenti, and W. G. M. Bastiaanssen, 1997, Distribution and seasonal variation of regional net radiation in the HEIFE area, *Chinese Journal of Atmospheric Sciences*, **21**(2): 410-416.
- (2) **Ma, Y.**, J. Wang, M. Menenti, and W. G. M. Bastiaanssen, 1999, Estimation of flux densities over the heterogeneous land surface with the aid of satellite remote sensing and ground observation, *ACTA Meteorological Sinica*, **57**(2): 180-189.
- (3) Wang, J., **Y. Ma**, M. Menenti, and W. G. M. Bastiaanssen, 1995, The scaling-up of processes in heterogeneous landscape of HEIFE with the aid of satellite remote sensing, *Journal of the Meteorological Society of Japan*, **73**(6): 1235-1244.

- (2) To determine the sensible heat flux H and latent heat flux λE using the *RS approach* presented in Chapter 3.
- (3) To assess the ability of bridging the gap of between local patch scale and larger length scale for heterogeneous land surfaces with the satellite data.

5.2 Methodology

The overall concept of the *RS approach* was dealt with in Chapter 3. A full diagram of the *RS approach* is given in Figure 5.1. The values of r_0 , T_0 and $NDVI$ are retrieved from Landsat-5 TM measurements. With these results R_n is determined. G_0 is estimated from R_n , T_0 , r_0 and $NDVI$. Sensible heat flux H is estimated from T_0 , surface measurements and variables taken from the literature. Finally λE is obtained as the residual of the energy budget.

5.2.1 Land surface variables

Surface reflectance $r_0(x, y)$

$r_0(x, y)$ can be derived pixel-wise from Landsat-5 TM data and the ground surface reflectance measurements r_0 . First, the hemispherical planetary reflectance can be obtained from the satellite remote sensing data through the following steps:

Step a: Determination of the spectral radiances in the visible and infrared regions

Remotely measured spectral radiances in the visible and near infrared, $K^{\uparrow}_{TOA}(\lambda)(x,y)$ range are represented in binary digital satellite image products by means of Digital Number (DN) which are calibrated radiance values in arbitrary units. In the case of Landsat-5 TM, to convert DN values to radiances, a simple linear interpolation is applied (Markham and Barker, 1987)

$$K^{\uparrow}_{TOA}(\lambda)(x, y) = a_1 + \frac{a_2 - a_1}{255} DN \quad (\text{W m}^{-2}\text{sr}^{-1}\mu\text{m}^{-1}) \quad (5.1)$$

where $K^{\uparrow}_{TOA}(\lambda)$ is the bi-directional spectral radiance at the sensor and a_1 and a_2 are the calibration parameters with a_1 being the spectral radiance at DN=0 and a_2 being the spectral radiance at DN=255. The values a_1 and a_2 vary for each reflectance band (Table 5.1).

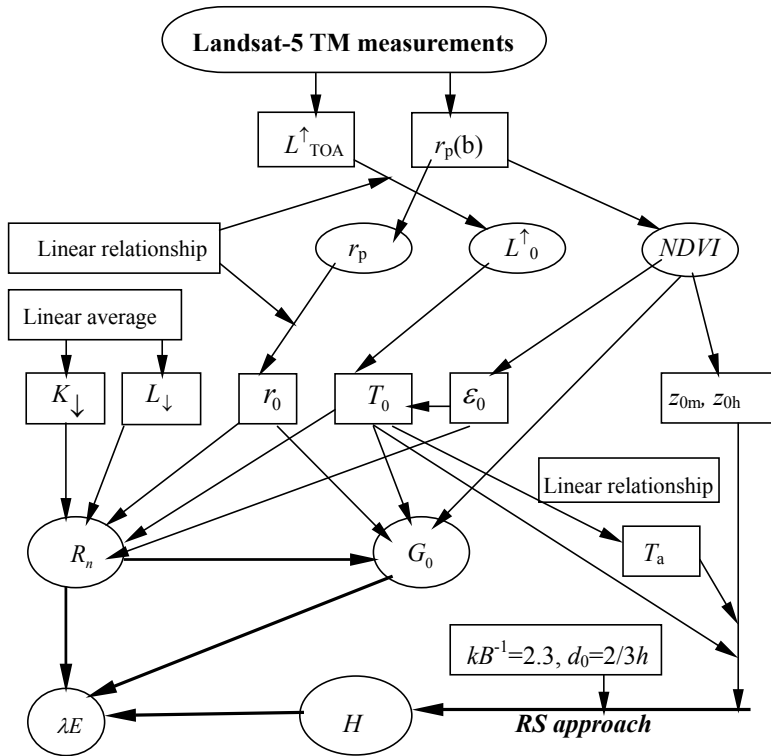


Figure 5.1 Diagram of the *RS approach*. The surface reflectance r_0 , land surface temperature T_0 and *NDVI* are retrieved from Landsat-5 TM measurements. With these results the surface net radiation flux (R_n) is determined. The soil heat flux (G_0) is estimated from R_n , T_0 , r_0 and *NDVI*. The sensible heat flux H is estimated from T_0 , surface measurements and variables taken from the literature with the aid of *RS approach*. Latent heat flux λE is finally obtained as the residual of the energy budget equation.

Table 5.1 The values of a_1 and a_2 (Eq.5.1) for TM measurements

Band	1	2	3	4	5	7
a_1	-0.15	-0.28	-0.12	-0.15	-0.37	-0.015
a_2	15.2	29.68	20.43	20.62	2.719	1.438

Step b: Determination of the solar declination δ

The solar declination, δ , is the angular height of the sun above the astronomical equatorial plane, with δ change in throughout the year according to (e.g. Duffie and Beckman, 1980)

$$\delta = 0.409 * \sin(0.0172J - 1.39) \quad (\text{rad}) \quad (5.2)$$

where J is the Julian day number (January 1 is day 1)

Step c: Determination of the solar angle hour $\omega(x)$

The longitude dependent solar angle hour, $\omega(x)$, reads as

$$\omega(x) = \pi \left[\frac{t(x) - 12}{12} \right] \quad (\text{rad}) \quad (5.3)$$

where $t(x)$ (decimal hours) is the local longitude time which can be obtained from the Greenwich Mean Time (GMT) t' at 0^0 longitude according to the following correction

$$t(x) = t' + \text{min}/60 + \text{long}(x) \frac{12}{\pi} \quad (\text{s}) \quad (5.4)$$

where long is the longitude.

Step d: Determination of the solar zenith angle ϕ_{su}

The solar zenith angle is the angle between a line normal to a particular point at a horizontal land surface and a line through the solar center. Iqbal (1983) gave a simplified goniometric function to describe solar zenith angle ϕ_{su}

$$\cos \phi_{su}(x, y) = \sin \delta \cdot \sin[\text{lat}(y)] + \cos \delta \cdot \cos[\text{lat}(y)] \cdot \cos[\omega(x)] \quad (-) \quad (5.5)$$

where lat is the latitude.

Step e: Determination of the relative earth-sun distance d_s

The relative earth-sun distance changes because of the elliptical orbit of the earth around the sun. The earth-sun distance reaches its minimum value at the beginning of January while

the beginning of June is marked by the largest distance among these celestial bodies. The motion of the relative earth-sun distance can be approximated by the function

$$d_s = 1 + 0.0167 \sin \left[\frac{2\pi(J - 93.5)}{365} \right] \quad (\text{AU}) \quad (5.6)$$

where d_s is the relative earth-sun distance in astronomical units (AUs). The absolute value of 1 AU is 1.496×10^8 km.

Step f: Determination of in-band spectral short wave hemispherical planetary reflectance $r_p(b)$

Values for in-band spectral reflectance $r_p(b)$ can be calculated from incoming and outgoing in-band radiances at the top of atmosphere. The in-band outgoing radiance $K^{\uparrow}_{\text{TOA}}(b)$ was obtained by multiplying $K^{\uparrow}_{\text{TOA}}(\lambda)$ from computation step (a) by its bandwidth b . Integration of $K^{\uparrow}_{\text{TOA}}(b)$ over zenith and azimuth angles gives the hemispherical radiance, $\pi K^{\uparrow}_{\text{TOA}}(b)$. If the reflecting surface is assumed to be isotropic (Lambertian reflector for azimuth and zenith effects), which yields the in-band hemispherical reflectance at the top of the atmosphere as

$$r_p(b)(x, y) = \frac{\pi K^{\uparrow}_{\text{TOA}}(b)(x, y)}{K^{\downarrow}_{\text{TOA}}(b)(x, y)} \quad (-) \quad (5.7)$$

and

$$K^{\downarrow}_{\text{TOA}}(b)(x, y) = \frac{K^{\downarrow}_{\text{exo}}(b) \cos(\phi_{\text{su}})(x, y)}{d_s^2} \quad (\text{W m}^{-2}) \quad (5.8)$$

where $K^{\downarrow}_{\text{exo}}(b)$ is the mean in-band solar exo-atmospheric irradiance undisturbed by the atmosphere at $\phi_{\text{su}}=0^{\circ}$. The value of $K^{\downarrow}_{\text{exo}}(b)$ used in Eq.5.8 is corrected for the sensor spectral response for consistency with $K^{\uparrow}_{\text{TOA}}(b)$.

Step g: Determination of the integrated clear sky short wave hemispherical planetary reflectance $r_p(x, y)$

The spectrally integrated planetary reflectance, $r_p(x, y)$, can be estimated by performing a narrow-band to broad-band integration covering all reflectance bands in the visible and near-infrared region. The results should be approximately similar to $\int_{0.3}^{3.0} r_p(\lambda) d\lambda$. The weighing factors, $c(b)$, account for the uneven distribution of $K^{\uparrow}_{\text{exo}}(\lambda)$ in the spectral

bands of a specific sensor

$$r_p(x, y) = \int_{0.3}^{3.0} r_p(\lambda) d\lambda \approx \sum_{i=1}^{7(i \neq 6)} c(b)_i r_p(b)_i \quad (-) \quad (5.9)$$

where n represents the total number of spectral bands i of the radiometer defined in the 0.3 and 3.0 μm region. The sum of the weighing factor $\sum c(b)_i$ should be equal to one..

Step h: Determination of the integrated clear sky short wave hemispherical surface reflectance $r_0(x, y)$

The integrated short wave hemispherical surface reflectance, r_0 , at each pixel can be determined from r_p by using a model to calculate atmospheric correction (Menenti, 1984; Menenti, et al., 1989; Menenti et al., 1991). A simplified linear relationship between r_0 and r_p founded in the HEIFE area (Figure 5.2; Wang et al., 1995; Ma et al., 1997; Ma et al., 1999) will be used to calculate the atmospheric correction in this chapter. It means that r_0 at

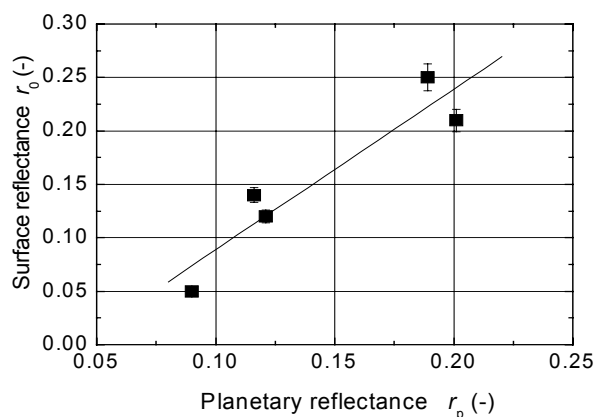


Figure 5.2 Hemispherical surface reflectance r_0 against hemispherical planetary reflectance r_p over the HEIhe basin Field Experiment (HEIFE) area.

each pixel of TM in the HEIFE area can be determined from

$$r_0(x, y) = 1.5053r_p(x, y) - 0.0618 \quad (-) \quad (5.10)$$

where the linear regression coefficient r is 0.94. Eq.5.10 was based on ground measurements of r_0 and satellite measurements of r_p .

Land surface temperature $T_0(x,y)$

Band 6 (10.45-12.46 μ m) of the TM covers part of the thermal infrared radiation, which is the radiance by a surface with temperature T_0 and surface emissivity ε_0 . As given by Plank's function

$$L(\lambda, T_0) = \varepsilon_\lambda \frac{2c_{\text{Planck}} c^2}{\lambda^5 (e^{c_{\text{Planck}} c / c_{\text{SB}} \lambda T_0} - 1)} \quad (\text{W m}^{-2}) \quad (5.11)$$

where $L(\lambda, T_0)$ is the spectral radiance at wave length λ by a surface with a physical temperature T_0 , c is light speed, c_{Planck} is Planck constant, and c_{SB} is Stefan Boltzmann constant. In estimating surface temperature from satellite remote sensing, the observed radiance must be corrected for atmospheric effects such as absorption, scattering etc., even in the atmospheric water vapour window. For the thermal infrared band radiance at the top of the atmosphere $L^{\uparrow}_{\text{TOA}}$ measured by TM, a satellite brightness temperature of the earth—atmosphere system is derived from

$$T_{\text{sat}}(x, y) = \frac{1260.56}{\ln\left(\frac{60.776}{L^{\uparrow}_{\text{TOA}}(x, y)} + 1\right)} \quad (\text{K}) \quad (5.12)$$

A crude atmospheric correction procedure is found between $L^{\uparrow}_{\text{TOA}}(x, y)$ and upward long-wave radiation measurements $L^{\uparrow}_0(x, y)$. It can be done using radio soundings and a radiation transfer model (e.g. Menenti, 1984; Menenti, et al., 1989). A simplified linear relationship between $L^{\uparrow}_0(x, y)$ and $L^{\uparrow}_{\text{TOA}}(x, y)$ that was found in the HEIFE area (Figure 5.3; Ma et al., 1997; Ma et al., 1999) will be used to calculate atmospheric correction. The upward long-wave radiation on each pixel $L^{\uparrow}_0(x, y)$ of TM in the HEIFE area can be determined from

$$L_0^\uparrow(x,y) = 1.9190L_{\text{TOA}}^\uparrow(x,y) + 528.9931 \quad (\text{W m}^{-2}) \quad (5.13)$$

where the linear regression coefficient r is 0.96. Then T_0 is derived pixel-wise from

$$L_0^\uparrow(x,y) = \varepsilon_0(x,y)\sigma T_0^4(x,y) \quad (\text{W m}^{-2}) \quad (5.14)$$

where surface emissivity $\varepsilon_0(x,y)$ is the function of $NDVI$ (Owe et al.,1993), i.e.

$$\varepsilon_0(x,y) = 1.009 + 0.047 \ln NDVI(x,y).$$

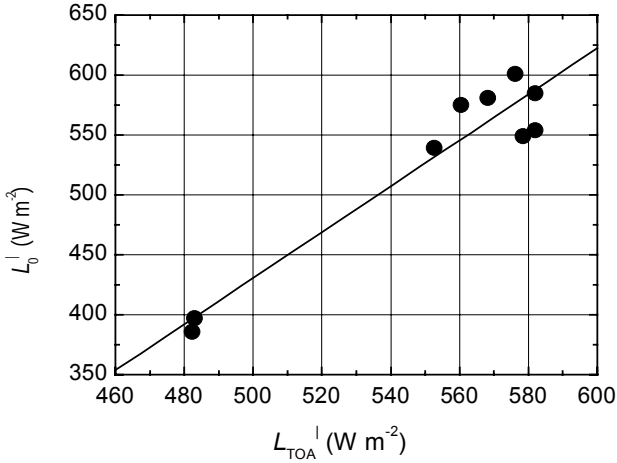


Figure 5.3 The upward long-wave radiation L_0^\uparrow at the land surface against the thermal infrared band radiance at the top of the atmosphere L_{TOA}^\uparrow over the HEIhe basin Field Experiment (HEIFE) area.

5.2.2 Net radiation flux R_n and soil heat flux G_0

The regional net radiation flux can be determined using Eq.2.3. The incoming short

wave radiation flux $K_{\downarrow}(x,y)$ and the incoming long wave radiation flux $L_{\downarrow}(x,y)$ in Eq.2.3 are to be derived from the ground experiments, i.e.

$$K_{\downarrow}(x,y) = \overline{K_{\downarrow}} = \frac{1}{n} \sum_{i=1}^n K_{\downarrow_i} \quad (\text{W m}^{-2}) \quad (5.15)$$

$$L_{\downarrow}(x,y) = \overline{L_{\downarrow}} = \frac{1}{n} \sum_{i=1}^n L_{\downarrow_i} \quad (\text{W m}^{-2}) \quad (5.16)$$

where K_{\downarrow_i} and L_{\downarrow_i} are the incoming short wave radiation flux and long-wave radiation flux in the station No. i .

The regional soil heat flux $G_0(x,y)$ will be estimated from Eq. 2.27.

5.2.3 Sensible heat flux H

The regional sensible heat flux $H(x,y)$ can be derived from Eq.2.34. The procedure is similar to the Surface Energy Balance Algorithm for Land (SEBAL, Bastiaanssen, 1995). For the HEIFE case, the assumptions and approximations shown in Table 5.2 will be used to calculate $H(x,y)$, and $T_a(x,y) = 0.40T_0(x,y) + 9.45$ was derived from Figure 5.4.

Table 5.2 The assumptions and approximations that were used to calculate the regional sensible heat flux $H(x,y)$.

Variable	Unit	Equation
$z_{0m}(x,y)$	m	$z_{0m}(x,y) = \exp[-7.13 + 9.33NDVI(x,y)]$ (Jia et al, 1999a)
$z_{0h}(x,y)$	m	$z_{0h}(x,y) = 0.01z_{0m}(x,y)$ (Bastiaanssen, 1995)
$\psi_h(x,y)$	-	Eq.2.46 and Eq.2.47 (Paulson, 1970; Webb, 1970)
$\psi_m(x,y)$	-	Eq.2.46 and Eq.2.47 (Paulson, 1970; Webb, 1970)
$d_0(x,y)$	m	$d_0 = (2/3)h_v$
$kB^{-1}(x,y)$	-	2.3
$T_a(x,y)$	$^{\circ}\text{C}$	$T_a(x,y) = 0.40T_0(x,y) + 9.45$

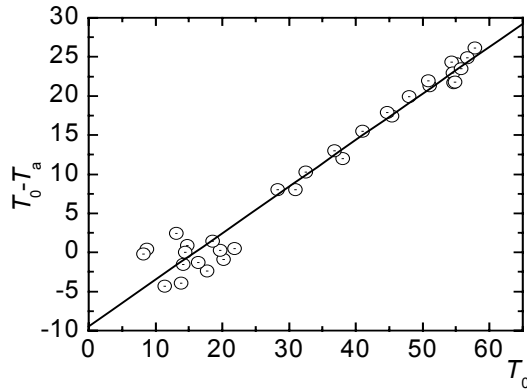


Figure 5.4 $T_0 - T_a$ versus surface temperature T_0 for the HEIhe basin Field Experiment (HEIFE) stations. $T_a(x, y) = 0.40T_0(x, y) + 9.45$, T_a is the air temperature.

5.2.4 Latent heat flux λE

The regional latent heat flux $\lambda E(x, y)$ can be determined from Eqs.2.50. But to determine $\lambda E(x, y)$ from the satellite measurements through Eq.2.50 we need to determine the turbulent transport resistances first. To avoid that difficulty, Eq.2.51 will be used to determine the regional $\lambda E(x, y)$ over the HEIFE area.

5.3 Analysis of the results

The Landsat-5 TM image of the HEIFE area used in this chapter was acquired on July 9, 1991: being a very clear day. A composite image of TM band 4, 5, and 3 at 10:00 (local time) July 9, 1991 over the HEIFE area has been displayed in Figure 4.5 b. An unsupervised classification of the land use has been compared with surface observations. Except for the southwest (lower left) mountainous area where the Heihe River flows down, there are two dominant land cover types: sand or Gobi desert (including low hilly land, some parts with sparse vegetation) and oasis.

Figure 5.5 shows the distribution maps of r_0 , $NDVI$, T_0 , R_n , G_0 , H and λE over the HEIFE area. Their frequency distributions are shown in Figures 5.6 and 5.7. The distribution ranges of these variables are shown in Table 5.3. The derived r_0 , T_0 , R_n , G_0 , H and λE can be validated against the ground measurements. In Figure 5.8, the determined values from TM are plotted against the measured values in the field for the R_n , G_0 , H and λE . The 1:1 line is also plotted in the graphs. Since it is difficult to determine where the exact locations of the experimental sites are, the values of a 5×5 pixel rectangle, surrounding the determined Universal Transfer Macerator (UTM) coordinate, are compared with the ground measurements. The relative deviation can quantitatively measure the difference between the derived results ($V_{\text{derived}(i)}$) and measured values ($V_{\text{measured}(i)}$) as

$$\frac{\delta V}{V} = \frac{|V_{\text{derived}(i)} - V_{\text{measured}(i)}|}{V_{\text{measured}(i)}} \quad (-) \quad (5.18)$$

The derived and measured land surface variables (r_0 and T_0) and land surface heat fluxes (R_n , G_0 , H and λE) in different stations are shown in Table 5.4. Their $\delta V/V$ is also shown in the Table.

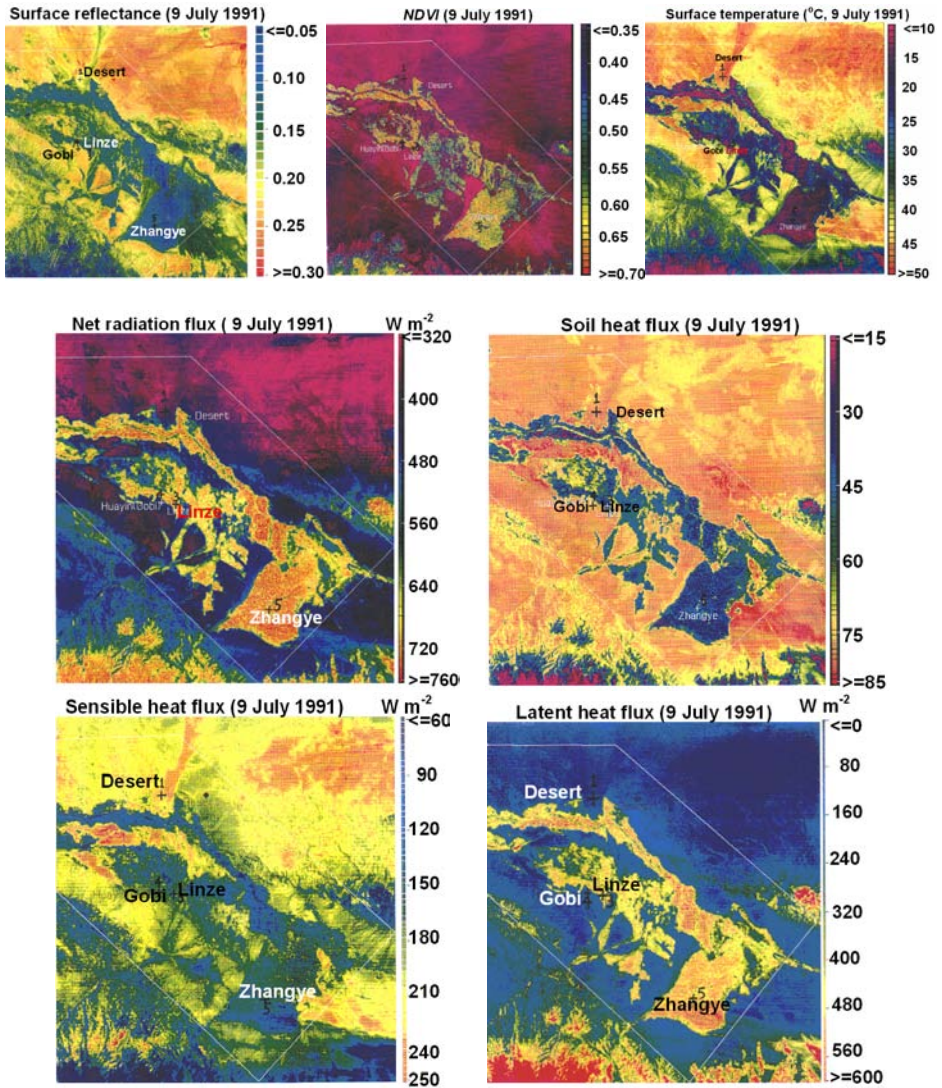


Figure 5.5 The distribution maps of surface reflectance r_0 , $NDVI$, surface temperature T_0 , net radiation flux R_n , soil heat flux G_0 , sensible heat flux H and latent heat flux λE over the HEIFE basin Field Experiment (HEIFE) area.

Table 5.3 The distribution range and peaks of surface reflectance r_0 , $NDVI$, surface temperature T_0 , net radiation flux R_n , soil heat flux G_0 , sensible heat flux H and latent heat flux λE over the HEIhe basin Field Experiment (HEIFE) area.

	Range	Oasis (peak)	Gobi desert (peak)
$NDVI$ (-)	0.01—0.75	~0.65	~0.15
r_0 (-)	0.10—0.30	~0.11	~0.24
T_0 ($^{\circ}C$)	2.0—52.0	~15.0	~45.0
R_n ($W\ m^{-2}$)	300—760	~700	~370
G_0 ($W\ m^{-2}$)	15—85	~38	~79
H ($W\ m^{-2}$)	20—270	~120	~225
λE ($W\ m^{-2}$)	-20—640	~500	~50

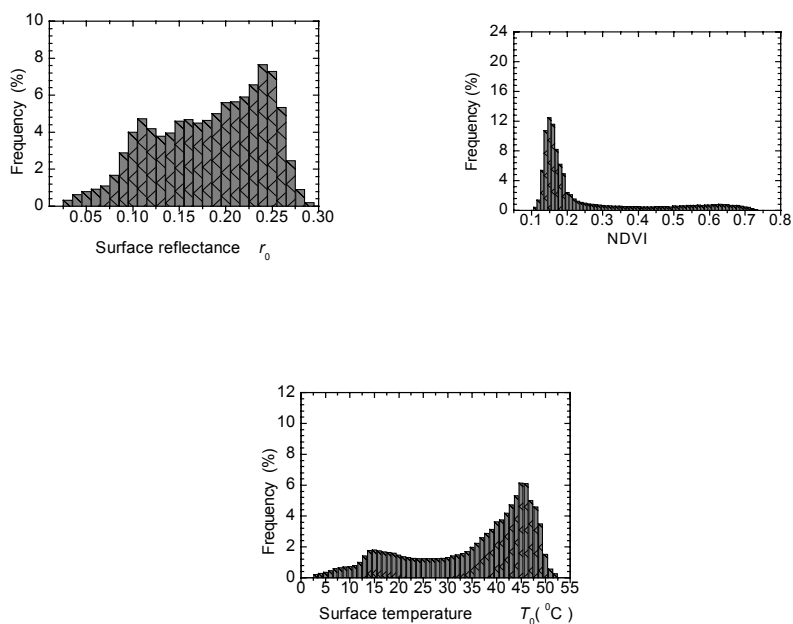


Figure 5.6 The frequency distributions of surface reflectance r_0 , $NDVI$ and surface temperature T_0 over the HEIhe basin Field Experiment (HEIFE) area.

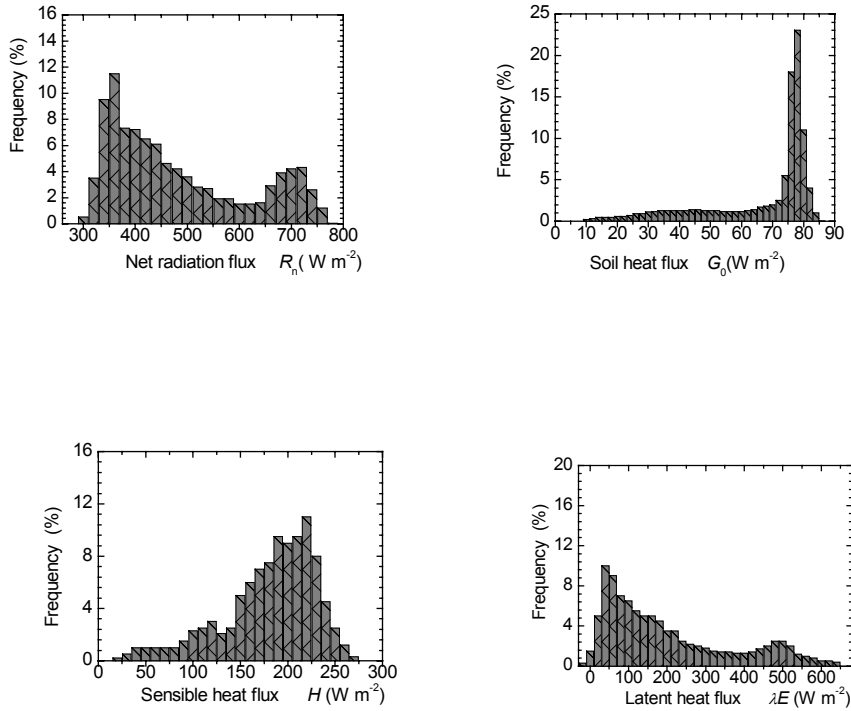


Figure 5.7 The frequency distributions of net radiation flux R_n , soil heat flux G_0 , sensible heat flux H and latent heat flux λE over the HEIhe basin Field Experiment (HEIFE) area.

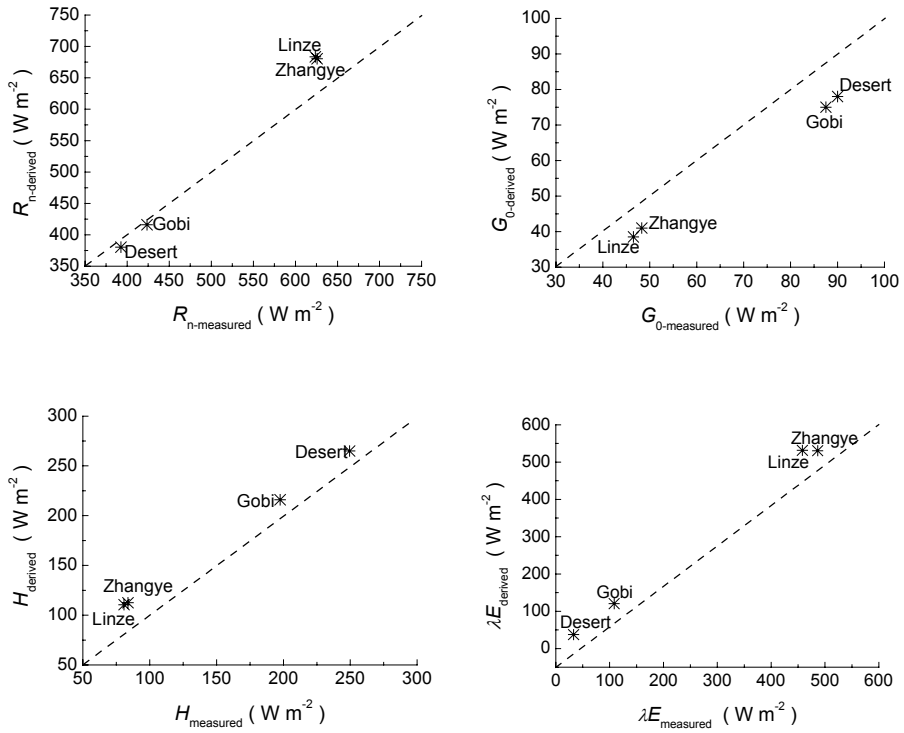


Figure 5.8 Validation of the derived results against the ground measurements for net radiation flux R_n , soil heat flux G_0 , sensible heat flux H and latent heat flux λE over the HEIhe basin Field Experiment (HEIFE) area, together with 1:1 line.

Table 5.4 The relative deviation $\delta V/V$ (Eq.5.18) between the derived results using RS approach (RS) and measured (Meas.) values of surface reflectance r_0 , surface temperature T_0 , net radiation flux R_n , soil heat flux G_0 , sensible heat flux H and latent heat flux λE at the HEIthe basin Field Experiment (HEIFE) sites.

Station	r_0 (-)			T_0 ($^{\circ}\text{C}$)			R_n (W m^{-2})		
	Meas.	RS	$\delta V/V$	Meas.	RS	$\delta V/V$	Meas.	RS	$\delta V/V$
Desert	0.25	0.22	12 %	44.8	46.5	4 %	392.6	380.5	3 %
Linze	0.12	0.11	8 %	15.4	16.5	7 %	625.7	680.5	9 %
Gobi	0.21	0.20	5 %	46.5	43.7	6 %	423.6	416.0	2 %
Zhangye	0.14	0.12	14 %	22.8	19.0	17 %	623.7	683.5	10 %
	G_0 (W m^{-2})			H (W m^{-2})			λE (W m^{-2})		
	Meas.	RS	$\delta V/V$	Meas.	RS	$\delta V/V$	Meas.	RS	$\delta V/V$
Desert	90.0	78.0	13 %	249.5	265.0	6 %	33.0	37.5	14 %
Linze	46.5	38.5	17 %	80.8	110.5	37 %	458.0	531.5	16 %
Gobi	87.5	75.0	14 %	197.5	216.0	9 %	108.5	120.5	11 %
Zhangye	48.3	41.0	15 %	83.7	112.5	34 %	486.5	530.5	9 %

It can be seen that:

- (1) The derived land surface variables (r_0 and T_0), $NDVI$ and land surface heat fluxes (R_n , G_0 , H and λE) over the HEIFE area are consistent with the land cover types (Figures 4.5 b, 4.6, 5.5, 5.6 and 5.7). These variables show a wide range (Table 5.3) due to the strong contrast of surface features (Figures 4.5 b, 4.6, 5.5, 5.6 and 5.7). There are two peaks in the figures of all frequency distributions in this area. The first peak corresponds to the oasis and another one corresponds to the Gobi desert (Figures 5.5 and 5.6 and Table 5.3).
- (2) The derived r_0 and T_0 based on the linear relationship here is not suitable for the whole area, and $\delta V/V$ in Zhangye (oasis) and Desert are higher than 10 % (Table 5.4). It means that there are some shortcomings existing in the procedure of deriving r_0 and T_0 from the linear relationship. *Firstly*, the ground measurement is only a point value, while the satellite pixel is the average of many point values. *Secondly*, fewer ground observation data coincide with satellite data when the satellite overpasses the observation sites, therefore better atmospheric correction procedures and algorithm to estimate r_0 and T_0 are needed. *Thirdly*, geo-location should be accurately made to establish the regression relationship.

- (3) The derived R_n is close to ground measurement with a $\delta V/V$ being less than 10 % (Table 5.4 and Figure 5.8).
- (4) The derived G_0 at the four validation sites are lower than the measured values, with a $\delta V/V$ being higher than 13 % (Table 5.4 and Figure 5.8). The first reason is that the derived soil heat flux was based on $NDVI$, but the problems exist in the $NDVI$ definition equation. The reason is the external factor effect, such as soil back-ground variations (Huete et al., 1985; Huete, 1989). The second reason is that we use the equation from literature (Bastiaanssen, 1995) directly.
- (5) The derived regional H with a $\delta V/V$ being less than 10 % at the sites of Desert and Gobi due to homogeneous land surface over there (Table 5.4 and Figure 5.8). But there is a large difference between the derived results and ground-measured values over oasis ($\delta V/V = 37\%$ in Linze and $\delta V/V = 34\%$ in Zhangye). It means that the method should be improved to estimate sensible heat flux over the canopy surface.
- (6) The derived regional λE , which is based on the energy balance equation, is larger than the measured values for four validation sites, and $\delta V/V$ is higher than 10 % at the validation sites of Desert, Linze (oasis) and Gobi (Table 5.4 and Figure 5.8).

5.4 Summary and conclusions

The regional distributions of land surface variables (surface reflectance r_0 and surface temperature T_0), $NDVI$ and land surface heat fluxes (net radiation flux R_n , soil heat flux G_0 , sensible heat flux H and latent heat flux λE) in the HEIhe basin Field Experiment (HEIFE) area were obtained by using the *RS approach*. It bridged the gap between the point local measurements and the regional scale over the arid area of the HEIFE, as well as formed a sound basis to study land surface variables and land surface fluxes over this area.

But the results showed that the satellite derived r_0 , T_0 , G_0 , H and λE of some areas were distinctly different from the ground measurements. The reason being that many assumptions and approximations were involved in the *RS approach* including some shortcomings:

- Linear relationships between T_a and T_0 , r_0 and r_p , L^{\uparrow}_0 and L^{\uparrow}_{TOA} etc. were used in the methodology. The linear relationships may however not be accurate, because the ground measurement was only a point value, while the satellite pixel was the average values of many points. Also the few ground observation data coincide with satellite measurements, the more sophisticated measurement techniques are needed. Also the

geo-location should be accurate provided to establish correct regression relationships. Furthermore, the land surface exhibited significant heterogeneity at all spatial scales (Chapter 3). Also the coupling of radiation from different surface components into the sensor receiving aperture, as expressed by radiative transfer equations, was nonlinear.

- The aerodynamic roughness length z_{0m} and the thermodynamic roughness length z_{0h} in Eq.2.34 were only estimated from *NDVI*. This implies that only the aerodynamic characteristics of the land surface were considered in the parameterization of z_{0m} and z_{0h} . But both the aerodynamic and the thermodynamic characteristics of the land surface are influencing on z_{0h} actually.
- The excess resistance to heat transfer $kB^{-1}=2.3$ was used for the whole area in the parameterization, but kB^{-1} had different values over different land surfaces (Chapter 6, Ma et al., 2002d).
- Zero-plane displacement height d_0 was estimated from the vegetation height h_v ($d_0 = (2/3)h_v$), but h_v cannot really be estimated from TM measurements.

Therefore, improvements are necessary in the *RS approach*. The atmospheric and the land surface variables have to be determined at heterogeneous landscapes by using the Surface Layer (SL) as well as Atmospheric Boundary Layer (ABL) observations instead of taking from linear relationships and data from the literature.

The analysis of land surface heterogeneity (Chapter 3), z_b and wind speed at the blending height u_b , the atmospheric variables (z_{0m} , z_{0h} and kB^{-1}) will in Chapter 6 be done and determined with the aid of SL and ABL observations. All of them will be used to improve the input variables in the parameterization methodology in Chapter 7.

6. Analysis of momentum and heat fluxes at the surface using local surface and atmospheric boundary layer observations

6.1 Introduction

The land surface in the experimental areas of GAME/Tibet, the CAMP/Tibet, the HEIFE, the AECMP'95 and the DHEX is heterogeneous (see Figures 4.1 - 4.7 including). This results in the heterogeneity of the energy partitioning at the surface, and further more, in the different structure of the Convective Atmospheric Boundary Layer (CABL) near the land surface. The land surface heterogeneity will be documented through the comparison of surface reflectance r_0 , surface temperature T_0 , net radiation flux R_n and sensible heat flux H partitioning over the different land cover types in the experimental areas.

The air flow and state over a heterogeneous land surface is influenced by surface heterogeneity, and it leads to spatial variability in the ABL state near the land surface (Chapter 3). In the Surface Layer (SL) this results in different vertical profiles of air temperature T_a (or potential temperature θ), wind speed u and humidity q in response to changes in land surface properties. But the development of CABL tends to smooth out the at-surface variability at the 'blending height', at which atmospheric characteristics such as θ , u and q become spatially uniform (Chapter 3).

The different vertical profiles of T_a , u and q in the near surface layer and above the blending height z_b will now be analyzed using the PBL tower data, radio sonde data and tethered balloon data.

This chapter is based on:

- (1) **Ma, Y.**, S. Fan, H. Ishikawa, O. Tsukamoto, T. Yao, T. Koike, H. Zuo, Z. Hu, and Z. Su, 2005, Diurnal and inter-monthly variation of land surface heat fluxes over the central Tibetan Plateau area, *Theoretical and Applied Climatology*, **80**: 259-273.
- (2) **Ma, Y.**, O. Tsukamoto, J. Wang, H. Ishikawa, and I. Tamagawa, 2002d, Analysis of aerodynamic and thermodynamic parameters on the grassy marshland surface of Tibetan Plateau, *Progress in Natural Science*, **12** (1): 36-40.
- (3) **Ma, Y.**, W. Ma, M. Li, O. Tsukamoto, H. Ishikawa, J. Wang, Z. Hu, and F. Gao, 2003e, The comparative analysis of characteristics of energy transfer in near surface layer over the area of GAME/Tibet, HEIFE and AECMP'95, *Chinese Journal of Atmospheric Sciences*, **27**(1):1-14.

The land surface heterogeneity leads to differences in the aerodynamic roughness length z_{0m} , the thermodynamic roughness length z_{0h} and the excess resistance to heat transfer kB^{-1} over the different land surfaces. These near surface boundary layer variables over the different land surfaces will be determined.

6.2 Land surface heterogeneity and its influences on the overlying surface layer and atmospheric boundary layer

The land surface heterogeneity and its influences on the overlying atmospheric layer over the different land surfaces of the HEIFE, the CAMP/Tibet and the DHEX will be documented in this section by using the surface and ABL observational data described in Chapter 4.

6.2.1 Diurnal variation of surface reflectance, surface temperature and surface heat fluxes over heterogeneous land surfaces

Figure 6.1 gives the diurnal variation of r_0 , T_0 , R_n and H over the oasis, Gobi desert in the HEIFE area on 9 July 1991. The diurnal variations of r_0 , T_0 , R_n and H over the CAMP/Tibet area in the months January, June and August are shown in Figure 6.2. All the curves were obtained under clear-sky conditions. In the Figures 6.1 and 6.2, T_0 was measured by an infrared radiometer, and r_0 was calculated from

$$r_0 = \frac{K_{\uparrow}}{K_{\downarrow}} \quad (-) \quad (6.1)$$

where K_{\downarrow} and K_{\uparrow} are the measured downward and upward short wave radiation flux respectively. R_n in the Figures 6.1 and 6.2 was calculated from

$$R_n = K_{\downarrow} - K_{\uparrow} + L_{\downarrow} - L_{\uparrow} \quad (\text{W m}^{-2}) \quad (6.2)$$

where L_{\downarrow} and L_{\uparrow} are the measured downward and upward long wave radiation flux respectively. H in the Figures 6.1 and 6.2 was calculated from the PBL tower data, which is

$$H = \rho c_p C_{HN} (u_{z2} - u_{z1}) (T_{z2} - T_{z1}) \quad (\text{W m}^{-2}) \quad (6.3)$$

where ρ is air density, c_p is air specific heat at constant pressure, u_{z1} and u_{z2} are the wind

speed at heights z_1 and z_2 respectively, and T_{z1} and T_{z2} are air temperature at the height z_1 and z_2 respectively. C_{HN} denotes the bulk transfer coefficient in the neutral state:

$$C_{HN} = \frac{k^2}{[\ln(z/z_{0m})]^2} \quad (-) \quad (6.4)$$

where k is Von Karman constant and z is the reference height.

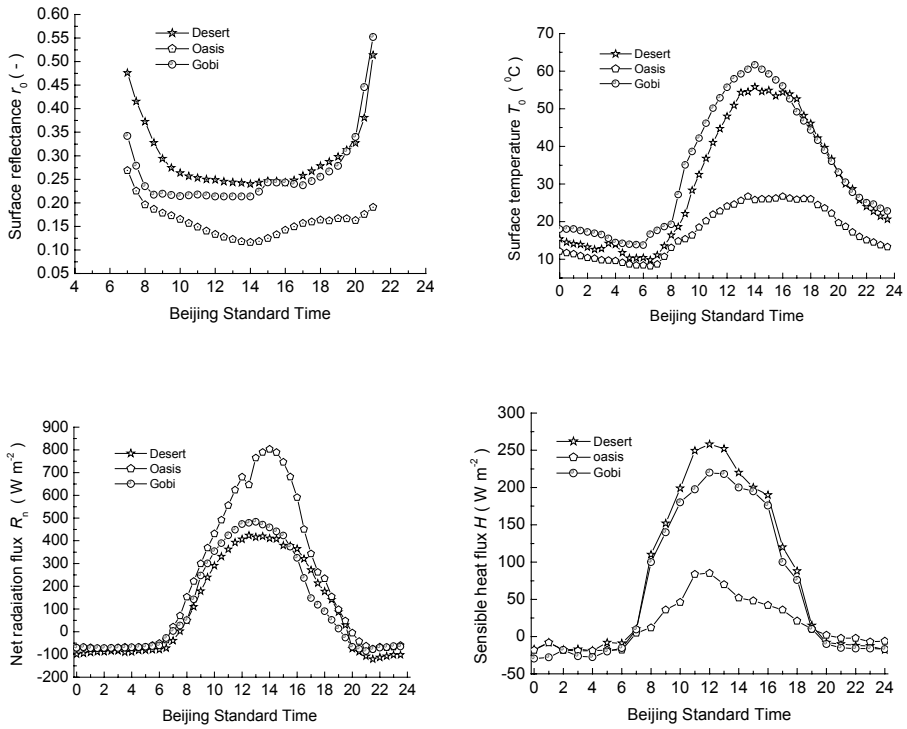


Figure 6.1 Comparisons of diurnal variations of surface reflectance r_0 , surface temperature T_0 , net radiation flux R_n and sensible heat flux H on 9 July 1991 above desert, oasis and Gobi surfaces obtained in the HEIhe basin Field Experiment (HEIFE) stations.

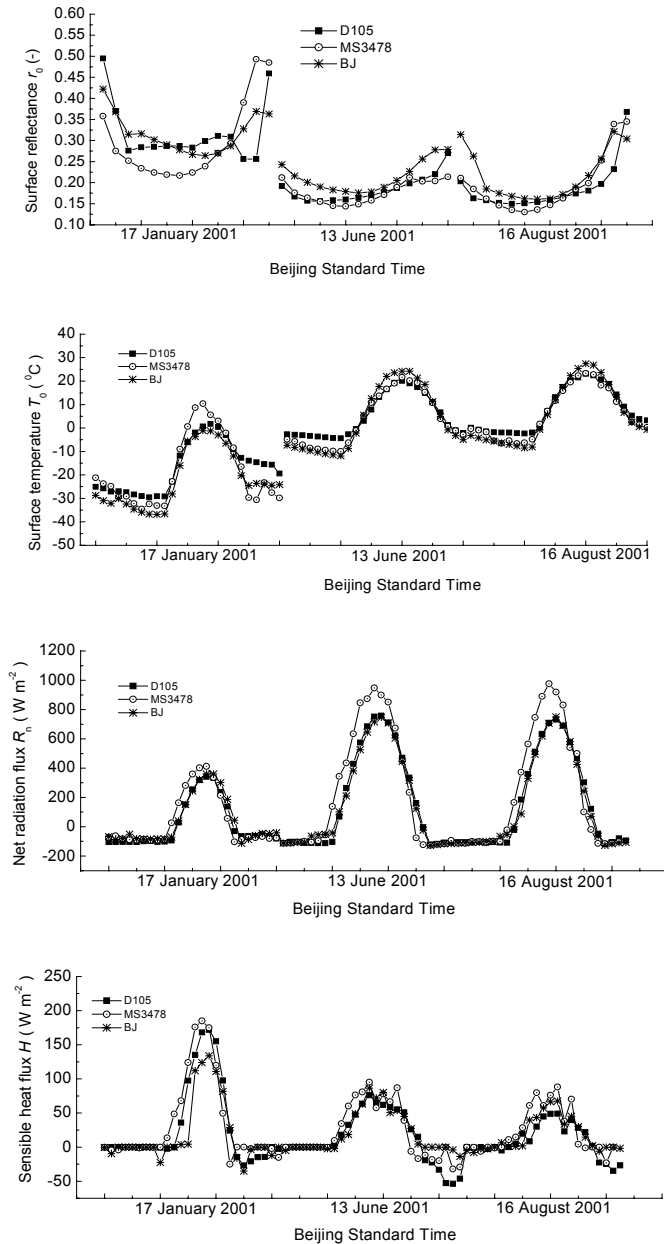


Figure 6.2 Comparisons of diurnal variations of surface reflectance r_0 , surface temperature T_0 , net radiation flux R_n and sensible heat flux H over the CAMP/Tibet stations D105, MS3478 and BJ.

The following can be concluded.

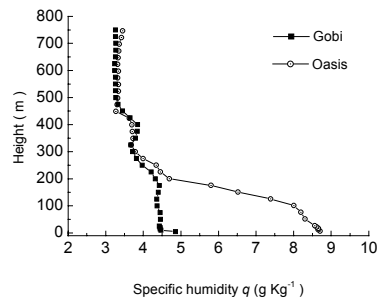
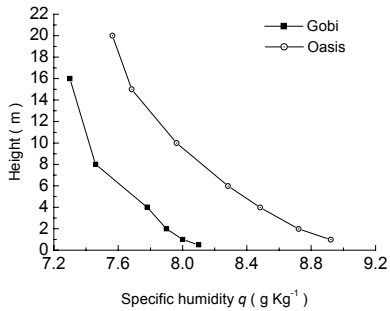
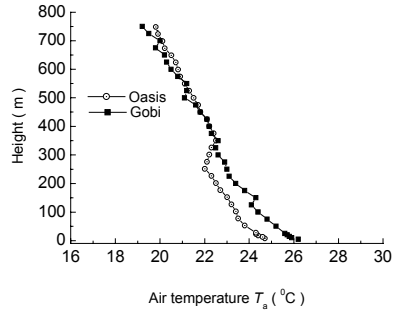
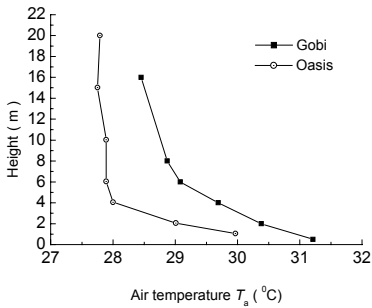
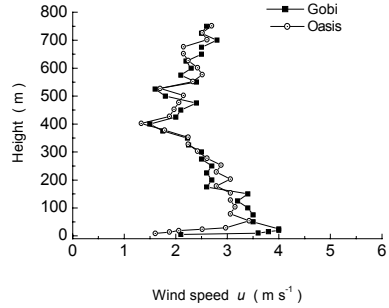
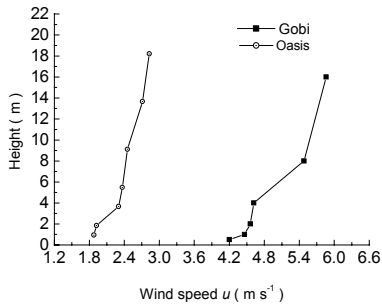
- (1) The surface heterogeneity resulted in different values of r_0 , T_0 , R_n and H over the HEIFE area. The values of r_0 , T_0 and H over the oasis surface are much lower than over the Gobi desert surfaces. R_n over the oasis is much higher than over Gobi and desert due to its lower r_0 and lower T_0 . The values of r_0 , T_0 , R_n and H in the Gobi zone and the desert zone are different, but the differences are not large.
- (2) Surface heterogeneity was observed at the stations in the CAMP/Tibet area: the MS3478 station has a relatively high vegetation fractional cover, while BJ and D105 have sparse vegetation covers. The land surface properties at the stations D105, MS3478 and BJ in the CAMP/Tibet are different i.e. r_0 is lower and R_n is higher over the MS3478 station. But the differences are not as large as between oasis and desert i. e. surface heterogeneity is not very large in the CAMP/Tibet area as compared to that in the HEIFE area.
- (3) The monthly variations of r_0 , T_0 , R_n and H over the CAMP/Tibet area are very clear: T_0 , R_n in summer (June and August) are higher than in winter (January), and r_0 and H in summer (June and August) are lower than in winter (January). The reason is that in summer the land surface is wet and the grass grows, and in winter the surface is covered by snow and ice and the grass is dry.

6.2.2 Influences of surface heterogeneity on the overlying convective atmospheric boundary layer

In order to show the influences of land surface heterogeneity on the overlying CABL, the vertical profiles of T_a , u and q will be shown in this section.

Figure 6.3 shows the vertical profiles of u , T_a and q over the very different surfaces of Gobi and oasis over the HEIFE area. Data used in Figure 6.3a was measured at a PBL tower and the ones shown in Figure 6.3b were measured by means of a Tethered balloon. Figure 6.4 gives the vertical profiles of u , T_a and q over the Gobi desert and oasis of the DHEX as measured by means of radio soundings (oasis) and Tethered balloon (Gobi) respectively. The vertical profiles of u , T_a and q observed from the radio sonde system at the BJ station of the CAMP/Tibet are shown in Figure 6.5. The results show that:

- (1) Due to the different surface properties the vertical profiles of u , T_a and q overlying the surfaces of Gobi and oasis in the HEIFE area are very different in the near surface layer. The values of u and T_a below a height of about 300 m over the Gobi surface are higher than over the oasis, q over the Gobi surface is lower than over the oasis. The values of u ,



(a)

(b)

Figure 6.3 The profiles of horizontal wind speed u , air temperature T_a and specific humidity q over the Gobi and oasis of the HEIhe basin Field Experiment (HEIFE). (a) Data are from the PBL tower observations at 12:00 on 8 August 1991; (b) Data are from the Tethered balloon observations at 12:00 on 15 August 1991.

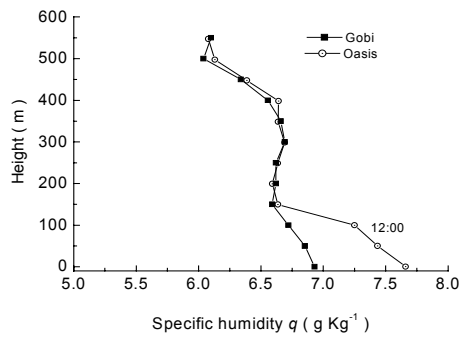
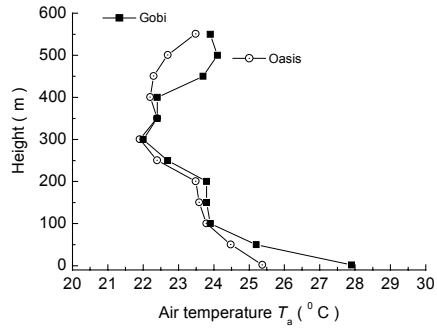
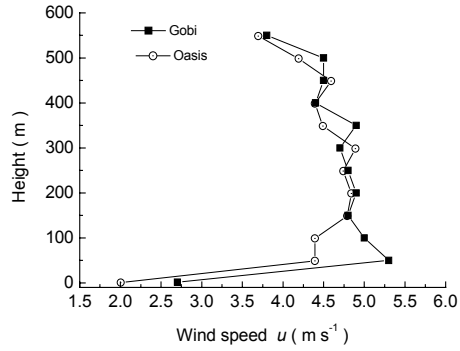


Figure 6.4 The profiles of horizontal wind speed u , air temperature T_a and specific humidity q on 3 June 2002 over the Gobi desert and oasis of the DunHuang EXperiment (DHEX).

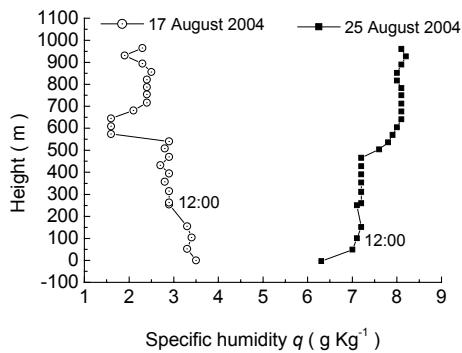
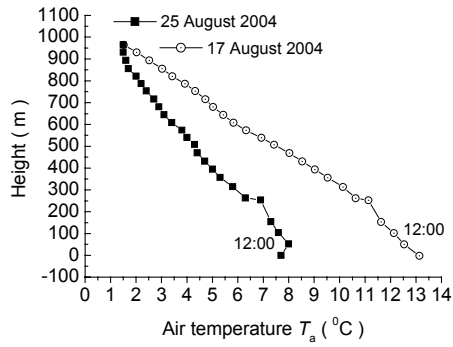
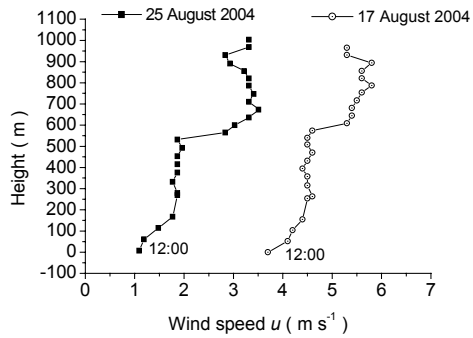


Figure 6.5 The profiles of horizontal wind speed u , air temperature T_a and specific humidity q on 17 and 25 August 2004 at the BJ station in the Tibetan Plateau (CAMP/Tibet).

T_a and q become almost the same at (and above) a height of about 300 m overlying the two very different land surfaces of Gobi and oasis. It means that u , T_a and q have become well mixed at (and above) the height of about 300 m. In other words, the surface heterogeneity has no influence above 300, and this height can be regarded as a blending height.

- (2) The vertical profiles of u , T_a and q overlying the surfaces of Gobi desert and oasis in the DHEX area are different in the near surface layer due to the different surface properties. The values of u and T_a below a height of about 150 m over the Gobi desert surface are higher than over the oasis, q over the Gobi desert surface is lower than over the oasis. The values of u , T_a and q become almost the same at (and above) a height of about 150 m overlying the two very different land surfaces of Gobi and oasis. It means that the ABL variables have become well mixed above the height of about 150 m. It can also be seen very clearly that the blending height (150m) over the DHEX area is lower than that over the HEIFE area. The reason is that the oasis spatial scale in the DHEX area is smaller than that in the HEIFE area (Figure 4.5b and Figure 4.7). Therefore the vertical structure of the air flow in the DHEX adjusted quickly to changes in the surface properties. The explanation of the relation between vertical and horizontal scales was given in Chapter 3.
- (3) Although only one radio sonde system was set up in the CAMP/Tibet area, the variability of the profiles of u , T_a and q overlying the grass land surface of the BJ station can also be seen clearly when we compare observations on two different days, i.e. 17 and 25 August 2004. Wind speed u increases with height at 12:00 (Beijing Standard Time, BST) on two days, and it becomes almost constant between 250 m and 550 m (u is about 4.5 m s^{-1} at 12:00 in 17 August 2004 and u is about 1.8 m s^{-1} at 12:00 on 25 August 2004). T_a decreases with height on both days. The q at 12:00 on 17 August 2004 decreases with height in the near surface atmospheric layer, and it becomes almost constant (about 2.9 g Kg^{-1}) between 250 m and 550 m. On the other hand, q at 12:00 in 25 August 2004 increases with height in the near surface layer (it was called “inverse humidity”), and it becomes almost constant (about 7.2 g Kg^{-1}) between 250 m and 480 m. Therefore, the height of about 250 m can be regarded as a blending height over the BJ station of the CAMP/Tibet area. The area of the experiment consists of typical pattern of very similar landscape units (see Figure 4.3). Each unit consists of a flat extensive area where the instrumented tower is located, surrounded by lower hills. The blending height derived at the BJ station can, therefore, be considered representative of

the entire experimental area.

6.2.3 Vertical variation of surface heat fluxes

Figure 6.6 shows the diurnal variations of H and λE at two levels (3 m and 20 m) on two very clear days of 24 June 2002 and 24 August 2002 at the BJ station of the CAMP/Tibet. The turbulence data, observed with a sonic anemometer-thermometer and an infrared hygrometer at two levels, was processed using the eddy correlation methodology. H and λE were calculated from

$$H = \rho c_p \overline{w'T_a'}$$
 (W m⁻²) (6.5)

$$\lambda E = \lambda \rho \overline{w'q'}$$
 (W m⁻²) (6.6)

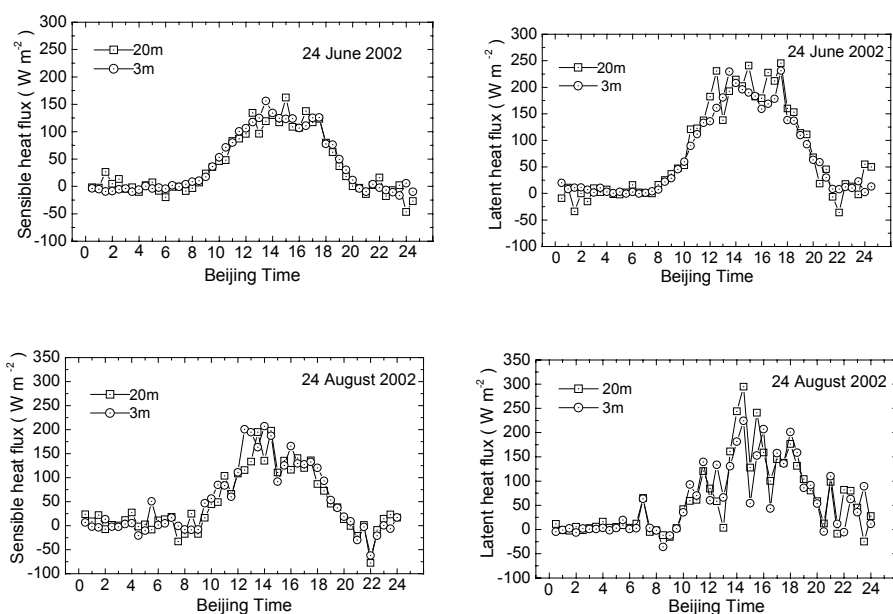


Figure 6.6 The diurnal variations of the sensible heat flux H and the latent heat flux λE at two levels (3 m and 20 m) on 24 June 2002 and 24 August 2002 over the BJ station at the Tibetan Plateau (CAMP/Tibet).

where ρ is air density, c_p is air specific heat at constant pressure, λ is latent heat of vaporization, E is evaporation flux, w' is the fluctuation of vertical wind velocity, T_a' is the fluctuation of air temperature, and q' is the fluctuation of specific humidity.

The results show that H and λE vary by less than 10 % of their magnitude with height over the BJ station. In other words, the surface layer (up to 20 m) over the BJ station is a constant flux layer, i.e. the Monin-Obukhov similarity theory applies to this height, and energy advection at BJ station can be neglected, at least up to 20 m.

6.3 Aerodynamic and thermodynamic variables over the different land surfaces

Land surface heterogeneity leads to different thermo-aerodynamic atmospheric variables (z_{0m} , z_{0h} and kB^{-1}) of the surface layer. Methods to estimate these variables will be described in this section.

6.3.1 Aerodynamic roughness length z_{0m}

The aerodynamic roughness length for momentum, z_{0m} , can be derived using two methods, i.e. the so called independent method (Chen et al., 1993) and the profile method.

The independent method using a single sonic anemometer-thermometer

According to the Monin-Obukhov similarity theory (Monin and Obukhov, 1954), the gradient of non-dimensional wind speed is written as:

$$\frac{kz}{u_*} \frac{\partial u}{\partial z} = \varphi_m \left(\frac{z}{L} \right) \quad (-) \quad (6.7)$$

Eq.6.7 is integrated to obtain the averaged wind speed U at height z as:

$$U = \frac{u_*}{k} \left[\ln \left(\frac{z}{z_{0m}} \right) - \psi_m \left(\frac{z}{L} \right) \right] \quad (\text{m s}^{-1}) \quad (6.8)$$

where $\varphi_m \left(\frac{z}{L} \right)$ is the similarity universal function and $\psi_m \left(\frac{z}{L} \right)$ is the stability function of the

wind profile, which becomes 0 under neutral conditions. The aerodynamic roughness length z_{0m} was derived from (Chen et al, 1993)

$$z_{0m} = ze^{-\frac{kU}{u_*} \psi_m\left(\frac{z}{L}\right)} \quad (\text{m}) \quad (6.9)$$

Through the same procedure the thermodynamic (heat transport) roughness length z_{0h} can be derived as:

$$z_{0h} = ze^{-\frac{k(T_a - T_0)}{T_0} \psi_h\left(\frac{z}{L}\right)} \quad (\text{m}) \quad (6.10)$$

where $\psi_h\left(\frac{z}{L}\right)$ is the stability function of the temperature profile and $\psi_h\left(\frac{z}{L}\right) = 0$ under neutral conditions.

The profile method

When the atmosphere is under near neutral conditions Eq.6.8 can be simplified to:

$$U = \frac{u_*}{k} \ln\left(\frac{z}{z_{0m}}\right) \quad (\text{m s}^{-1}) \quad (6.11)$$

According to Eq.6.11, if the averaged wind speed is observed at two different levels (z_1, z_2), the following expressions can be derived:

$$U_1 = \frac{u_*}{k} \ln\left(\frac{z_1}{z_{0m}}\right) \quad (\text{m s}^{-1}) \quad (6.12)$$

$$U_2 = \frac{u_*}{k} \ln\left(\frac{z_2}{z_{0m}}\right) \quad (\text{m s}^{-1}) \quad (6.13)$$

Finally, z_{0m} can be derived as:

$$z_{0m} = e^{\left(\frac{U_2 \ln z_1 - U_1 \ln z_2}{U_2 - U_1}\right)} \quad (\text{m}) \quad (6.14)$$

Observations of the non-dimensional wind speed kU/u_* versus the stability parameter

$\zeta = z/L$ over the Amdo and NPAM stations of the GAME/Tibet are shown in the Figures 6.7 and 6.9. Figure 6.8 shows the aerodynamic roughness length z_{0m} derived from the wind

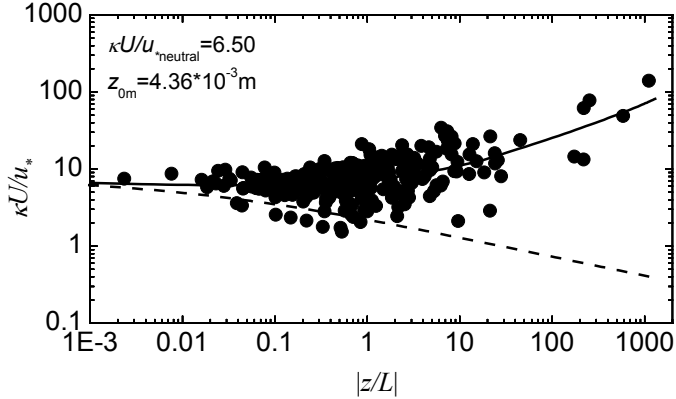


Figure 6.7 Non-dimensional wind speed kU/u^* versus the stability parameter $\zeta=z/L$ as derived by the independent method over the NPAM (MS3478) station at the Tibetan Plateau (GAME/Tibet).

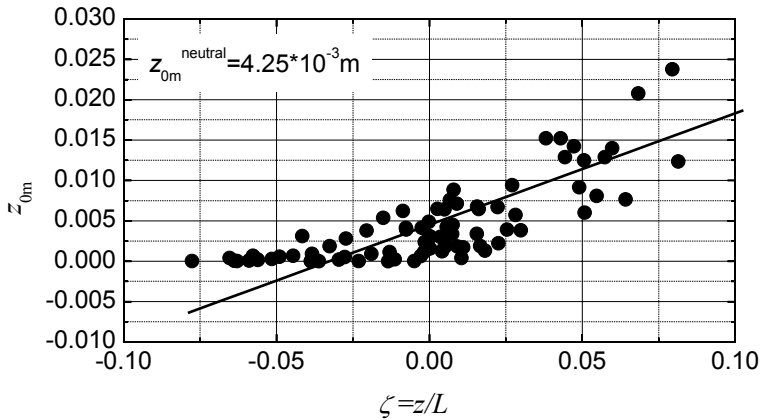


Figure 6.8 The surface momentum roughness length z_{0m} derived from the wind profile at the Amdo station in the Tibetan Plateau (GAME/Tibet).

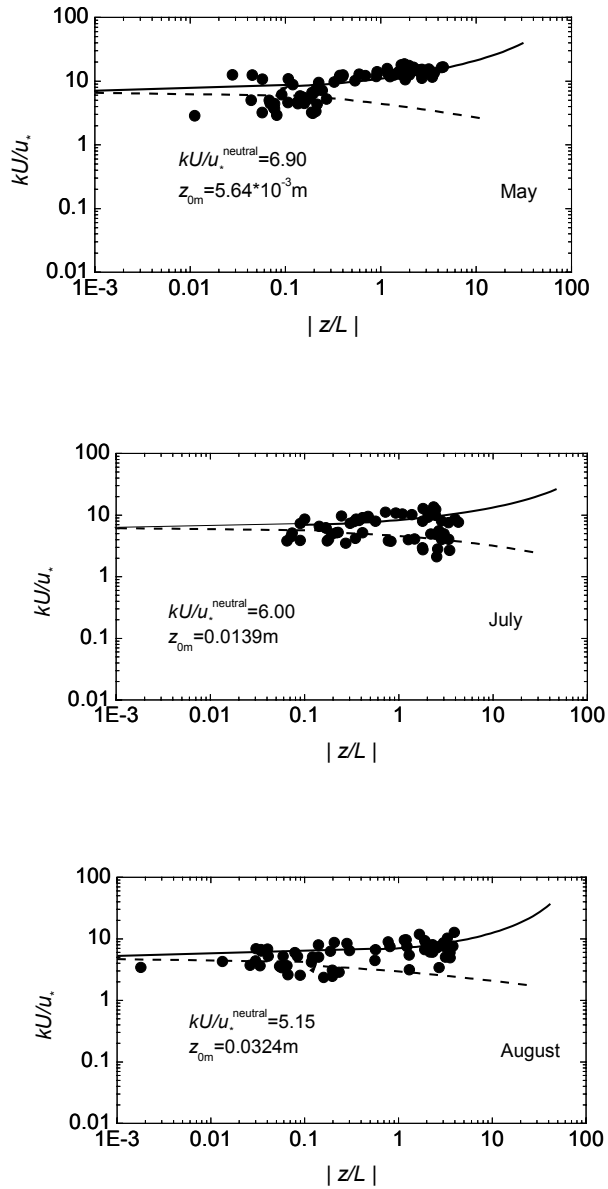


Figure 6.9 Non-dimensional wind speed kU/u_* versus the stability parameter $\zeta=z/L$ at the NPAM (MS3478) station in the Tibetan Plateau (GAME/Tibet) in the months May, July and August.

profile at the Amdo station. Using the Eqs.6.9 and 6.14, the aerodynamic roughness length z_{0m} at the NPAM and Amdo stations in the GAME/Tibet area can be determined. The stability parameter $\zeta = z/L$ between -0.100 and 0.100 applies to neutral conditions. The values of z_{0m} in the HEIFE and AECMP'95 areas were derived by the same method. All the results are shown in Table 6.1.

Table 6.1 Aerodynamic roughness length z_{0m} derived from different land surfaces by using the independent method

	Amdo	NPAM	HEIFE	HEIFE	HEIFE	HEIFE	AECMP'95
Land surface	Grass land, ~5cm	Grass land, ~15cm	Sand desert	Very sparse vegetation (Gobi)	Bean, ~0.4m	Wheat, ~1.0m	Corn, ~1.8m
Observation height(m)	2.90	5.60	2.90	2.90	2.90	2.90	4.90
z_{0m} (m)	0.00436 ±0.00040	0.00564 (May) 0.0139 (July) 0.0324 (August)	0.00267 ±0.0003	0.00280 ±0.00030	0.06100 ±0.00400	0.16800 ±0.03000	0.30200 ±0.0200

Summarizing:

- z_{0m} is significantly different for grassland, sand desert, Gobi and oasis.
- z_{0m} at the Amdo and NPAM stations of the GAME/Tibet is higher than the value obtained for Gobi and sand desert (HEIFE), but is lower than those obtained for the oasis (HEIFE: three sites); z_{0m} at the NPAM station is larger than at the Amdo station.
- The values of z_{0m} obtained at the Amdo station with different methods (independent method and profile method) are comparable (Figure 6.7 and Figure 6.8).
- z_{0m} at the NPAM station has a different value in different months (May, July and August) due to the high vegetation fractional cover in the station. It is clear that canopy height determines the aerodynamic roughness length z_{0m} at this station.

6.3.2 Thermodynamic roughness length z_{0h}

Figure 6.10 shows the non-dimensional air temperature $k(T_a - T_0)/T_*$ versus the stability parameter $\zeta = z/L$ at the Amdo station in the Tibet Plateau. These observations

yield $z_{0h-Amdo}=0.000409$ m with $\zeta = z/L$ between -0.100 and 0.100 applying to neutral conditions. The thermodynamic roughness length z_{0h} of grassland, sand desert, Gobi and oasis are given in Table 6.2. They were obtained by the same method as mentioned in the previous section. It indicates that z_{0h} has very different values for different land cover types and z_{0h} is one order of magnitude smaller than z_{0m} in the GAME/Tibet area. The reason is that the thermodynamic roughness length z_{0h} is not only a function of temperature gradient, but is also affected by the canopy height and fractional vegetation cover.

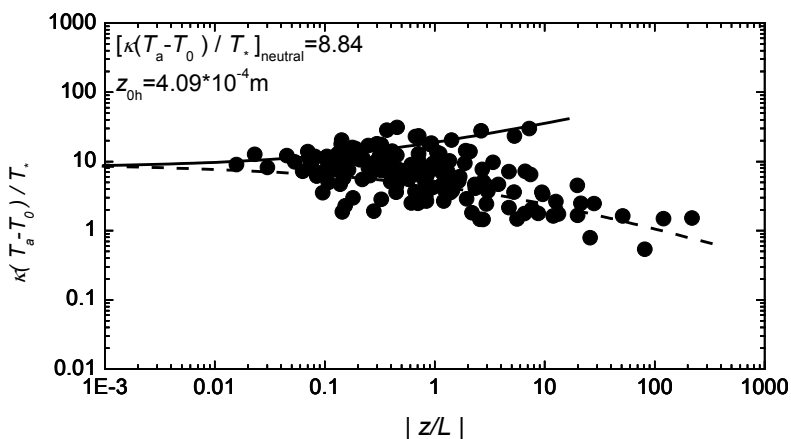


Figure 6.10 Non-dimensional air temperature $k(T_a - T_0) / T_*$ versus the stability parameter $\zeta = z/L$ at the Amdo station in the Tibetan Plateau (GAME/Tibet).

Table 6.2 Thermodynamic roughness length z_{0h} derived from different land surfaces

	Amdo	NPAM	HEIFE	HEIFE	HEIFE	HEIFE	AECMP'95
Land surface	Grass land, ~5cm	Grass land, ~15cm	Sand desert	Very sparse vegetation (Gobi)	Bean, ~0.4m	Wheat, ~1.0m	Corn, ~1.8m
Height(m) of observation	2.90	5.60	2.90	2.90	2.90	2.90	4.90
z_{0h}(m)	0.00041 ±0.00005	0.00051 (May) 0.00114 (July) 0.00231 (August)	0.000049	0.000011	0.000685	0.00132	0.00227

6.3.3 Excess resistance to heat transfer kB^{-1}

The excess resistance to heat transfer kB^{-1} is used to parameterize the sensible heat exchange between the land surface and atmosphere. It appears as a variable in many numerical models and satellite remote sensing parameterization methods, and can be derived from the equation (Owen and Thomson, 1963; Chamberlain, 1968):

$$kB^{-1} = \ln\left(\frac{z_{0m}}{z_{0h}}\right) \quad (-) \quad (6.15)$$

An alternative expression for kB^{-1} can be obtained from the bulk transfer equation as (Monteith, 1973):

$$kB^{-1} = \frac{ku_*(T_0 - T_a)}{H_{\text{obs}}/\rho c_p} - \left[\ln \frac{z - d_0}{z_{0m}} - \psi_h\left(\frac{z}{L}\right) \right] \quad (-) \quad (6.16)$$

where u_* , H_{obs} , and L can be derived from the data observed by using a PBL tower and sonic anemometer-thermometer. Based on turbulent measurements and $k=0.40$, z_{0m} was derived from Eqs 6.9 and 6.14, zero-plane displacement d_0 was obtained from $d_0 = (2/3) h_v$ (Brutsaert, 1984) for every station, which h_v being the canopy height. The diurnal variations of kB^{-1} were derived through Eq.6.16 for the GAME/Tibet area and the HEIFE area. The results are shown in Figure 6.11 and Figure 6.12. Figure 6.13, Figure 6.14 and Figure 6.15 show the values of kB^{-1} versus T_0 , $T_0 - T_a$ and $U(T_0 - T_a)$ over grassland, Gobi, sand desert and oasis in the GAME/Tibet and HEIFE areas. The kB^{-1} values derived from Eq. 6.15 for different land cover types are shown Table 6.3.

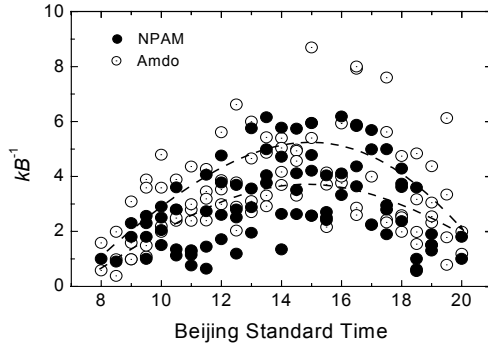


Figure 6.11 Diurnal variations of the excess resistance to heat transfer kB^{-1} derived through Eq.6.16 over the Amdo and NPAM stations at the Tibetan Plateau (GAME/Tibet).

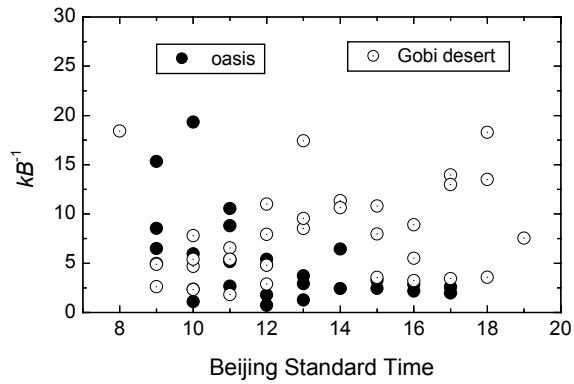


Figure 6.12 Diurnal variations of the excess resistance to heat transfer kB^{-1} , derived through Eq.6.16 over the Gobi desert and the oasis of the HEIhe basin Field Experiment (HEIFE) area.

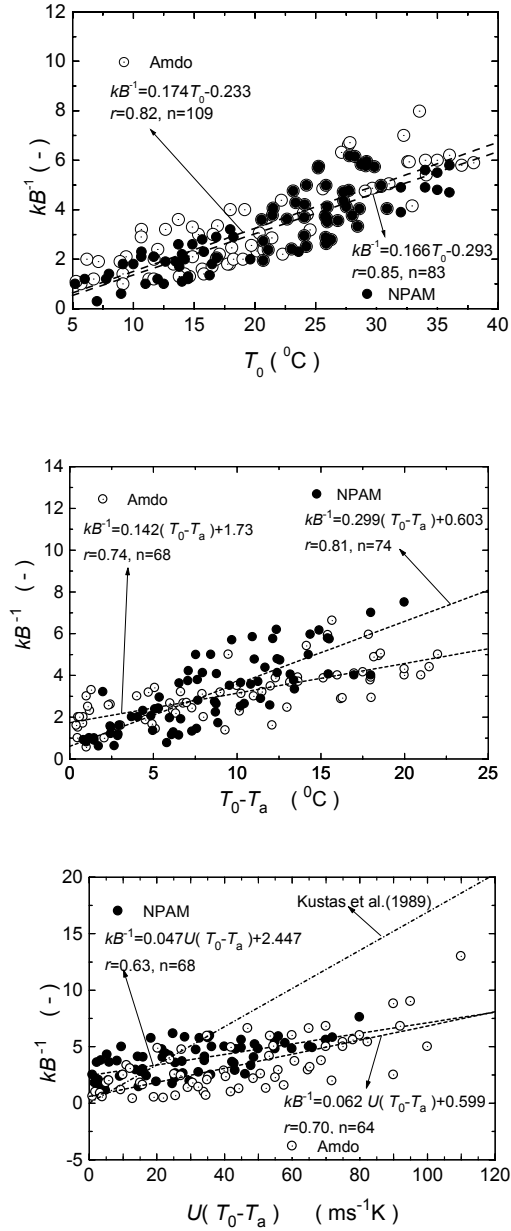


Figure 6.13 Values of the excess resistance to heat transfer, kB^{-1} (Eq.6.16) versus T_0 , $T_0 - T_a$ and $U(T_0 - T_a)$ over the Amdo and NPAM stations at the Tibetan Plateau (GAME/Tibet).

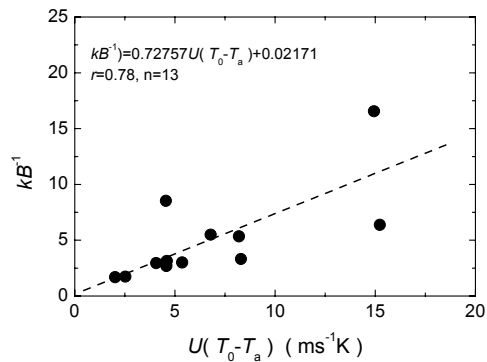
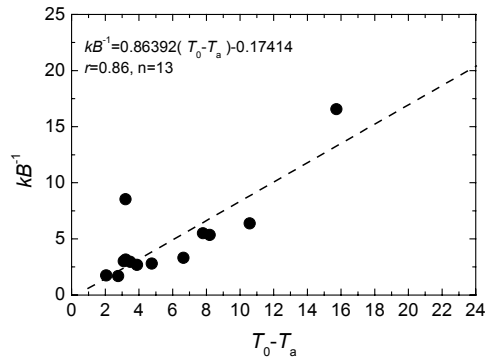
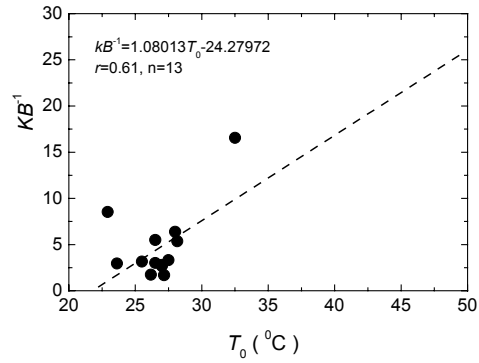


Figure 6.14 Values of the excess resistance to heat transfer, kB^{-1} (Eq.6.16) as plotted versus T_0 , $T_0 - T_a$ and $U(T_0 - T_a)$ over the oasis surface of the HEIhe basin Field Experiment (HEIFE) area.

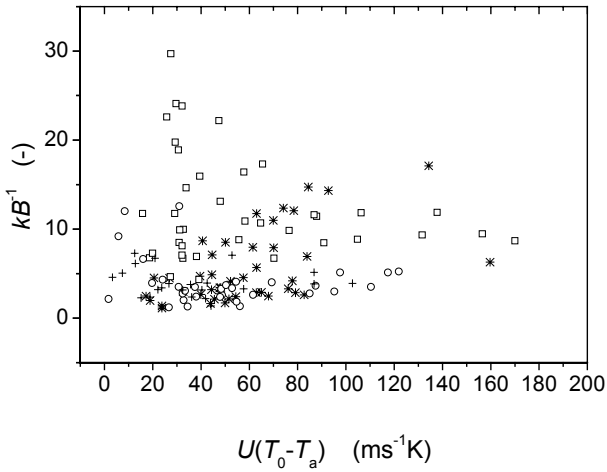
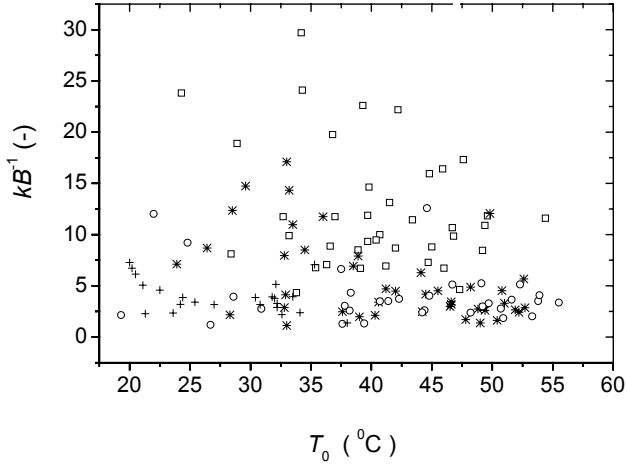


Figure 6.15 Values of the excess resistance to heat transfer, kB^{-1} (Eq.6.16) as plotted versus T_0 and $U(T_0-T_a)$ over the Gobi and desert surface of the HEIhe basin Field Experiment (HEIFE) (after Jia et al., 2000). (\circ : desert-August 1995, $+$: desert-October 1992, $*$: Gobi-October 1992, \square : D1-August 1995)

Table 6.3 Excess resistance to heat transfer kB^{-1} of different land cover types

	Amdo	NPAM	HEIFE	HEIFE	HEIFE	HEIFE	AECMP'95
Land surface	Grass land ~5cm	Grass land ~15cm	Sand desert	Very sparse vegetation (Gobi)	Bean ~0.4m	Wheat ~1.0m	Corn ~1.8m
Observed height (m)	2.90	5.60	2.90	2.90	2.90	2.90	4.90
$\overline{kB^{-1}}$	2.36	2.50	4.00	5.50	4.49	4.85	4.89

The following conclusions can be drawn:

- The values of kB^{-1} have obvious diurnal variations for the GAME/Tibet area. Although the values of kB^{-1} are different at different hours, they show no distinct diurnal variations over the HEIFE area. Because of this temporal variability, the values derived by other researchers cannot directly be used. Also in satellite remote sensing parameterization methods over our study area, kB^{-1} cannot be considered as a constant (e.g. Garratt et al., 1973; Garratt 1978; Guo and Wang, 1993; Verhoef et al., 1997), and different values of kB^{-1} should be used at different hours of the day.
- For the GAME/Tibet area a linear relationship exists between: a) kB^{-1} and T_0 (the correlation coefficient $r=0.82$ for Amdo and $r=0.85$ for NPAM); b) kB^{-1} and T_0-T_a ($r=0.74$ for Amdo and $r=0.81$ for NPAM); and c) kB^{-1} and $U(T_0-T_a)$ ($r=0.70$ for Amdo and $r=0.63$ for NPAM). The linear relationship between kB^{-1} and T_0 is the best and can be applied to estimate the heat fluxes using satellite data for the GAME/Tibet area. The results derived in the literature (e.g. Kustas et al., 1989) cannot be used for the grass marshland surface of the Tibetan Plateau (Figure 6.13).
- Due to the very different surface properties in the two areas the relations between kB^{-1} and other atmospheric parameters are quite different over the surfaces of Gobi desert and oasis in the HEIFE area. For the oasis in the HEIFE area there exist linear relationships between: a) kB^{-1} and T_0 (correlation coefficient $r=0.61$); b) kB^{-1} and T_0-T_a ($r=0.86$); and c) kB^{-1} and $U(T_0-T_a)$ ($r=0.78$). Among them the relationship between kB^{-1} and T_0-T_a is the best. For Gobi desert in the HEIFE area (Figure 6.15) there exist no similar relationships. *It means that no common relationship between kB^{-1} and other variables can be used to parameterize heat fluxes over the HEIFE area.*
- The average values of $kB^{-1}_{NPAM}=2.50$ and $kB^{-1}_{Amdo}=2.36$ derived from Eq.6.15 are very close to the results of $kB^{-1}_{NPAM}=2.56$ and $kB^{-1}_{Amdo}=2.40$ derived from Eq.6.16. The latter two values were averaged over 10 observations from 9:00 PM Beijing Standard Time (BST) to 6:00 AM BST (see Figure 6.11).
- The averaged kB^{-1} of the GAME/Tibet area agree with the well known result $kB^{-1}=2.3$

(Choudhury, 1989), but it is larger than 2.3 in the HEIFE area.

6.4 Summary and conclusions

Understanding of the Surface Layer (SL) and Atmospheric Boundary Layer (ABL) processes over heterogeneous land surfaces is very important in the procedure of scaling up heat fluxes from the observational station i.e. “point” level to the regional scale. The land surface heterogeneity and its influences on the overlying atmospheric layer and the aerodynamic and thermodynamic parameters has been analyzed by using SL and ABL observations during the GAME/Tibet, the CAMP/Tibet, the HEIFE, the DHEX and the AECMP’95. The results described in this chapter can be summarized as follows.

- Very different values of surface reflectance r_0 , surface temperature T_0 , net radiation flux R_n and sensible heat flux H between the Gobi desert and oasis show that land surface heterogeneity is very significant in the HEIFE area. Surface heterogeneity at the CAMP/Tibet area is less significant than in the HEIFE area.
- The land surface heterogeneity leads in the near surface layer to different vertical profiles of horizontal wind speed u , air temperature T_a and specific humidity q overlying the surfaces of Gobi and oasis in the areas of the HEIFE and DHEX. The values of u , T_a and q become well mixed above a height of about 300 m at the HEIFE and 150 m at the DHEX. It means that a clearly defined blending height z_b can be observed over both experimental areas. The difference of z_b results from the oasis horizontal scale. In other words, the larger oasis scale will lead to a higher z_b value (see Chapter 3). Although one radio sonde system data was available, on a normal summer day about 250 m can be regarded as a blending height over the whole CAMP/Tibet area. It is also very clear that z_b determined by the ABL observations over the experimental areas is a direct and correct way. It is better than estimations from the Eqs.3.8 and 3.9 (Chapter 3 and Chapter 5).
- H and λE vary with height over the CAMP/Tibet station by less than 10% of their magnitude. It means that the surface layer (up to 20m) of the CAMP/Tibet area can be regarded as a constant flux layer and the energy advection in the near surface layer can be neglected. Therefore, the Monin-Obukhov similarity theory can be used for the surface layer in the CAMP/Tibet area.
- The aerodynamic roughness length z_{0m} and the thermodynamic roughness length z_{0h} are significantly different over the different land surfaces of grassland, Gobi, sand desert and oasis. For the GAME/Tibet area z_{0h} is one magnitude smaller than z_{0m} . It

means that both the aerodynamic and thermodynamic characteristics of the land surface have effects on z_{0m} and z_{0h} . In other words, it is not correct that estimate z_{0m} and z_{0h} would have been estimated from *NDVI* only (Chapter 5).

- The excess resistance to heat transfer, kB^{-1} , has obvious characteristics over different land cover types. It has different values for grassland, Gobi, sand desert and oasis. It is very clear that a kB^{-1} -value of 2.3 cannot be used as a general value for the HEIFE area (Chapter 5). kB^{-1} over the GAME/Tibet area show evidently diurnal variations. Hence, kB^{-1} values derived by other researchers cannot directly be applied to parameterize heat fluxes from satellite data. In other words, the different values of kB^{-1} should be used at different hours of a day. There are better linear relationships between kB^{-1} and surface temperature T_0 over the GAME/Tibet area, while no similar relationship between kB^{-1} and other atmospheric and surface parameters (T_0 , T_a and horizontal averaged wind speed U) was observed over the HEIFE area.

Some more general conclusions that can be drawn are the following.

- 1) *Very different land cover types and hydrological conditions (e.g. the oasis and the Gobi desert over the HEIFE area and the DHEX area) lead to different Surface Layer Atmospheric Boundary Layers. These layers however adjust to land surface properties over spatial scales varying from 1 to 10 km (Chapter 3).* It means that different ABL vertical profiles and different resistances exist over quite different land surfaces.
- 2) *Limited land surface heterogeneities such as the grass land and topography over the areas of GAME/Tibet and CAMP/Tibet, results however in the same SL and ABL over the whole area.* In other words, in these areas the land surface is statistically homogeneous and the ABL adjusts to a mixture combination of small scale heterogeneities. *Therefore, effective variables and one resistance may for such conditions be used to determine the sensible and latent heat fluxes.*

The above mentioned concepts, as well as the aerodynamic and thermodynamic variables determined in this chapter will further be used in Chapter 7 to parameterize the near surface heat fluxes using in addition satellite measurements.

7. Estimation of regional surface heat fluxes using satellite measurements in combination with surface layer and atmospheric boundary layer observations

7.1 Introduction

In Chapter 5, the *RS approach* was used to estimate the regional distribution of sensible heat flux H and latent heat flux λE over the HEIFE area. But the results showed that the estimated H and λE over some areas were not accurate due to the shortcomings of the applied parameterization methodology.

In order to overcome these shortcomings, the *Tile approach* can be used to estimate regional distributions of H and λE using satellite measurements and Surface Layer (SL) observations (Chapter 3). But the *Tile approach* needs many measurements for each *tile*. To avoid this shortcoming, as a simplification of the *Tile approach*, i.e. the *Blending height approach* (Chapter 3) was used to estimate regional distributions of H and λE over heterogeneous land surfaces.

The objective of the present chapter is to *apply the Tile approach as well as the*

This chapter is based on:

- (1) **Ma, Y.**, O. Tsukamoto, H. Ishikawa, Z. Su, M. Menenti, J. Wang, J., and J. Wen, 2002a, Determination of Regional land surface heat flux densities over heterogeneous landscape of HEIFE Integrating satellite remote sensing with ground observations, *Journal of Meteorological Society of Japan*, **80**(3): 485-501.
- (2) **Ma, Y.**, H. Ishikawa, O. Tsukamoto, M. Menenti, Z. Su, T. Yao, T. Koike, and T. Yasunari, 2003a, Regionalization of surface fluxes over heterogeneous landscape of the Tibetan Plateau by using satellite remote sensing, *Journal of Meteorological Society of Japan*, **81**(2): 277-293.
- (3) **Ma, Y.**, J. Wang, R. Huang, G. Wei, M. Menenti, Z. Su, Z. Hu, F. Gao, and J. Wen, 2003b, Remote sensing parameterization of land surface heat fluxes over arid and semi-arid areas, *Advances in Atmospheric Sciences*, **20**(4):530-539.
- (4) **Ma, Y.**, 2003c, Remote sensing parameterization of regional net radiation over heterogeneous land surface of GAME/Tibet and HEFE, *International Journal of Remote Sensing*, **24** (15): 3137-3148.
- (5) **Ma, Y.**, M. Menenti, O. Tsukamoto, H. Ishikawa, J. Wang, and Q. Gao, 2004a, Remote sensing parameterization of regional land surface heat fluxes over arid area in northwestern China, *Journal of Arid Environments*, **57**: 117-133.
- (6) **Ma, Y.**, L. Zhong, Z. Su, H. Ishikawa, M. Menenti, and T. Koike, 2006, Determination of regional distributions and seasonal variations of land surface heat fluxes from Landsat-7 Enhanced Thematic Mapper data over the central Tibetan Plateau area, *Journal of Geophysical Research*, **111**, D10305, doi: 10.1029/2005JD006742.

Blending height approach to estimate the regional land surface heat fluxes over the experimental areas of the HEIFE, the AECMP'95, the DHEX, the GAME/Tibet and the CAMP/Tibet. The plan of this chapter is as follows.

- a) The general procedures of the *Tile approach* and the *Blending height approach* and the comparison between the *RS approach*, the *Tile approach* and the *Blending height approach* will be summarized in Section 7.2.
- b) The satellite data, the ground observational data and the approaches to apply in the experimental case studies areas will be summarized in Section 7.3. The results from these approaches applied to the case studies areas will also be shown.
- c) Finally the summary and conclusions will be given in Section 7.4.

7.2 Implementation of the Tile approach and the Blending height approach

7.2.1 Tile approach

The overall concept of the *Tile approach* was treated in Chapter 3. Its parameterization diagram is shown in Figure 7.1 (Ma et al., 2004a). Values of surface reflectance r_0 and surface temperature T_0 are derived from Landsat-5 Thematic Mapper (TM) measurements and Landsat-7 Enhanced Thematic Mapper (ETM) measurements. These satellite data are corrected for atmospheric effects using the radiative transfer model MODTRAN (Berk et al. 1989). For this purpose surface and atmospheric observational data are used. This radiative transfer model also computes the downward short wave surface radiation flux K_{\downarrow} and the downward long wave surface radiation flux L_{\downarrow} . With these results the net radiation flux R_n is determined. Soil heat flux G_0 is estimated from R_n , T_0 , r_0 and *MSAVI* (Ma et al., 2002a; Ma et al., 2002b; Ma et al., 2003a; Ma et al., 2003b; Ma et al., 2004a; Ma et al., 2004b; Ma et al., 2005), as well as derived from Landsat-5(7) TM (ETM) measurements. H is estimated from T_0 , surface and atmospheric data with the aid of the *Tile approach* (Ma et al., 2004a, Chapter 3). Finally λE is obtained as the residual of the energy budget equation.

Net radiation flux R_n

The regional net radiation flux $R_n(x,y)$ was derived from Eq.2.3. The variables in the Eq.2.3 were determined in different ways according to the different satellite data. Eq.2.19

was used to determine $\varepsilon_0(x, y)$. Eq.2.6 and Eq.2.17 were applied to determine $r_0(x, y)$ and $T_0(x, y)$ using the Landsat-5 (7) TM (ETM) data. The incoming short-wave radiation flux $K_{\downarrow}(x, y)$ in Eq.2.3 was derived from Eq.2.22. In the same way the incoming long-wave radiation flux $L_{\downarrow}(x, y)$ in Eq.2.3 was derived from MODTRAN directly (Chapter 2).

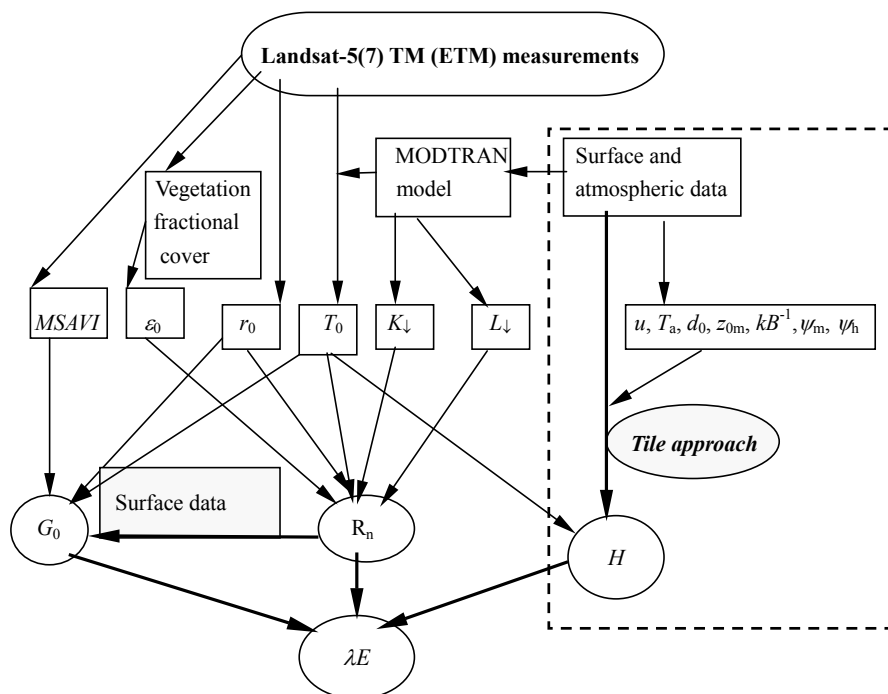


Figure 7.1 Diagram of the *Tile approach*. Surface reflectance r_0 and surface temperature T_0 are derived from Landsat-5(7) TM (ETM) measurements. These data are corrected for atmospheric effects using the radiative transfer model MODTRAN. For these purpose surface and atmospheric observational data are used. This radiative transfer model also computes the surface downward short- and long- wave radiation. With these results R_n is determined. G_0 is estimated from R_n , T_0 , r_0 and $MSAVI$. H is estimated from T_0 , surface and atmospheric observational data with the aid of the *Tile approach*. Finally λE is obtained as the residual of the energy budget equation.

Soil heat flux G_0

The regional soil heat flux $G_0(x,y)$ was determined through Eq.2.28 (Ma et al., 2002a; Ma et al., 2002b; Ma et al., 2003a; Ma et al., 2003b; Ma et al., 2004a; Ma et al., 2004b; Ma et al., 2005). Based on ground observations, the constants in Eq.2.28 applying to the experimental areas are shown in Table 7.1.

Table 7.1 Constants in Eq.2.28 over the experimental areas of the HEIFE, the AECMP'95, the DHEX and the GAME/Tibet.

	<i>a</i>	<i>b</i>	<i>c</i>	<i>d</i>	<i>e</i>
HEIFE	0.00028	0.004364	0.00846	-0.97892	4
AECMP'95	0.00025	0.004364	0.00845	-0.97900	4
DHEX	0.00028	0.004240	0.00875	-0.98200	4
GAME/Tibet	0.00029	0.004540	0.00878	-0.96400	4

Sensible heat flux H

In the areas of the DHEX and the AECMP'95 only agricultural oasis and Gobi desert exist. The length scales of heterogeneity for these areas were relative small (Chapter 4 and Chapter 6). The atmospheric variables have been measured or derived over each land cover type. In other words, the atmospheric variables at the reference height (e.g. 20 m) over the oasis and Gobi desert have been measured as: u_{oasis} and $u_{\text{Gobi-desert}}$, $T_{\text{a-oasis}}$ and $T_{\text{a-Gobi-desert}}$. Also the other atmospheric variables below the reference height have been derived as: $d_{0\text{-oasis}}$ and $d_{0\text{-Gobi-desert}}$, $z_{0\text{m-oasis}}$ and $z_{0\text{m-Gobi-desert}}$, kB^{-1}_{oasis} and $kB^{-1}_{\text{Gobi-desert}}$, $\psi_{\text{m-oasis}}$ and $\psi_{\text{m-Gobi-desert}}$, and $\psi_{\text{h-oasis}}$ and $\psi_{\text{h-Gobi-desert}}$. Hence, the sensible heat flux H was then calculated from Eq.3.18 over different land surface types according to:

$$H_{\text{oasis}}(x, y) = \rho c_p k^2 u_{\text{oasis}} \frac{[T_0(x, y) - T_{\text{a-oasis}}]}{\left[\ln \frac{z - d_{0\text{-oasis}}}{z_{0\text{m-oasis}}} + kB^{-1}_{\text{oasis}} - \psi_{\text{h-oasis}} \right] \cdot \left[\ln \frac{z - d_{0\text{-oasis}}}{z_{0\text{m-oasis}}} - \psi_{\text{m-oasis}} \right]} \quad (\text{Wm}^{-2}) \quad (7.1)$$

$$H_{\text{Gobi-desert}}(x, y) = \rho c_p k^2 u_{\text{Gobi-desert}} \cdot \frac{[T_0(x, y) - T_{\text{a-Gobi-desert}}]}{\left[\ln \frac{z - d_{0\text{-Gobi-desert}}}{z_{0\text{m-Gobi-desert}}} + kB^{-1}_{\text{Gobi-desert}} - \psi_{\text{h-Gobi-desert}} \right] \cdot \left[\ln \frac{z - d_{0\text{-Gobi-desert}}}{z_{0\text{m-Gobi-desert}}} - \psi_{\text{m-Gobi-desert}} \right]}$$

Hence, H over whole area was derived through Eq.3.19 as:

$$H(x, y) = a(\text{oasis})H_{\text{oasis}}(x, y) + a(\text{Gobi - desert})H_{\text{Gobi-desert}}(x, y) \quad (\text{Wm}^{-2}) \quad (7.2)$$

where a (oasis) and a (Gobi-desert) were the fractional ratios of oasis and Gobi desert over the experimental areas of the DHEX and the AECMP'95.

Latent heat flux λE

The regional $\lambda E(x, y)$ was determined from Eq.2.50, Eq.3.18 and Eq.3.19. But to determine $\lambda E(x, y)$ from the satellite measurements through Eq.2.50, Eq.3.18 and 3.19 we needed to determine the turbulent transport resistances first. To avoid the difficulty, Eq.2.51 was used to determine the regional $\lambda E(x, y)$ over the experimental areas of the AECMP'95 and the DHEX.

7.2.2 Blending height approach

The overall concept of the *Blending height approach* was shown in Chapter 3. Its parameterization diagram is shown in the Figures 7.2 (Ma et al., 2002a; Ma et al., 2003a; Ma et al., 2005; Ma et al., 2006). The determination procedures of r_0 , T_0 , $MSAVI$, vegetation fractional cover, ϵ_0 , K_{\downarrow} , L_{\downarrow} , R_n and G_0 are the same as that in the *Tile approach*. H is estimated from T_0 , surface and atmospheric observational data with the aid of the *Blending height approach*. Finally λE is obtained as the residual of the energy budget. The main differences between the *Blending height approach* and the *Tile approach* are shown in the right dash frames in the Figures 7.1 and 7.2. They will be documented in the next section.

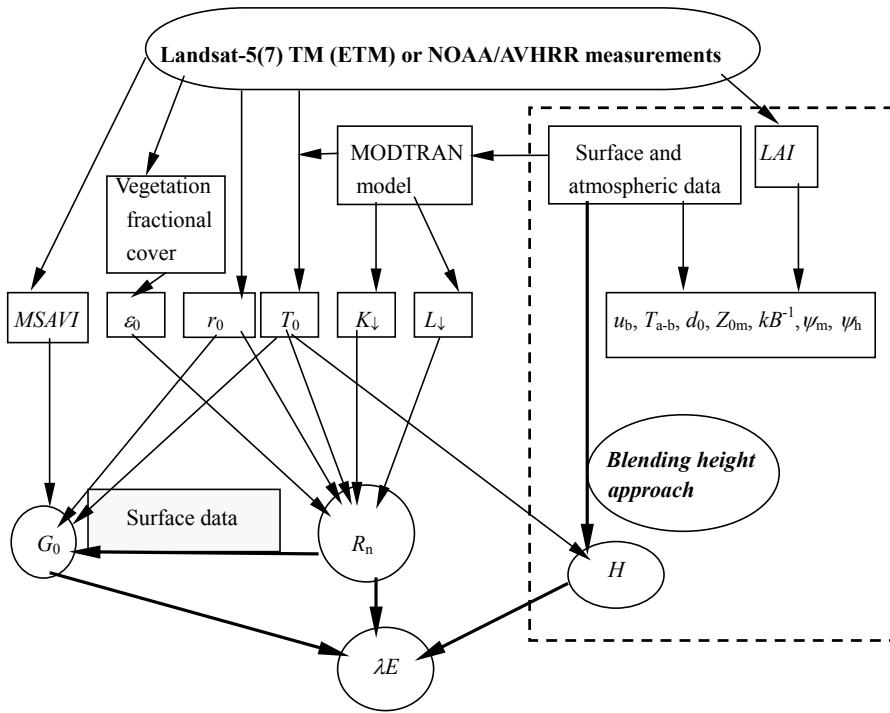


Figure 7.2 Diagram of the *Blending height approach*. The determination procedures of surface reflectance r_0 , surface temperature T_0 , *MSAVI*, vegetation fractional cover, emissivity ε_0 , downward surface short wave radiation flux K_{\downarrow} , downward surface long wave radiation flux L_{\downarrow} , net radiation flux R_n and soil heat flux G_0 are the same as in Figure 7.1. Sensible heat flux H is estimated from T_0 , surface and atmospheric observational data with the aid of *Blending height approach*. Finally λE is obtained as the residual of the energy budget equation.

Net radiation flux R_n

The determination procedures of regional net radiation flux $R_n(x,y)$ was the same as in the *Tile approach*. The only differences were the determinations of r_0 and T_0 from the NOAA/AVHRR measurements in the Tibetan Plateau. Based on the Tibetan Plateau NOAA/AVHRR measurements, surface and atmospheric data and Eq.2.7, the surface reflectance over the Tibetan Plateau was estimated as (Ma et al., 2003a):

$$r_{\text{broadband}}(x, y) = 0.546r_{\text{AVHRR-1}}(x, y) + 0.454r_{\text{AVHRR-2}}(x, y) + 0.038 \quad (-) \quad (7.3)$$

Based on case studies in the Tibetan Plateau area and Eq.2.9, T_0 over this area was determined from (Ma et al., 2003a)

$$T_0(x, y) = T_4(x, y) + 1.56[T_4(x, y) - T_5(x, y)] + 0.28[T_4(x, y) - T_5(x, y)]^2 + (48 - 5W)(1 - \varepsilon) \quad (\text{K}) \quad (7.4)$$

where $\varepsilon = (\varepsilon_4 + \varepsilon_5)/2$ (Becker and Li, 1995).

Soil heat flux G_0

The determination procedures of the regional soil heat flux $G_0(x, y)$ was the same as in the *Tile approach*. But Eq.2.28 could not be correctly used for the 2 December 2002 case over the CAMP/Tibet area, because this equation was based on $T_0(^{\circ}\text{C}) > 0$ and in winter T_0 was much below 0°C . The relationship between $G_0(x, y)$ and $R_n(x, y)$ found over the Tibetan Plateau area ($G_0(x, y) = 0.35462(\pm 0.00235)R_n(x, y) - 47.79(\pm 0.7005)$, Ma et al., 2002c) was applied to determine $G_0(x, y)$ over the CAMP/Tibet area (Ma et al., 2006).

Sensible heat flux H

The regional sensible heat flux $H(x, y)$ was estimated from Eq.3.23.

HEIFE and AECMP'95 cases

Two different land surfaces (oasis and Gobi desert) exist in the HEIFE and AECMP'95 areas (Chapter 4 and Chapter 6). It meant that two aerodynamic resistances for heat should be applied in Eq.3.23, i.e.

$$\begin{aligned}
H(x, y) &= a(\text{oasis})H_{\text{oasis}}(x, y) + a(\text{Gobi} - \text{desert})H_{\text{Gobi-desert}}(x, y) \\
&= \rho c_p k^2 u_b [T_0(x, y) - T_{a-b}] \bullet \\
&\left(\begin{aligned}
&a(\text{oasis}) \bullet \frac{1}{\left[\ln \frac{z_b - d_{0-\text{oasis}}(x, y)}{Z_{0\text{m-oasis}}} + kB^{-1}(x, y) - \psi_h(x, y) \right] \bullet \left[\ln \frac{z_b - d_{0-\text{oasis}}(x, y)}{Z_{0\text{m-oasis}}} - \psi_m(x, y) \right]} \\
&+ a(\text{Gobi} - \text{desert}) \bullet \frac{1}{\left[\ln \frac{z_b - d_{0-\text{Gobi-desert}}(x, y)}{Z_{0\text{m-Gobi-desert}}} + kB^{-1}(x, y) - \psi_h(x, y) \right] \bullet \left[\ln \frac{z_b - d_{0-\text{Gobi-desert}}(x, y)}{Z_{0\text{m-Gobi-desert}}} - \psi_m(x, y) \right]}
\end{aligned} \right) \\
&\hspace{20em} (\text{W m}^{-2}) \quad (7.5)
\end{aligned}$$

where z_b was blending height, u_b was wind speed at z_b , T_{a-b} was the air temperature at z_b . z_b , u_b and T_{a-b} can be determined by using the ABL observations or numerical ABL models. They were determined with the aid of measurements by radio sonde system and tethered balloon in the HEIFE and AECMP'95 area (Chapter 6).

The effective roughness length $Z_{0\text{m-oasis}}$ in Eq.7.5 over the HEIFE and the AECMP'95 areas was determined through Eq.3.10. $Z_{0\text{m-Gobi-desert}}$ was regarded as the same as the local roughness length $z_{0\text{m}}$ due to the flat Gobi desert surface in the experimental areas. The results obtained in Chapter 6 (Table 6.1) and Jia et al. (1999b) over the areas of the HEIFE and the AECMP'95 was used.

Eq.2.43 was used to derive the zero-plane displacement $d_0(x, y)$ in Eq.7.5 over the cases study areas. The value of h_v was 1.0 m for the HEIFE area (wheat field) and h_v was 1.8 m for the AECMP'95 area (corn field). As regards the Gobi desert area in the HEIFE and the AECMP'95, approximation $d_0(x, y) \approx 0$ was used ($LAI \rightarrow 0$, $d_0(x, y) / h_v(x, y) \rightarrow 0$, Raupach, 1994).

The excess resistance to heat transfer $kB^{-1}(x, y)$ in Eq.7.5 over the areas of the HEIFE and the AECMP'95 was determined from LAI by using a widely-used model (Qualls and Brutsaert, 1995) since no general relationship between kB^{-1} and T_0 , kB^{-1} and $T_0 - T_a$, kB^{-1} and $u(T_0 - T_a)$ was found over the two areas (see Chapter 6).

Integrated stability functions $\psi_h(x, y)$ and $\psi_m(x, y)$ in Eq.7.5 were determined through

Eqs.2.46 and 2.47.

GAME/Tibet and CAMP/Tibet cases

The surface heterogeneity in the GAME/Tibet and the CAMP/Tibet areas was less significant than in the HEIFE area (Chapter 4 and Chapter 6), one aerodynamic resistance for heat was applied in Eq.3.23, i.e.

$$H(x, y) = \rho c_p k^2 u_b \frac{[T_0(x, y) - T_{a-b}]}{[\ln \frac{z_b - d_0(x, y)}{Z_{0m}} + kB^{-1}(x, y) - \psi_h(x, y)] \bullet [\ln \frac{z_b - d_0}{Z_{0m}} - \psi_m(x, y)]} \quad (\text{W m}^{-2}) \quad (7.6)$$

where z_b , u_b and T_{a-b} were determined using radio sonde system in the GAME/Tibet and the CAMP/Tibet areas (Chapter 6)

The effective roughness length Z_{0m} in Eq.7.6 over the GAME/Tibet and the CAMP/Tibet areas was determined through Eq.3.11 and the results in the Table 6.1 were also used.

Eq.2.43 was used to derive the zero-plane displacement $d_0(x, y)$ in Eq.7.6 over the cases study areas. Value of h_v was 10 cm for the GAME/Tibet and the CAMP/Tibet areas.

The excess resistance to heat transfer $kB^{-1}(x, y)$ in Eq.7.6 over the GAME/Tibet and the CAMP/Tibet areas was determined from the relationship between kB^{-1} and T_0 (Chapter 6).

Integrated stability functions $\psi_h(x, y)$ and $\psi_m(x, y)$ in Eq.7.6 were also determined through Eqs.2.46 and 2.47.

Latent heat flux λE

Eq.2.51 was used to determine the regional $\lambda E(x, y)$ over the experimental areas of the HEIFE, the AECMP'95, the GAME/Tibet and the CAMP/Tibet.

7.2.3 Comparison between the RS approach, the Tile approach and the Blending height approach

The *RS approach*, the *Tile approach* and the *Blending height approach* are compared in Table 7.2 and Table 7.3. It is very clear that many differences exist between these approaches. The advantages of the *Tile approach* and the *Blending height approach* will be documented by the following case studies.

Table 7.2 Comparison between the *RS approach*, the *Tile approach* and the *Blending height approach* in estimating the sensible heat flux H .

Variables	RS approach	Blending height approach	Tile approach
Wind speed $u(x,y)$	Wind speed at the reference height was estimated from SEBAL model	Wind speed at the blending height u_b was determined using ABL observations	The reference height z was selected nearby
Air temperature $T_a(x,y)$	Air temperature at the reference height was estimated from $T_a(x,y) = 0.40T_0(x,y) + 9.45$	Air temperature at blending height T_{a-b} was determined using ABL observations	the land surface (e.g.20m); u , T_a , z_{0m} , KB^{-1} , d_0 , ψ_m and ψ_h were measured or derived at
Reference height z	~2.0 m	Blending height z_b was determined using ABL observations	and below the reference height over each kind of land surface cover types.
Aerodynamic roughness length $z_{0m}(x,y)$	$z_{0m}(x,y) = f(NDVI(x,y))$	Arya's model (Eq.3.10), Taylor's model (Eq.3.11) and land surface and surface layer observations	
Excess resistance to heat transfer $KB^{-1}(x,y)$	2.3	$KB^{-1} = k(\frac{120}{LAI} \sqrt{wu_s} - 2.5)$ (HEIFE and AECMP'95) and the relationship between KB^{-1} and T_0 (GAME/Tibet and CAMP/Tibet)	
Zero-plane displacement $d_0(x,y)$	$d_0=(2/3)h_v$	$d_0 = f(LAI)$	

Table 7.3 Comparison between the *RS approach*, the *Tile approach* and the *Blending height approach* in estimating surface reflectance r_0 , surface temperature T_0 , fractional vegetation cover P_v , LAI , net radiation flux R_n , soil heat flux G_0 using Landsat-5(7) TM (ETM) measurements

Items	RS approach	Tile approach and Blending height approach
$r_0(x, y)$	Linear relationship between surface reflectance r_0 and planetary reflectance r_p	Verhoef's model and the surface and atmospheric observations
$T_0(x, y)$	Linear relationship between the upward long-wave radiation flux on the surface L^{\uparrow}_0 and the upward long-wave radiation flux of the earth—atmosphere system at the top of atmosphere L^{\uparrow}_{TOA}	Radiative transfer model and the surface and atmospheric observations
$P_v(x, y)$	no	$P_v = \left[\frac{NDVI - NDVI_{\min}}{NDVI_{\max} - NDVI_{\min}} \right]^2$
$LAI(x, y)$	no	$LAI = -\frac{1}{2k} \ln \left[\frac{r_0 - r_v}{r_s - r_v} \right]$
$\varepsilon_0(x, y)$	$\varepsilon_0(x, y) = 1.009 + 0.047 \ln NDVI(x, y)$	$\varepsilon_0 = f(P_v)$
$K_{\downarrow}(x, y)$	Linear average of the ground measurement $K_{\downarrow}(x, y) = \overline{K_{\downarrow}} = \frac{1}{n} \sum_{i=1}^n K_{\downarrow_i}$	MODTRAN model and the surface and atmospheric observations
$L_{\downarrow}(x, y)$	Linear average of the ground measurement $L_{\downarrow}(x, y) = \overline{L_{\downarrow}} = \frac{1}{n} \sum_{i=1}^n L_{\downarrow_i}$	MODTRAN model and the surface and atmospheric observations
$G_0(x, y)$	$G_0 = f(NDVI)$	$G_0 = f(MSAVI)$

7.3 Experimental case studies

Five TM (ETM) images and three scenes of AVHRR data were used to derive the regional land surface heat fluxes (Table 7.4). The most relevant in-situ data, collected at the stations of the HEIFE, the AECMP'95, the DHEX, the GAME/Tibet and the CAMP/Tibet (Chapter 4) to support the determination of regional land surface heat fluxes are also shown in Table 7.4.

Table 7.4 The satellite data and in-situ data used in this chapter.

	Satellite data	In-situ data
HEIFE	Landsat-5 TM: 10:00, July 7, 1991	– Surface radiation budget components. – Surface radiation temperature T_{rad} .
AECMP'95	Landsat-5 TM: 10:00, August 21, 1995	– Surface reflectance r_0 .
DHEX	Landsat-7 ETM: 10:00, August 22, 2000	– Vertical profiles of air temperature T_a , humidity q , wind speed u and wind direction.
CAMP/Tibet	Landsat-7 ETM 10:00, June 9, 2002, 10:00, December 2, 2002	– Turbulent fluxes. – Soil heat flux. – Soil temperature profiles.
GAME/Tibet	NOAA/AVHRR: 14:43, June 12, 1998, 13:21, 16 July, 1998, 13:25, August 21, 1998	

The approaches applied over the case studies areas are summarized in Table 7.5.

Table 7.5 The *RS approach*, the *Tile approach* and the *Blending height approach* that were used over the case studies areas

	RS approach	Tile approach	Blending height approach
HEIFE	×		×
AECMP'95		×	×
DHEX		×	
GAME/Tibet			×
CAMP/Tibet			×

The regional distribution of r_0 , T_0 , $NDVI$, $MSAVI$, P_v , LAI , R_n , G_0 , H and λE over the areas of the HEIFE, the AECMP'95, the DHEX, the GAME/Tibet and the CAMP/Tibet are shown here, and the derived r_0 , T_0 , R_n , G_0 , H and λE are validated by using the measurements in the stations. The relative deviation $\delta V/V$ (Eq.5.18) was used.

In order to compare surface heterogeneity over the experimental areas, the distribution ranges of r_0 , T_0 , $MSAVI$, R_n , G_0 , H and λE over the HEIFE, the AECMP'95, the DHEX, the CAMP/Tibet and GAME/Tibet are shown in Table 7.6.

Table 7.6 The distribution ranges of r_0 , T_0 , $NDVI$, $MSAVI$, P_v , LAI , R_n , G_0 , H and λE over the HEIFE, the AECMP'95, the DHEX, the CAMP/Tibet and GAME/Tibet. “**BH**”: *Blending height approach*; “**Tile**”: *Tile approach*.

	$MSAVI$ (-)	r_0 (-)	T_0 (°C)	R_n (Wm^{-2})	G_0 (Wm^{-2})	H (Wm^{-2})	λE (Wm^{-2})
HEIFE	0.10~0.88	0.10~0.28	10~50	300~680	35~100	30~260	0~620
AECMP'95	0.10~0.80	0.10~0.35	25~44	310~540	45~68	40~300 (BH) 50~235 (Tile)	100~470 (BH) 100~450 (Tile)
DHEX	0.10~0.65	0.12~0.34	10~55	300~630	20~110	0~280	0~600
GAME/Tibet	0.00~0.25	0.13~0.22	25~44	500~700	100~150	140~300	130~450
(Jun., Jul., Aug.)	0.05~0.39	0.10~0.20	20~35	650~800	90~120	50~150	400~650
	0.06~0.46	0.05~0.20	18~30	660~810	70~110	40~120	400~680
CAMP/Tibet	0.05~0.24	0.10~0.25	10~42	500~650	130~180	60~350	50~450
(Jun., Dec.)	0.02~0.20	0.10~0.25	-40~0	250~450	75~120	150~280	10~110

7.3.1 HEIFE

Figure 7.3 shows the distribution maps of r_0 , T_0 , H and λE over the HEIFE area based on 2600×2600 pixels. Their frequency distributions are also shown in Figure 7.3. The *Blending height approach* was used to determine H and λE . In Figure 7.4, the derived r_0 , T_0 , R_n , G_0 , H and λE in different stations are plotted against ground measured values. The 1:1 line is also plotted in the graphs. The values of r_0 , T_0 , R_n , G_0 , H and λE derived from the *RS approach* (Chapter 5) are plotted in Figure 7.4 as well.

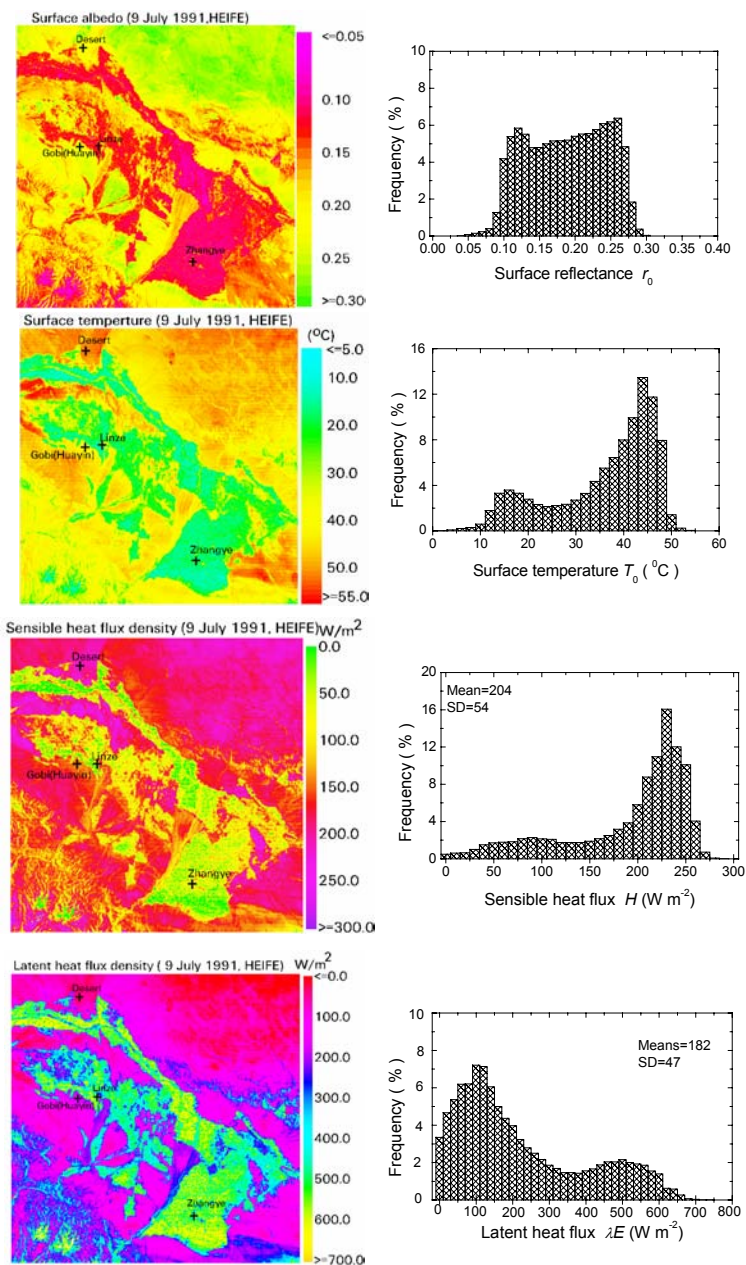


Figure 7.3 The distribution maps of land surface reflectance r_0 , surface temperature T_0 , sensible heat flux H and latent heat flux λE and their frequency distributions for the HEIFE basin Field Experiment (HEIFE) area on 9 July 1991.

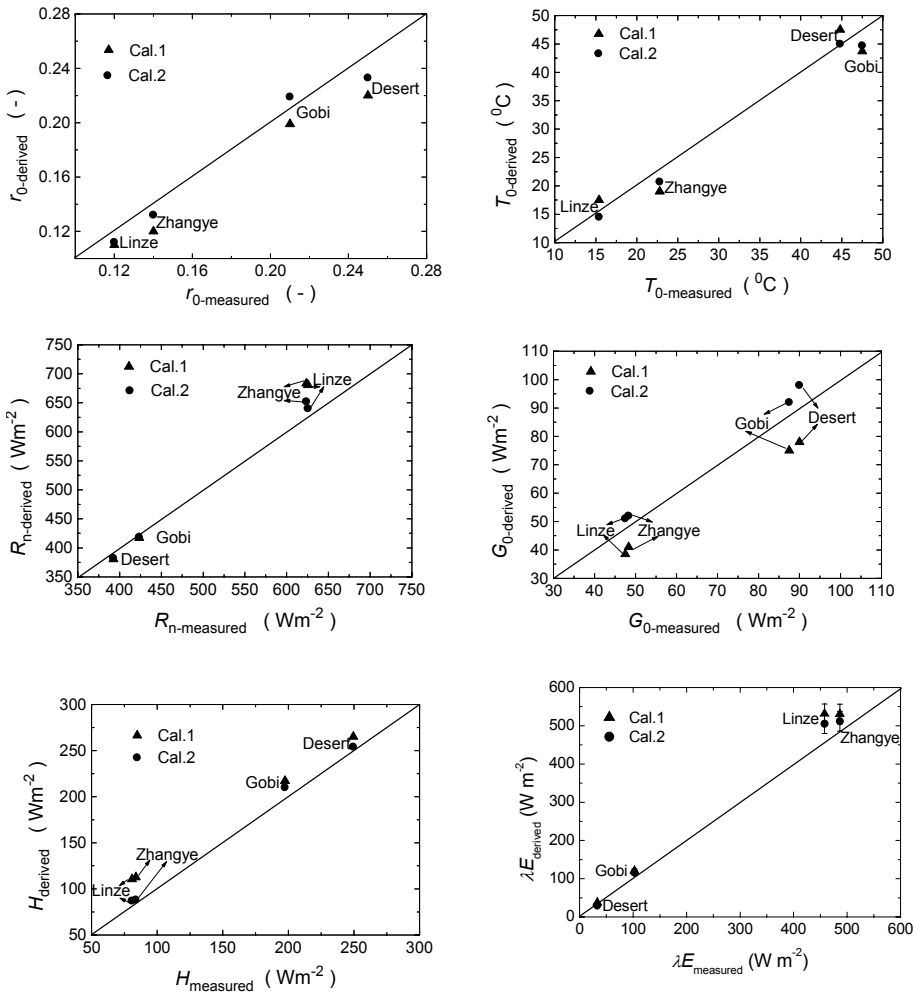


Figure 7.4 Validation of the derived land surface reflectance r_0 , surface temperature T_0 , sensible heat flux H and latent heat flux λE against the ground measurements over the HEIhe basin Field Experiment (HEIFE) stations, Gobi (Huayin), Desert, Zhangye (oasis) and Linze (oasis), together with 1:1 line. Cal.2: derived from *Blending height approach*; Cal.1: results derived from the *RS approach* (Chapter 5).

It can be seen that:

- (1) The derived r_0 , T_0 , $NDVI$, $MSAVI$, P_v , LAI , R_n , G_0 , H and λE over the HEIFE area are consistent with the land cover type (Figures 4.5b and 7.3). Due to the strong contrast of surface features these variables show a wide range (Table 7.6 and Figure 7.3). For examples, net radiation flux is from 300 to 680 W m⁻² and latent heat flux changes from 300 to 680 W m⁻² (Table 7.6). There are two peaks in the frequency distributions in this area. The first peak corresponds to the oasis and another one corresponds to the Gobi desert (Figure 7.3).
- (2) The derived r_0 and T_0 in this chapter are much better than the results derived from the linear relationship (Chapter 5, Figure 7.4). It means that r_0 and T_0 derived from the radiative transfer assumption for atmospheric correction in this chapter are much better than it derived from the linear relationship in Chapter 5. The reason is its much better consideration of the radiative transfer processes (Chapter 2, Table 7.3).
- (3) The derived R_n is very close to the ground measurement with a $\delta V/V$ being less than 5 %. It is much better than the former results at the Zhangye and Linze stations (oasis) due to the improvements in determining $r_0(x, y)$, $T_0(x, y)$, $\varepsilon_0(x, y)$, $K_{\downarrow}(x, y)$ and $L_{\downarrow}(x, y)$ in this chapter (Figure 7.2 and Table 7.3).
- (4) The parameterization method for G_0 based on $MSAVI$ for a heterogeneous land surface is much better than the one based on $NDVI$. Although the derived G_0 based on $MSAVI$ is a bit higher than the measured value, the $\delta V/V$ (i.e. less than 10 %) becomes smaller than the former derived value based on the $NDVI$ (Figure 7.4).
- (5) The derived values of H with a lower $\delta V/V$ (i.e. less than 10 %) at four validation sites are consistent with ground measurements. The peaks of oasis and Gobi desert in the histogram of H (Figure 7.3) are clearer than the previous results (Chapter 5: Figure 5.7). The derived H from the *Blending height approach* is much better than from the *RS approach* (Chapter 5) due to the advantage in calculating scheme of $T_a(x, y)$, $kB^{-1}(x, y)$, $Z_{0m}(x, y)$ and $d_0(x, y)$ (Figure 7.2 and Table 7.2). The previous results derived in Chapter 5 are acceptable over the Gobi and desert surface ($\delta V/V=9\%$ and $\delta V/V=7\%$), but there are large differences between the derived results and the ground-measured values over oasis ($\delta V/V=38\%$ at Linze station and $\delta V/V=34\%$ at Zhangye station).
- (6) The derived λE , which is based on the energy balance equation, is acceptable for the whole HEIFE area. The calculated value of $\delta V/V$ is less than 10 % for the four validation sites (Figure 7.4).

7.3.2 AECMP'95

Figure 7.5 shows the distribution maps of H and λE over the AECMP'95 area based on 400×750 pixels with a size of about $30 \times 30 \text{ m}^2$. Their frequency distributions are also shown in Figure 7.5. Both the *Tile approach* and the *Blending height approach* are used for determining H and λE here. In Figure 7.6, the derived H and λE in different stations are plotted against field measured values. The 1:1 line is also plotted in the graphs.

The results indicate that:

- (1) The derived sensible heat flux H and latent heat flux λE over the AECMP'95 area are consistent with the land cover type (Figure 4.5a, Figure 7.5). Due to the strong contrast of surface features H and λE have a wide distribution ranges (Table 7.6): H changes from 40 to 300 W m^{-2} (*Blending height approach*) and from 50 to 235 W m^{-2} (*Tile approach*); λE varies from 100 to 470 W m^{-2} (*Blending height approach*) and from 100 to 450 W m^{-2} (*Tile approach*). There are two peaks in the all distribution histograms over the study area (Figure 7.5). The first peak corresponds to the oasis and another one corresponds to the Gobi desert.
- (2) H and λE estimated from the *Tile approach* were slightly better than from the *Blending height approach* over the AECMP'95 area (Figure 7.6). Even the estimated values of H and λE from the *Blending height approach* are a little higher than from the *Tile approach* over the AECMP'95 area, but they are close to the ground measurements in the stations with a $\delta V/V$ being less than 10 % (Figure 7.6). It means that both the *Tile approach* and the *Blending height approach* are suitable to heterogeneous landscapes of the AECMP'95 area.

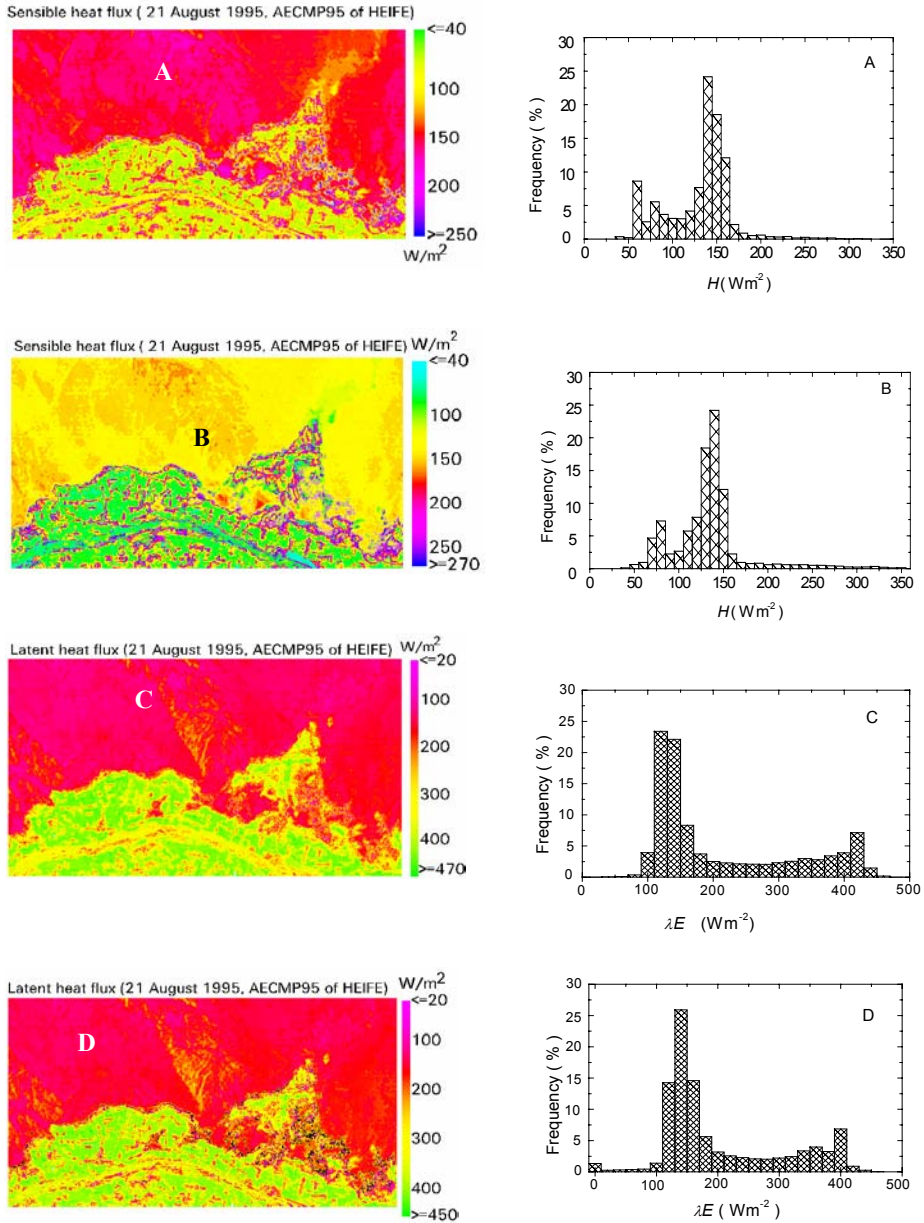


Figure 7.5 The distribution maps of sensible heat flux H and latent heat flux λE and their frequency distributions for the Arid Environment Comprehensive Monitoring Plan, 95 (AECMP'95) area on 21 August 1995. A and C is the distribution of H and λE derived from the *Blending height approach*; B and D is the distribution of H and λE derived from the *Tile approach*.

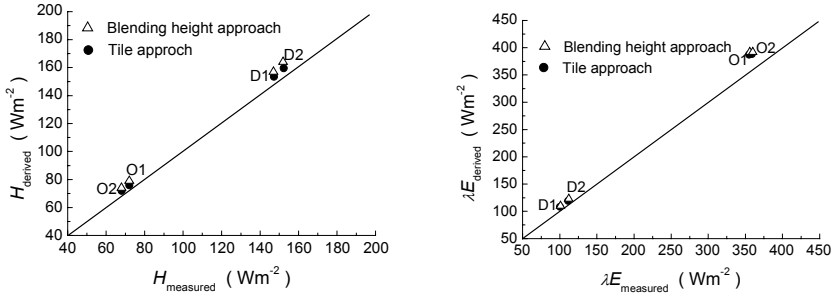


Figure 7.6 Validation of the derived sensible heat flux H and the derived latent heat flux λE against ground measurements over the Arid Environment Comprehensive Monitoring Plan, 95 (AECMP'95) stations, D1, D2, O1 and O2, together with 1:1 line.

7.3.3 DHEX

Figure 7.7 shows the frequency distributions of r_0 , T_0 , H and λE over the DHEX area. The *Tile approach* was used for determining H and λE over this area. The variables of z_{0m} , z_{0h} and kB^{-1} that were determined by other researchers over the DHEX area (Zhang et al, 2001; Hu, et al., 2002; Hu, 2004) have been used in the present approach. In Figure 7.8, the derived H and λE are plotted against the measured values at the stations of the DHEX (in order to validate the derived results more accurately, two cases of 3 June 2000 and 29 January 2001 are also shown in the figures). The 1:1 line is also plotted in the figures.

The results show that:

- (1) Due to the strong contrast of surface features over the DHEX area (Figure 4.7), the derived r_0 , T_0 , R_n , G_0 , H and λE show a wide distribution range (Table 7.6): r_0 is from 0.12 to 0.34, T_0 changes from 10 to 55 °C, R_n varies from 300 to 630 $W m^{-2}$, G_0 is from 20 to 110 $W m^{-2}$, H changes from 0 to 280 $W m^{-2}$ and λE varies from 0 to 600 $W m^{-2}$. There are two peaks in the figures of all distribution maps and all frequency distributions histograms. The first peak is corresponding to the oasis and the other peak corresponds to the Gobi desert (see Figure 7.7).
- (2) The derived H and λE at the validation sites of the DHEX area are in good agreement with ground measurements (Figure 7.8) with a $\delta V/V$ being less than 10 %. It means that the *Tile approach* can accurately be used to the relative small length scale of mixing oasis and desert area when the Surface Layer (SL) observations were performed over

oasis and Gobi desert respectively.

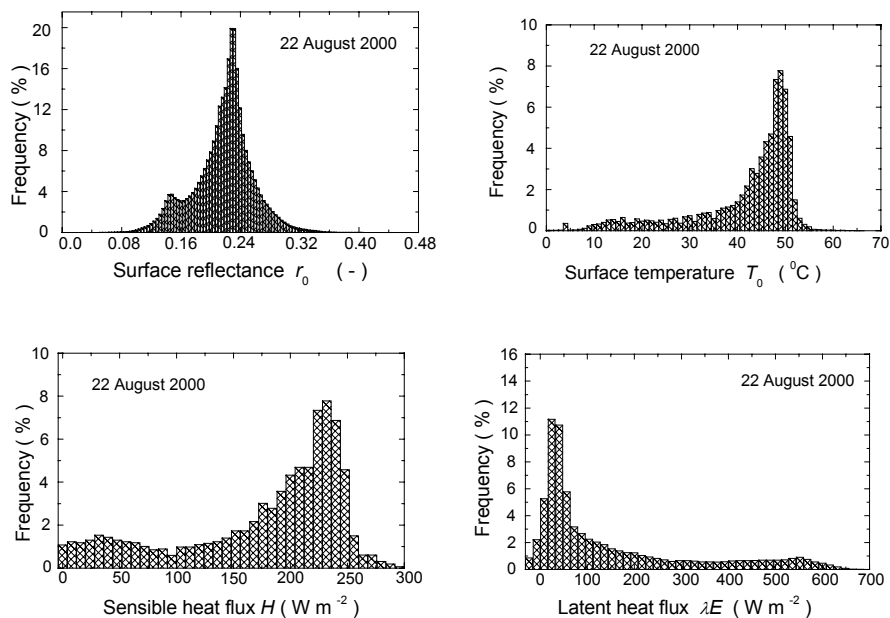


Figure 7.7 The frequency distributions of the surface reflectance r_0 , surface temperature T_0 , sensible heat flux H and latent heat flux λE for the Dunhuang Experiment (DHEX) area on 22 August 2000.

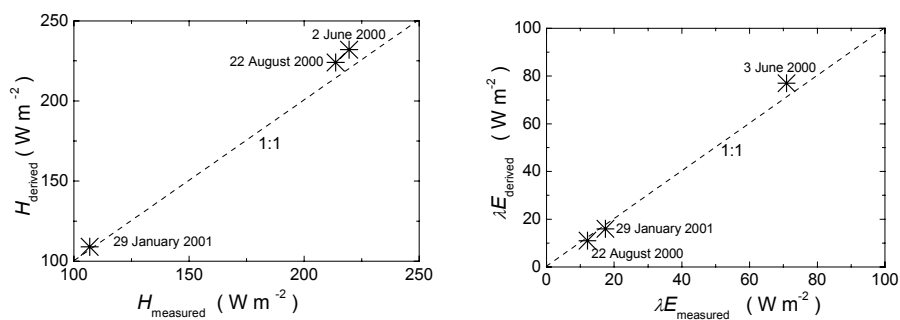


Figure 7.8 Validation of the derived results against the ground measurements for sensible heat flux H and latent heat flux λE for the Dunhuang Experiment (DHEX) area, together with 1:1 line.

7.3.4 CAMP/Tibet

It was better to select the satellite data taken on clear days to study the distribution of r_0 , T_0 , $NDVI$, $MSAVI$, P_v , LAI , R_n , G_0 , H and λE over the Tibetan Plateau area. Unfortunately, it was difficult to meet real cloud-free conditions because of the strong convective clouds being present during the Landsat-7 ETM overpass. Only two ETM data, 9 June 2002 (summer) and 2 December 2002 (winter), were used to estimate the land surface variables, vegetation variables and land surface heat fluxes. Figure 7.9 shows the summer distribution maps of r_0 , T_0 , H and λE around the CAMP/Tibet area based on 3400×2000 pixels, their frequency distributions are also shown in the figures. In Figure 7.10, the derived r_0 , T_0 , R_n , G_0 , H and λE are plotted against the measured values at the stations of the CAMP/Tibet. The *Blending height approach* was used to determine land H and λE .

The following can be concluded.

- (1) The derived r_0 , T_0 , R_n , G_0 , H and λE in two different months over the study area are consistent with the land cover type (Figures 4.3, 4.4 and 7.9). The experimental area includes a variety of land cover types such as a large area of grassy marshland, some desertification grass-land areas, many small rivers and several lakes, therefore, these derived land surface variables and surface heat fluxes show a relative wide range due to the contrast of surface features (Table 7.6). But they are not wide as that in the areas of the HEIFE, the AECMP'95 and the DHEX (Table 7.6). For examples, R_n is from 500 to 650 $W m^{-2}$ over the CAMP/Tibet area, it changes from 300 to 680 $W m^{-2}$ over the HEIFE area, it varies from 310 to 540 $W m^{-2}$ over the AECMP'95 area and it is from 300 to 630 $W m^{-2}$ over the DHEX area. The reason being that the surface heterogeneity is not very larger in the CAMP/Tibet area as in the areas of the HEIFE, the DHEX and the AECMP'95 (Chapter 4 and Chapter 6). The values of r_0 , T_0 and H around the lake in the distribution maps are much higher in June, and at the same time, R_n , G_0 and λE are lower over there. The reason being that most of around lake area consisted of the desertification grass land. It was dry and soil moisture was low.
- (2) The derived pixel value and average value (Figure 7.9) of T_0 , R_n , G_0 and λE in June are higher than in December. It means that in the central Tibetan Plateau area is much more evaporation in summer than in winter. It is also pointed out that the heating density ($H + \lambda E = R_n - G_0$) in summer is much higher than it in winter in the central Tibetan Plateau area. The reason being that most the land surface was on the

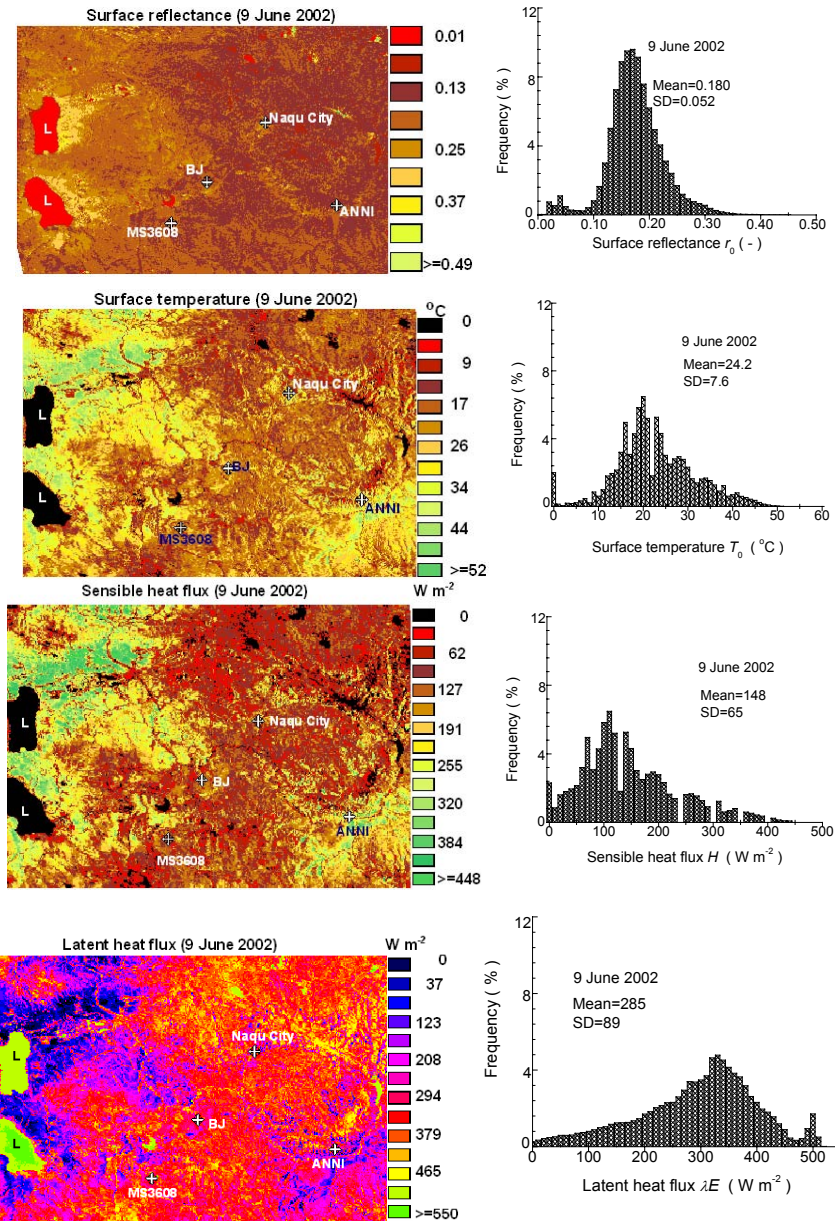


Figure 7.9 The distribution maps of land surface reflectance r_0 , surface temperature T_0 , sensible heat flux H and latent heat flux λE and their frequency distributions for the Coordinated Enhanced Observing Period (CEOP) Asia-Australia Monsoon Project on the Tibetan Plateau (CAMP/Tibet) area at 10:00(LST) on 9 June 2002. L denotes lake.

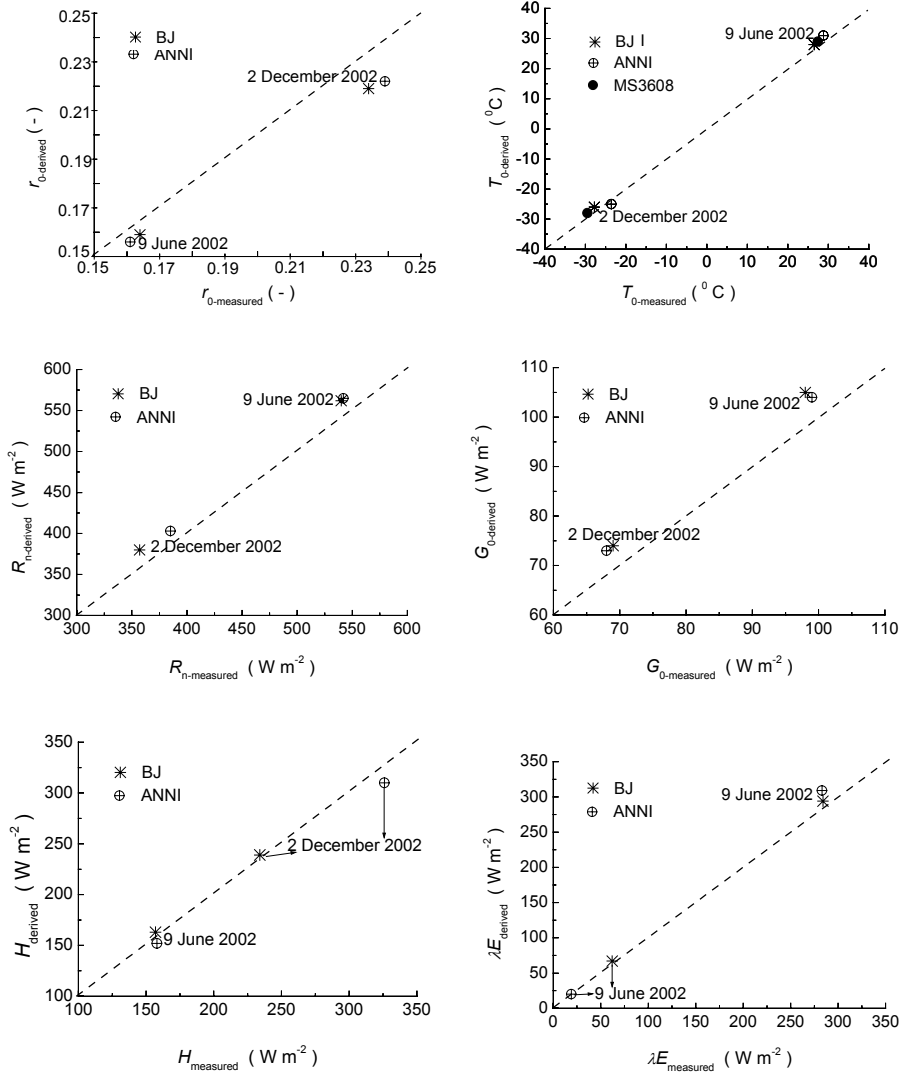


Figure 7.10 Validation of the derived land surface reflectance r_0 , surface temperature T_0 , net radiation flux R_n , soil heat flux G_0 , sensible heat flux H and latent heat flux λE against ground measurements over the Coordinated Enhanced Observing Period Asia-Australia Monsoon Project on the Tibetan Plateau (CAMP/Tibet) stations, BJ and ANNI, together with 1:1 line.

experimental area covered by green grass in summer and it was covered by snow and ice during the winter.

- (3) The derived r_0 , T_0 and R_n , over the study area are very close to the ground measurements with a $\delta V/V$ being less than 8 % (Figure 7.10). The reason is its better consideration of the radiative transfer processes in determining r_0 and T_0 (Chapter 2, Table 7.3)
- (4) The regional soil heat flux G_0 derived from the relationship between G_0 and R_n is suitable for heterogeneous land surface of the CAMP/Tibet area with a $\delta V/V$ being less than 10 % at validation sites (Figure 7.10) because the relationship itself was derived from the same area (Ma et al., 2002c).
- (5) The derived regional H and λE with a $\delta V/V$ being less than 10 % at the validation sites in the CAMP/Tibet area are in good agreement with ground measurements (Figure 7.10). The reason being that the process of Surface Layer (SL) and Atmospheric Boundary Layer (ABL) was considered in more detail in the parameterization methodology. It has to be pointed out that the presented *Blending height approach* for H and λE is reasonable for the central Tibetan Plateau area.

7.3.5 GAME/Tibet

The Asian Monsoon system-Tibetan Plateau interaction is very important for the climate change in the Tibetan Plateau area. It would be better to select more satellite data on clear days to study this interaction. Unfortunately, because of the strong convective clouds at the NOAA-14/AVHRR overpass only three scenes of the NOAA-14/AVHRR could be selected during the whole intensive observation period of the GAME/Tibet. The scene of June 12, 1998 was selected as a case of pre-monsoon and mesoscale area. The scenes of July 16, 1998 and August 21, 1998 were selected as the cases of mid-monsoon and the post-monsoon. The images around the Anduo (Amdo) stations and NPAM stations were selected as comparable areas because flux measurements with sonic anemometer-thermometer were taken at the two stations. It was also a very clear day around these two stations on the images of NOAA-14/ AVHRR.

Figure 7.11 shows the frequency distributions maps of r_0 , T_0 , R_n , G_0 , H and λE of the mesoscale experimental area of the GAME/Tibet. The distribution maps of r_0 , T_0 , H and λE around the Anduo (Amdo) station and the NPAM station based on 45 by 40 pixels are compared in Figure 7.12. The quantities of r_0 , T_0 , R_n , G_0 , H and λE derived from the

Blending height approach are compared with those measurements at the Anduo station and the NPAM station (see Figure 7.13).

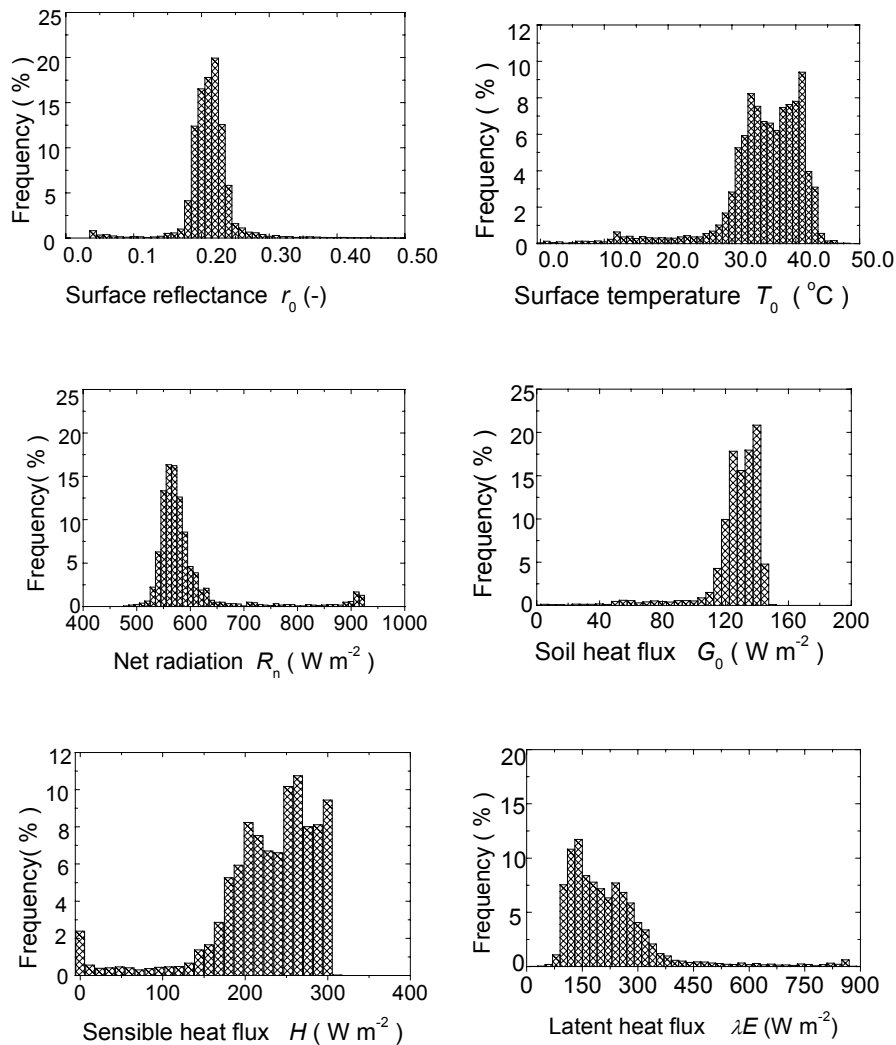


Figure 7.11 The frequency distributions of land surface reflectance r_0 , surface temperature T_0 , net radiation flux R_n , soil heat flux G_0 , sensible heat flux H and latent heat flux λE over the Global Energy and Water cycle EXperiment Asian Monsoon Experiment on the Tibetan Plateau (GAME/Tibet) area on 12 June 1998.

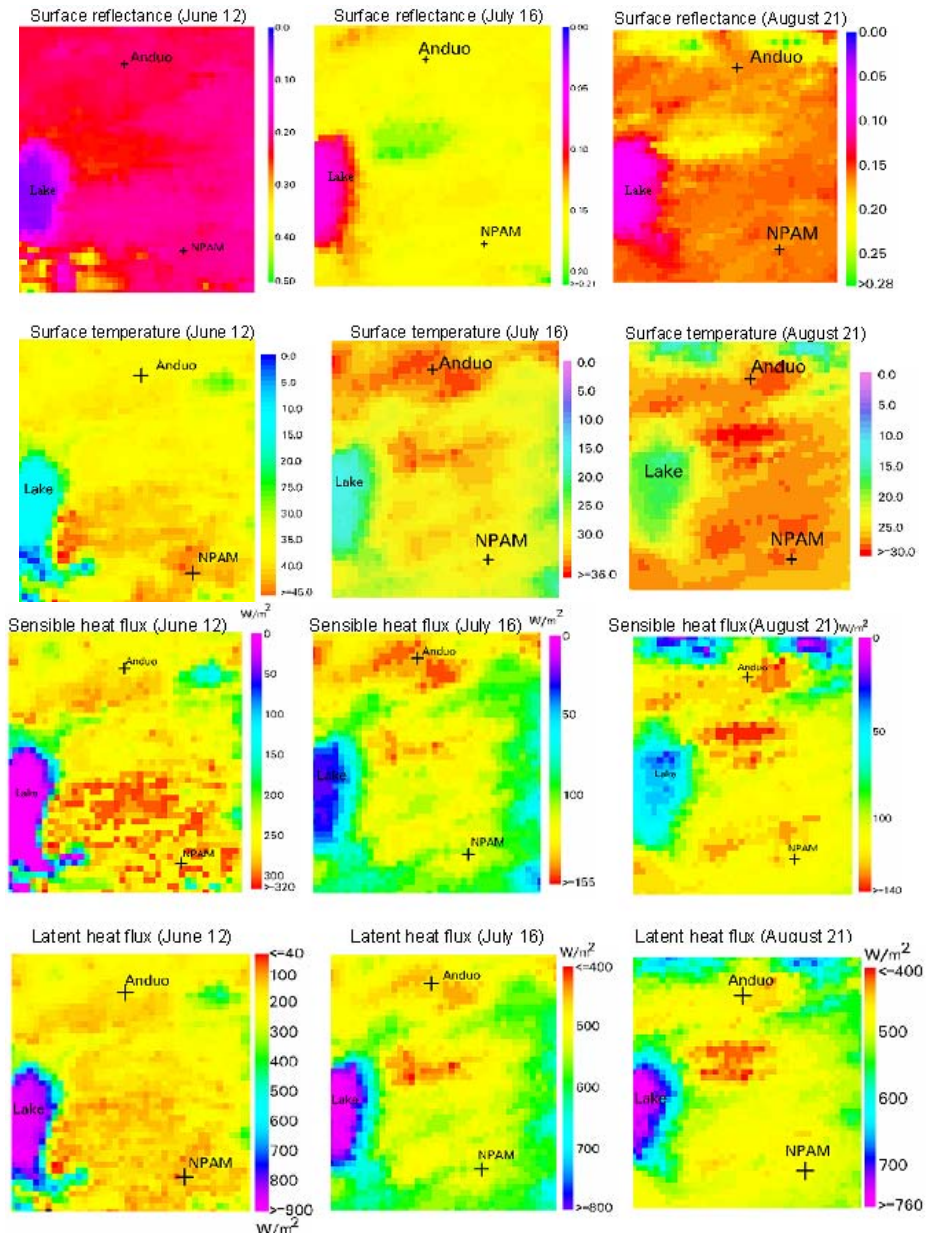


Figure 7.12 The distribution maps of land surface reflectance r_0 , surface temperature T_0 , sensible heat flux H and latent heat flux λE over the Global Energy and Water cycle EXperiment Asian Monsoon Experiment on the Tibetan Plateau (GAME/Tibet) area on June 12, July 16 and August 21, 1998

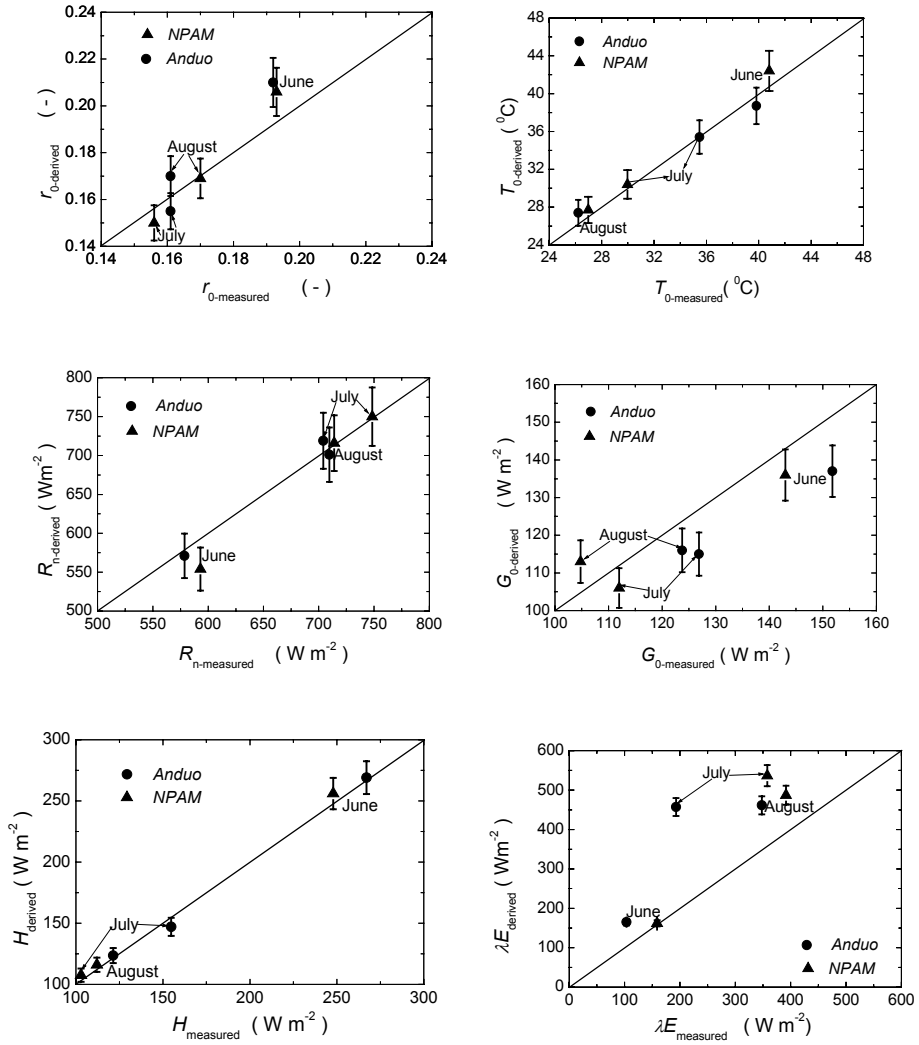


Figure 7.13 Validation of the derived land surface reflectance r_0 , surface temperature T_0 , net radiation flux R_n , soil heat flux G_0 , sensible heat flux H and latent heat flux λE against ground measurements over the Global Energy and Water cycle EXperiment Asian Monsoon Experiment on the Tibetan Plateau (GAME/Tibet) Global Energy and Water cycle EXperiment Asian Monsoon Experiment on the Tibetan Plateau (GAME/Tibet) stations, Anduo and NPAM, together with 1:1 line.

The following can be concluded.

- (1) The derived land surface variable (r_0 and T_0) and surface heat fluxes (R_n , G_0 , H and λE) for the whole meaoscale area on 12 June 1998 were consistent with the land cover types (Figures 4.1, 4.2, 7.11 and 7.12). These land surface variables and surface heat fluxes show a relative wide range of variations due to the contrast of surface features in the study area. But the distribution ranges are not wide as those in the areas of the HEIFE, the AECMP'95 and the DHEX (Table 7.6). The reason being that the surface heterogeneity was not quite larger in the GAME/Tibet area than in the areas of the HEIFE, the DHEX and the AECMP'95 (Chapter 4 and Chapter 6).
- (2) Not only on June 12, but also on July 16 and August 21, the derived r_0 , T_0 , R_n , G_0 and H are close to ground measurements with a $\delta V/V$ being less than 10% (Figure 7.13).
- (3) During the experimental periods, the derived net radiation flux is larger than that in the HEIFE area (Figures 7.12 and 7.3) due to the high altitude (the higher value of downward short-wave radiation) and land surface coverage of grassy marshland (the lower value of the upward long-wave radiation) in this area. For example, the regional average value of net radiation flux is 470 Wm^{-2} over the HEIFE area on 9 July, 1991 and that is 750 Wm^{-2} over the GAME/Tibet area on 16 July, 1998.
- (4) The derived land surface variables and land surface heat fluxes over the Tibetan Plateau area show that they are sensitive to the Asian Monsoon system and the seasons change (Figure 7.12). The values of r_0 , T_0 , G_0 and H in June over this area were larger than these values in July and August. The values of R_n and λE in June were lower than their values in July and August. The reason is that June 12 was the day before the onset of the Asia Monsoon. The land surface was dry on that day. July 16 and August 21 were within and after Asia Monsoon. The land surface was wet and the grass was high and growing.
- (5) All elements of the heat balance equation at the NPAM site on June 12 correspond well with the satellite measurements. On the other hand, all but latent heat flux corresponds to the satellite measurements in other seasons and at the Anduo station and the NPAM station. The reason is that the measured one dimensional energy budget did not balance due to large error of the latent heat flux through the surface observation and advection at the Anduo station and the NPAM station in other seasons. The large error of the measurement on latent heat flux may depend on the accuracy of the turbulence measurement sensors (e.g. Ishikawa et al.1999; Wang et al., 1999; Tsukamoto et al., 1999; Ma et al., 2000; Tanaka et al., 2001; Tsukamoto et al., 2001).

7.4 Summary and conclusions

In this chapter, the *Tile approach* and the *Blending height approach* have been applied for deriving the regional land surface variables (surface reflectance r_0 and surface temperature T_0) and land surface heat fluxes (net radiation flux R_n , soil heat flux G_0 , sensible heat flux H and latent heat flux λE) over heterogeneous land surfaces of the HEIFE, the AECMP'95, the DHEX, the GAME/Tibet and the CAMP/Tibet. The derived results have been validated by using the ground measurement (“ground truth”) at the stations.

The Surface Layer (SL) and Atmospheric Boundary Layer (ABL) observations were used as much as possible in the *Tile approach* and the *Blending height approach*. The atmospheric variables such as the aerodynamic roughness length z_{0m} , the thermodynamic roughness length z_{0h} and the excess resistance to heat transfer kB^{-1} derived in Chapter 6 were also used.

The results derived from this chapter can be summarized as follows.

- The values of land surface variables derived from the radiative transfer assumption of atmospheric correction and the surface and atmospheric observations were much better than derived from the linear relationships of Chapter 5 (Figure 7.4).
- The surface heterogeneity leads to very different values of land surface variables and surface heat fluxes over the areas of the HEIFE, the AECMP'95 and the DHEX (Table 7.6). The derived values of land surface variables and land surface heat fluxes were consistent with the land cover types, and they showed a wide distribution range due to the strong contrast of surface features in the areas (Table 7.6). There were two peaks in the all distribution maps and all frequency distributions histograms. The first peak was corresponding to the oasis and the other peak corresponding to the Gobi desert. The distribution ranges of the derived values of land surface variables and surface heat fluxes were not wide in the areas of the GAME/Tibet and the CAMP/Tibet as that in the areas of the HEIFE, the AECMP'95 and the DHEX (Table 7.6).
- The estimated net radiation flux over *all the case studies areas* was close to the ground measurements with a relative deviation $\delta V/V$ being less than 10%. It shows that the present parameterization of net radiation flux could be applied to heterogeneous landscapes of arid and high altitude areas.
- The derived soil heat flux based on *MSAVI* over the areas of the GAME/Tibet, the HEIFE, the AECMP'95 and the DHEX were close to the ground measurements with a $\delta V/V$ being less than 10 %. It was much better than the derived regional soil heat

fluxes based on *NDVI*.

- The values of sensible heat flux estimated from the *Tile approach* over the DHEX area and the AECMP'95 area were close to the ground measurements at the validation stations, with a $\delta V/V$ being less than 10 %. It means that the *Tile approach* is suitable to apply to heterogeneous landscapes of arid and semi-arid areas when the surface and Surface Layer (SL) measurements is done over each land cover type.
- The values of sensible heat flux estimated from the *Blending height approach* over the areas of the HEIFE, the AECMP'95, the CAMP/Tibet and the GAME/Tibet were close to ground measurements at the validation stations with a $\delta V/V$ being less than 10 %. The derived sensible heat flux from the *Blending height approach* was much better than from the *RS approach* over the HEIFE area. It shows that the *Blending height approach* can be used to heterogeneous arid areas and high altitude areas when the length scales of land heterogeneity are relatively larger.
- The derived latent heat flux based on the energy balance equation was accurately for the entire areas of the HEIFE, the AECMP'95, the DHEX and the CAMP/Tibet. But the error was larger over the GAME/Tibet area.

In order to show the advantages as well as shortcomings between the *RS approach*, the *Tile approach* and the *Blending height approach*, the relative deviations between the derived net radiation flux, soil heat flux, sensible heat flux and latent heat flux using the approaches and the ground measurement surface fluxes *as averaged over the four experimental areas* ($\overline{\delta V/V}$) are shown in Table 7.7. The four experimental areas of the HEIFE, the AECMP'95, the DHEX and the CAMP/Tibet are selected due to the higher spatial resolution satellite measurements being used over there.

Table 7.7 The relative deviation between the derived land surface heat fluxes using the *RS approach*, the *Tile approach* and the *Blending height approach* and the ground measured fluxes *as averaged over the four experimental areas*($\overline{\delta V/V}$).

Approaches	RS approach	Tile approach	Blending height approach
R_n ($W m^{-2}$)	6 %	5 %	5 %
G_0 ($W m^{-2}$)	15 %	6 %	7 %
H ($W m^{-2}$)	22 %	5 %	6 %
λE ($W m^{-2}$)	13 %	8 %	9 %
Number of validation sites	4	7	12

It is seen that the values of $\overline{\delta V / V}$ from the *RS approach* are much larger than from the *Tile approach* and the *Blending height approach*.

It is therefore concluded that *in determining the land surface heat fluxes the Tile approach and the Blending height approach did provide better results than the RS approach. The Tile approach and the Blending height approach can accurately be applied to estimate regional land surface variables and surface heat fluxes over heterogeneous landscapes.*

Summary and conclusions

Problem statement

Land-atmosphere interactions over heterogeneous landscapes have increased the attention of meteorologists and hydrologists in the recent years. The regional heat flux exchange between the land surface and the atmosphere is of paramount importance for land-atmosphere interactions. Satellite remote sensing measurements offer the possibility to estimate regional distribution of land surface heat fluxes over heterogeneous landscapes. Recent studies have explored several satellite remote sensing parameterization methodologies to estimate the regional surface heat fluxes. They bridge the gap between the point/local measurements and the regional scale. But these methodologies do not pay sufficient attention to the aspects of the Surface Layer (SL) and the Atmospheric Boundary Layer (ABL). The investigations in heterogeneous landscapes of arid areas and high altitudes are quite rare.

The main objective of this thesis is therefore provide a better parameterization methodology of at-surface heat fluxes using satellite measurements to estimate at-surface bio-geophysical variables and surface heat fluxes over heterogeneous landscapes, thereby including SL and ABL observations.

Theoretical framework

Based on satellite measurements, SL and ABL observations, the theoretical framework to estimate the regional land surface heat fluxes (net radiation heat flux R_n , soil heat flux G_0 , sensible heat flux H and latent heat flux λE) were established in Chapter 2. *Net radiation flux at the land surface* was determined from Eq. 2.3 when the incoming solar radiation flux, the incoming long-wave radiation flux, surface reflectance, surface temperature and surface emissivity have been estimated. *Soil heat flux at the land surface* was derived from Eq.2.28 with the variables in this equation being determined from ground and satellite measurements. *Sensible heat flux at the land surface* was derived from Eq.2.34 with the pixel values of surface temperature and atmospheric variables (air temperature, aerodynamic roughness length, thermodynamic roughness length, excess resistance to heat transfer and stability correction function) at and below the reference height being determined by satellite measurements, SL and ABL observations and some assumptions or

approximations. *Latent heat flux at the land surface* was finally obtained as a residual of the surface energy balance equation at the land surface (Eq.2.51)

Parameterization methodology

The land surface heat fluxes can be estimated from the theory presented in Chapter 2. But parameterization methodologies are necessary when the surface heat fluxes are to be determined over heterogeneous landscapes. It results from that the surface variables and atmospheric variables are difficult to be determined at each satellite pixel over a heterogeneous landscape.

The characteristics of a heterogeneous landscape and its length scale of heterogeneity, the response of SL and ABL at the Surface Energy Balance (SEB) to large scale heterogeneity, the blending height assumption, its height z_b and relative length scale X over a heterogeneous landscape have firstly been described and determined in Chapter 3.

Based on the analysis of the land surface heterogeneity and its effects on the overlying air flow, on the SL and ABL observations, and satellite Remote Sensing (RS) measurements, *three parameterization methodologies, i.e. RS approach (RS+SL-assumptions), Tile approach (RS+SL-observations) and Blending height approach (RS+SL-observations +ABL-observations), have been developed to estimate the surface heat fluxes over heterogeneous landscapes* in Chapter 3. The *RS approach* (Figure 3.4) uses satellite measurements and assumptions on the SL. When the length scales of land surface heterogeneity are relatively small the *Tile approach* (Figures 3.4 and 3.5) uses satellite measurements and SL observations. In other words, the sensible heat flux and latent heat flux can be calculated from Eq.3.18 and Eq.3.19. When the length scales of land surface heterogeneity are relatively larger the *Blending height approach* uses satellite measurements in combination with SL and ABL observations. In other words, the sensible heat flux and latent heat flux can then be calculated from Eqs.3.20, 3.23 and 3.24.

Study areas and satellite measurements

In order to implement and test the developed *RS approach*, the *Tile approach* and the *Blending height approach*, five land surface processes experiments were performed over heterogeneous landscapes of China and described in Chapter 4: i.e. the Global Energy and Water cycle EXperiment Asian Monsoon Experiment on the Tibetan Plateau (GAME/Tibet),

the Coordinated Enhanced Observing Period Asia-Australia Monsoon Project on the Tibetan Plateau (CAMP/Tibet), the HEIhe basin Field Experiment (HEIFE), the Arid Environment Comprehensive Monitoring Plan, 95 (AECMP'95) and the DunHuang EXperiment (DHEX). Many different instruments (e.g. PBL tower, radiation system, radio sonde system, turbulent fluxes measured by eddy-correlation technique, soil moisture and soil temperature measurement system, PAM, Wind Profiler with RASS, tethered sonde system, radio sonde system and radar system and the like) were set up.. A large amount of observational data of soil, surface, SL and ABL has been collected, providing a sound base in deriving the input variables to the *RS approach*, the *Tile approach* and the *Blending height approach* for determining regional surface heat fluxes over heterogeneous landscapes.

Satellite remote sensing measurements provide consistent and frequent observations of spectral reflectance and emittance of radiation at patches landscape. The data of Landsat-5 Thematic Mapper (TM), Landsat-7 Enhanced Thematic Mapper (ETM) and NOAA-14 Advanced Very High Resolution Radiometer (AVHRR) have also been described in Chapter 4. The higher spatial resolution measurements of TM and ETM give the possibility to accurately estimate the regional land surface heat fluxes over heterogeneous landscapes.

Implementation of the parameterization methodologies and conclusions

The proposed parameterization methodologies (Chapter 3) of estimating surface heat fluxes over heterogeneous landscapes were implemented and validated with results obtained from the five case studies areas.

Using the *RS approach* (Figures 3.4 and 5.1) and Landsat-5 TM measurements, the regional distributions of land surface variables (land surface reflectance and surface temperature), *NDVI* and land surface heat fluxes (net radiation flux, soil heat flux, sensible heat flux and latent heat flux) have been obtained from the heterogeneous landscape of the HEIFE area (Chapter 5). The results showed how the proposed *RS approach* bridges the gap between the point/local measurements and the regional scale. But the results also indicated that the derived land surface variables and land surface heat fluxes of some areas were distinctly different from the ground measurements. The reason being that many assumptions and approximations were involved in the methodology and that some shortcomings exist.

To evaluate in more detail the assumptions and approximations involved in the *RS*

approach, the land surface heterogeneity and its influences on wind speed, air temperature, specific humidity, surface reflectance, surface temperature and surface heat fluxes have been further analyzed (Chapter 6). The atmospheric variables such as aerodynamic roughness length, thermodynamic roughness length and excess resistance to heat transfer were determined over the heterogeneous land surfaces of the study areas. The results showed that the *land surface heterogeneity has a very strong effect on the overlying near surface atmospheric layer*. It leads to the different values of land surface variables, atmospheric variables and surface heat fluxes on the land surface and in the near surface atmospheric layer. It also resulted in different vertical profiles of wind speed, air temperature and specific humidity in the surface layer. *But the effect of the land surface heterogeneity becomes uniform at a blending height z_b : at and above z_b the atmospheric variables like wind speed, air temperature and specific humidity were homogeneous.*

The *Tile approach* (Figures 3.4, 3.5 and 7.1) and the *Blending height approach* (Figures 3.4, 3.6 and Figure 7.2) based on Landsat-5 (7) TM (ETM) measurements, NOAA-AVHRR measurements, SL and ABL observations were applied in order to derive the regional land surface variables and surface heat fluxes over the heterogeneous landscapes of the study areas (Chapter 7). The result of the analysis and the atmospheric variables (aerodynamic roughness length, thermodynamic roughness length and excess resistance for heat transfer) that have been derived in Chapter 6, have been used in both approaches. The *comparisons between the RS approach, Blending height approach and the Tile approach* are also shown in the Tables 7.2 and 7.3. The derived values of regional land surface variables and land surface heat fluxes have been validated by using the independent ground measurements.

The results obtained in Chapter 7 showed the following.

- The derived regional land surface variables (surface reflectance and surface temperature) and land surface heat fluxes (net radiation flux, soil heat flux, sensible heat flux and latent heat flux) over the case studies areas are in good agreement with the land surface conditions.
- Land surface heterogeneity leads to very different values of land surface variables and surface heat fluxes over the areas of the HEIFE, the AECMP'95 and the DHEX. These variables and land surface heat fluxes show a wide distribution range, with two peaks in all the distribution maps and frequency distribution histograms. The first peak corresponds to the oasis and the other peak to the Gobi desert (Table 7.6). The

distribution ranges of the derived values of regional land surface variables and land surface heat fluxes are not wide in the areas of the GAME/Tibet and the CAMP/Tibet as those in the areas of the HEIFE, the AECMP'95 and the DHEX (Table 7.6).

- The estimated regional land surface variables and land surface heat fluxes from the *Tile approach* and the *Blending height approach* were consistent with ground measurements, and all their relative deviations $\delta V/V$ (Eq.5.18) were less than 10 % in the validation sites (Figures 7.4, 7.6, 7.8, 7.10 and 7.13). In other words, a better regional distribution of land surface variables and land surface heat fluxes over heterogeneous landscapes was obtained by using the *Tile approach* and the *Blending height approach* rather than the *RS approach*. It means that *the Tile approach and the Blending height approach can accurately be applied to estimate regional land surface heat fluxes over the heterogeneous landscapes of arid areas and high altitude areas.*

In conclusion:

- 1) *The parameterization methodologies to determine land surface heat fluxes as developed in this thesis bridge the gap between local patch scale and large length scale over heterogeneous landscapes using satellite measurements in combination with SL and ABL observations.*
- 2) *The Tile approach and the Blending height approach can be accurately applied to heterogeneous landscapes.*

Perspectives for future research

In this thesis the proposed *Tile approach*, the *Blending height approach* and the *RS approach* have only been applied to five different experimental case studies. For a more general understanding of the heat exchanges between heterogeneous landscapes and the overlying atmospheric layer, more SL and ABL observations (using e.g. PBL tower, eddy correlation turbulent measurement system, AWS, radio sonde system, tethered balloon, winder profiler, Radio Acoustic Sounding System, radar.) should be used. In addition more satellite measurements should be introduced to study the diurnal variation, seasonal variation and even the inter-annual variation of regional land surface heat fluxes.

Samenvatting en conclusies

Probleemstelling

Meteorologen en hydrologen bestuderen met toenemende belangstelling de land-atmosfeer-interacties boven heterogene landoppervlakken. Warmte-uitwisseling tussen het landoppervlak en de atmosfeer is namelijk van groot belang voor het beter kunnen begrijpen van deze interacties.

Aardobservatie door satellieten biedt de mogelijkheid om de regionale verdeling van de warmtestromen aan heterogene landoppervlakken te schatten. Recente studies hebben daarbij verschillende mogelijkheden van parameterisaties onderzocht. Deze parameterisaties overbruggen namelijk het gat tussen de lokale/punt-waarnemingen en de regionale schaal. Daarbij worden echter verschillende aspecten van de Oppervlaktelaag (SL) en de Atmosferische Grenslaag (ABL) uit het oog verloren. Dergelijke onderzoeken in heterogene, droge landschappen en hooggelegen gebieden zijn tot op heden schaars.

Het hoofddoel van dit proefschrift is dan ook om met behulp van satellietgegevens, SL- en ABL-waarnemingen een betere parameterisatie van de bio-geofysische eigenschappen van het landoppervlak en de warmtestromen boven heterogene landschappen te realiseren. Daarbij is in het bijzonder aandacht geschonken aan respectievelijk de Heihe River Basin en het Tibetaanse Plateau.

Theoretisch kader

In Hoofdstuk 2 wordt de theorie uiteen gezet om met behulp van satelliet-, SL- en ABL-waarnemingen, de regionale warmtestromingen aan het land oppervlak te bepalen, i.e. nettostraling R_n , bodemwarmtestroom G_0 , voelbare warmtestroom, H en latente warmtestroom, λE . De nettostraling aan het landoppervlak wordt met behulp van Eq. 2.3 berekend aan de hand van de inkomende zonnestraling, inkomende lang-golvige stralingsflux, oppervlaktereflectie, oppervlaktetemperatuur en oppervlakte-emissiviteit. De bodemwarmtestroom wordt afgeleid m.b.v. Eq.2.28, waarbij de variabelen in deze vergelijking worden bepaald m.b.v. terrein- en satellietmetingen.. De voelbare warmtestroom aan het landoppervlak wordt afgeleid m.b.v. van Eq.2.34, waarbij de pixel waarden van de oppervlaktetemperatuur en de atmosferische variabelen (luchttemperatuur, aerodynamische ruwheidslengte, thermodynamische ruwheidslengte, additionele weerstand

voor warmteoverdracht en stabiliteitscorrectie functie) worden bepaald met behulp van satellietwaarnemingen. De atmosferische variabelen aan en onder de referentiehoogte worden vastgesteld m.b.v. RS- SL- en ABL-waarnemingen met inbegrip van enkele veronderstellingen/ benaderingen. Tenslotte, wordt de latente warmtestroom aan het landoppervlak uit de energiebalansvergelijking, Eq.2.51, verkregen.

Gevolge parameterisatie methodologie

De warmtestromingen aan het landoppervlak kunnen aan de hand van de in Hoofdstuk 2 uiteengezette theorie worden geschat, maar een nadere parameterisatie is noodzakelijk om de voorgestelde benadering voor heterogene landschappen te kunnen toepassen. Als gevolg van de heterogeniteit wordt het bepalen van zowel de oppervlakte- als de atmosferische variabelen voor elke pixel van de toegepaste satellietbeelden moeilijker. In Hoofdstuk 3 worden de kenmerken van een heterogeen landschap en zijn lengte- schaal van heterogeniteit, de opbouw van de SL en ABL en de invloed van de verdeling van de warmte aan het land oppervlak in combinatie met grootschalige heterogeniteit, de menhoogte aanname z_b , en de daarbijhorende lengte schaal X over een heterogeen landschap beschreven en vastgesteld.

Gebaseerd op de analyse van de heterogeniteit van het landoppervlak en zijn effecten op de daarboven liggende luchtstroom op de SL, ABL en satelliet waarnemingen, worden in Hoofdstuk 3 de drie parameterisatie benaderingen [te weten de RS-benadering (RS+SL-aanname's), de Tegel-benadering (RS+SL-waarnemingen) en de Menghoogte-benadering (RS+SL+ ABL- waarnemingen)], gebruikt om de warmtestromingen aan het heterogene landoppervlak vast te stellen. De RS benadering (Eq. 3.4) maakt gebruik van satellietwaarnemingen in combinatie met aannames over de SL. Wanneer de lengteschalen van de heterogeniteit van het landoppervlak betrekkelijk klein zijn, wordt de Tegel benadering (Eq. 3.4 en 3.5) gebruikt, i.e. satelliet- en SL waarnemingen. Met andere woorden de voelbare en de latente warmtestroom kunnen m.b.v. Eq.3.18 en Eq.3.19 worden berekend. Wanneer de lengteschalen van heterogeniteit van het landoppervlak betrekkelijk groot zijn wordt de Menghoogte benadering gebruikt, dwz. satellietwaarnemingen in combinatie met SL- en ABL-waarnemingen. Met andere woorden de voelbare en latente warmtestromen kunnen m.b.v. Eqs.3.20, 3.23 en 3.24 worden berekend.

Studiegebieden en satellietwaarnemingen

Om de respectievelijk ontwikkelde RS-, Tegel- en Menghoogte-benaderingen toe te kunnen toepassen en te evalueren, werden in China een 5-tal heterogene landoppervlakken experimenten verricht. Deze worden in Hoofdstuk 4 beschreven, te weten de Globale Energie en Water Cyclus Aziatische Monsoon Experiment op het Tibetaans Plateau (GAME/Tibet), de Gecoördineerde Intensieve Waarnemings Periode Azië-Australië Moesson Project op het Tibetaan Plateau (CAMP/Tibet), het HEIhe stroomgebied Experiment (HEIFE), de Ariede Gebieden met het uitvoerige waarnemingsprogramma '95 (AECMP '95) en het Dunhuang-EXperiment (DHEX). Vele verschillende instrumenten werden daarbij gebruikt, waaronder de PBL-toren, het stralings-meetsysteem, het radio sonde systeem, turbulente fluxen gemeten met eddy-correlatie-instrumenten, bodemvocht en bodemtemperatuur-meetsystemen PAM, windprofiel metingen met RASS, tethered en radiosonde systemen, radarsysteem e.a.. Een grote hoeveelheid aan observatiegegevens over bodem, oppervlak, SL en ABL werden verzameld, welke een goede basis vormen voor het afleiden van de invoervariabelen ten behoeve van het toepassen van de RS-, de Tegel- en de Menghoogte-benadering voor de vaststelling van regionale warmtestromingen boven heterogene landschappen. Aardobservatie via satellieten levert voor de afzonderlijke landschapselementen consequente en frequente waarnemingen op van de spectrale reflectie en de emissie. De gegevens verkregen met de Landsat-5 Thematische Mapper (TM), Landsat-7 Verbeterde Thematisch Mapper (ETM) en de NOAA-14 Geavanceerd Zeer Hoge Resolutie Radiometer (AVHRR) worden eveneens in Hoofdstuk 4 beschreven. De hogere ruimtelijke resolutie van de TM en ETM geven de mogelijkheid om nauwkeurig de regionale warmtestromingen boven heterogene landschappen te schatten.

Implementatie van de parameterisatie benaderingen en conclusies

De in Hoofdstuk 3 voorgestelde parameterisatiebenaderingen voor het schatten van de warmtestromingen boven heterogene landschappen, werden toegepast en gevalideerd aan de hand van de in de 5 experimenten verzamelde waarnemingen.

Door het toepassen van de RS-benadering (Eq. 3.4 en 5.1) met behulp van Landsat-5 TM gegevens, is de regionale verdeling van de variabelen aan het land oppervlak (reflectie en temperatuur), NDVI en stralings- en warmtestromingen, d.w.z. nettostralings-, voelbare- en latente warmtestroom voor het heterogene landschap van het HEIFE gebied verkregen (Hoofdstuk 5). De resultaten tonen aan hoe de voorgestelde RS- benadering het gat tussen de lokale/punt-waarnemingen en de regionale schaal overbrugt. In sommige gevallen gaven

de resultaten echter ook duidelijke verschillen aan tussen de afgeleide variabelen van het landoppervlak, de warmtestromingen en de waarnemingen in het veld. De verklaring daarvan is te vinden in de vele veronderstellingen en benaderingen die aan de methodologie ten grondslag liggen.

Om de bij de voorgestelde parameterisaties betrokkene aanname's in de RS-benadering beter te kunnen evalueren, is in Hoofdstuk 6 vervolgens de heterogeniteit van het landoppervlak en de invloeden daarvan op windsnelheid, luchttemperatuur, specifieke vochtigheid, oppervlaktereflectie, -temperatuur en -warmtestroom verder geanalyseerd. De atmosferische variabelen zoals de aerodynamische ruwheidslengte, de thermodynamische ruwheidslengte en de additionele weerstand voor warmteoverdracht werden voor de heterogene landoppervlakken van de verschillende studiegebieden vastgesteld. De resultaten toonden o.a. aan dat de heterogeniteit van het landoppervlak een heel duidelijke invloed heeft op de aangrenzende atmosferische laag. Dit leidt tot verschillende waarden van de ruimtelijke variabiliteit van het landoppervlak en de atmosfeer, alsmede van de warmtestromingen. Dit resulteerde ook in verschillende verticale profielen van windsnelheid, luchttemperatuur en specifieke vochtigheid in de oppervlaktelaag. Maar het resultaat van de heterogeniteit van het landoppervlak wordt pas uniform bij een menghoogte z_b . Aan en boven z_b worden de atmosferische variabelen zoals windsnelheid, luchttemperatuur en specifieke vochtigheid homogeen.

De Tegel-benadering (Fig. 3.4, 3.5 en 7.1) en de Menghoogte-benadering (Fig. 3.4, 3.6 en 7.2) gebaseerd op Landsat-5 (7) TM (ETM), NOAA-AVHRR, SL en ABL waarnemingen zijn toegepast om de regionale variabelen van het landoppervlak en de warmtestromingen te bepalen boven de heterogene landschappen van de studie gebieden (Hoofdstuk 7). Het resultaat van deze analyse en de atmosferische variabelen (aerodynamische ruwheidslengte, thermodynamische ruwheidslengte en additionele weerstand voor warmteoverdracht) die in Hoofdstuk 6 werden afgeleid, zijn voor beide benaderingen verder toegepast. De resultaten van de vergelijking tussen de RS-benadering, de Tegel-benadering en Menghoogte-benadering zijn in de Tabellen 7.2 en 7.3 weergegeven. De afgeleide waarden van de regionale variabelen en warmtestromingen van het landoppervlak werden ter validatie vergeleken met veldwaarnemingen

De in Hoofdstuk 7 gepresenteerde resultaten tonen het volgende aan.

- De afgeleide regionale landoppervlak variabelen (oppervlaktereflectie en -temperatuur) en oppervlaktewarmtestromingen (nettostraling, bodemwarmte, voelbare en latente warmte) over de studiegebieden komen goed overeen met de waargenomen karakteristieken van het landoppervlak.

- De heterogeniteit van het landoppervlak leidt tot heel verschillende waarden van de landoppervlak-variabelen en –warmtestromingen over de HEIFE-, AECMP '95 en DHEX gebieden. Deze variabelen en warmtestromingen laten in alle ruimteverdelingskaarten en frequentieverdeling-histogrammen uiteenlopende waarden zien, die geconcentreerd zijn rond een tweetal relatieve maxima's. Het eerste maximum is aan de oase gerelateerd en de tweede aan de Gobi woestijn (Tabel 7.6). De afgeleide waarden van landoppervlak-variabelen en –warmtestromingen in de GAME/Tibet en CAMP/Tibet gebieden zijn minder gespreid ten opzichte van de HEIFE-, AECMP '95 en DHEX gebieden (Tabel 7.6).
- De m.b.v. de Tegel- en de Menghoogte-benadering geschatte regionale landoppervlak -variabelen en –warmtestromingen wijken (zie Eq. 5.18) bij de meetplaatsen (Eqs. 7.4, 7.6, 7.8, 7.10 en 7.13) minder dan 10% af van de veldwaarnemingen. Met andere woorden: de met de Tegel- en de Menghoogte benadering verkregen regionale verdeling van land oppervlak -variabelen en –warmtestromingen over heterogene landschappen zijn nauwkeuriger dan de met de RS benadering verkregen schattingen. Dit betekent dat de Tegel- en de Menghoogte-benaderingen toegepast kunnen worden om nauwkeurig de warmtestromen boven het regionale landoppervlak van de heterogene landschappen van ariede en de hooggelegen gebieden. te schatten.

Conclusies:

- 1) *De in dit proefschrift beschreven parameterisaties om voor heterogene landschappen warmtestromingen aan het landoppervlak te bepalen m.b.v. satelliet-, SL- en ABL-waarnemingen overbruggen inderdaad het gat tussen de lokale/puntwaarnemingen en grote lengteschaal van deze landschappen.*
- 2) *De Tegel- en de Menghoogte-benadering kunnen nauwkeurig worden toegepast boven heterogene landschappen.*

Perspectieven voor toekomstig onderzoek

In dit proefschrift zijn de voorgestelde Tegel-, Menghoogte- en de RS-benadering toegepast op een vijf-tal verschillende experimenten. Voor het beter begrijpen van de warmteuitwisseling tussen heterogene landschappen en de atmosferische laag daarboven, zijn meer SL- en ABL-waarnemingen noodzakelijk.. Bovendien zou een meer systematisch gebruik van meteorologische en remote sensing waarnemingen dienen te worden gemaakt,

teneinde het dagelijks-, seizoens en zelfs inter-jaarlijks verloop van regionale warmtestromingen aan het landoppervlak nog beter te kunnen bestuderen.

References

- Anthes, R. A., 1983, Regional models of atmosphere in middle latitude, *Monthly Weather Review*, **110**: 1306-1335.
- Anthes, R. A., E. Y. Hsie, and Y. H. Kuo, 1987, Description of Penn.State/NCAR Mesoscale Model Version4(MM4), *NCAR/TN-282+STR*.
- Arya, S. P. S., 1975, A drag partition theory for determining the large-scale roughness parameter and wind stress on arectic pack ice. *Journal of Geophysics Research*, **80**: 3447-3454.
- Avissar, R., and R. A. Pielke, 1989, A parameterization of heterogeneous land surfaces for atmospheric numerical models and it impact on regional meteorology, *Monthly Weather Review*, **117**: 2113-2136.
- Avissar, R., 1991, A statistical-dynamical approach to parameterize subgrid-scale land-surface heterogeneity in climate models, *Surveys in Geophysics*, **12**: 155-178.
- Avissar, R., 1995, Scaling of land-atmosphere interactions: an atmospheric modelling perspective, *Hydrological Processes*, **9**: 679-695.
- Baret, F., and G. Guyot, 1991: Potential and limits of vegetation indices for LAI and APAR assessment, *Remote Sensing Environment*, **35**: 161-173.
- Baret, F., G. Guyot, J. M. Teres, and D. Rigal, 1988, Profile spectral et estimation de la biomass. *Proceeding of 4th International Colloquium on Spectral Signatures of Objects in Remote Sensing*, Aussois, France: 93-98.
- Baret, F., G. Guyot, and D. J. Major, 1989, TSAVI: A vegetation index which minimizes soil brightness effects on LAI and APAR estimation. *Proceedings of the 12th Canadian Symposium on remote Sensing*, Vancouver, Canada: 1355-1358.
- Bastiaanssen W. G. M., 1995, *Regionalization of surface fluxes and moisture indicators in composite terrain*, PhD Thesis, Wageningen Agricultural University, 273pp.
- Becker, F., and Z.-L., Li, 1990, Towards a local split window method over land surfaces, *International Journal of Remote Sensing*, **11**(3): 369- 393.
- Becker, F., and Z.-L., Li, 1995, Surface temperature and emissivity at various scales: definition, measurement and related problems, *Remote Sensing Review*, **12**: 225-253.
- Belcher, S. E., D. P. Xu, and J. C. R. Hunt, 1990, The response of a turbulent boundary layer to arbitrarily distributed two-dimensional roughness changes, *Quarterly Journal of the Royal Meteorological Society*, **116**: 611-635.
- Berk, A., L. S. Bernstein, and D. C. Robertson, 1989, *MODTRAN: a moderate resolution model for LOWTRAN 7*, GL-TR-89-0122, Geophysics Laboratory, Hanscom AFB, MA

01732.

- Blyth, E. M., A. J. Dolman, and N. Wood, 1993, Effective resistance to sensible and latent heat flux in heterogeneous terrain, *Quarterly Journal of the Royal Meteorological Society*, **119**: 423-442.
- Bolle, H. J., J. C. Andre, and J. L. Arrue, 1993, EFEDA: The European field experiment in a desertification threatened area, *Annual Geophysics*, **II**: 173-189
- Bradley, E. F., 1968, A micrometeorological study of velocity profiles and surface drag in the region modified by a change in surface roughness, *Quarterly Journal of the Royal Meteorological Society*, **94**: 361-379.
- Brest, C. L., and S.N. Goward, 1987, Deriving surface reflectance from a narrow band satellite data. *International Journal of Remote Sensing*, **8**: 351-367.
- Brutsaert, W., 1984, *Evaporation into the atmosphere-Theory, History, and Applications*. Kluwer Academic Publishers, Dordrecht, the Netherlands, 299pp.
- Businger, J. A., 1988, A note on the Businger-Dyer profiles, *Boundary Layer Meteorology*, **42**: 145-151.
- Carlson, T. N., and D. A. Ripley, 1997, On the relation between NDVI, fractional vegetation cover, and leaf area index. *Remote Sensing of Environment*, **62**: 241-252.
- Chamberlain, A. C., 1968, Transport of gases to and from surfaces with bluff and wave-like roughness elements, *Quarterly Journal of the Royal Meteorological Society*, **94**: 318-332
- Chen, J., J. Wang, Y. Mitsuta, 1993, An independent method to determine the surface roughness length, *Chinese Journal of Atmospheric Sciences*, **17**(1): 21-26 (in Chinese with English abstract).
- Choudhury, B. J., S. B. Idso, and R. J. Reginato, 1987, Analysis of an empirical model for soil heat flux under a growing wheat crop for estimating evaporation by infrared-temperature based energy balance Eq., *Agricultural and Forest Meteorology*, **39**: 283-297.
- Choudhury, B. J and J. L. Monteith, 1988, A four-layer model for the heat budget of homogeneous land surfaces, *Quarterly Journal of the Royal Meteorological Society*, **114**: 373-398.
- Choudhury, B. J., 1989, Estimating evaporation and carbon assimilation using infrared temperature data: Vistas in modeling, (ed.) G.Asrar, *Theory and application of optical remote sensing*, John Wiley, New York: 628-690.
- Claussen, M., 1990, Area-averaging of surface fluxes in a neutrally stratified, horizontally

- inhomogeneous atmospheric boundary layer, *Atmospheric Environment*, **24a**: 1349-1360.
- Claussen, M., 1991, Estimation of areally averaged surface fluxes, *Boundary-Layer Meteorology*, **54**: 387-410.
- Cleugh, H. A., and C. S. B. Grimmond, 1993, A comparison between measured local-scale suburban and areally-averaged urban heat and water vapour fluxes, in Bolle, H.-J., Feddes, R.A., and Kalma, J.D.(Eds), *Exchange processes at the Land Surface for a range of Space and time Scales, Proc.Symp.J3.1, joint Scientific Assembly of IAMAP and IAHS, Yokohama, Japan, 11-23 July, 1993, IAHS Publ.*, **212**: 155-163.
- Clevers, J. G. P.W., 1988, The derivation of simplified reflectance model for the estimation of leaf area index, *Remote Sensing of Environment*, **25**: 53-69.
- Clothier, B. E., K. L. Clawson, P. J. Pinter, M. S. Moran, R. J. Reginato, and R. D. Jackson, 1986, Estimating of soil heat flux from net radiation during the growth of alfalfa, *Agricultural and Forest Meteorology*, **37**: 319-329.
- Cowan, I. R., 1968, The interception and absorption of radiation in plants stands, *Journal of Applied Ecology*, **5**: 367-379.
- Cram, J. M., R. A. Pielke and W. R. Cotton, 1992 a, Numerical simulation and analysis of prefrontal squall line, Part I: Observation and basic simulation results, *Journal of Atmospheric Sciences*, **49**: 189-208.
- Cram, J. M., R. A. Pielke and W. R. Cotton, 1992 a, Numerical simulation and analysis of prefrontal squall line, Part II: Propagation of the squall line as an internal gravity wave, *Journal of Atmospheric Sciences*, **49**: 209-225.
- Daughtry, C. S. T., W. P. Kustas, M. S. Moran, P. J. Pinter, R. D. Jackson, P. W. Brown, W. D. Nichols, and L. W. Gay, 1990, Spectral estimates of net radiation and soil heat flux, *Remote Sensing Environment*, **32**: 111-124.
- Davis, P. A. and J. D. Tarpley, 1983, Estimation of shelter temperature from operational satellite sounder data, *Climate and Applied Meteorology*, **22**: 369-376.
- Deardorff, J. W., 1978, Efficient prediction of ground surface temperature and moisture, with inclusion of a layer of vegetation, *Journal of Geophysical Research*, **83**: 1889-1903.
- De Bruin, H. A. R., and A. A. M. Holtslag, 1982, A simple parameterization of the surface fluxes of sensible and latent heat during daytime compared with Penman-Monteith concept, *Journal of Applied Meteorology*, **21**: 1610-1621.
- Dickinson, R. E., A. Henderson-Shellers, P. J. Kennedy, and M. F. Wilson, 1986, *Biosphere-Atmosphere Transfer Scheme (BATS) for the NCAR Community Climate Model*,

- NCAR/TN-275+STR, National Center for Atmospheric Research, Boulder Colorado:pp69.
- Ding, Y., 1989, *The diagnostic analysis methodology in the dynamic weather*, Science Press, Beijing: 13 (in Chinese).
- Dolman, A. J., Wallace, J. S., 1991, Lagrangian and K-theory approaches in modelling evaporation from sparse canopies, *Quarterly Journal of the Royal Meteorological Society*, **117**: 1325-1340.
- Duffie, J. A., and W. A. Beckman, 1980, *Solar Engineering of Thermal Processes*, A Wiley-Interscience Publication, John Wiley & Sons, pp199
- Enthekabi, D., and P.S. Eagleson, 1989, Land surface hydrology parameterization for atmospheric general circulation models including sub-grid scale variability, *Journal of Climate*, **8**: 816-831.
- Famiglietti, J. S. and E. F. Wood, 1991, Evapotranspiration and runoff from large land areas: land surface hydrology for atmospheric general circulation models, *Surveys in Geophysics*, **12**: 179-204.
- Feddes, R. A., P. J. Kowalk, and H. Zaradny, 1978, *Simulation of field water use and crop yield*, PUDOC, Wageningen, pp189.
- Finnigan, J. J., M. R. Raupach, E.F. Bradley, and G. K. Aldis , 1990, A wind tunnel study of turbulent flow over a two-dimensional ridge, *Boundary-Layer Meteorology*, **50** : 277-317
- Fuchs, M. and A. Hadas, 1972, The heat flux in a nonhomogeneous bare loessial soil. *Boundary-Layer Meteorology*, **3**: 191-200
- GAME International Science Panel, *GEWEX Asian Monsoon Experiment (GAME) Implementation Plan*, March, 1998, pp136.
- Garratt, J. R., and B. B. Hicks, 1973, Momentum, heat, and water vapor transfer to and from natural and artificial surfaces, *Quarterly Journal of the Royal Meteorological Society*, **99**: 680-687.
- Garratt, J. R., 1978, Transfer characteristics for a heterogeneous surface of large aerodynamic roughness, *Quarterly Journal of the Royal Meteorological Society*, **104**: 491-502.
- Garratt, J. R., 1992, *The Atmospheric Boundary Layer*, Cambridge University Press, Cambridge, 366pp.
- Goutorbe J. P., T. Lebel, and A. Tinga, 1994, A large scale study of land-atmosphere interaction in the semi-arid tropics (HAPEX-Sahel), *Annual Geophysics*, **12**: 53-64.
- Guo, X., and J. Wang, 1993, Analysis of sensible heat flux by using the simplified

- aerodynamic approach method over HEIFE area, *Plateau Meteorology*, **12**(2): 133-140 (in Chinese with English abstract).
- Gutman, G., 1987, The derivation of vegetation indices from AVHRR data, *International Journal of Remote Sensing*, **8**: 1235-1243.
- Hall, F. G., and P. J. Sellers, 1993, M Apps BOREAS: Boreal Ecosystem Atmosphere Study, *IEEE Geosciences Remote Sensing Society Newsletter*, March: 9-17
- Hinzman, L. D., M. E. Bauer, and C. S. T. Daughtry, 1986, Effects of nitrogen fertilization on growth and reflectance characteristics of winter wheat, *Remote Sensing of Environment*, **19**: 47-61.
- Holtzlag, A. A. M., and M. EK, 1996, Simulation of surface heat fluxes and boundary layer development over the pine forest in HAPEX-MOBILHY, *Journal of Applied Meteorology*, **35**, 202-213.
- Hu, Y., 1990, On some aspects of the observations of turbulent fluxes in surface layer, *Plateau Meteorology*, **9**: 74-86. (in Chinese with English abstract).
- Hu, Y., Y. Gao, J. Wang, G. Ji, Z. Shen, L. Cheng, J. Chen, and S.Li, 1994, Some achievements in scientific research during HEIFE, *Plateau Meteorology*, **13**(3): 225-236 (in Chinese with English abstract).
- Hu, Z., 2004, *Land surface processes experiment and its related issues study in the Tibetan Plateau and northwest arid area of China*. PhD thesis, Cold and Arid Regions Environmental and Engineering Research Institute, Chinese Academy of Sciences, Lanzhou, China.(in Chinese with English abstract).
- Hu, Z., R. Huang, G. Wei, and H. Gao, 2002, Variations of surface atmospheric variables and energy budget during a sandstorm passing Dunhuang on June 6 of 2000, *Chinese Journal of Atmospheric Sciences*, **26**(1), 1-8. (in Chinese with English abstract)
- Huete, A. R., R. D. Jackson, and D. F. Post, 1985, Spectral response of a plant canopy with different soil backgrounds, *Remote Sensing of Environment*, **17**: 37-53.
- Huete, A. R., 1987, Soil and sun angles interaction on partial canopy spectra, *International Journal of Remote Sensing*, **8**: 1307-1317.
- Huete, A. R., 1988, A soil-adjusted vegetation index (SAVI), *Remote Sensing of Environment*, **25**: 295-309.
- Huete, A. R., 1989, Soil influences in remotely sensed vegetation-canopy spectra, *Theory and Applications of Optical Remote Sensing* (G.Asrar, Ed.): 107-141.
- Huete, A. R. and A. W. Warrick, 1990, Assessment of vegetation and soil water regimes in practical canopies with optical remotely sensed data, *Remote Sensing of Environment*,

32: 155-167.

- Huete, A. R. and C. J. Tucker, 1991, Investigation of soil influences in AVHRR red and near-infrared vegetation index imagery, *International Journal of Remote Sensing*, **12**(6): 1223-1242.
- Idso, S. B., J. K. Aaase, and R. D. Jacson, 1975, Net radiation-soil heat flux relations as influenced by soil water content variations, *Boundary-Layer Meteorology*, **9**: 113-122.
- IGBP, 1992, *Global Change: Reducing Uncertainties*, Publicized by Royal Swedish Academy, ISBN 91-630-1086-0
- Iqbal, M., 1983, *An introduction to solar radiation*, Academic Press, Toronto.
- Ishikawa, H., O. Tsukamoto, T. Hayashi, I. Tamagawa, Sh. Miyazaki, J. Asanuma, and Y. Qi, 1999, Summary of the boundary layer observation and preliminary analysis, *Preprint Volume of Third International Scientific Conference on the Global Energy and Water Cycle*, Beijing, China: 458-459.
- Jackson, P. S., J. C. R. Hunt, 1975, Turbulent wind flow over a low hill, *Quarterly Journal of the Royal Meteorological Society*, **101**: 929-955.
- Jackson, R. D., P. J., Jr. Pinter, S. B. Idso, and R. J. Idso, 1979, Wheat spectral reflectance: Interactions between crop configuration, sun elevation and azimuth angle, *Applied Optics*, **18**: 3730-3735.
- Jackson, R. D., P. J., Jr. Pinter, and R. J. Reginato, 1985, Net radiation calculated from remote multispectral and ground station meteorological data, *Agricultural and forest Meteorology*, **35**: 153-164.
- Jackson, R. D., M. S. Moran, L. W. Gay, and L. H. Raymond, 1987, Evaluating evaporation from field crops using airborne radiometry and ground-based meteorological data, *Irrigation Science*, **8**: 81-90.
- Jensen, N. O., and P. Hummelshøj, 1995, Derivation of canopy resistance for water vapor fluxes over a spruce forest using new technique for the viscous sublayer resistance, *Agricultural and Forest Meteorology*, **73**: 339-352.
- Jia, L., M. Menenti, and J. Wang, 1999a, Estimation of area roughness length for momentum using remote sensing data and measurements in field, *Chinese Journal of Atmospheric Sciences*, **23**: 632-640. (in Chinese with English abstract).
- Jia, L., J. Wang, M. Menenti, 1999b, The local and effective aerodynamic roughness of complex landscape of oasis and desert, *ACTA Meteorological Sinica*, **57**(3): 46-356 (in Chinese with English abstract).
- Jia, L., J. Wang, Z. Hu, 2000, The characteristics of roughness length for heat and its

- influence on determination of sensible heat flux in arid zone, *Plateau Meteorology*, **19**(4): 495-503(in Chinese with English abstract).
- Jia, L., 2004, *Modeling heat exchanges at land-atmosphere interface using multi-angular thermal infrared measurements*, PhD Thesis, Wageningen University, 199pp.
- JSC, 1994, *Report of 15th Session of the Joint Scientific Committee of WCRP*, WMO/TD, No.632, WMO, Geneva, pp136.
- Justice, C. O., J. R. G. Towensend, B. N. Holben, and C. J. Tucker, 1985, Analysis of the phenology of global vegetation using meteorological satellite data, *International Journal of Remote sensing*, **6-8**:1271-1318.
- Kahle, A. B., and R. E. Alley, 1992, Separation of temperature and emittance in remotely sensed radiance measurements, *Remote Sensing of Environment*, **42**: 107-112.
- Kaimal, J. C., J. J. Finnigan, 1994, *Atmospheric Boundary Flows: Their Structure and Measurement*, Oxford University Press, Oxford, 289pp.
- Kimes, D. S., 1983, Dynamic of directional reflectance factor distributions for vegetation canopies, *Applied Optics*, **22**: 1364-1372.
- Kimes, D. S., J. M. Norman, and C. L. Walthall, 1985, Modeling the radiant transfers of sparse vegetation canopies. *I.E.E.E. Transactions Geosciences and remote Sensing*, **23**: 695-704
- Kirchner, J. A., D. S. Kimes, and J. E. McMurtrey, III, 1982, Variation of directional reflectance factors with structural changes of developing alfalfa canopy, *Applied Optics*, **21**: 3766-3774.
- Kenizys, F.X., L.W. Abreu, G.P. Anderson, J.H., Chetwynd, E.P. Shettle, A. Berk, L.S. Bernstein, D.C. Robertson, P. Acharya, L.S. Rothman, J.E.A. Selby, W.O. Gallery, and S.A. Clough, *The MODTRAN3/2 report and LODTRAN 7 Model*. (L.W. Abreu and G.P. Anderson, Eds), prepared by Ontar Corp., North Andover, MA, for Phillips Laboratory, Geophysical Directorate, Hanscom AFB, MA., Contract No.F19628-91-C-0132, 1996.
- Koepke, P., K.T. Kriebel, and B. Dietrich, 1985, The effect of surface reflection and of atmospheric parameters on the shortwave radiation budget, *Advances in Space Research*, **5**: 351-354.
- Kohsiek, W., H. A. R. De Bruin, and B. J. J. M. ven den Hurk, 1993, Estimation of the sensible heat flux of a semi-arid area using surface radiative temperature measurements. *Boundary Layer Meteorology*, **63**: 213-230.
- Koike, T., 2002, CEOP starts-A step for predictability improvement of the water cycle and water resources, *CEOP News Letter*, **1**: 1-2.

- Kollenkark, J. C., C. S. T. Daughtry, M. E. Bauer, and T. L. Housley, 1982a, Effects of cultural practices on agronomic and reflectance of characteristics of soybean canopies, *Agronomic Journal*, **74**: 751-758.
- Kollenkark, J. C., V. C. Vanderbilt, C. S. T. Daughtry, M. E. Bauer, 1982b, Influence of solar illumination angle on soybean canopy reflectance, *Applied Optics*, **21**: 1179-1184.
- Kond, J., 1975, Air-sea bulk transfer coefficients in diabatic conditions, *Boundary Layer Meteorology*, **9**: 91-112.
- Koster, R. D., and M. J. Suarez, 1992, Modeling the land surface boundary in climate models as a composite of independent vegetation stands, *Journal of Geophysical Research*, **97**(D3): 2697-2715.
- Kroon, L. J. M. and H. A. R. de Bruin, 1993, Atmosphere-vegetation interaction in local advection conditions: effect of lower boundary conditions, *Agricultural and forest Meteorology*, **64**: 1-28.
- Kustas, W. P., B. J. Choudhury, M. S. Moran, R. J. Reginato, R. D. Jackson, L. W. Gay, and H. L. Weaver, 1989, Determination of sensible heat flux over sparse canopy using thermal infrared data, *Agricultural and Forest Meteorology*, **44**: 197-216.
- Kustas, W. P., 1990, Estimates of evapotranspiration with a one –and two-layer model of heat transfer over partial canopy cover, *Journal of Applied Meteorology*, **29**: 704-715.
- Kustas, W. P., and C. S. T. Daughtry, 1990, Estimation of the soil heat flux/net radiation ratio from spectral data, *Agricultural and Forest Meteorology*, **39**:205-223.
- Kustas, W. P., and J. M. Norman, 1997, A two-source approach for estimating turbulent fluxes using multiple angle thermal infrared observations, *Water Resources Research*, **33**: 1495-1508.
- Li, J., J. Huang, X. Wang, 1997, *Grassland remote sensing*, China Meteorological Press, pp242 (in Chinese).
- Li, Z-L., and F. Becker, 1993, Feasibility of land surface temperature and emissivity determination from AVHRR data, *Remote Sensing of Environment*, **43**: 67-85.
- Liang, S., 2004, *Quantitative Remote Sensing of Land Surfaces*, John Wiley and Sons, Inc., 534pp .
- Lu, D., 1997, Mongolia semi-arid grassland soil-vegetation-atmosphere interaction (IMGRASS), *Global Change News Letter*, **31**: 4-5
- Ma, Y., J. Wang, M. Menenti, and W. G. M. Bastiaanssen, 1997, Distribution and seasonal variation of regional net radiation in the HEIFE area, *Chinese Journal of Atmospheric Sciences*, **21**(2): 410-417. (Chapter 5)

- Ma, Y., J. Wang, M. Menenti, and W. G. M. Bastiaanssen, 1999, Estimation of fluxes over the heterogeneous land surface with the aid of satellite remote sensing and ground observation, *ACTA Meteorological Sinica*, **57**(2): 180-189 (in Chinese with English abstract) (Chapter 5)
- Ma, Y., O. Tsukamoto, X. Wu, I. Tamagawa, J. Wang, H. Ishikawa, Z. Hu, and H. Gao, 2000, Characteristics of energy transfer and micrometeorology in the surface layer of the atmosphere above marshland of the Tibetan Plateau area, *Chinese Journal of Atmospheric Sciences*, **24**(5): 715-722(in Chinese with English abstract). (Chapter 6)
- Ma, Y., O. Tsukamoto, H. Ishikawa, Z. Su, M. Menenti, J. Wang, and J. Wen, 2002a, Determination of Regional land surface heat flux densities over heterogeneous landscape of HEIFE Integrating satellite remote sensing with field observations, *Journal of Meteorological Society of Japan*, **80**(3): 485-501. (Chapter 7)
- Ma, Y., O. Tsukamoto, H. Ishikawa, 2002b, Remote sensing parameterization of energy and water cycle over desertification area, *Science in China (D)*, **45**(Supp):47-53.
- Ma, Y., Z. Su, Z-L. Li, T. Koike, and M. Menenti, 2002c, Determination of regional net radiation and soil heat flux densities over heterogeneous landscape of the Tibetan Plateau, *Hydrological Processes*, **16**(15): 2963-2971.
- Ma, Y., O. Tsukamoto, J. Wang, H. Ishikawa, and I. Tamagawa, 2002d, An analysis of aerodynamic and thermodynamic parameters over the grassy marshland surface of Tibetan Plateau, *Progress in Natural Science*, **12**(1): 36-41. (Chapter 6)
- Ma, Y., H. Ishikawa, O. Tsukamoto, M. Menenti, Z. Su, T. Yao, T. Koike, and T. Yasunari, 2003a, Regionalization of surface fluxes over heterogeneous landscape of the Tibetan Plateau by using satellite remote sensing, *Journal of the Meteorological Society of Japan*, **81**: 277-293. (Chapter 7)
- Ma, Y., J. Wang, R. Huang, G. Wei, M. Menenti, Z. Su, Z. Hu, F. Gao, and J. Wen, 2003b, Remote sensing parameterization of land surface heat fluxes over arid and semi-arid areas, *Advances in Atmospheric Sciences*, **20**(4): 530-539. (Chapter 7)
- Ma, Y., 2003c, Remote sensing parameterization of regional net radiation over heterogeneous land surface of GAME/Tibet and HEFE, *International Journal of Remote Sensing*, **24** (15): 3137-3148. (Chapter 7)
- Ma, Y., Z. Su, T. Koike, T. Yao, H. Ishikawa, K. Ueno, M. Menenti, 2003d, On measuring and remote sensing surface energy partitioning over the Tibetan Plateau-from GAME/Tibet to CAMP/Tibet, *Physics and Chemistry of the Earth*, **28**: 63-74.
- Ma, Y., W. Ma, M. Li, O. Tsukamoto, H. Ishikawa, J. Wang, Z. Hu, and F. Gao, 2003e, The

- comparative analysis of characteristics of energy transfer in near surface layer over the area of GAME/Tibet, HEIFE and AECMP'95, *Chinese Journal of Atmospheric Sciences*, **27**(1): 1-14. (Chapter 6).
- Ma, Y., M. Menenti, O. Tsukamoto, H. Ishikawa, J. Wang, and Q. Gao, 2004a, Remote sensing parameterization of regional land surface heat fluxes over arid area in northwestern China, *Journal of Arid Environments*, **57**: 117-133. (Chapter 7)
- Ma, Y., W. Ma, M. Li, Z. Su, M. Menenti, O. Tsukamoto, H. Ishikawa, T. Koike, and J. Wen, 2004b, Determination of regional heat fluxes over heterogeneous land surfaces, GIS and Remote Sensing in Hydrology, Water Resources and Environment, *IAHS Publ.* **289**: 206-214.
- Ma, Y., S. Fan, H. Ishikawa, O. Tsukamoto, T. Yao, T. Koike, H. Zuo, Z. Hu, and Z. Su, 2005, Diurnal and inter-monthly variation of land surface heat fluxes over the central Tibetan Plateau area, *Theoretical and Applied Climatology*, **80**: 259-273. (Chapter 6, Chapter 7)
- Ma, Y., L. Zhong, Z. Su, H. Ishikawa, M. Menenti, T. Koike, 2006, Determination of regional distributions and seasonal variations of land surface heat fluxes from Landsat-7 Enhanced Thematic Mapper data over the central Tibetan Plateau area, *Journal of Geophysical Research*, **111**, D10305, doi:10.1029/2005JD006742. (Chapter 7)
- Manabe, S., 1969, Climate of the ocean simulation, the atmospheric circulation and the hydrology of the earth's surface, *Monthly Weather Review*, **97**: 739-774.
- Markham, B. L. and J. L. Barker, 1987, Thematic mapper bandpass solar exoatmospheric irradiances, *International Journal of Remote Sensing*, **8** (3): 517-523.
- Mason, P., 1988, The formation of areally averaged roughness lengths, *Quarterly Journal of the Royal Meteorological Society*. **114**: 399-420
- McNaughton, K. G., T. W. Spriggs, 1986, A mixed-layer model for regional evaporation, *Boundary Layer Meteorology*, **34**: 243-262.
- McNaughton, K. G., 1989, Regional interaction between canopies and atmosphere, in Russell, G., Marshall, B., and Jarvis, P.G. (Eds), *Plant Canopies: their Growth, Form and Function*, Cambridge University Press, Cambridge: 63-81.
- McNaughton K. G., P. G. Jarvis, 1991, Effects of spatial scale on stomatal control of transpiration, *Agricultural and Forest Meteorology*, **54**: 279-301.
- McNaughton, K. G., and B. J. J. M. van den Hurk, 1995, A "Lagrangian" revision of resistors in the two-layer model for calculating the energy budget of a plant canopy. *Boundary Layer Meteorology*, **74**: 261-288.

- McNaughton, K. G., and M. R. Raupach, 1996, Response of the convective boundary layer and the surface energy balance to large scale heterogeneity, *Scaling up in hydrology using remote sensing* (Editors: Stewart, J.B., E. T. Engman, R. A. Feddes, and Y. H. Kerr), John Wiley & Sons: 171-182.
- Menenti, M., 1984, *Physical aspects and determination of evaporation in deserts applying remote sensing techniques*, PhD Thesis, Instituut voor Cultuurtechniek en Waterhuishouding, Wageningen, 202pp.
- Menenti, M., W. G. M. Bastiaanssen, and D. Van Eick, 1989, Determination of hemispheric reflectance with Thematic Mapper data, *Remote Sensing of Environment* (special issue), **28**: 327-337.
- Menenti, M., W. G. M. Bastiaanssen, K. Hefny, and M. H. Abd El Karim, 1991, Mapping of ground water losses by evaporation in the Western Desert of Egypt, *DLO Winand Staring Centre, Report No.43*, Wageningen, The Netherlands: 116pp.
- Menenti, M., and B. J. Choudhury, 1993, Parameterisation of land surface evaporation by means of location dependent potential evaporation and surface temperature range, in (eds.)Bolle, Feddes and Kalma, *Exchange processes at the land surface for a range of space and time scales*, IAHS Publ. **212**: 561-568.
- Menenti, M., and J. C. Ritchie, 1994, Estimation of effective aerodynamic roughness of Walnut Gulch watershed with laser altimeter data, *Water Resources Research*, **30**: 1329-1337.
- Menenti, M., W. G. M. Bastiaanssen, (eds.), 1997. Mesoscale climate hydrology: *Earth Observation System-Definition Phase*, Report 106, DLO-Winand Staring Centre, Wageningen, The Netherlands (appeared also as BCRS Report NRSP-2 95-15), 199pp.
- Monin, A. S., A. M.Obukhov, 1954, Basic laws of turbulent mixing the atmospheric near the ground, *Akad. Nauk.SSR., Geophys. Inst.*, 151
- Monteith, J. L., 1965, Evaporation and environment, *Symposium of Society Experimental Biology*, Academic Press, Inc., NY, 19: 206-234.
- Monteith, J. L., 1973, *Principles of Environmental Physics*, Edward Arnold, London, 241pp
- Norman, J. M., W. P. Kustas, and K. S. Humes, 1995, A two-source approach for estimating soil and Vegetation energy fluxes from observations of directional radiometric surface temperature, *Agricultural and Forest Meteorology*, **77**: 263-293
- Oku, Y., and H. Ishikawa, 2004, Estimation of land surface temperature over the Tibetan Plateau using GMS data, *Journal of Applied Meteorology*, **43**(4): 548-561.

- Owen, P. R., and W. R. Thomson, 1963, Heat transfer across rough surfaces, *Journal of Fluid Mechanics*, **15**: 321–334.
- Owe, M., 1992, Measurements of surface resistance, reflectance and thermal emissivity during EFEDA, *Proc. European Geophysical Society*, Edinburgh 1992, Supplement II to Vol. 10: C280.
- Owe, M., A. A. Van de Griend, and D. C. Carter, 1993, Modelling of longterm surface moisture and monitoring vegetation response by satellite in semi-arid Botswana, *Geo-Journal*, **29**(4): 335-342.
- Owen, P. R., and W. R. Thomson, 1963, Heat transfer across rough surface, *Journal of Fluid Mechechim.*, **15**:321-334.
- Paltridge, W., R. M. Mitchell, 1990, Atmospheric and viewing angle correction of vegetation indices and grassland fuel moisture content derived from NOAA/AVHRR. *Remote Sensing of Environment*, **31**: 121-135.
- Paulson, C. A., 1970, The mathematic representation of wind speed and temperature profiles in the unstable atmospheric surface layer, *Journal of Applied Meteorology*, **9**: 856-861.
- Peterson, D. L., M. L. Spanner, S. W. Running, and K. B. Toker, 1987, Relationship of the thermatic mapper simulator data to leaf area index of temperate coniferous forests, *Remote Sensing of Environment*, **22**: 323-341.
- Pielke, R. A., X. Zeng, T. J. Lee, and G. A. Dalu, 1995, Mesoscale fluxes over heterogeneous flat landscape for use large scale models *Journal of Hydrology*, **141**: 79-94.
- Pinker, R. T., 1990, Satellites and our understanding of the surface energy balance, *paleogeography, palaeoclimatology, palaeoecology (Global and planetary change Section)*, **82**: 321-342.
- Pinty, B., and D. Ramond, 1987, A method for the estimate of broadband directional albedo from a gestationary satellite, *Journal of Climate and Applied Meteorology*, **26**: 1709-1722.
- Pinter, P. J., Jr., G. Zipoli, G. Marachhi, and R. J. Reginato, 1987, Influence of topography and sensor view angles on NIR/Red ratio and greenness vegetation indices of wheat, *International Journal of remote Sensing*, **8**: 953-957.
- Pirrier, A., 1975, Assimilation nette, utilization de l'eau et micriclimat d'un champ de maïs. *Annual Agronomy*, **26**: 139-157.
- Price, J. C., 1992, Estimating vegetation amount from visible and near infrared reflectance, *Remote Sensing of Environment*, **41**: 29-34.
- Price, J. C., 1993, Estimating leaf area index from satellite data, *I.E.E.E. Transactions on*

- Geoscience and Remote Sensing*, **31**: 727-734.
- Qi, J., A. Chehbouni, A. R. Huete, Y. H. Kerr, and S. Sorooshian, 1994, A Modified Soil Adjusted Vegetation Index, *Remote Sensing of Environment*, **48**:119-126
- Qualls, R. J., and W. Brutsaert, 1995, The effect of vegetation density on the parameterization of scalar roughness to estimate spatially distributed sensible heat fluxes, *Water Resource Research*, **32**: 645-652.
- Ranson, K. J., C. S. T. Daughtry, L. L. Biehl, and M. E. Bauer, 1985, Sun-view angle effects on reflectance factors of corn canopies, *Remote sensing Environment*, **18**: 147-161.
- Ranson, K. J., C. S. T. Daughtry, and L. L. Biehl, 1986, Sun angle, view angle and background effects on spectral response of simulated balsam fir canopies, *Photogramm. Eng. Remote Sensing*, **52**: 649-658.
- Raupach, M. R., 1991, Vegetation-atmosphere interaction in homogeneous terrain, *Vegetatio*, **91**: 105-120.
- Raupach, M. R., 1994, Simplified expressions for vegetation roughness length and zero-plane displacements as functions of canopy height and area index, *Boundary Layer Meteorology*, **71**: 211-216.
- Raupach, M. R., 1995, Vegetation-atmosphere interaction and surface conductance at leaf, canopy and regional scales, *Agricultural and Forest Meteorology*, **73**: 151-179.
- Raupach, M. R., J. J. Finnigan, 1995, Scale issues in boundary-layer meteorology: surface energy balances in heterogeneous terrain, *Hydrological Processes*, **9**: 589-612.
- Reginato, R. J., R. D. Jackson, P. J. Jr., Pinter, 1985, Evapotranspiration calculated from remote multispectral and ground station meteorological data, *Remote Sensing Environment*, **18**: 75-89.
- Roerink, G. J. and M. Menenti, M. (eds.), 1997, *Climate and hydrology at mesoscale: the contribution of future sensor systems, final report of bridging phase*, BCRS NUSP 98-01, 172pp.
- Rouse, J. W., 1972, Monitoring the vernal advancement and retro-gradation (Green wave effect) of natural vegetation. *NASA/GSFCT Type I Report*, Greenbelt, MD.USA.
- Rouse, J. W., R. W. Haas, J. A. Schell, D. W. Deering, and J. C. Hhharlan, 1974, Monitoring the vernal advancement and retro-gradation (Green wave effect) of natural vegetation. *NASA/GSFCT Type I Report*, Greenbelt, MD.USA.
- Rowntree, P. R., 1991, Atmospheric parameterization schemes for evaporation over land: basic concepts and climate modeling aspects. In: Schmugge, T.J. and J.-C. Andre (eds), *Land surface evaporation*. Springer-Verlag, New York, 5-29.

- Saunders., R. W., 1990, The determination of broad band surface reflectance from AVHRR visible and near –infrared radiances, *International Journal of Remote Sensing*, **11**: 49-67.
- Schmidt, J. M., and W. R. Cotton, 1990, Interactions between upper and lower troposphere gravity waves on squall line structure and maintenances, *Journal of Atmospheric Sciences*, **47**: 1205-1222.
- Schmugge, T. J. and J. C. Andre, 1991, Land surface evaporation measurement and parameterization, Springer Verlag, New York, 424
- Schmugge, T. J., S. Hook, and A. Kahle, 1995, TIMS observation of surface emissivity in HAPEX-Sahel, *Proceeding of IGARSS 1995 July*, Florence, Italy.
- Seginer, I., 1974, Aerodynamic roughness of vegetated surfaces, *Boundary Layer Meteorology*, **5**: 383-393.
- Sellers, A. H., and F. G. Hall, 1992, FIFE special Issue, *Journal of Geophysics Research*, **97** (D17): 18343-19109.
- Sellers, A. H., and J. A. Pitman, 1992, Land-Surface schemes for future climate models: Specification, Aggregation and heterogeneity, *Journal of Geophysics Research*. **97**(D3):2687-2696.
- Sellers, A. H., J. A. Pitman, P. Irannejad, and T. H. Chen, 1995, The project for intercomparison of land surface parameterization schemes (PILPS):Phases 2 and 3: *Bulletin of America Meteorological Society*, **76**(4):489-503.
- Sellers, P. J., 1985, Canopy reflectance photosynthesis and transpiration, *International Journal of Remote Sensing*, **6**: 1335-1372.
- Sellers, P. J, Y. Mintz, Y. C. Sud, and A. Dalcher, 1986, A simple Biosphere model(SiB) for use within general circulation models, *Journal of Atmospheric Sciences*, **43**(6): 505-531.
- Sellers, P. J., S. I. Rasool, and H. J. Bolle, 1990, A review of satellite data algorithms for studies of the land surface, *Bulletin of America Meteorological Society*, **71**(12): 1429-1447.
- Sellers, P. J., C. A. Norbre, D. J. Fitzjarrald, 1993, LAMBADA-BATERISTA: A preliminary science plan for a large scale biosphere-atmosphere field experiment in Amazon Basin, ISLSCP, IGPO Washington D.C., 49
- Sheppard, P. A., 1958, Transfer across the earth's surface and through the air above, *Quarterly Journal of the Royal Meteorological Society*, **84**: 205-224.
- Shi, L., and E.A. Smith, 1992, Surface forcing of the infrared cooling profile over Tibetan Plateau. Part II: Cooling rate variation over large scale plateau domain during summer

- monsoon transition. *Journal of Atmospheric Sciences*, **49**: 823-844.
- Sobrino, J. A., V. Caselles, and F. Becker, 1990, Significance of remotely sensed thermal infrared measurements obtained over a citrus orchard, *Photogrammetric Engineering and Remote Sensing*, **44**: 343-354.
- Sobrino, J. A., Z-L. Li, M.P. Stoll, and F. Becker, 1994, Improvement in the Split-Window Technique for Land Surface Temperature Determination, *IEEE Transactions on Geoscience and Remote Sensing*, **32**: 243-253.
- Sobrino, J. A., and N. Raissouni, 2000, Toward remote sensing methods for land cover dynamic monitoring: application to Morocco, *International Journal of Remote Sensing*, **21**(2): 353-366.
- Stanhill, G., 1969, A simple instrument for the ground measurement of turbulent diffusion flux, *Journal of Applied Meteorology*, **8**: 509-513.
- Stewart, J. B., 1995, Turbulent surface fluxes from remotely sensed skin temperature of sparse prairie grass, *Journal of Geophysics Research*, **100**(D12): 25429-25433.
- Stewart, J. B., E. T. Engman, R. A. Feddes, and Y. H. Kerr, 1998, Scaling up in hydrology using remote sensing: summary of a workshop, *International Journal of Remote Sensing*, **19**(1): 181-194.
- Strack, J. E., R. A. Pielke, and J. Adegoke, 2003, Sensitivity of Model-Generated Daytime Surface Heat Fluxes over Snow to Land-Cover Changes, *Journal of Hydrometeorology*, **4**(1): 24-42.
- Su, Z., M. Menenti, H. Pelgrum, B. J. J. M. Van den Hurk, and W. G. M. Bastiaanssen, 1998, Remote sensing of land surface heat fluxes for updating numerical weather predictions, In Nieuwenhuis, G.J.A., Vaughan, R.A., and Molenaar, M.(eds), *Operational Remote Sensing for Sustainable Development*, Balkema: 393-402.
- Su, Z., and M. Menenti, 1999, *Mesoscale Climate Hydrology: The contribution of the new observing systems. Pre-Execution Phase, Final Report*, BCRS NUSP-2, 99-05, 141pp.
- Su, Z., 2002, The Surface Energy Balance System (SEBS) for estimation of turbulent heat fluxes, *Hydrology and Earth System Sciences*, **6**(1): 85-99.
- Sugita, M., and M. Brusaert, 1990, Regional surface fluxes from remotely sensed skin temperature and lower boundary layer measurements, *Water Resources Research*, **26**:2937-2944.
- Susskind, J, J. Rosenfield, D. Reuter, and M. T. Chahine, 1984, Remote sensing of weather and climate parameters from HIRS2/MSU on TIROS-N, *Journal of Geophysics Research*, **89**: 467-469.

- Sverdrup, H.U., 1937, On the evaporation from the oceans, *Journal of Marine Research*, **8**: 3-14.
- Tanaka, K., H. Ishikawa, T. Hayashi, I. Tamagawa, and Y. Ma, 2001, Surface Energy Budget of Amdo on the Eastern Tibetan Plateau using GAME/Tibet IOP98 Data, *Journal of the Meteorological Society of Japan*, **79**(1B): 505-517.
- Taylor, P. A., R. I. Sykes, and P. J. Mason, 1989, On the parameterization of drag over small scale topography in neutrally stratified Boundary flow, *Boundary Layer Meteorology*, **48**: 409-422.
- Thom, A. S., 1972, Momentum, mass, and heat exchange of the vegetation, *Quarterly Journal of the Royal Meteorological Society*, **98**: 124-134.
- Troen, I. B., L. Marhrt, 1986, A simple model of atmospheric boundary layer: sensitive to surface evaporation, *Boundary Layer Meteorology*, **37**: 129-148.
- Tsukamoto, O., H. Fudeyasu, Sh. Miyazaki, K. Ueno, Y. Qi, and Y. Ma, 1999, Turbulent surface flux measurements over Tibetan Plateau with flux-PAM system, *Preprint Volume of Third International Scientific Conference on the Global Energy and Water Cycle*, Beijing, China, 411-412.
- Tsukamoto, O., H. Ishikawa, Sh. Miyazaki, J. Kim, Y. Ma, and Z. Hu, 2001, Diurnal variations of surface fluxes and boundary layer over Tibetan Plateau, *Proceedings of the International Workshop on GAME-AAN/Radiation*, Phuket, Thailand, 36-39.
- Tucker, C. J., 1979, Red and photographic infrared linear combination for monitoring vegetation, *Remote Sensing of Environment*, **17**: 223-249.
- Tucker, C.J., I. Fung, C. Keeling, and R. Gammon, 1986. Relationship between atmospheric CO₂ variations and satellite-derived vegetation index, *Nature*, **319**: 195-199
- Tucker, C. J., (ed), 1987, Monitoring the grasslands of semi-arid Africa using NOAA AVHRR data, *International Journal of Remote Sensing*, (special Issue), **7-11**:1383-1622.
- Valiente, J. A., M. Nunez, E. Lopez-Baeza, and J. F. MORENO, 1995, Narrow-band to broad-band conversion for Meteosat-visible channel and broad-band reflectance using both AVHRR-1 and -2 channels. *International Journal of Remote Sensing*, **16**(6):1147-1166.
- Valor, E. and V. Caselles, 1996, Mapping land surface emissivity from NDVI: application to European, African, and South American areas, *Remote Sensing of Environment*, **57**: 167-184.
- Van de Griend, A. A., and M. Owe, 1993, Determination of microwave vegetation optical

- depth and single scattering albedo from large scale moisture and Nimbus/SMMR satellite observations, *International Journal of Remote Sensing*, **14**(10): 1875-1886.
- Van den Hurk, B. J. J. M., W. G. M., Bastiaanssen, H. Pelgrum, and E., van Meijgaard, 1997, A new methodology for assimilation of initial soil moisture fields in weather prediction models using meteosat and NOAA data, *Journal of Applied Meteorology*, **36**(9): 1271-1283.
- Van den Hurk, B. J. J. M., 2001, Energy balance based surface flux estimation from satellite data, and its application for surface moisture assimilation, *Meteorology and Atmospheric Physics*, **76**: 43-52.
- Verhoef, A., H. A. R. de Bruin, and B. J. J. M. van den Hurk, 1997, Some practical notes on the parameter kB^{-1} for sparse vegetation, *Journal of Applied Meteorology*, **36**:560-572.
- Verhoef, W., 1997, *Theory of radiative transfer models applied in optical remote sensing of vegetation canopies*, PhD Thesis, Remote Sensing Department of National Aerospace Laboratory, The Netherlands.
- Walko, R. L., C. J. Tremback, and R. F. A. Hertenstein, 1995, RAMS-The regional atmospheric modelling system version 3b: *User's guide*, Published by ASTER, Inc.
- Wan, Z., and J. Dozier, 1989, land surface temperature measurement from space: Physical principles and inverse modelling, *IEEE Transactions on Geoscience and Remote Sensing*, **27**(3):268-278.
- Wang, J., Y. Gao, and Y. Hu, 1993, An overview of the HEIFE experiment in the People's Republic of China, *Exchange processes at the land surface for a range of space and time scales*, IAHS Publication, **212**: 397-403.
- Wang, J., Y. Ma, M. Menenti, and W. G. M. Bastiaanssen, 1995, The scaling-up of processes in the heterogeneous landscape of HEIFE with the aid of satellite remote sensing, *Journal of the Meteorological Society of Japan*, **73**(6): 1235-1244. (Chapter 5)
- Wang, J., J. Kim, Y. Liou, Z. Gao, Y. Yan, T. Choi, and H. Lee, 1999, Energy balance analysis and one-dimensional simulation of land surface process in a short-grass site of Central Tibetan Plateau, *Preprint Volume of Third International Scientific Conference on the Global Energy and Water Cycle*, Beijing, China, 424-425.
- Watson, K., F. Kruse, and S. Hummer-Miler, 1990, Thermal infrared exploration in the Carlin trend, *Geophysics*, **55**(1): 70-79.
- Webb, E. K., 1970, Profile relationships: the log-liner range and extension to strong stability, *Quarterly Journal of the Royal Meteorological Society*, **96**: 67-90.
- Webster, P. J., T. N. Palmer, M. Yanai, J. Shukla, V. Magana, T. Yasunari, and R. Tomas,

- 1998, The monsoon: Processes and prediction. *Journal of Geophysics Research*, 103, (TOGA special issue): 14451-14510.
- Wen, J., 1999, *Land surface variables estimated from remote sensing and the correction of atmospheric effects*, PhD. Thesis, Lanzhou Institute of Plateau Atmospheric Physics, The Chinese Academy of Sciences, Lanzhou, China: 115pp(in Chinese with English abstract).
- Wieringa, J., 1986, Roughness-dependent geographical interpolation of surface wind speed averages. *Quarterly Journal of the Royal Meteorological Society*, **112**: 867-889.
- Wieringa, J., 1992, Updating the Davenport roughness classification. *Journal of Wind Engineering and Industrial Aerodynamics*, **44**: 357-368.
- Wooding, R. A., E. F. Bradeley, and J. K., MA shall, 1973, Drag due to regular arrays of roughness elements of varying geometry, *Boundary Layer Meteorology*, **5**: 285- 308.
- Wood, N., P. J. Mason, 1991, The influence of static stability on the effective roghness lengths for momentum and temperature, *Quarterly Journal of the Royal Meteorological Society*, **117**: 1025-1057.
- Wu, K., X. Wang, S. Wang, W. Zhao, F. Yang, and Z. Pan, 1993, An analysis of urban island effect for air temperature using NOAA satellite data, *ACTA, Meteorological Sinica*, **51**, **2**: 203-208. (in Chinese with English abstract).
- Xue, Y., and J. Shukla, 1993, The influence of surface properties on Sahel climate. PartI: desertification, *Journal of Climate*, **6**: 2232-2245.
- Xue, Y., F. J. Zeng, K. Mitchell, Z. Janjic, and E. Rogers, 2001, The impact of land surface processes on the simulation of the U.S. hydrological cycle: A case study of 1993 US flood using the Eta/SSiB regional model, *Monthly Weather Review*, **129**: 2833-2860.
- Yan, Y., 1999, *Numerical simulation study of land atmosphere interaction on heterogeneous terrain*, PhD thesis, Lanzhou Institute of Plateau Atmospheric Physics, the Chinese Academy of Sciences, China, 134pp. (in Chinese with English abstract).
- Yanai, M., C. Li, and Z. Song, 1992: Seasonal heating of the Tibetan Plateau and its effects on the evolution of the Asian summer monsoon. *Journal of Meteorological Society of Japan*, **70**: 319-351.
- Ye, D., and Y. Gao, 1979, *The Meteorology of the Qinghai-Xizang (Tibet) Plateau*. Science Press, Beijing, 278 pp (in Chinese).
- Zhang, Q. G. Wei, and R. Huang, 2001: Bulk transfer coe_cients of momentum and sensible heat over the Gobi desert surface in north-western arid area. *Science in China (Series D)*, **31**(9): 783-792. (in Chinese)

Zhou, D., Y. Hu, 1988, A numerical study of internal boundary layer caused by abrupt change of the underlying surface characteristics, *Plateau Meteorology*, 7: 357-366. (in Chinese with English abstract)

List of peer-reviewed publications by the candidate during the PhD study period

First-author publications

- Ma, Y.,** H. Tian, J. Wang, H. Ishikawa, R. Ohba, H. Ueda, J. Wen, 2006, Determination of regional land surface heat fluxes over heterogeneous landscape of Jiddah area of Saudi Arabia by using Landsat-7 ETM data, *Hydrological Processes*, (in press).
- Ma, Y.,** L. Zhong, Z. Su, H. Ishikawa, M. Menenti, and T. Koike, 2006, Determination of regional distributions and seasonal variations of land surface heat fluxes from Landsat-7 Enhanced Thematic Mapper data over the central Tibetan Plateau area, *Journal of Geophysics Research*, 111, D10305, doi:10.1029/2005JD006742.
- Ma, Y.,** S. Fan, H. Ishikawa, O. Tsukamoto, T. Yao, T. Koike, H. Zuo, Z. Hu, and Z. Su, 2005, Diurnal and inter-monthly variation of land surface heat fluxes over the central Tibetan Plateau area, *Theoretical and Applied Climatology*, 80, 259-273.
- Ma, Y.,** M. Menenti, O. Tsukamoto, H. Ishikawa, J. Wang, and Q. Gao, 2004, Remote sensing parameterization of regional land surface heat fluxes over arid area in northwestern China, *Journal of Arid Environments*, 57: 117-133.
- Ma, Y.,** W. Ma, M. Li, Z. Su, M. Menenti, O. Tsukamoto, H. Ishikawa, T. Koike, and J. Wen, 2004, Determination of regional heat fluxes over heterogeneous land surfaces, GIS and Remote Sensing in Hydrology, Water Resources and Environment, *IAHS Publ.* 289: 206-214.
- Ma, Y.,** Z. Su, T. Koike, T. Yao, H. Ishikawa, K. Ueno, and M. Menenti, 2003, On measuring and remote sensing surface energy partitioning over the Tibetan Plateau-from GAME/Tibet to CAMP/Tibet, *Physics and Chemistry of the Earth*, **28**: 63-74.
- Ma, Y.,** H. Ishikawa, O. Tsukamoto, M. Menenti, Z. Su, T. Yao, T. Koike, and T. Yasunari, 2003, Regionalization of surface fluxes over heterogeneous landscape of the Tibetan Plateau by using satellite remote sensing, *Journal of Meteorological Society of Japan*. **81**(2): 277-293.
- Ma, Y.,** 2003, Remote sensing parameterization of regional net radiation over heterogeneous land surface of GAME/Tibet and HEFE, *International Journal of Remote Sensing*, **24** (15): 3137-3148.
- Ma, Y.,** J. Wang, R. Huang, G. Wei, M. Menenti, Z. Su, Z. Hu, F. Gao, and J. Wen, 2003, Remote sensing parameterization of land surface heat fluxes over arid and semi-arid

areas, *Advances in Atmospheric Sciences*, **20**(4):530-539.

- Ma, Y.**, W. Ma, M. Li, O. Tsukamoto, H. Ishikawa, J. Wang, Z. Hu, and F. Gao, 2003, The comparative analysis of characteristics of energy transfer in the atmospheric surface layer over GAME/Tibet, HEIFE and AECMP'95, *Chinese Journal of Atmospheric Sciences*, **27**(1): 1-14.
- Ma, Y.**, O. Tsukamoto, J. Wang, H. Ishikawa, and I. Tamagawa, 2002, Analysis of aerodynamic and thermodynamic parameters over the grassy marshland surface of Tibetan Plateau, *Progress in Natural Sciences*, **12**(1): 36-40.
- Ma, Y.**, O. Tsukamoto, H. Ishikawa, Z. Su, M. Menenti, J. Wang, and J. Wen, 2002, Determination of regional land surface heat flux densities over heterogeneous landscape of HEIFE Integrating satellite remote sensing with field observations, *Journal of Meteorological Society of Japan*, **80**(3): 485-501.
- Ma, Y.**, Z. Su, Z-L. Li, T. Koike, and M. Menenti, 2002, Determination of regional net radiation and soil heat flux densities over heterogeneous landscape of the Tibetan Plateau, *Hydrological Processes*, **16**(15): 2963-2971.
- Ma, Y.**, O. Tsukamoto, and H. Ishikawa, 2002, Remote sensing parameterization of energy and water cycle over desertification area, *Science in China (D)*, **45**(Supp): 47-53.
- Ma, Y.**, Ma, W., Hu, Z., Li, M., Wang, J., H. Ishikawa, and O. Tsukamoto, 2002, Similarity analysis of turbulent variances over the grassland surface of Tibetan Plateau, *Plateau Meteorology*, **21**(5): 514-517. (in Chinese with English abstract).
- Ma, Y.**, O. Tsukamoto, X. Wu, I. Tamagawa, J. Wang, H. Ishikawa, Z. Hu, and H. Gao, 2000, Characteristics of energy transfer and micrometeorology in the surface layer of the atmosphere above marshland of the Tibetan Plateau area, *Chinese Journal of Atmospheric Sciences*, **24**(5): 715-722(in Chinese with English abstract).
- Ma, Y.**, J. Wang, M. Menenti, and W. G. M. Bastiaanssen, 1999, Estimation of flux densities over the heterogeneous land surface with the aid of satellite remote sensing and field observation, *ACTA Meteorological Sinica*, **57**(2): 180-189.(in Chinese with English Abstract)

Co-author publications

- Li, M., **Y. Ma**, W. Ma, Z. Hu, H. Ishikawa, Z. Su, and F. Sun, 2006, Analysis of turbulence characteristics over the northern Tibetan Plateau area, *Advances in Atmospheric Sciences*, **23**(4): 579-585.

- Oku, Y., H. Ishikawa, S. Haginoya, and **Y. Ma**, 2006, Recent trends in land surface temperature on the Tibetan Plateau, *Journal of Climate*, **19**(12): 2995-3003.
- Asanuma, J., H. Ishikawa, I. Tamagawa, **Y. Ma**, T. Hayashi, Y. Qi, and J. Wang, 2005, Application of the band-pass covariance technique to portable flux measurements over the Tibetan Plateau, *Water Resources Research*, **41**, W09407, doi:10.1029/2005WR003954.
- Zuo, H., Y. Hu, D. Li, Sh. Lu, and **Y. Ma**, 2005, Seasonal transition and its boundary characteristics in Anduo area of Tibetan Plateau, *Progress in Natural Sciences*, **15** (3): 239-245.
- Wen, J., Z. Su, and **Y. Ma**, 2004, Reconstruction of cloud-free vegetation index time series for the Tibetan Plateau, *Mountain Research and Development*, **24**(4): 348-353.
- Yang, K., T. Koike, H. Ishikawa, and **Y. Ma**, 2004, Analysis of the surface energy budget at a site of GAME/Tibet using a single-source model, *Journal of Meteorological Society of Japan*, **82**(1): 131-153.
- Choi, T., J. Hong, J. Kim, H. Lee, J. Asanuma, H. Ishikawa, O. Tsukamoto, Z. Gao, **Y. Ma**, K. Ueno, J. Wang, T. Koike, and T. Yasunari, 2004, Turbulent exchange of heat, water vapor, and momentum over a Tibetan prairie by eddy covariance and flux variance measurements, *Journal of Geophysical Research*, **109**, D21106, 10.1029/2004JD004767.
- Wen, J., Z. Su, and **Y. Ma**, 2003, Determination of land surface temperature and soil moisture from Tropic Rainfall Measuring Mission/Microwave Imager remote sensing data, *Journal of Geophysical Research*, **108**(D2), 4038, doi: 10.1029/2002JD002176,2003.
- Tanaka, K., I. Tamagawa, H. Ishikawa, **Y. Ma**, and Z. Hu, 2003, Surface energy budget and closure of the eastern Tibetan Plateau during the GAME/Tibet IOP 1998, *Journal of Hydrology*, **283**:169-283.
- Tanaka, K., H. Ishikawa, T. Hayashi, I. Tamagawa, and **Y. Ma**, 2001, Surface energy budget at Amdo on the Tibetan Plateau using GAME/Tibet IOP98 data, *Journal of Meteorological Society of Japan*, **79**(1B): 505-517.
- Gao, Z., J. Wang, **Y. Ma**, J. Kim, T. Choi, H. Lee, J. Asanuma, and Z. Su, 2000, Calculation of Near-surface Layer Turbulent Transport and Analysis of Surface Thermal Equilibrium Features in Naqu of Tibet, *Physics and Chemistry of the Earth (B)*, **25**(2): 135-139.
- Gao, Z., J. Wang, **Y. Ma**, J. Kim, T. Choi, H. Lee, J. Asanuma, and Z. Su, 2000 Study of

roughness lengths and drag coefficients over Nansha Sea Region, Gobi, Desert, Oasis and Tibetan Plateau, *Physics and Chemistry of the Earth* (B), **25** (2): 141-145.

Curriculum Vitae

Yaoming Ma was born in Xia County, Shanxi Province, China, on July 22, 1964. He went to Lanzhou University on 1983 and obtained a Bachelor Degree in Atmospheric Physics in June 1987. He obtained his Master Degree in Atmospheric Physics from the Chinese Academy of Sciences (CAS) in 1995 at the Postgraduate School of the Chinese University of Science and Technology and Lanzhou Institute of Plateau Atmospheric Physics (LIPAP), CAS. He became employed at LIPAP, CAS in 1987. In 2000, he became employed at Cold and Arid Regions Environmental and Engineering Research Institute (CAREERI), CAS, and in March 2002, he became a professor of CAREERI, CAS. In April 2004, he joined the Institute of Tibetan Plateau Research (ITP), CAS, and worked as a professor in ITP, CAS. He is also the director of Lhasa Branch of ITP, CAS.

As an atmospheric boundary layer researcher, he has been actively involved in many land surface (sea surface) experiments in China. He has also been actively involved in the GEWEX Asia Monsoon Experiment on the Tibetan Plateau (GAME/Tibet, 1996-2000) for its entire duration. He was coordinating the participation of Chinese team in the GAME/Tibet. He is still in charge of the long term atmospheric monitoring on the Tibetan Plateau, which including one Planetary Boundary Layer (PBL) tower and radiation system station, eleven Automatic Weather Stations (AWSs), two Portable Automated Meso-net (PAM) stations, five flux measurement towers and nine Soil Moisture and Soil Temperature Measurement Systems (SMTMSs). He is also one of the overall coordinators of Coordinated Enhanced Observing Period (CEOP) Asian-Australian Monsoon Project (CAMP) on the Tibetan Plateau (CAMP/Tibet, 2001-2010). He is also the director of Comprehensive Observation and Research Station on Mt. Qomolangma (Mt. Everest), the Chinese Academy of Sciences.

As a scientific researcher, except his domestic research work, he cooperated with the foreign scientists on atmospheric boundary layer and the application of satellite remote sensing. His cooperative institutions and universities are including Alterra (SC-DLO), Wageningen University and Research Center (WUR) and International Institute for Geo-Information Science and Earth Observation (ITC) (The Netherlands), University of Tokyo, Nagoya University, Kyoto University, Tsukuba University and Okayama University (Japan) etc.

Yaoming Ma is married and has one daughter.

This research reported in this thesis was founded and supported by the Wageningen University and Research Centre through a 'sandwich' PhD fellowship, the Chinese National Key Programme for Developing Basic Sciences (2005CB422003 and G1998040900), the National Natural Science Foundation of China (40520140126) and the Innovation Project of Chinese Academy of Sciences (KZCX3-SW-231 and KZCX3-SW-339).